Ref. Ares(2021)6888450 - 09/11/2021

Horizon 2020
European Union Funding
for Research & Innovation

GEARBODIES

Grant Agreement Number: 101013296
Project Acronym: GEARBODIES
Project title: Innovative Technologies for Inspecting Carbodies and for Development of Running Gear

DELIVERABLE D 2.1

Modelling investigation and assessment

Project acronym:	GEARBODIES
Starting date:	01/12/2020
Duration (in months):	25
Call (part) identifier:	H2020-S2R-OC-IP1-02-2020
Grant agreement no:	101013296
Grant Amendments:	N/A
Due date of deliverable:	30-07-2021
Actual submission date:	09-11-2021
Coordinator:	Alkiviadis Tromaras
Lead Beneficiary:	CERTH
Version:	1
Type:	Report
Sensitivity or Dissemination level:	Public
Contribution to S2R TDs or WAs	TD1.3 Carbody Shell Demonstrator
Taxonomy/keywords:	Non-destructive testing; Active thermography modelling; Ultrasonic testing modelling; optical pulsed thermography modelling; optical lockin thermography modelling; Lamb waves modelling; pulse echo modelling; ThermoCalc 3D thermography modelling; Ultrasonic testing modellig with Comsol; composite rail carbodies; inspection methods for rail carbodies

This project has received funding from the Shift2Rail Joint Undertaking (JU) under grant agreement 101013296. The JU receives support from the European Union's Horizon 2020 research and innovation programme and the Shift2Rail JU members other than the Union.

Document history

Date	Name	Affiliation	Position/Project Role	Action/ Short Description
07/06/2021	Alkiviadis Tromaras	CERTH	WS1 leader	First draft
20/06/2021	Alkiviadis Tromaras	CERTH	WS1 leader	Thermography modelling literature review and thermography software overview
14/07/2021	Alkiviadis Tromaras	CERTH	WS1 leader	Ultrasonic modelling literature review
19/10/2021	Alkiviadis Tromaras	CERTH	WS1 leader	Thermography modelling and simulations on ThermoCalc3D software
19/10/2021	Eduardo Moreno Hernandez, Roberto Giacchetta, David Sánchez Pariente	DASEL	Deliverable contributor	Ultrasonic modelling and simulations for sandwich component using Comsol software
26/10/2021	Celestino Sánchez	EUR	Project coordinator	Internal review
27/10/2021	Alkiviadis Tromaras	CERTH	WS1 leader	Modifications, corrections, and review
28/10/2021	Eduardo Moreno Hernández	DASEL	Deliverable contributor	Additional contributions on ultrasonic modelling using Comsol software
30/10/2021	Vasilis Kappatos	CERTH	WS1 leader	Internal review
1/11/2021	Alkiviadis Tromaras	CERTH	WS1 leader	Additional ultrasonic modelling on monolithic composite using SimNDT software
8/11/2021	Celestino Sánchez	EUR	Project coordinator	Final review

Disclaimer

The information in this document is provided "as is", and no guarantee or warranty is given that the information is fit for any particular purpose. The content of this document reflects only the author's view – the Shift2Rail Joint Undertaking is not responsible for any use that may be made of the information it contains. The users use the information at their sole risk and liability.

Table of contents

Executive Summary

The present document represents Deliverable D 2.1 "Modelling investigation and assessment" of the GEARBODIES project funded by the European Commission within the framework of Shift2Rail (S2R) programme. D 2.1 is the second deliverable withing the research process followed under Work Stream 1 of the project, where the application of NDT methods for inspecting surface and subsurface defects/damage on new composite rail carbodies (from PIVOT2 project), is explored. In the previous Deliverable D1.1 "Terms of reference, requirements and specifications for Carbody Inspection Technology" a state-of-the-art literature review was conducted on suitable NDT methods for such applications. In D 2.1, the research focuses specifically on the suitability of active thermography and ultrasonic testing, through the aid of software modelling and simulation packages such as ThermoCalc 3D, Comsol and SimNDT.

To explore the capabilities of infrared thermography and ultrasonic testing, two types of composite components were modelled based on input from PIVOT2 project. Specifically, a monolithic Carbon Fibre Reinforced Polymer (CFRP) component of 20mm thickness and a composite sandwich component consisting of 5mm thickness CFRP skins and a Polyethylene terephthalate (PET) foam core of 30mm thickness (40mm overall thickness). Dimensional, mechanical and thermal material properties were based on input from PIVOT2 project and literature.

The IRT simulations, that were carried out in ThermoCalc 3D, focused on techniques such as optical pulsed thermography and lockin thermography as they are most commonly used in the field and were also reviewed for potential application under D 1.1. A series of subsurface defects, of various sizes and at different depths, were introduced on the modelled specimens, in order to simulate delaminations and disbonds. The IRT simulations have proven that both thermography methods can detect these defects up to a certain depth. However, there are limitations on both techniques. In the case of pulsed thermography, the technique has proven to be more effective for defects at 5-10 mm depth for both samples. Deeper defects (at 15mm) on the monolithic component, were mostly detectable using optical lockin method where heat is applied on the specimen for much longer time up to 2mins. Hence, defects beneath the foam core of the sandwich component were not detectable with any IRT technique.

In addition, ultrasonic modelling and simulations were carried out, to test the detectability of defects on the two model components, using low frequency ultrasonic excitation pulse. The frequency range was from 15 KHz to 200 KHz, where the formation of Lamb waves is expected. The models and simulations were developed using Finite Elements Methods (FEM) on Comsol 5.6 software. A novel FEM tool called Discontinuous Galerkin method was used to simulate pulse propagations with low mesh sizes. Apart from the FEM models, dispersion curves models, were also developed in Matlab, for the foam core and CFRP skins in order to understand better the frequency ranges that are required in the simulations. The

results showed the predominant propagation of antisymmetric Lamb wave modes. On the simulations of the sandwich component, a leakage from the top CFRP skin to the PET core material has been observed under the simulations of 200 KHz. Overall, the simulations have proven that Lamb waves can be used for NDT testing of the monolithic and sandwich components. Pulse echo simulations were also conducted on the monolithic component where the usage of this technique has proven to be a viable option for deeper defects not previously detected by IRT.

D 2.1 concludes that simulations have been a useful tool. However, they remain a theoretical tool. Therefore, further experimentation is required under lab conditions where IRT and UT tests will be carried out on fabricated samples. This remains future work to be carried out in following deliverables and WP2.

List of abbreviations, acronyms and definitions

Abbreviation / Acronym	Definition
AES	Algebraic equation system
AUT	Automated Ultrasonic Testing
BB	Building block
CAD	Computer Aided Design
CAE	Computer Aided Engineering
CAM	Computer Aided Manufacturing
CFD	Computational Fluid Analysis
CFM	Call for Members
CFRP	Carbon Fibre Reinforced Polymer
DDF	Digital damage fingerprints
FEA	Finite element analysis
FEM	Finite element method
FT	Fourier Transformation
GRP	Glass Reinforced Polymer
IP1	Innovation Programme 1 of Shift2Rail (Cost-efficient and reliable trains, including high-capacity trains and high-speed trains)
IR	Infrared
IRT	Infrared Thermography
MAAP	Multi Annual Action Plan (of Shift2Rail Joint Undertaking)
NEDT	Noise Equivalent Temperature Difference
NDE	Non-destructive Evaluation
NDT	Non-destructive Testing
PA	Phased Array
PCA	Principle Component Analysis
PDE	Partial Differences Equations
PE	Pulse Echo
PET	Polyethylene terephthalate
PIVOT2	Performance Improvement for Vehicles on Track 2 (S2R IP1 project)
PT	Pulsed Thermography
RF	Repetitive Frequency
S2R	Shift2Rail Joint Undertaking (under the H2020 framework)
SNR	Signal-to-noise ratio
SP	Sandwich plate

SV	Shear vertical
TD1.3	Technology Demonstrator 1.3 within IP1 of S2R (Carbody Shell Demonstrator)
TOFD	Time-of-flight diffraction
TRL	Technology Readiness Level
UT	Ultrasonic Testing
WP	Work Package
WS	Work Stream (of the GEARBODIES project)

List of Figures

List of Tables

List of Graphs

Graph 51 Delta T profiles for different rows of defects using optical lockin simulation ML2 settings. Row#1 in blue, Row #2 in green, Row# 3 in Orange and Row#4 in red 126

Graph 179 Delta T profiles for different rows of defects using optical pulsed thermography simulation SP5. Row#1 in blue, Row #2 in green, Row# 3 in Orange, Row# 4 in yellow and Row #5 in red 222

Graph 180 Delta T profiles for Row #4 and #5 of defects using optical lockin simulation SP4. Row #4 yellow, Row #5 in red 222

Graph 181 Space profiles of the different rows of defects using optical pulse simulation SP5 settings 223

Graph 182 Delta T profiles for different rows of defects using optical pulsed thermography simulation SP5. Row#1 in blue, Row #2 in green, Row# 3 in Orange, Row# 4 yellow and Row #5 in red 224

Graph 183 Delta T profiles for Row #4 and #5 of defects using optical lockin simulation SP5. Row #4 yellow, Row #5 in red 224

Graph 184 Space profiles of the different rows of defects using optical pulse simulation SP6 settings 225

Graph 185 Delta T profiles for different rows of defects using optical pulsed thermography simulation SP6. Row#1 in blue, Row #2 in green, Row# 3 in Orange, Row# 4 in yellow and Row #5 in red 226

Graph 186 Delta T profiles for Row #4 and #5 of defects using optical lockin simulation SP4. Row #4 yellow, Row #5 in red 226

Graph 187 Space profiles of the different rows of defects using optical pulse simulation SP7 settings 227

Graph 188 Delta T profiles for different rows of defects using optical pulsed thermography simulation SP7. Row#1 in blue, Row #2 in green, Row# 3 in Orange, Row# 4 in yellow and Row #5 in red 228

Graph 189 Delta T profiles for Row #4 and #5 of defects using optical lockin simulation SP7. Row #4 yellow, Row #5 in red 228

Graph 190 Space profiles of the different rows of defects using optical pulse simulation SP8 settings 229

Graph 191 Delta T profiles for different rows of defects using optical pulsed thermography simulation SP8. Row#1 in blue, Row #2 in green, Row# 3 in Orange, Row# 4 in yellow and Row #5 in red 230

Graph 192 Delta T profiles for Row #4 (yellow) and Row#5 (red) of defects using optical lockin simulation SP8. 230

Graph 193 Space profiles of the different rows of defects using optical pulse simulation SP9 settings 231

1 Introduction

The present document represents Deliverable D 2.1 “Modelling investigation and assessment” of the GEARBODIES project, funded by the European Commission within the framework of Shift2Rail (S2R) programme.

The GEARBODIES project is part of Innovation Programme 1 (IP1) “Cost-efficient and reliable trains, including high-capacity trains and high-speed trains” of the Shift2Rail Joint Undertaking, within the framework of Horizon 2020. According to the Shift2Rail Annual Work Plan and Budget 2020 (Shift2Rail, 2020), it is expected that GEARBODIES will contribute to two Technology Demonstrators (TD) in IP1, i.e.:

- TD1.3 Carbody Shell Demonstrator;
- TD1.4 Running Gear Demonstrator.

Therefore, the GEARBODIES consortium will collaborate with PIVOT2 (Performance Improvement for Vehicles on Track 2), the complementary project for S2R members, which will run in the same period.

The work carried out within the Work Stream 1 of GEARBODIES (WS1: Inspection methods for carbodies using new materials) will contribute to TD1.3, in particular to its building block (BB) BB1.3_1 “Composite-hybrid carbodyshell” and its associated deliverables D1.3_1 and D1.3_2 (Figure 1).

Figure 1 The building block associated with TD1.3 and its related deliverables

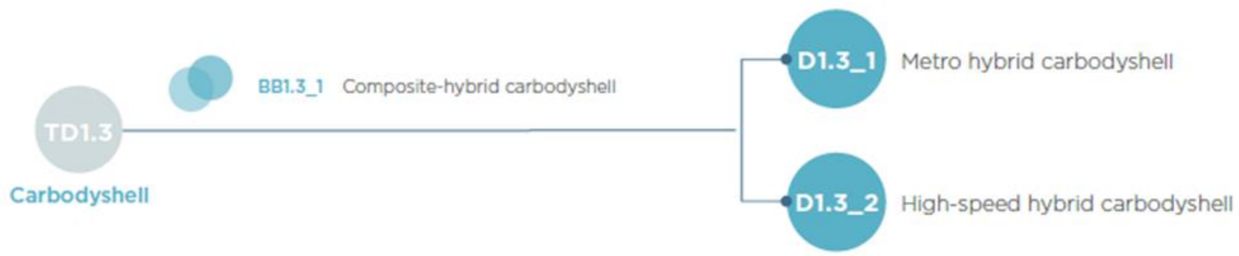

Source: S2R (2019)

D 1.1 “Terms of reference, requirements and specifications for carbody inspection technology” presented a state-of-the-art literature review of thermographic and ultrasonic Non-Destructive inspection techniques that can be applied on surface and sub-surface inspection of composite and hybrid components, including both monolithic and sandwich types for usage in rail carbodies. Thus, D 2.1 will explore, on a theoretical level, the suitability of such NDT methods from D 1.1 with the means of modelling and simulation.

2 Objectives/aim

Deliverable D 2.1 "Modelling investigation and assessment", reports the first research outcomes of Work Package 2 "Development of inspection methods for composite and hybrid components for both monolithic and sandwich types" in relation to Work Stream (WS) 1. The latter aims to develop a prototype NDT inspection platform that will be capable of inspecting the PIVOT2 prototype composite carbody using inspection techniques such as Infrared thermography and ultrasonic testing. D 2.1 is the second step of the research process (Figure 2) of WS1, for identifying suitable thermographic and ultrasonic Non-Destructive inspection techniques that can be applied on surface and sub-surface inspection of composite and hybrid components, including both monolithic and sandwich components for usage in rail carbodies. D 2.1 aims to explore the suitability of NDT techniques, that were previously identified in D 1.1, for potential usage on inspecting composite rail carbodies. Therefore, D2.1 will assess, through software modelling and simulations, whether the simulated NDT techniques, can detect defects/ damage such as impact damage, delamination, disbonds only through the front surface of the component. The latter is the result of PIVOT 2 project's requirement, that the NDT system to be developed in WP3 "Development of prototype equipment for inspection of carbody shell", can only carry out inspections from the exterior of the composite cardoby, without access to the interior of the train. The two components to be modelled in D 2.1 are based structural sections of the PIVOT2 composite rail carbody shell prototype. Specifically, the components will be: 1) a sandwich type composite, consisting of Carbon Fibre Reinforced Polymer (CFRP) skins and polyethylene terephthalate (PET) foam core and 2) a monolithic CFRP material. The sandwich component will be located at the side wall sections of the carbody while the monolithic CFRP component will be located between the windows. Further details about the components and their materials are provided in Section 4.1

Figure 2 Research process of WS1

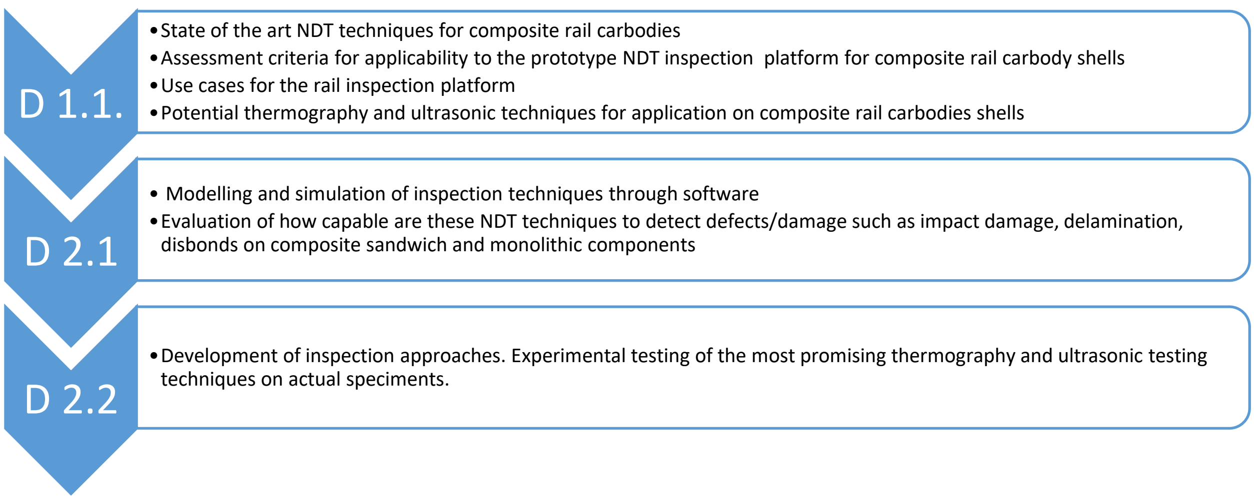

Source: own elaboration

3 Introduction to modelling software

Section 3 presents a brief overview of why modelling and simulation will be used.

3.1 Overview of modelling and simulation

Digital simulation tools that belong to the general spectrum of Computer Aided Engineering (CAE) have various applications within the engineering field. CAE is a growing and established field in the engineering world, that offers deeper understanding and analysis of objects or processes, with applications ranging from design and virtual testing to planning and manufacturing (Design academy, 2021; Simscale, 2021). Common applications of CAE are Computer Aided Design (CAD), Computer Aided Manufacturing (CAM), Finite Element Analysis (FEA), Computational Fluid Dynamics (CFD), Thermal Analysis, dynamics, kinematics, noise vibration and harness, reliability analysis, material properties and many other specialised fields where complex physics and mathematical calculations are required. Modelling of processes such as thermography and ultrasonic testing falls within these aforementioned specialised fields. Such software allows the modelling and simulation of specific processes. In the first case, specialised software allows the simulation of the heating and heat transfer process of thermography on a specimen that is modelled in a virtual environment that carries user defined material properties and defects. Respectively, the concept remains the same in the case of ultrasonic testing where a software is used to simulate ultrasound propagation in a specimen with defects.

In general, the reason for using CAE tools, is that they offer a series of benefits. CAE offers the capability of modelling objects that are complicated while they allow visualisation and testing in a virtual risk-free environment. CAD/CAM tools are used by many industries not only to model and design but also to solve mathematical 2D and 3D problem (Vavilov and Burleigh, 2020). The models created in one software can be exchanged between different ones thus offering time reduction in carrying out various types of analyses. According to Umaz et al. (2008) thermography research funds can be significantly reduced by first modelling potential test procedures on simulation software. Simulations, can enable a wider range of experimenting with heating protocols and testing different heating duration times on a theoretical level, thus saving time from lab environment experimentations. Usually in the case of thermography, experimentations are always required on the spot to get optimum results. The concept of experimenting in a theoretical level through simulations also applies to UT. Despite these benefits, modelling and simulations in thermography and UT remain a more academic/ research related topic. Companies that carry out thermography inspections as a service or industries that apply NDT methods in-house, usually tend to ignore the use of simulations simply because they have a range of equipment that can be used to test various techniques.

3.2 Thermography modelling and simulations background

Specialised thermography software has been created by companies in order to solve classical heat conduction multidimensional problems (in 1D, 2D or 3D). Such software use analytical and numerical methods to analyse heat conduction in solids that contain subsurface defects (Vavilov and Burleigh, 2020). The capabilities of each software differs and can be found on each software's website as seen on Table 1. The cost of many of these software is significant. Many of such software do not serve the purpose of solving thermography calculations. Instead, they can do Multiphysics calculations and be used, including others purposes, to see the behaviour of the materials under heat. Some of the most the most well-known software are Comsol Multiphysics and Ansys.

Table 1 Software capable of thermophysics modelling and simulations

Program/Thermophysical module	*Website*	*Characteristics*
Abaqus/Standard	https://www.3ds.com/products-services/simulia/products/abaqus/abaqusstandard/	FEA software
Adina Thermal	http://www.adina.com/adina-thermal.shtml	Heat transfer problems software
Algor/ Multiphysics	https://download.autodesk.com/us/algor/userguides/mergedProjects/master/index.htm	FEA software, heat transfer, thermal stress analysis
Ansys/Multiphysics	https://www.ansys.com	FEA software
Comsol/ Multiphysics	https://www.comsol.com/	FEA, heat transfer, CFD,
Marc	https://www.mscsoftware.com/product/marc	FEA software
MuSES TAIThermIR	https://www.thermoanalytics.com/	Thermal IR signatures for objects. Heat transfer solver
ThermoCalc-3D	Tomsk Polytechnic University (Russia)	Finite Difference Method software that uses numerical solutions for heating 3D bodies with different parallepiped-like defects. Offers different heating functions that can simulate thermography techniques and produces IR image sequences

Source: Adapted from (Vavilov and Burleigh, 2020; 105, 106)

The last software on Table 1, ThermoCalc-3D, is a software specifically designed to model and simulate thermography related problems and offers calculations accuracy similar to Comsol. It has been developed by Tomsk Polytechnic University and is the one that will be used to carry out the simulations in D2.1.

ThermoCalc-3D is software specifically designed for modelling thermal non-destructive testing and is capable of solving three-dimensional heat conduction problems of heating a 36-layer solid body containing up to 40 subsurface defects. It can be used to model and analyse different heating functions as well as arbitrary heating. It offers simplicity in designing the specimens by creating parallelepiped specimens made of user defined materials and adding defects that are normally simulated as air gaps. Thus, ThermoCalc-3D does not require the use of importing complex CAD designs like other commercial software and offers good computational accuracy that is difficult to achieve by other software (ThermoCalc 3D, 2018). ThermoCalc-3D is going to be used to carry out all IRT modelling and simulation with D 2.1.

The main characteristics of the software are listed below (ThermoCalc 3D, 2018; 2):

- User-friendly interface
- Uniquely fast computation time
- Sample may include up to 36 layers and contain up to 40 defects
- Defects may intersect and cross layer boundary, as well as reach sample external surface
- Thin defects in thick samples can be modeled
- Anisotropic layers can be characterized by different layup angles
- Non-adiabatic heat exchange
- Heating with both a square and cosine pulse, periodic square pulses
- Modelling arbitrary heating with a piece-wise (arbitrary) function
- Additional heating by the ambient can be modeled
- Heat conduction within defects is taken into account (capacitive defects)
- Cross-influence of defects and 3D heat diffusion can be analyzed
- Uneven heating phenomena (Gaussian heat flux) can be introduced
- Unique feature of introducing a heat mask to model an arbitrary spatial distribution of absorbed energy
- Performing the pixel-based Fourier transform in time (Pulse Phase Thermography) and Principle Component Analysis (PCA)
- Saving calculated data as a sequence of synthetic images (in Byte of float format)
- Saving calculated data as a sequence of *.txt files (MS Excel compatibility)
- Saving calculated image sequences in the MatLab format

- Saving calculated data in text form
- Black & White (B&W) and color temperature images
- Temporal profiles of true temperatures, differential temperature signals and dimensionless temperature contrasts as functions of time
- Spatial profiles of temperature and 3D presentation of both the object and IR thermograms

When starting the ThermoCalc 3D, a demonstration scenario loads up by default thus making easier to simply modify the different variables and properties according to the user's needs and create new scenarios. Figure 3 presents the main window when starting Thermocalc 3D which includes all the menus and the demonstration scenario. The brown rectangle presents the front side of a sample that contains 9 defects which are numbered and presented with different colours. The software also has the ability to display the object in six directions front, rear, left, right, top and bottom as well as a 3D view. Figure 4 presents various details of the representations of the object that are available from the software. The top right picture b) shows a top view of the object where the different material layers of the composite are presented. The top view also presents the location of the 9 defects and the direction of the excitation heat Q that reaches the front of the object. The different side views and the 3D view allows the user to see the depth where the defects are located.

Figure 3 Main window of the ThermoCalc 3D software

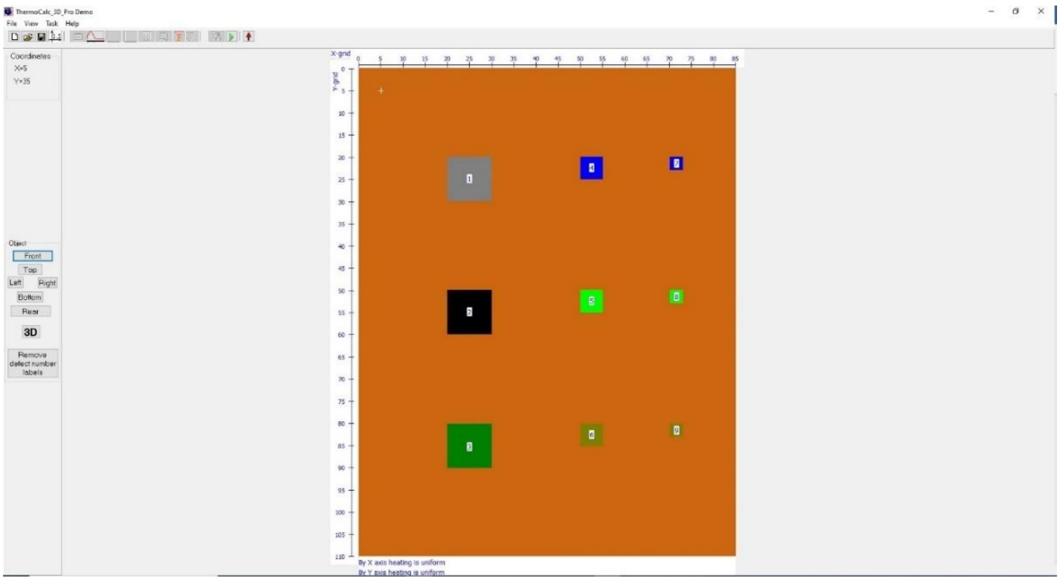

Source: ThermoCalc 3D own software

Figure 4 Various representations of the modelled object. a) Representation of the defects (left side). b) Top view of the object. c) 3D view

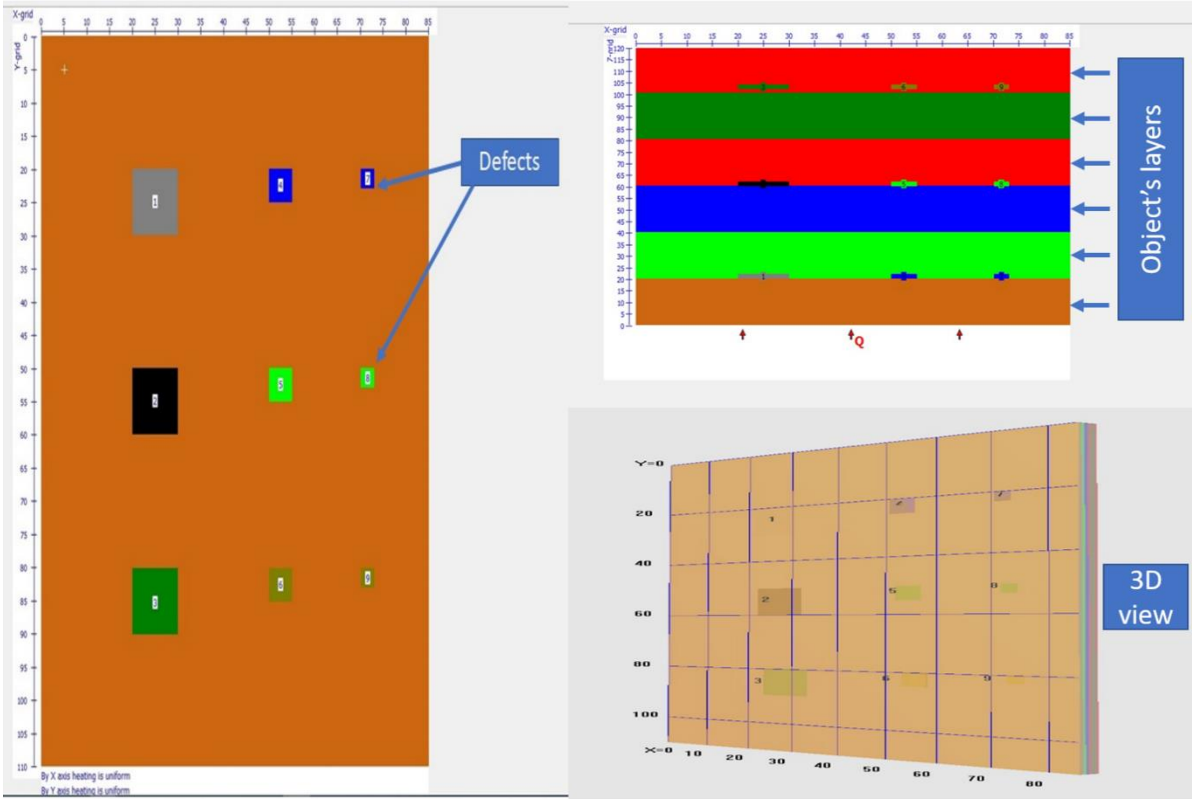

Source: ThermoCalc 3D own software

The parameters menu, consists of the main menu for inputting data regarding the characteristics of the object that is modelled in the software. The six tabs contained under the parameters menu consist of:

<u>Specimen</u>: this tab allows the user to define general characteristics about the specimen to be modelled. The menu its explanations are presented at Figure 5 and Table 2.

Figure 5 Specimen menu

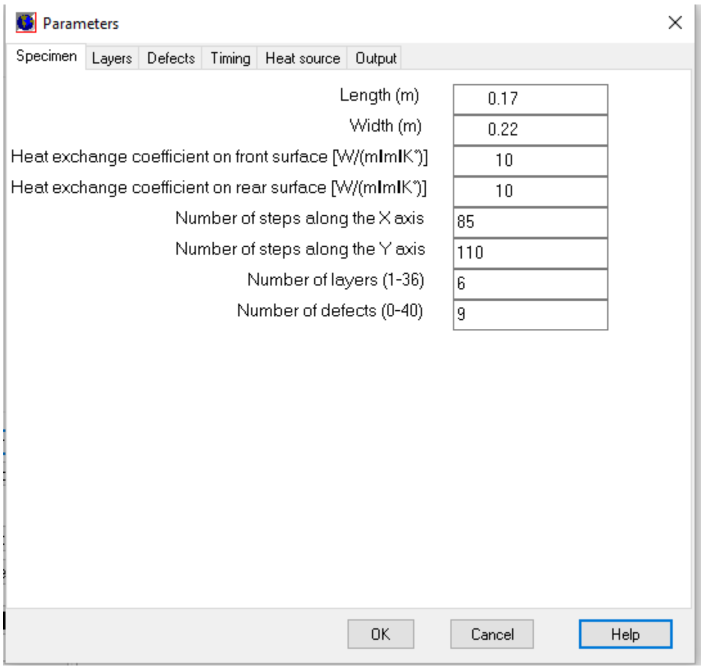

Source: ThermoCalc 3D own software

Table 2 Specimen menu explanation

Parameter	Explanation
Length [m] Width [m]	General dimensions of the specimen in XY axis
Heat exchange coefficient on front surface $[W/(m^2 \cdot K)]$ Heat exchange coefficient on rear surface $[W/(m^2 \cdot K)]$	Heat exchange coefficient is usually assumed to be 10 $W/(m^2.K)$ at ambient temperatures and is the same for both front and back surfaces (Vavilov and Burleigh, 2020)
Number of steps along the X axis Number of steps along the Y axis	Refers to the number of spatial grid steps chosen by the user along the X or Y axis. As a rule, a defect of 5mm should have 3-5 steps covering the area. Thus, steps can be 1mm. The lateral number of steps are not as crucial as the number of steps in the Z axis.
Number of layers (from 1 to 36)	The number of layers the user wants to define according to the specimen they want to model
Number of defects (from 0 to 40 with 0 (zero) corresponding to a non-defect specimen).	The number of defects the user wants to introduce

Layers: The layers tab menu allows the user to define the different layers of the specimen. This section is actually where the specimen is characterised and the user inputs the type of material that each layer consists of. The number of layers is more relevant to composites and sandwich components that can contain skin, core and adhesives between the skins and core. Also, the software allows to model isotropic and anisotropic materials by defining the direction of the different plies i.e. 0°, 45°, 90° as shown on Figure 6. The layer properties are actually the ones that allow the user to define the material properties (heat capacity, heat conductivity, density, layer thickness) of the specimen. Such values about material heat capacity, density etc. can be found in the software's manual (ThermoCalc 3D, 2018) as well as Vavilov and Burleigh (2020) and different internet sources.

Figure 6 a) Fibre reinforced composite laminate and b) Rotation from the natural (global)to the principal system.

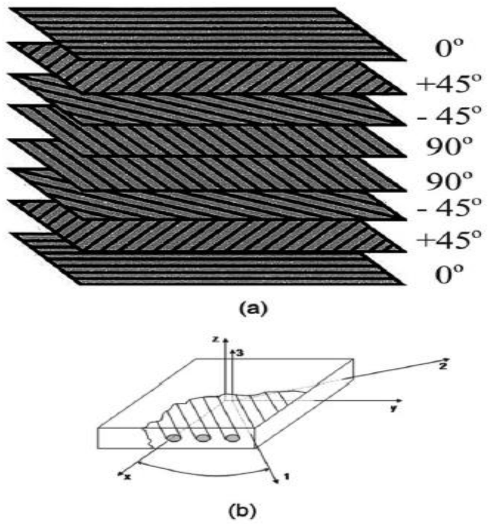

Source: Kalogiannakis et al. (2006; 063521-2)

The layers menu is shown in Figure 7

Figure 7 Layers menu

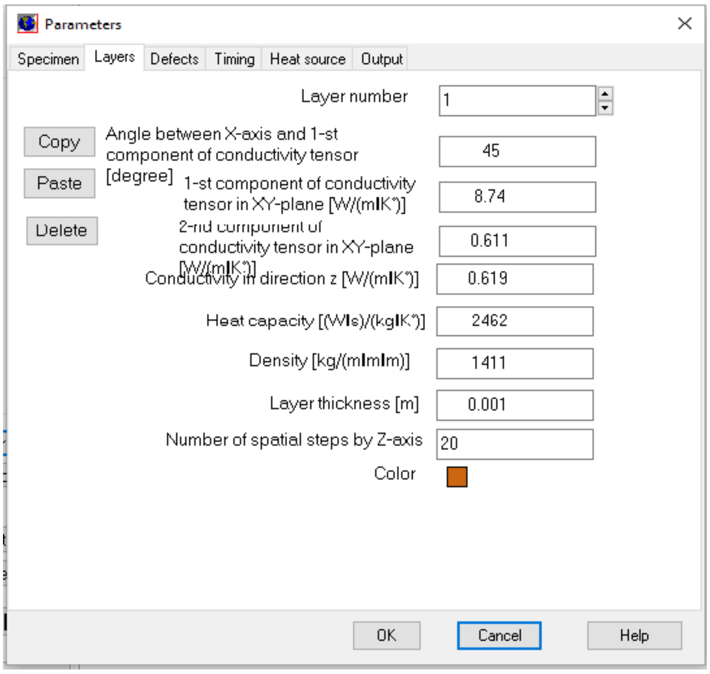

Source: ThermoCalc 3D own software

A detailed explanation of the items from the Layers menu can be seen in Table 3 Layers menu explanationTable 3

Table 3 Layers menu explanation

Parameter	Explanation
Layer number	The number of layers that the specimen will have. A simple composite that consists of a 2 skins (without different plies) and a core should be modelled with 3 layers.
Angle between X-axis and 1st component of conductivity tensor (in degree)	Refers to the direction of plies as explained earlier i.e. 0°, 45°, 90°
1st component of conductivity tensor in XY plane [$W/(m \cdot K)$] 2st component of conductivity tensor in XY plane [$W/(m \cdot K)$]	The conductivity depends on the type of materials and whether it is isotropic or anisotropic. The conductivity can changes depending on the direction of the plies Values for different materials can be found in ThermoCalc 3D (2018) as well as Vavilov and Burleigh (2020)

Conductivity in direction Z [$W/(m \cdot K)$]	Conductivity in the Z axis. This value can be found from literature sources such as ThermoCalc 3D (2018) as well as Vavilov and Burleigh (2020). The conductivity for fibrous materials can be higher along the fibres and smaller on the z axis where the heat is perpendicular to the fibres.
Heat Capacity (Specific Heat) that is constant in all three coordinate directions [$(W \cdot s)/(kg \cdot K)$]	The amount of heat required to change its temperature by one degree. Heat capacity of materials varies in literature especially for CFRP and GFRP based on material technology and manufacturer (fabrication process).
Density that is constant in all three coordinate directions [kg/m^3]	The density of the material. The density of the material varies in literature especially for CFRP and GFRP based on material technology and manufacturer (fabrication process).
Layer thickness [m]	The thickness of the layer
Number of spatial steps by the Z-axis	As opposed to the XY axis spatial steps, Z axis steps should be many to achieve better accuracy. The thickness of a defect should be covered at least by 3 steps. For example, if the defect thickness is 0.1 mm the Z-steps should be of 0.025 mm
Color (to select the layer color for the sample scheme)	The user defined colour for each layer

<u>Defects:</u> The defects tab menu allows the user to define the individual characteristics of the defects that have been introduced earlier in the specimen tab. The way that defects are modelled is explained after the presentation of the defect's menu. As a general rule cracks, delamination, corrosion and disbonding are normally modelled as air gaps in the material by using the thermal properties of air. The defects menu is shown in Figure 8.

Figure 8 Defects menu

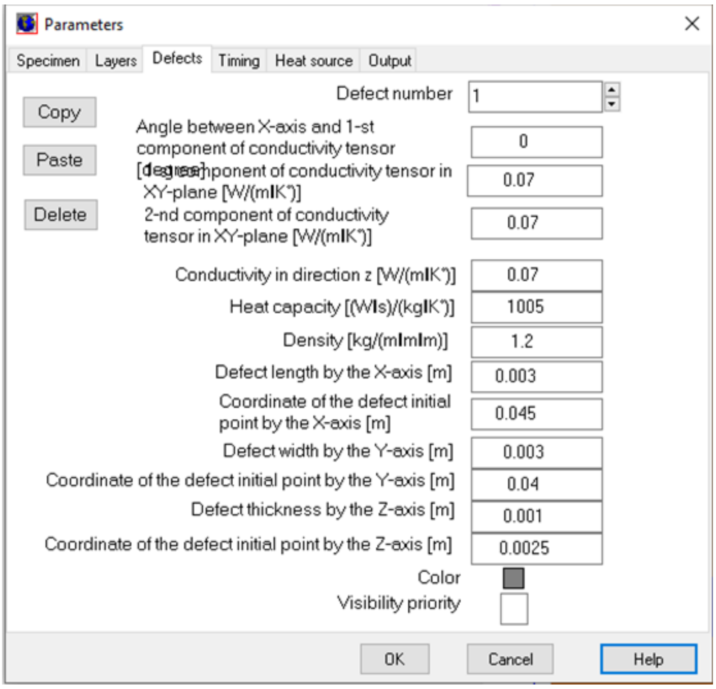

Source: ThermoCalc 3D own software

A detailed explanation of the items from the Defect menu can be seen in Table 4

Table 4 Defect menu explanation

Parameter	Explanation
Defect number (from 1 to 40 - to be selected with the counter on the right)	The number of defects to be introduced in the specimen
Angle between X-axis and 1st component of conductivity tensor (in degree)	The angle between the component and the X axis
1st component of conductivity tensor in XY plane [$W/(m \cdot K)$]	Since defects are modelled as a different type of material within a layer i.e. an air gap, the thermal conductivity of the defects will be the same as air. Values for different materials can be found in ThermoCalc 3D (2018) as well as Vavilov and Burleigh (2020)
2nd component of conductivity tensor in XY plane [$W/(m \cdot K)$]	The defects can have different “layers” hence they can exhibit anisotropic or isotropic properties having the same thermal properties in the XYZ axis. Values for different materials can be found in ThermoCalc 3D (2018) as well as Vavilov and Burleigh (2020)
Conductivity in direction Z [$W/(m \cdot K)$]	See above

Heat Capacity (Specific Heat) that is constant in all three coordinate directions $[(W \cdot s)/(kg \cdot K)]$	See 1st conductivity tensor explanation
Density that is constant in all three coordinate directions $[kg/m^3]$	See above
Defect length by the X axis $[m]$	Length of the defect
Coordinate of the defect initial point by the X axis $[m]$	Coordinate location of the defect in X axis
Defect width by the Y axis $[m]$	Width of the defect
Coordinate of the defect initial point by the Y axis $[m]$	Coordinate location of the defect in Y axis
Defect thickness by the Z axis $[m]$	Thickness of the defect in the Z axis
Coordinate of the defect initial point by the Z axis (defect depth) $[m]$	Coordinate location of the defect in z axis
Color	The user defined colour for each defect
Visibility priority	The user can prioritise a defect so it can appear first (i.e. not to be overshadowed by other defects).

Modelling of defects in the thermal NDT and ThermoCalc 3D

Defects in ThermoCalc 3D are modelled with parallelepiped sections whose material properties are defined to be the same as air. Thus, the software recognises the specified area as an air gap. In other cases, where water has accumulated in a honeycomb sandwich structure, the defect is modelled as parallelepiped gap that exhibits the material properties of water (Vavilov et al., 2016). Examples of how different defects can be modelled are given below at Figure 9 according to the software's manual.

Figure 9 Modelling of defects with ThermaCalc 3D

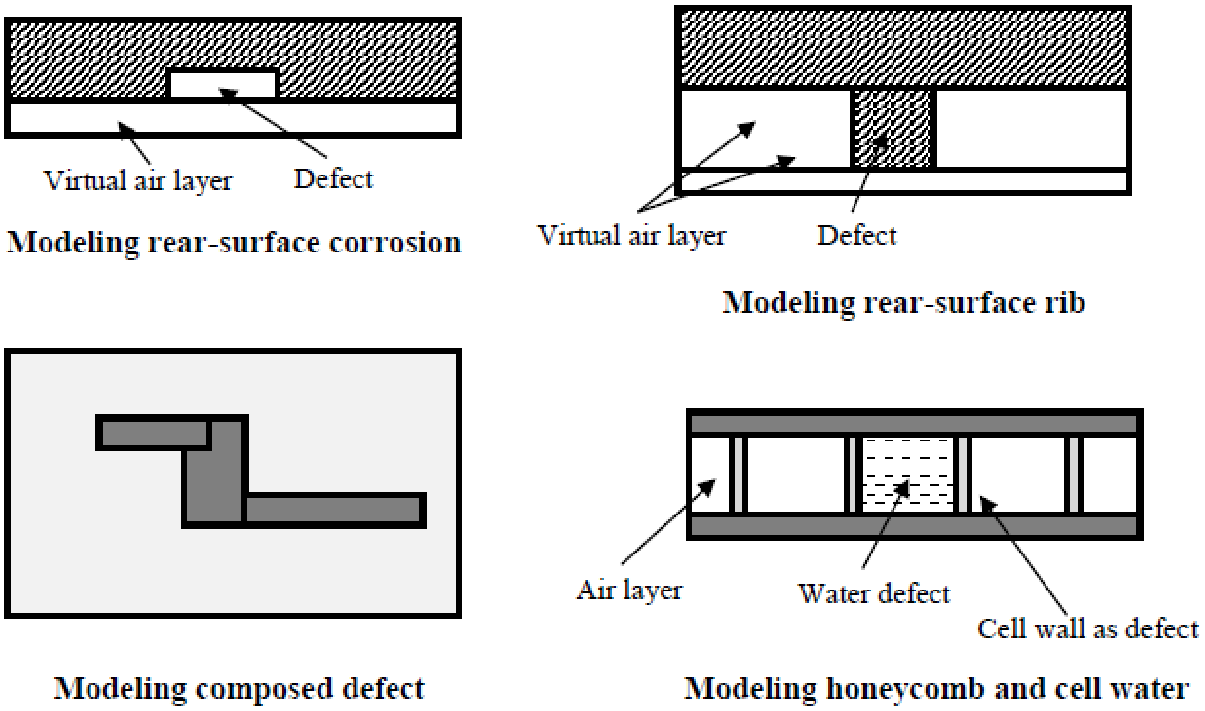

Source: ThermoCalc 3D (2018; 34)

Timing

The timing menu allows the user to define what type of heating process wants to be introduced on the specimen as seen in Figure 10. This menu allows the use replicate what thermography method would like to model based on the heating functions incorporated into the software. Table 5 and Figure 11 present the explanation of the menu and the heating functions used to replicate the thermography techniques.

Figure 10 Timing menu

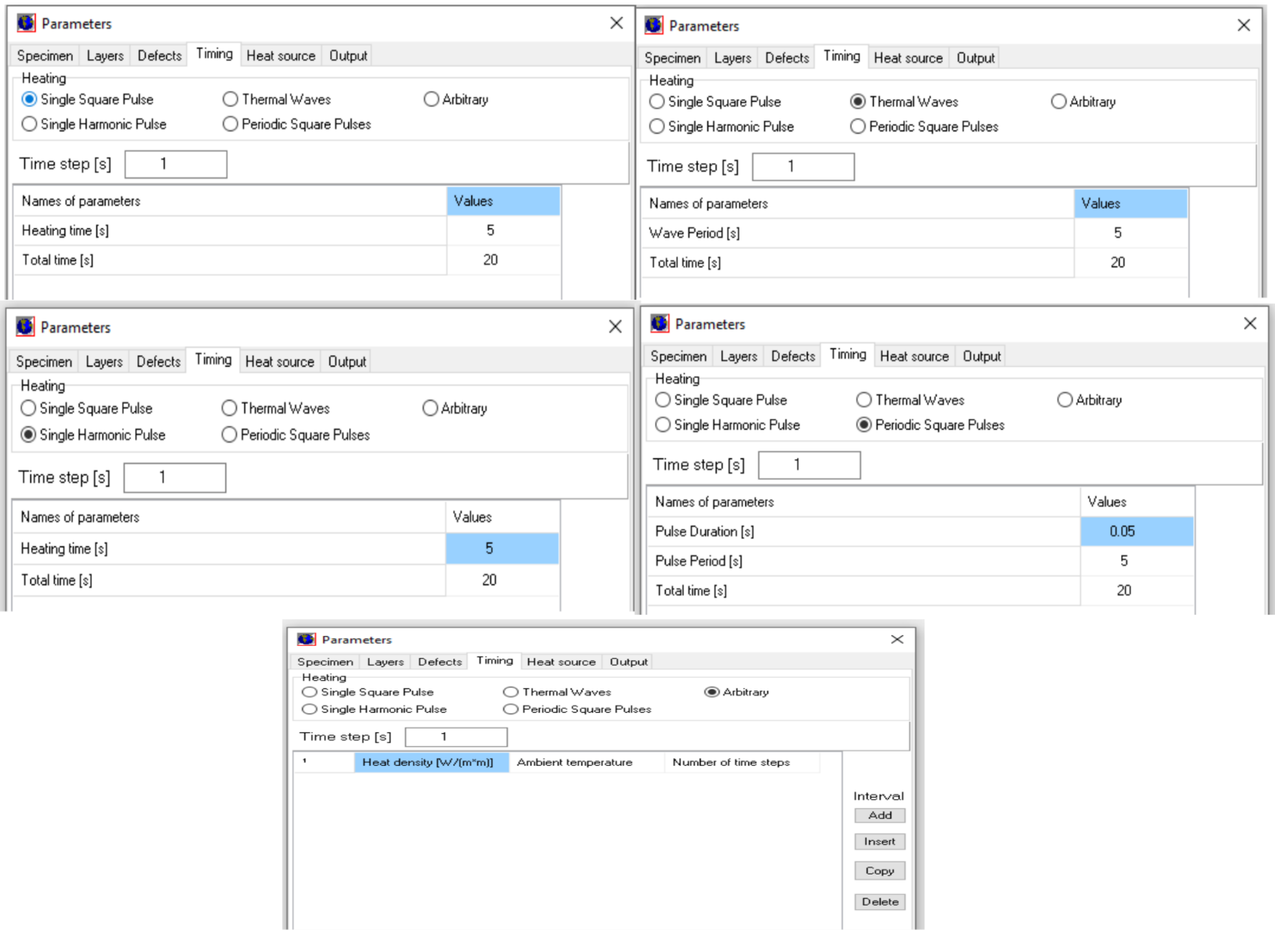

Source: ThermoCalc 3D own software

Table 5 Timing menu explanation

Parameter	Explanation
Single Square Pulse heating	This type of heating corresponds to pulsed or square pulse thermography where Q_m is the pulse amplitude and τ_h is the heat time, or pulse duration
Single Harmonic Pulse (cosine) heating	This type of heating is more relevant optical lock in thermography or to outdoor passive thermography where the heat source is only solar radiation during daytime. Q_m is the maximum pulse power amplitude and τ_h is the pulse period. Thermal waves heating function is closer to optical lock-in thermography technique

Thermal Waves option allows heating with multiple cosine pulses	This option allows heating with multiple cosine pulses simulating periodical harmonic stimulation of the sample. Thermal waves heating function is closer to optical lock-in thermography technique.
Periodic Square Pulse	This option heating with a number of square pulses similar to stepped heating thermography
Arbitrary heating	This option allows the user to create different heating with square pulses where is the pulse amplitude Q_m which can vary between time intervals

Figure 11 Types of heating available in ThermoCalc 3D software.

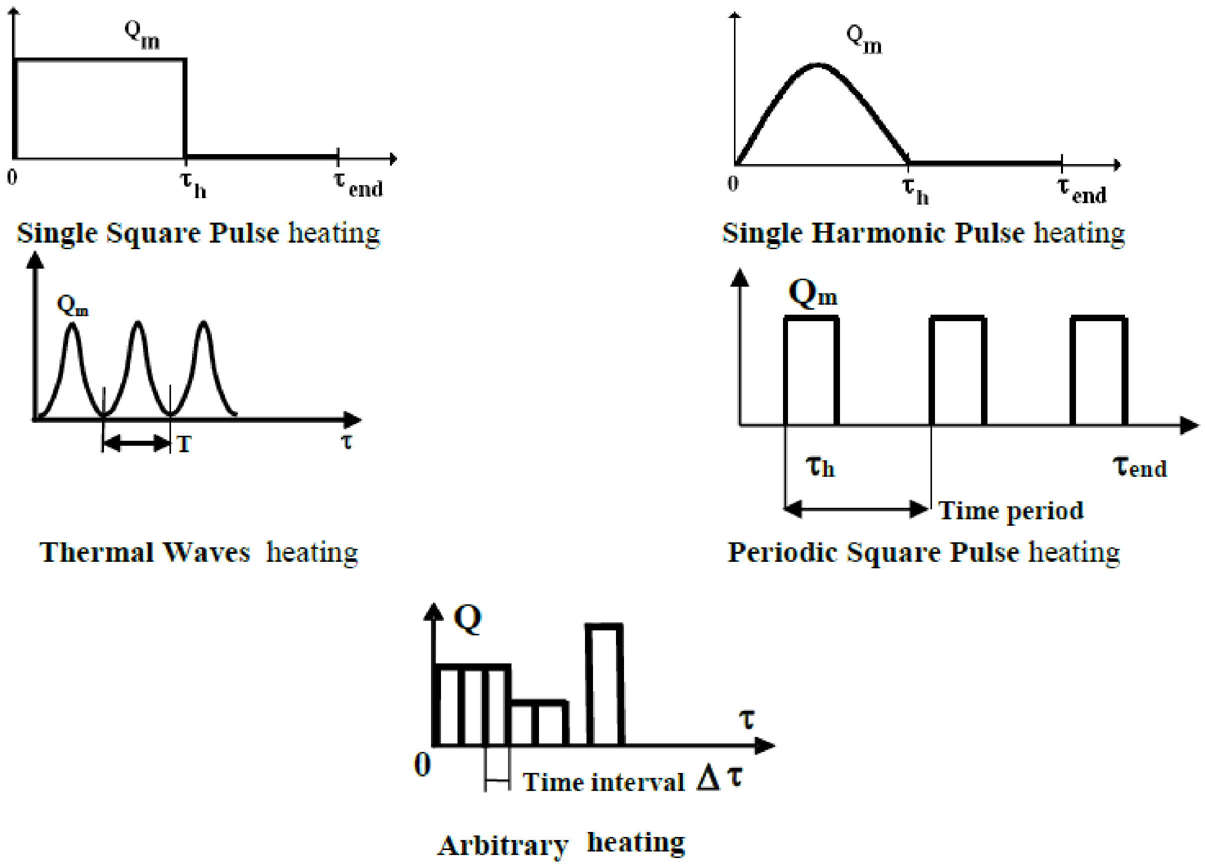

Source: ThermoCalc 3D (2018; 34)

Heat source

The heat source menu allows the user to set characteristics of the heating source such as its intensity, the heating centre on the specimen as well as to create other effects like uneven heating. Heat Source menu can be seen in Figure 12

Figure 12 Heat Source menu

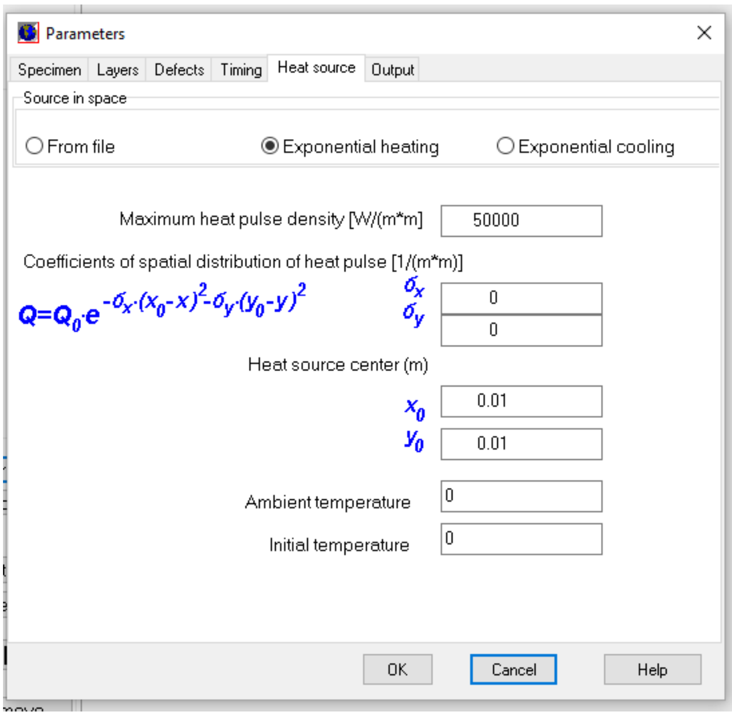

Source: ThermoCalc 3D own software

A detailed explanation of the items from the Heat Source menu can be seen in Table 6

Table 6 Heat Source menu explanation

Parameter	Explanation
Source in space: From file Exponential heating Exponential cooling	Allows to model heating on the specimen in three ways. 1) Using a two-dimensional mask that is a file contained within the software. The heat mask simulates uneven heating where in experimental cases when defects are not yet seen, they can serve as a mask. 2) As square-pulse or cosine-pulse heating with a Gaussian or uniform source, or 3) as forced cooling a specimen with a square-pulse (Gaussian or uniform) source.
Maximum heat pulse density $[W/m^2]$	This describes the heat pulse power in the form of density and should replicate the heat that the experimental equipment should create. Thus this is a good measure to test in simulation whether the equipment that will be in used in the actual experimentation, are adequate to detect the defects on a specimen with certain characteristics. Because the heat pulse power is expressed as power density ($W/1m^2$) in the software, it requires conversion based on the desired power needed for the specific dimensions of the modelled specimen. Hence the heat pulse density per m^2 will be significantly larger.

Coefficients of spatial distribution of heat pulse in both the X and Y direction $[1/m^2]$	These coefficients describe the spatial distribution of a Gaussian pulse on XY coordinates. The zero values indicates uniform heating while the higher the value is the heat is more localised to the heat centre
Heat source center position in both X and Y directions $[m]$	Coordinates of where the heat source centre will be on the specimen. The user can choose the centre of the specimen or another location depending on where the defects that have been created on the model. The heat source centre is indicated on the specimen with a small white cross
Ambient temperature $[^0C]$	The ambient temperature is set by default to 0° C. Non zero values will specify additional heating of the sample to the required temperature. Respectively a below zero ambient temperature will specify additional cooling of the sample
Initial temperature $[^0C]$	The initial temperature is set by default to 0° C. The initial temperature should be higher than the Ambient temperature in order for the simulation to model cooling by convection.

<u>Output</u>

The output menu allows the temperature distribution to be exhibited in the different sections of the specimen's surface (front, tear, top, bottom, left and right buttons). The custom option allows the user to define the position of plane for output temperature data on the XY, X-Z or Y-Z axis. The output time steps shown on Figure 13 is related to the number of computational steps of the simulation and have to be greater or equal to that number.

Figure 13 Output menu

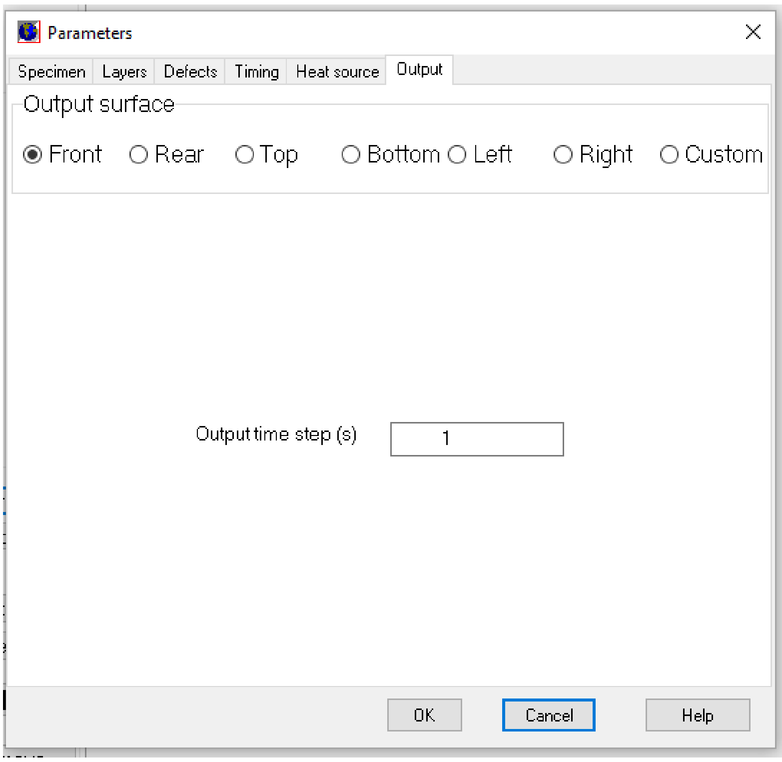

Source: ThermoCalc 3D own software

3.3 Ultrasonic testing modelling and simulations background

Computer modelling and simulation of ultrasonic testing has the same potential as for thermography which is to provide a cost and time-effective alternative to experiments in the lab or field. UT modelling and simulations are typically carried out using Finite element method (FEM) software as the most popular solutions. These simulations are representation of wave generation, propagation and interaction with discontinuities in materials (Dib et al., 2018). Finite element analysis (FEA) is one of the most commonly used methods to solve numerical problems (Petrov et al., 2017). FEA Modelling allows the user to confirm the right choice of technique before actual experimentation while being able to virtually test for sensitivity, accuracy, flaw detectability under specific material properties and conditions (Petrov et al., 2017). Regardless, software modelling is based on approximations and in most cases does not capture the entire complexity that real-life experimentation has, yet it is sufficient to explain empirical results (Did et al. 2018).

Two main modelling approaches exist in UT. Beam models and flaw response models respectively (Dib et al., 2018). Beam models visualise the propagation within a material of ultrasound, generated by a transducer. Beam models also offer 3D visualisation where structures can be complex, something that is difficult to obtain in actual experimentation. One of the main advantages of this method is that beam models can supplement actual experimentation especially for probe design. Also, beam models do not require long computational time (Dib et al., 2018). In contrary, flaw response model, simulates the interaction of the flaws in an object with the ultrasonic wave. This type of modelling is more time consuming and can find application in replacing experimentation for assessing and qualifying UT methods. Common features amongst most of the modelling software is that an object needs to be created where the user defines the mechanical properties of the materials that are modelled and tested. The user also defines the damage or defect they would like to introduce into the object. As explained in the thermography section, the damage or defect is modelled by defining its location and material properties in order for the software to be able to understand that there is a discontinuity on the object and that it has certain type of properties. In some cases the software depending on how sophisticated it is, allows to create transducer geometries with certain properties. Finally, depending on the software's physics engine, different ultrasonic techniques can be modelled with more types of waves, and more customisation options as well as visualisation of the inspection process.

All the previously arguments are quite good for volumetric components. But in this project we are dealing with composite monolithic and sandwich structures. In this case it is necessary to use Lamb waves technique and develop mathematic models for wave propagation. This is a consequence that maybe it could not be possible to use the same technology as used in volumetric homogeneous samples. In sandwich structures, such as the PIVOT2 prototype carbody, the PET foam component has a low acoustic impedance. Thus, this is a very complex situation for phased array or simple pulse echo techniques because it uses higher frequencies than the Lamb waves case. The Lamb waves technique has been applied to the inspection of multidirectional composites laminated for sandwich structures. Results from experimentations in literature have shown that the technique is applicable for the inspection of relatively long sandwich structures and that it can detect damage that is located in any position though the thickness of a component even if only one side is accessible for testing (Diamanti et al., 2005). Also, techniques such as through thickness that requires access to both sides of the material are also excluded based on the requirements from PIVOT2 project. These user requirements can be found in D 1.1.

Lamb waves is one case of the guided waves that propagated in plates. Specifically, it corresponds with the SV (Shear Vertical) solution of the wave equation in a plate. This kind of waves have two fundamental modes: symmetric and antisymmetric with several overtones. A good review can be obtained from Viktorov (1967). The fundamental idea for these waves, is that they have the dispersion phenomenal which means that the group and phase velocity depend on the frequency and the thickness of the plate (also depend on elastic constant). Figure 14 shows the fundamental modes symmetric and antisymmetric.

Figure 14 Two fundamental mode A0 (a) and S0 (s).

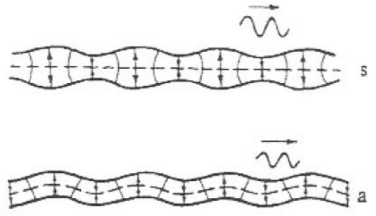

Source: Viktorov (1967)

From the point of view of NDT methods, the dispersion phenomena could be considered a limitation compared with other methods that use non dispersive waves like longitudinal and shear waves. However, Lamb waves have a relative low attenuation and propagate at great distance inside the material. In the case of thin plates with high attenuation for instance, this could be the only option relative to other ultrasonic methods.

For the case of multidirectional composite laminates, where the attenuation is a great limitation, the Lamb waves have been studied mostly in this century. Zhongqing Su et al. (2006) made a review with 176 references for the use of Lamb waves for the identification of damage in composites. In the aforementioned paper, several technologies that uses Lamb waves in composite plates were described. Covering the basic concepts of guided Lamb waves, the authors also include several conditions for its emission. Algorithms for signal processing including fuzzy logic, inductive learning, genetic algorithms, and artificial neural networks are presented along with Bayesian inference. Finally, Zhongqing Su et al. (2006) analysed the concept of digital damage fingerprints (DDF). Other authors like Diamanti et al (2005, 2007, 20120) show the uses of Lamb waves with array transducers on aircraft composite structures. In another paper Mustapha et al. (2011) use FEM for the simulation of Lamb waves propagation. Watkins et al (2012) use the time reversal mirror to analyses several signals obtained in plate element.

Figure 15 Experimental signal obtained with several conditions from healthy structure to damage ones.

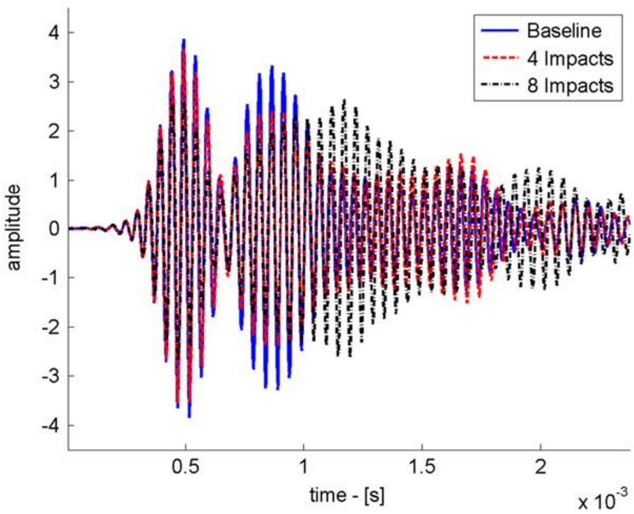

Source: Watkins and Jha (2012; 352)

Figure 15 shows an interesting idea of how to compare a healthy structure with a damaged structure. Finally, Castaings et al (2001, 2005) and Kazys et al. (2006) show the use of air transducers for Lamb waves generation on composite plate elements like CFRP (such as the one in Figure 15). All the above have been very well documented for the case of CFRP and other “monolithic” structures. However, for the case of sandwich with foam core and two skin layers of CFRP, there is a significant difference between the acoustic impedance of the core and the skins and there is also a high core to skin thickness ratio (see section 4.1). In this case, the benefit of using of the “classic” Lamb waves, is not so obvious as it is the case of the monolithic CFRP. A possible solution is the use of Leaky Lamb Waves, where the Lamb waves propagated at the skin with a leakage phenomenon. Both situations, the classic Lamb waves and the Leakage Lamb waves should be studied by simulations and experimentally. Diamanti et al (2005) studied, from an experimental point of view, the classic form of Lamb waves applied on sandwich structures.

Theoretical model of wave propagation in composite plates

An orthotropic material could be conceived as a generalization for the first level of the material relative to the second level that will be isotropic. Following this idea, the physical equations for wave propagation in an orthotropic material will be presented and these equations will be simplified later to depict the wave propagation in an isotropic material. Considering a 2D plate as shown in Figure 16.

Figure 16 2D plate represented as a slice of the 3D case.

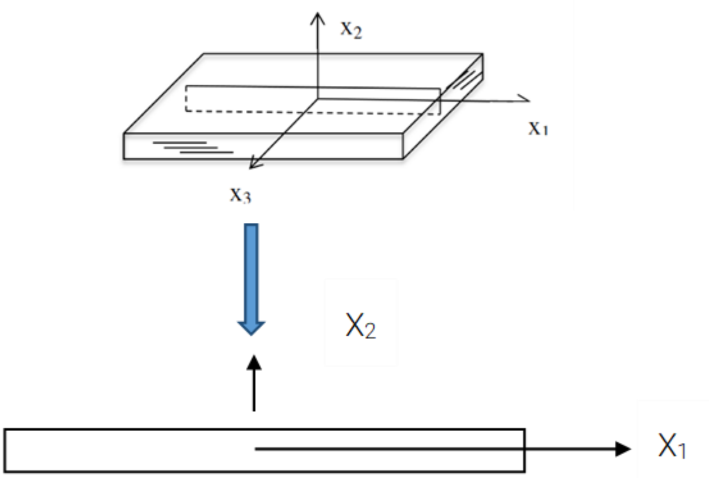

Source: own elaboration

The wave equations for orthotropic material for 2D case, could be expressed as (Martincek, 1975) :

$$
\begin{aligned}
\rho\frac{\partial^2 u_1}{\partial t^2} &= C_{11}\frac{\partial^2 u_1}{\partial x_1{}^2} + C_{12}\frac{\partial^2 u_2}{\partial x_1 \partial x_2} + C_{66}\frac{\partial^2 u_1}{\partial x_2{}^2} + C_{66}\frac{\partial^2 u_2}{\partial x_1 \partial x_2} \\
\rho\frac{\partial^2 u_2}{\partial t^2} &= C_{12}\frac{\partial^2 u_1}{\partial x_1 \partial x_2} + C_{22}\frac{\partial^2 u_2}{\partial x_2{}^2} + C_{66}\frac{\partial^2 u_1}{\partial x_1 \partial x_2} + C_{66}\frac{\partial^2 u_2}{\partial x_1{}^2}
\end{aligned} \tag{1}
$$

Where ρ is the density, C_{11}, C_{12} C_{22} and C_{66} are the elastic constant in Voigt notation, and u_1, u_2 are the displacements in the x_1 and x_2 respectively. For the case of isotropic material (1) could be simplified by assuming that:

$$
C_{11} = C_{22} = \Lambda + 2\mu
$$

$$
\begin{gathered}
C_{12} = \Lambda \\
C_{66} = \mu
\end{gathered} \tag{2}
$$

Λ and μ are the Lame elastic constants for the isotropic material which describe these properties as well as the Young modulus E and the Poisson ratio σ (Mason, 1958). Equations (1) are the fundamental equations that will be used for FEM simulation assuming pulse excitation. This could be considered as a first objective. However, it is convenient to develop a second model for the harmonic propagation in order to obtain the dispersion curves. From (1) assuming sinusoidal propagation, it is possible to obtain the following dispersion equation (Moreno et al. 2015; Martincek ,1975):

$$
\left(\frac{th\left(\frac{sh}{2}\right)}{th\left(\frac{qh}{2}\right)} \right)^{+/-1} = \frac{B_0 C_0}{A_0 D_0} \tag{3}
$$

Where +1 is for the symmetrical Lamb wave mode and -1 for the antisymmetrical case. The arguments of *th(x)* functions are given by:

$$
\frac{qh}{2} = \pi\frac{h}{\lambda}\sqrt{-\frac{a}{2} + \sqrt{\left(\frac{a}{2}\right)^2 - b}} \qquad \frac{sh}{2} = \pi\frac{h}{\lambda}\sqrt{-\frac{a}{2} - \sqrt{\left(\frac{a}{2}\right)^2 - b}}
$$

$$a = \frac{C_{12}^2}{C_{22}C_{66}} + \frac{2C_{12}}{C_{22}} - \frac{C_{11}}{C_{66}} + \rho c^2\left(\frac{1}{C_{66}} + \frac{1}{C_{22}}\right)$$

$$b = \frac{C_{11}}{C_{22}} - \rho c^2\frac{(C_{11} + C_{66})}{C_{22}C_{66}} + \rho^2 c^4\left(\frac{1}{C_{66}C_{22}}\right) \tag{4}$$

and

$$A_0 = \frac{q}{k}\left[-\rho c^2 + C_{11} - \frac{C_{12}(C_{12} + C_{66})}{C_{22}}\right] - C_{66}\left(\frac{q}{k}\right)^3$$

$$B_0 = \frac{s}{k}\left[-\rho c^2 + C_{11} - \frac{C_{12}(C_{12} + C_{66})}{C_{22}}\right] - C_{66}\left(\frac{s}{k}\right)^3$$

$$C_0 = -\rho c^2 + C_{11} + C_{12}\left(\frac{q}{k}\right)^2$$

$$D_0 = -\rho c^2 + C_{11} + C_{12}\left(\frac{s}{k}\right)^2 \tag{5}$$

Where k is wavevector modulus expressed as $k=2\pi/\lambda$ and λ is the wavelength.

Results of Dispersion curves

For the case of monolithic CFRP Figure 17 shows an example of the dispersion curves for a 5 mm of plate thickness obtained in Matlab according to the previous equations and Table 18 from Castaings (2001).

Figure 17 Dispersion curves obtained from matlab for the fundamental modes A_0 and S_0 and 5 mm thickness

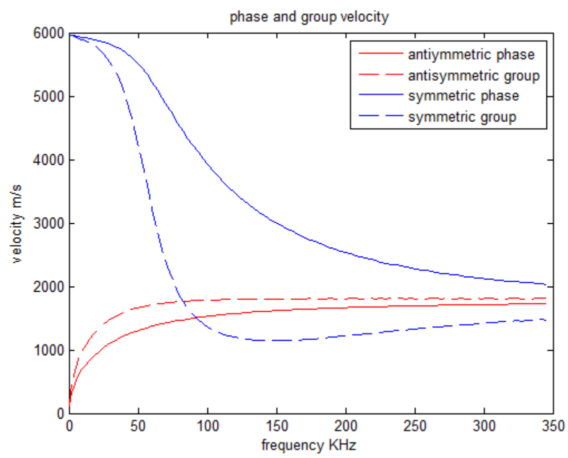

Source: own elaboration

These curves are used to obtain a frequency range for Lamb waves propagations. In this case, for experimental and FEM modelling, it is recommended to work at a frequency below 50 KHz. At such frequency range, phase and group velocity depend on the frequency but also on the thickness. Delamination defect introduces a new equivalent thickness which is equivalent to a frequency increase. This leads toa higher group and phase velocity and then to a phase a change amplitude of the received signal.

<u>Available software</u>

Below, a list of available software for ultrasonic modelling and their main characteristics has been shown

Table 7 Ultrasonic modelling and simulation software

Software	*Website*	*Characteristics*
UTMan	http://www.utsim.co.uk/index.html	Ultrasonic weld inspection practice software. Allows the user to practice in Manual Ultrasonic and time-of-flight diffraction (TOFD) techniques by simulating the probe path and presenting the various readings and settings that are available in a UT flaw detector screen
CIVA	https://www.extende.com/civa-in-a-few-words	CIVA Ultrasound software is a specialised software specifically built simulating UT inspection processes such as pulse echo, tandem or TOFD techniques with a wide range of probes (conventional, Phased- Arrays or Electromagnetic Acoustic Transducer -EMAT). The software allows to create or import components (from simple shapes to complex 3D CAD geometries) and create a variety of defect types.
Comsol Multiphysics	https://www.comsol.com/	FEA software that allows solving problems such as piezoelectric physics, linear and non-linear mechanical wave propagation, heat generation and thermal diffusion. Comsol through the Multiphysics module allows the modelling and simulation of elastic waves in materials as well as the design of transducers

SimNDT	https://github.com/mmolero/SimNDT	Open-source software that runs on Python capable of simulating Pulse echo, Through transmission, Linear Scan, Radial Scan and Tomography techniques. The software allows to set dimensions of the transducer, the type of pulse to be used including its amplitude and frequency. SimNDT uses Elastodynamic Finite Integration to model in a simple environment a sample with certain properties and the defects that might be presents. It a also, allows to simulate in real time the elastic wave propagation within the sample.
Abaqus /CAE	https://www.3ds.com/products-services/simulia/products/abaqus/	FEA software that allows the user to create 3D drawings of objects and carry out Finite Element modelling and simulations of ultrasonic wave propagation in materials.
k-Wave	http://www.k-wave.org/	Open source MATLAB toolbox that allows simulation of acoustic wave propagation (photoacoustic or ultrasonic) acoustic heterogeneities, and power law absorption (1D, 2D, and 3D). The software tool also allows the creation of geometric shapes.
ANSYS	https://www.ansys.com/	FEA software capable of carrying out ultrasonic modelling and simulation of wave propagation in materials

4 Modelling and simulation results

D2.1 will use a series of software such as ThermoCalc-3D and Comsol to model and simulate IRT and UT experiments in order to test whether specific inspection techniques are suitable of detecting subsurface defects/damage in composite rail carbodies. To achieve this task the first thing that was required was to establish what would have to be modelled in the virtual environment and its properties. Hence, PIVOT2 project provided some limited information regarding the mechanical and thermal properties of the rail carbody material and its dimensions. In order to carry out the IRT and UT simulations a significant part of overall material mechanical and thermal properties had to be extracted from literature.

4.1 Material description

The main task for the IRT and UT simulations was to model the two specific types of components that will be used by PIVOT2 composite rail carbody and then simulate specific techniques in the virtual environment. It needs to be noted that the thermal and mechanical properties of the composite rail carbody to be modelled and simulated were unavailable from PIVOT2 during the write up process of D 2.1. Therefore, a large part of the properties were assumed based on existing literature of materials for rail applications. Samples of the components were also unavailable in order to experimentally establish the thermal or mechanical properties. The values in italics in the table below indicate assumptions that were made due to unavailable information from PIVOT2.

<u>Monolithic CFRP material</u>

Table 8 Monolithic CFRP component specifications

Parameter	Value
Overall thickness	20 mm
CF layer direction top skin	Unidirectional 0/90, +/-45
Cf layer direction bottom skin	Unidirectional 0/90, +/-45

<u>Sandwich CFRP-PET-CFRP material</u>

Table 9 Sandwich component specifications

Parameter	Value
Composition	CFRP skins, PET foam core
Overall thickness	40 mm

CF skin thickness	*5 mm (front & back)*[1]
CF layer direction top skin	Unidirectional 0/90, +/-45
Cf layer direction bottom skin	Unidirectional 0/90, +/-45
PET core	30 mm

4.2 Infrared thermography modelling, simulations and results

As mentioned earlier two types of components were modelled in ThermoCalc3D software where IRT simulations took place. Since the software offers specific types of heating functions, 2 main types of IRT techniques were simulated. Table 10 presents the thermal properties that were used to model the material and defect thermal properties.

<u>Material thermal properties used for IRT simulations</u>

Table 10. Thermal properties of materials used in the IRT modelling & simulations

Material	Density ρ, kg/m^3	Heat capacity Cp, J/ (kg·K)	Thermal conductivity λ, W/ (m·K)
Air (in thin gaps)[2]	1.2	1005	0.070
Carbon fibre reinforced plastic (CFRP)[3]	*1600*	*1200*	*0.8* (⊥)[4] *7* (‖)[5]
PET foam	*250*[6]	524[7]	0.047[8]

It needs to be noted CFRP thermal properties vary between fibre manufacturers as well as at the finished product after fabrication and curing. The CFRP density that was used for the thermal simulations was 1600 Kg/m^3 which is a typical value found in literature which can vary between 1500-1600 Kg/m^3 .

[1] The 5mm skin thickness of the CF-PET-CF sandwich is considered significantly large. Although the value was an assumption based on an overall sandwich thickness of 40mm and the availability of the PET core at certain thickness of 30, 40, 50 mm, it has been decided to use 5mm as skin thickness..
[2] Thermal properties for air taken from Vavilov & Burleigh (2020)
[3] Thermal properties for CFRP taken from Avdelidis & Almond (2004)
[4] ⊥ signifies thermal properties of the material in perpendicular direction to the fibers (in Z axis)
[5] || signifies thermal properties of the material in parallel direction to the fibers (in XY axis)
[6] Density for PET foam was based on available PET products in the market used for rail applications
[7] Calculated value for based on PET foam density
[8] Thermal conductivity values taken from Diab (2021) and Armacell (2021) for the specific PET densities

4.2.1 Monolithic CFRP modelling and simulations

A series of 12 subsurface defects were designed, using air gaps, at various depths on the monolithic CF block in order to test the ability of optical pulsed and lockin thermography to detect them. The dimensions and depth of the defects are shown on Table 11, Figure 18, Figure 19. The defects that represent delaminations, were designed to grow progressively by 2mm while retaining 1 mm thickness. It needs to be noted that the CF monolithic component is considered extremely thick (20mm) based on a) typical thickness of CF components used in various applications, b) limitations of thermography for such thickness, as well as c) due to CF's thermal conductivity compared to metals.

Table 11 Dimensions of defects on the monolithic CF block

Row #	Depth	Location	Defect size
1	2.5 mm	Top skin surface	3mm, 5mm,7mm (length & width), 1mm thickness
2	5 mm	Top front	9mm,11mm,13mm (length & width), 1mm thickness
3	10 mm	Middle	15mm, 17mm, 19mm (length & width), 1mm thickness
4	15 mm	Middle back	21mm, 23mm, 25mm (length & width), 1mm thickness

Figure 18 Monolithic CF component defects and dimensions

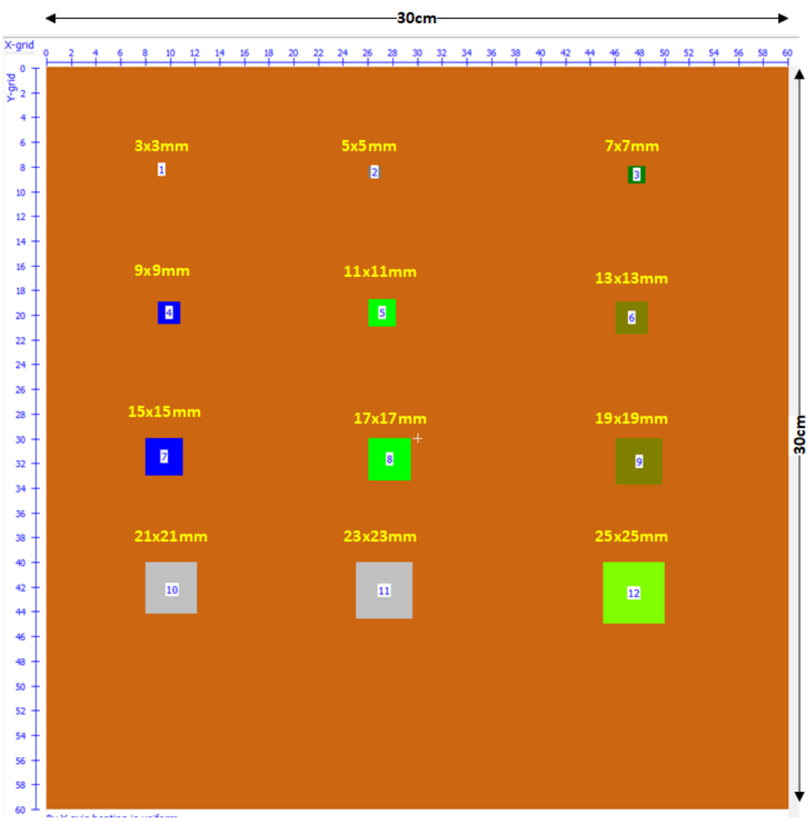

Figure 19 Top view of CF monolithic block and depth of defects

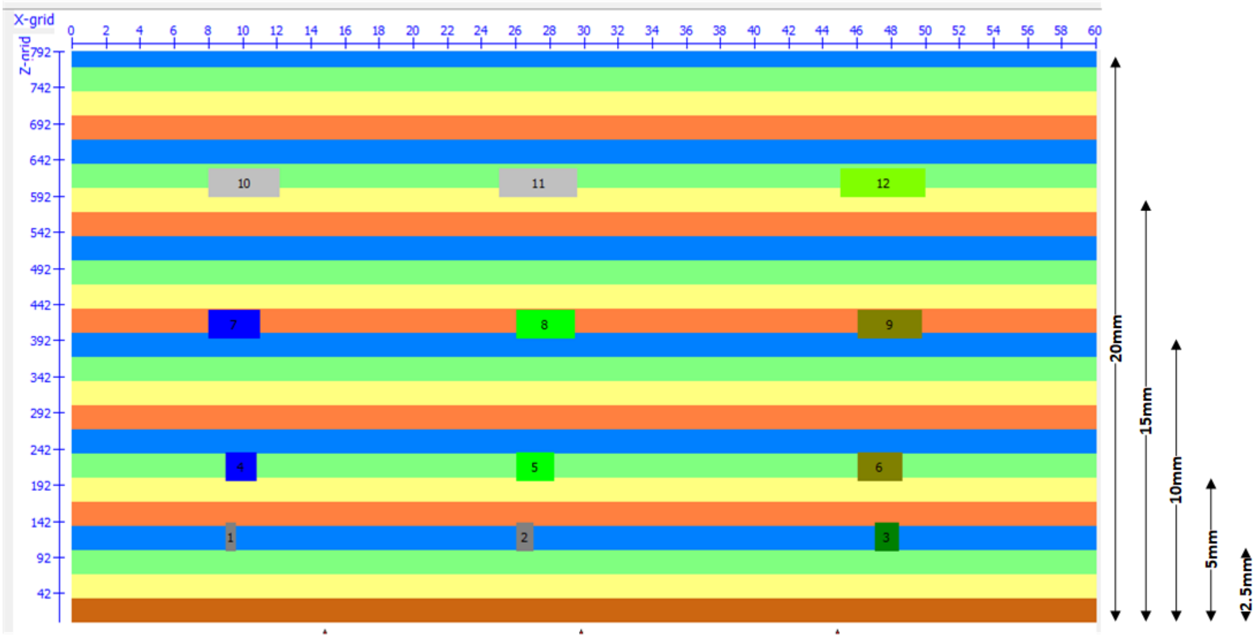

For the detection of the defects 3 typical qualitative and quantitative types of thermography analyses were used: 1) temperature image, 2) space profile, 3) Delta Profile.

Table 12 IRT analysis used and explanation

IRT Analysis	Example
The **Temperature image** presents what a thermal camera would see, therefore it shows an image of the temperature across the sample without any noise due to being a simulation. The temperature image shows what defects are visually detectable based on its temperature difference. Brighter spots indicate the presence of defects. In the current case there should be 4 rows of defects in total, while only 2 have are visibly detected	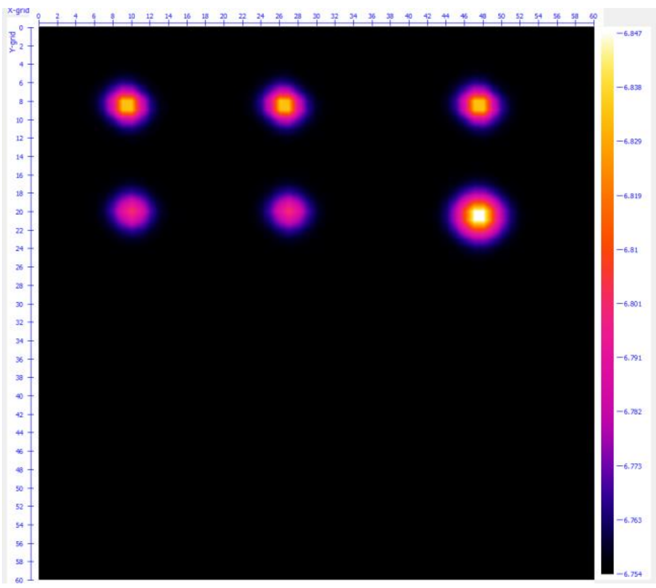

Space profile is an easy and quick method of detecting defects at specific grid areas[9] of the sample where defects have been modelled. The image on the right shows the temperature rise of the sample which is set at a specific grid step on the Y axis and moment in time. Hence, the 3 temperature spikes indicate the presence of defects at grid 10, 26, 48 on X axis. This specific space profile is based on Row 2 of the previous thermal image. In cases where the temperature line is flat the defects are non-detectable or have extremely low temperature (0.001°C or even less).	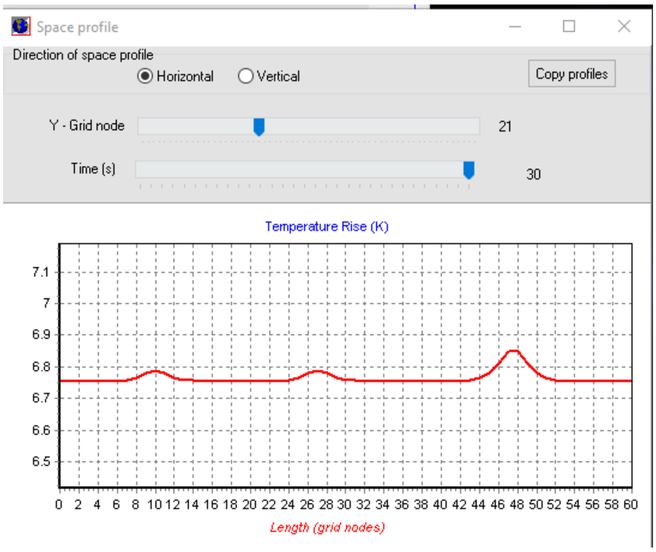
Delta profile (ΔT[10]) is expressed as a temperature difference at a point of interest over time and can indicate the presence of a defect. The Delta T rise shows the rise of temperature for a specific location of a know defect over the duration of the simulation (30s in this case). Thus, the temperature rise in this case means that the defect is detectable. The specific Delta T profile of the 3 defects is taken from Row 1 of the defects from the first picture.	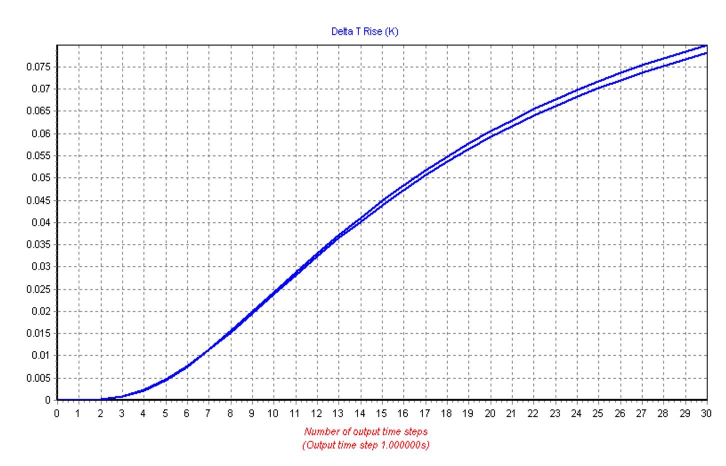

[9] In the ThermoCalc 3D software the sample is divided into grid areas (on XY axis) that signify the computational grid that is used to model the sample

[10] $\Delta T = Td - Tnd$ where ΔT is the temperature difference between T_d for the temperature of the defect at a given point in time and T_{nd} for the temperature of the non defective area.

4.2.1.1 Optical lockin simulations for monolithic CFRP component

The first method to be simulated was optical lockin using the thermal waves heating function of the software. This is the closest function available by the software that can simulate optical lockin thermography type of heating without necessarily performing the lockin signal function that occurs in actual experiments. Different simulations were conducted in order to gradually begin detecting deeper defects and to test heating power and times.

Figure 20 Thermal waves heating function

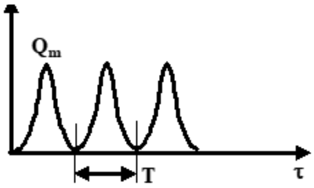

Table 13 Settings for optical lockin simulation used on the monolithic CFRP sample and results

Simulation #	Heating density (W/m^2)	Wave period (s)	Total time (s)	Time step (s)	No. defects detected	Detection depth limit
ML1[11]	3000	3	30	0.5	6/12	5mm
ML2	3000	3	25	0.5	6/12	5mm
ML3	6000	5	20	0.5	6/12	5mm
ML4	6000	7	20	0.5	6/12	5mm
ML5	6000	3	30	0.5	6/12	5mm
ML6	6000	4	40	0.5	9/12	10mm
ML 7	6000	4	60	0.5	9/12	10mm
ML 8	11111	3	60	0.5	9/12	10mm
ML 9	11111	4	60	0.5	9/12	10mm
ML 10	11111	7	60	0.5	9/12	10mm
ML 11	11111	4	90	0.5	9/12	15mm
ML 12	11111	4	120	0.5	12/12	15mm
ML 13	22222	4	20	0.5	6/12	5mm
ML 14	22222	4	30	0.5	6/12	5mm
ML 15	22222	4	60	0.5	9/12	10mm
ML 16	22222	4	90	0.5	9/12	10mm
ML 17	22222	4	120	0.5	12/12	15mm

Although the different settings of ThermoCalc 3D have been explained in section 3.2.1,

[11] A coding for the simulations was used. ML= Monolithic Lockin

further explanation of Table 13 is required in order for the reader to understand.

Heating density: Max heating power (Q_m see Figure 20) is expressed in the form of heating density in the ThermoCalc 3D software, which means that the user depending on the sample size that has been modelled, will have to calculate the equivalent heating power that is desired for the sample and then express it in a value for 1 m^2.

Wave period: The wave period can be seen in Figure 20 as T and signifies the heating time of the sample. Longer wave period means slower heating time and vice versa.

Total time: When using the thermal waves heating function, the total time signifies the total duration of all the heating wave periods and thus the process.

Time step: signifies the duration of the calculation steps. Therefore, small the time steps are used for more accurate simulation in order to observe smaller variations of temperature while heating. Smaller time steps are also used for very fast heating time in the region of ms where the time step needs to be within similar range. In order to improve accuracy and potentially missing detection of the deeper defects, 0.5 sec calculation steps were used.

No. of defects: this show the amount of defects that are detectable in the sample. The monolithic CF component has 12 defects.

Detection depth limit: This shows the max depth where the defects are no longer detectable using the stated heating power and time settings.

<u>Optical lockin simulation results</u>

The simulations begun using low power settings in order to establish what potential settings will be used and see how many defects are detectable. Therefore, as shown on Table 13, simulation ML1 was based on 3000 W/m^2 power density with a short wave period of 3s. Only the most significant simulation results will be presented in the main body text. The remaining results can be found in Appendix 1. This is because many of the simulation in Table 13 were trials trying to establish what difference, changing wave period time and total time or heating power density, would have on the detectability of the defects. Figure 21 shows the thermal image from simulation ML1 where only 2 rows of defects are visually detectable under these settings.

Figure 21 Thermal image for simulation ML1 using Optical lockin: Heating density 3000W/m^2, Wave period 3s, Total time 30s

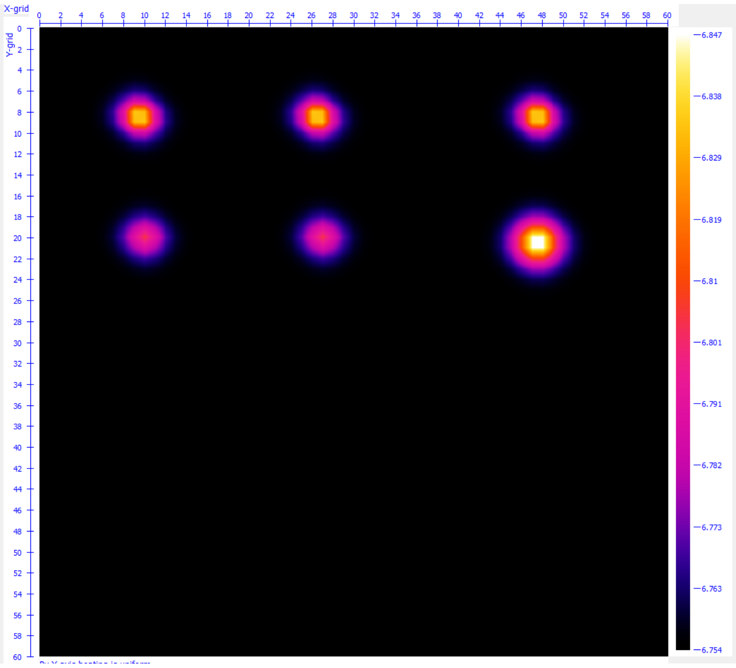

Graph 1 shows the space profiles for the 4 rows of defects on the monolithic CFRP sample, using simulation ML1 settings. Row 1 and 2 show clear signs of temperature spikes at the point of interests where the defects are located. Rows 3 and 4 at 10 and 15mm depth respectively, show no temperature signals.

Graph 2 presents the Delta T (ΔT) profiles of the different rows of defects for the monolithic CFRP sample using simulation ML1 settings. The graph basically shows the temperature difference between defective and sound areas in order to show the temperature difference at the point of interest. The different lines plots present each row of defects Row#1 in blue, Row #2 in green, Row# 3 in Orange and Row# 4in red. Since ThermoCalc3D software has a limit of plotting only 10 defects on the graph and the sample defects are 12 in number, only 10 defects are displayed in the graph. Specifically, 3 defects from Row 1-3 and 1 from Row 4. Although, Row 3 and 4 can hardly been seen on the graph since their temperature rise is minute <0.001 °C, it means that additional heat power might reveal the defects. It is also important to note that as the depth increases in the sample the ΔT decreases while deeper defects take more time to start getting detectable. This observation is also in line with IRT principles which means that the model and the simulations are working as intended and according to the same principles.

Graph 1 Space profiles of the different rows of defects using optical lockin simulation ML1 settings

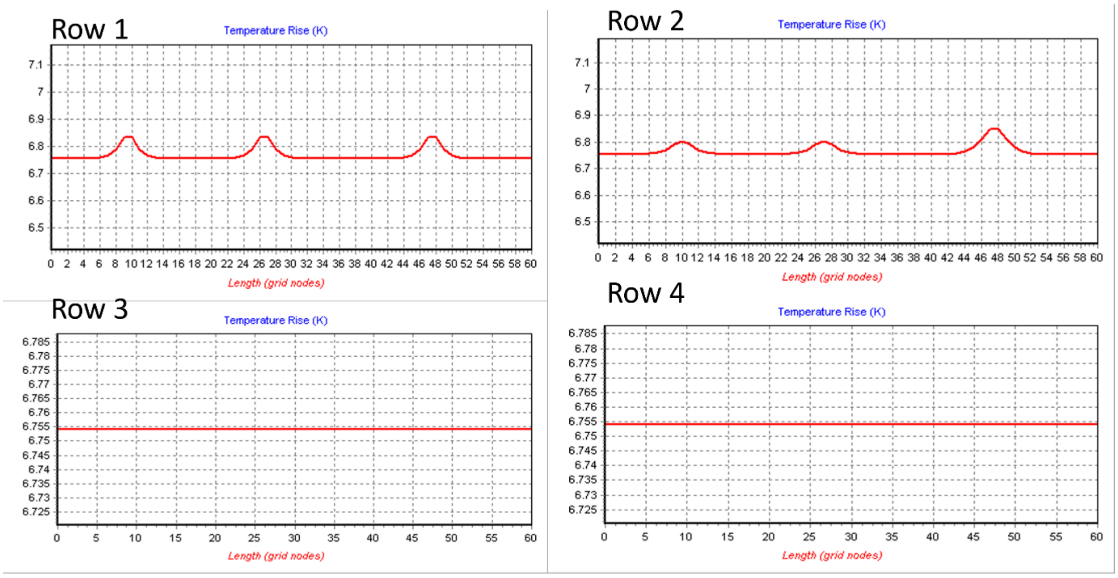

Graph 2 Delta T profiles for different rows of defects using optical lockin simulation ML1 settings. Row#1 in blue, Row #2 in green, Row# 3 in Orange and Row#4 in red

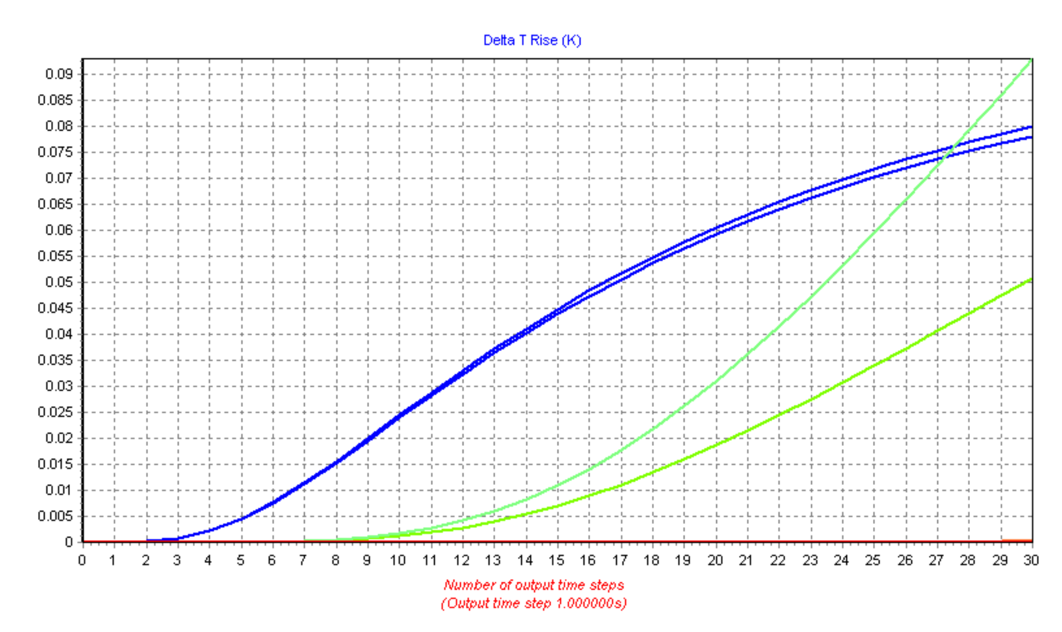

As the experimentations progressed with increasing heating power density and lowering total heating time it was noticed that the total time of lower than 20sec was not enough. Hence, the simulations with short total heating time that were made and longer heating wave period led to no significant changes in term of detecting defects from Row #3 and #4.

Figure 22 Thermal image for simulation ML7 using Optical lockin: Heating density 6000W/m^2, Wave period 4s, Total time 60s

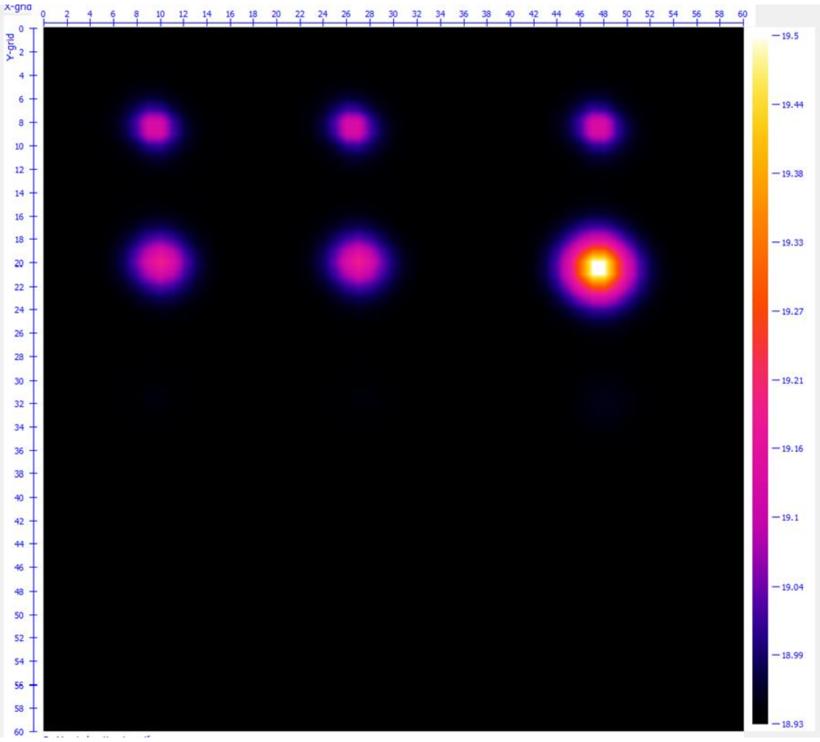

Simulation ML6 was the first “breakthrough” in beginning to detect stronger temperature signals from Row #3 where a longer total time (40s) with a heating wave period of 4s were used. Therefore, at simulation ML7, a longer total heating time was used of 60s. Figure 22 still shows only 2 rows of defects being detected visually, although Row #3 is beginning to show up very faintly with a slightly blue colour. The space profiles of the temperature signal from row #3 at Graph 3 are also becoming more distinct. This means that the thermal wave is reaching 10mm and the defects are causing enough temperature variation to be detected., Delta T profile as shown on Graph 3 for row #3 is also beginning to pick up in range. An individual Graph 5 was used only for Row #3 and #4 where the temperature rise this time is above 0.001. Row#4 still remains undetected but is less flat on the graph than before.

Graph 3 Space profiles of the different rows of defects using optical lockin simulation ML7 settings

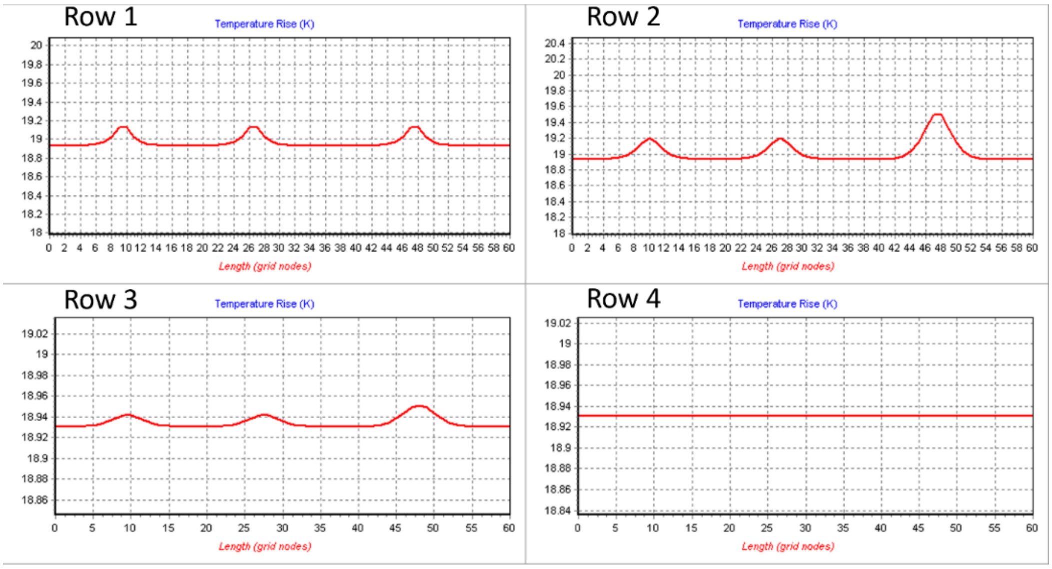

Graph 4 Delta T profiles for different rows of defects using optical lockin simulation ML7. Row#1 in blue, Row #2 in green, Row# 3 in Orange and Row#4 in red

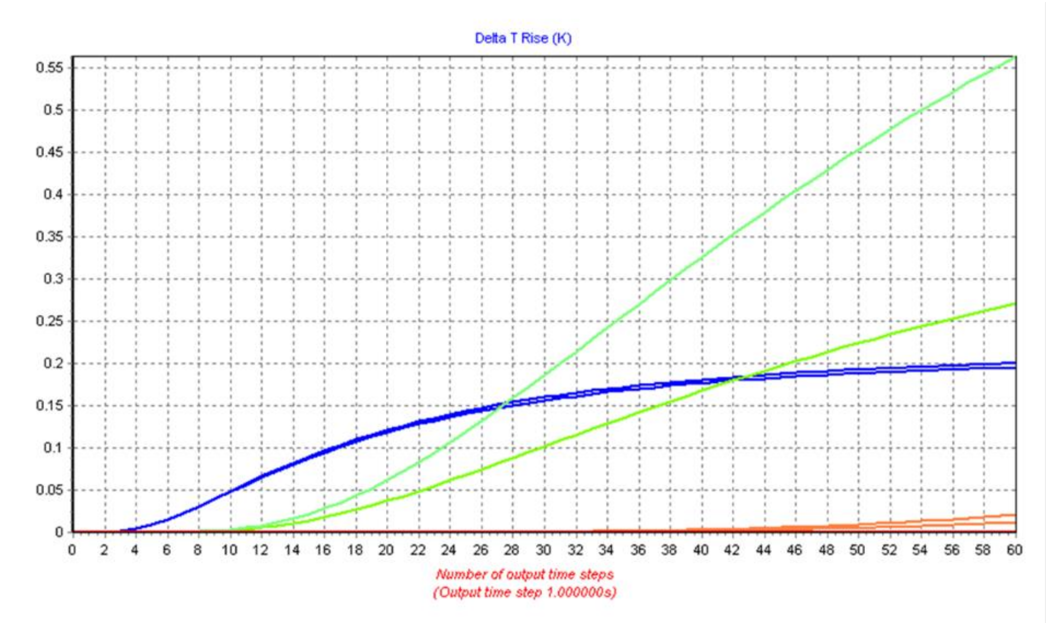

Graph 5 Delta T profiles for Row #3 and #4 of defects using optical lockin simulation ML7. Row# 3 in orange and Row#4 in red

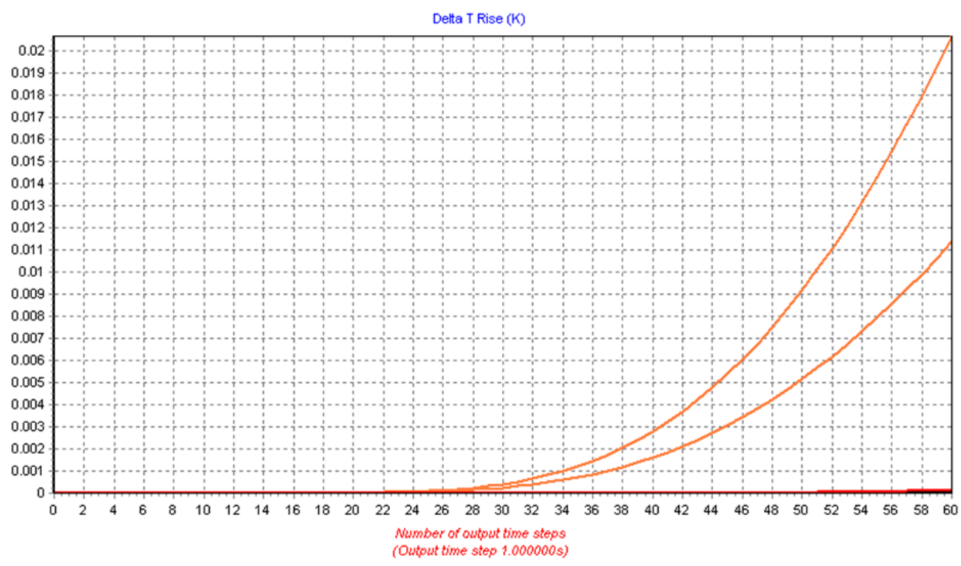

Based on the simulation results it was decided that 4sec wave period was giving satisfactory results for detectability of Row 3 and 4, which are the main points of interest since it has been already established that Row #1 and #2 can be detected through all the types of IRT analysis. Longer or shorter wave periods of 3 and 7sec gave similar results, without necessary improving Delta T other than increase the sample's overall temperature. Therefore, the next step was to increase heating power density to 11,111W/m^2 which is equivalent to 1000W on the 30x30 specimen that was modelled. The results are shown in Figure 23, Graph 6, Graph 7 and Graph 8. Compared to the previous simulations at 6000W/m^2, Delta T has increased for Row #3 making it more distinct while Row #4 temperature signal remains similar. This led to the conclusion that in order to reach the 15mm of depth, more total heating time will be required.

Figure 23 Thermal image for simulation ML9 using Optical lockin: Heating density 11111W/m^2, Wave period 4s, Total time 60s

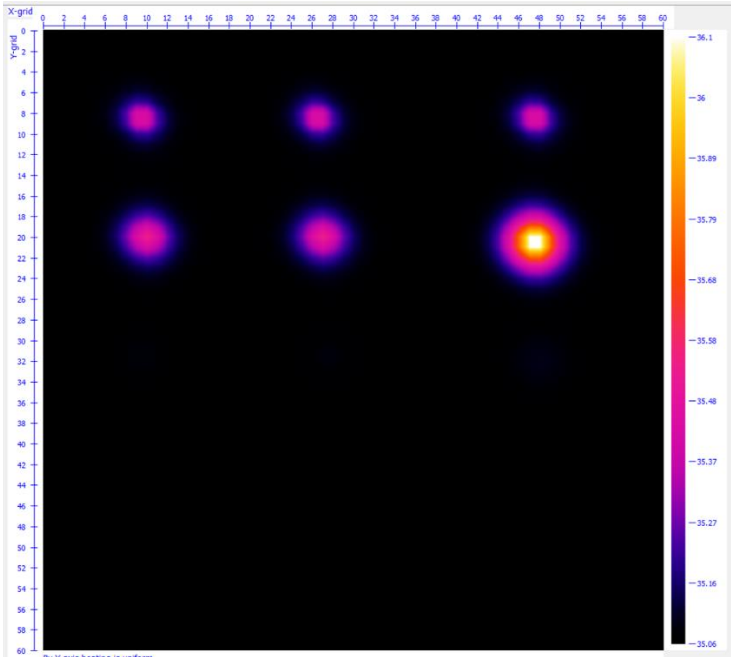

Graph 6 Space profiles of the different rows of defects using optical lockin simulation ML9 settings

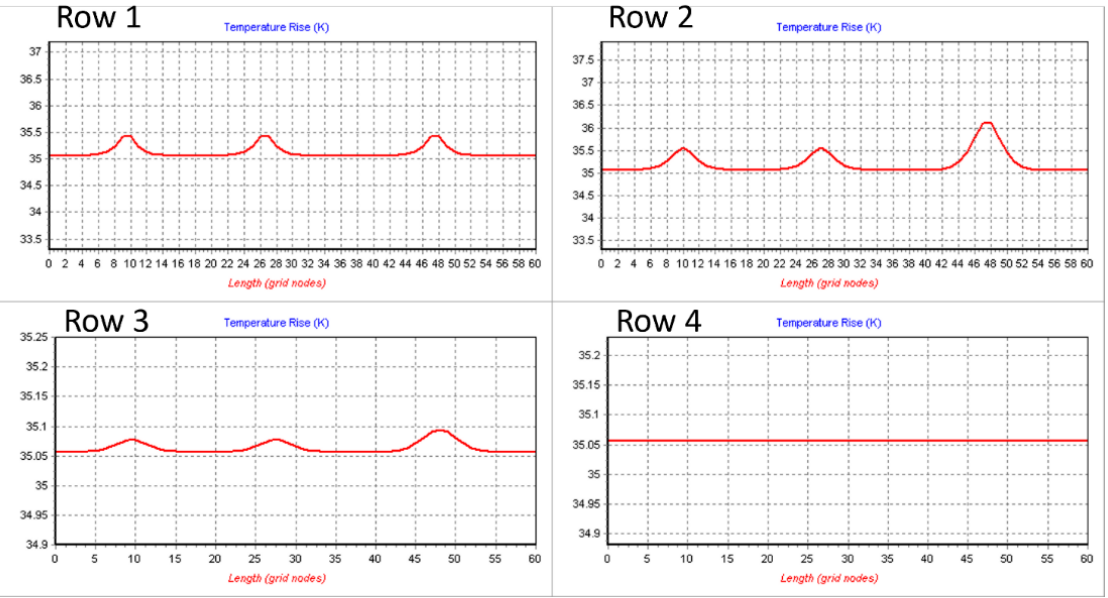

Graph 7 Delta T profiles for different rows of defects using optical lockin simulation ML9. Row#1 in blue, Row #2 in green, Row# 3 in Orange and Row#4 in red

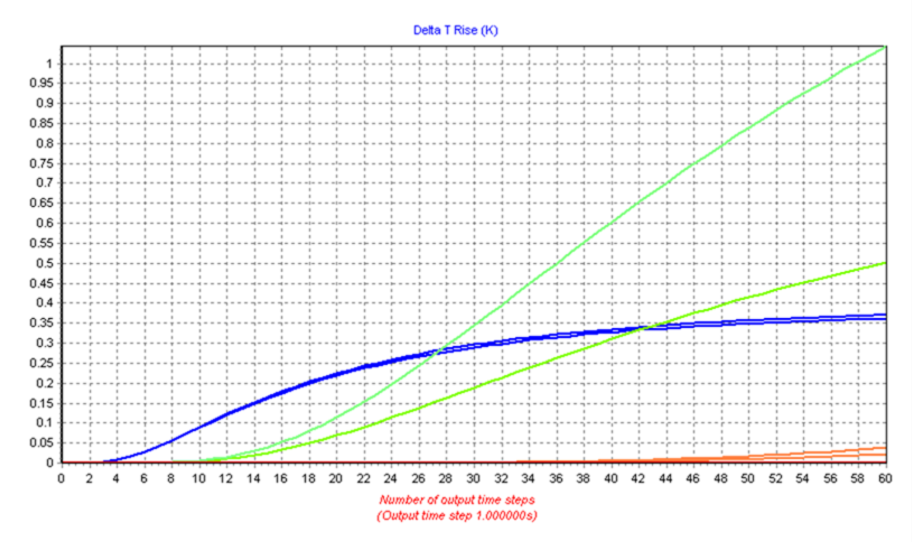

Graph 8 Delta T profiles for Row #3 and #4 of defects using optical lockin simulation ML9. Row# 3 in orange and Row#4 in red

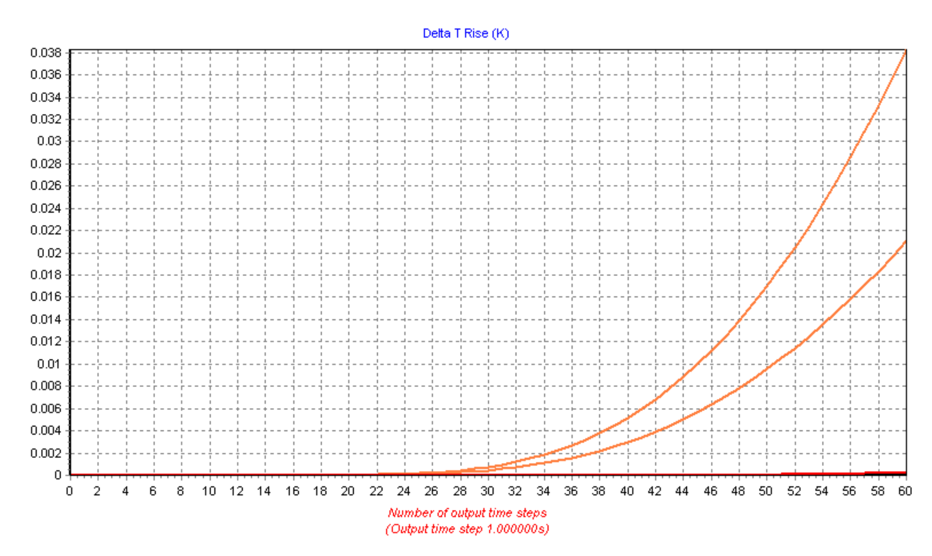

After running simulation 11 with 90 seconds total heating time, row #4 begun to show signs of detection at the space profile. Thus, at simulation 12 120 seconds of total heating time were used where row #4 actually begun to show a delta rise of 0.021°C. Row #3 is also more visually distinct even through the thermal image. All thermal images are depicted at the end-time of the simulation which means that in some cases, especially for long heating time procedures like ML12, heat from the shallow defects would start to dissipate and the deeper defects might be more visible as shown on Figure 24.

Figure 24 Thermal image for simulation ML12 using Optical lockin: Heating density 11111W/m^2, Wave period 4s, Total time 120s

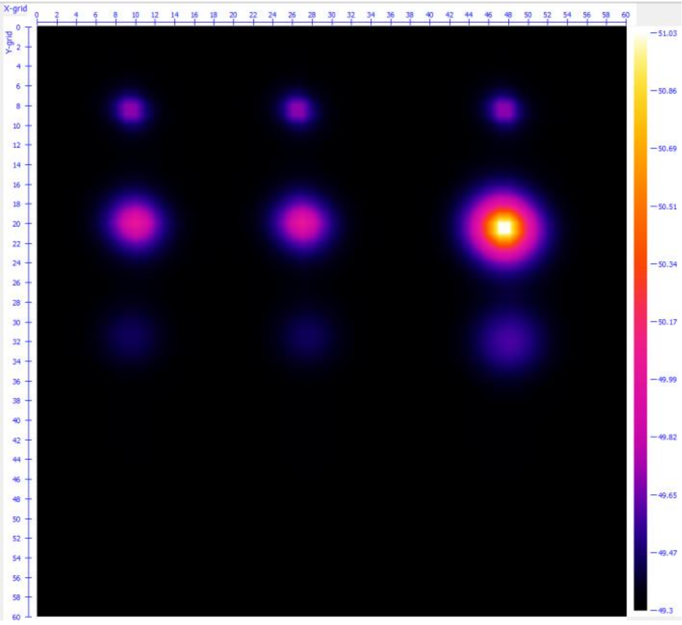

Graph 9 Space profiles of the different rows of defects using optical lockin simulation ML12 settings

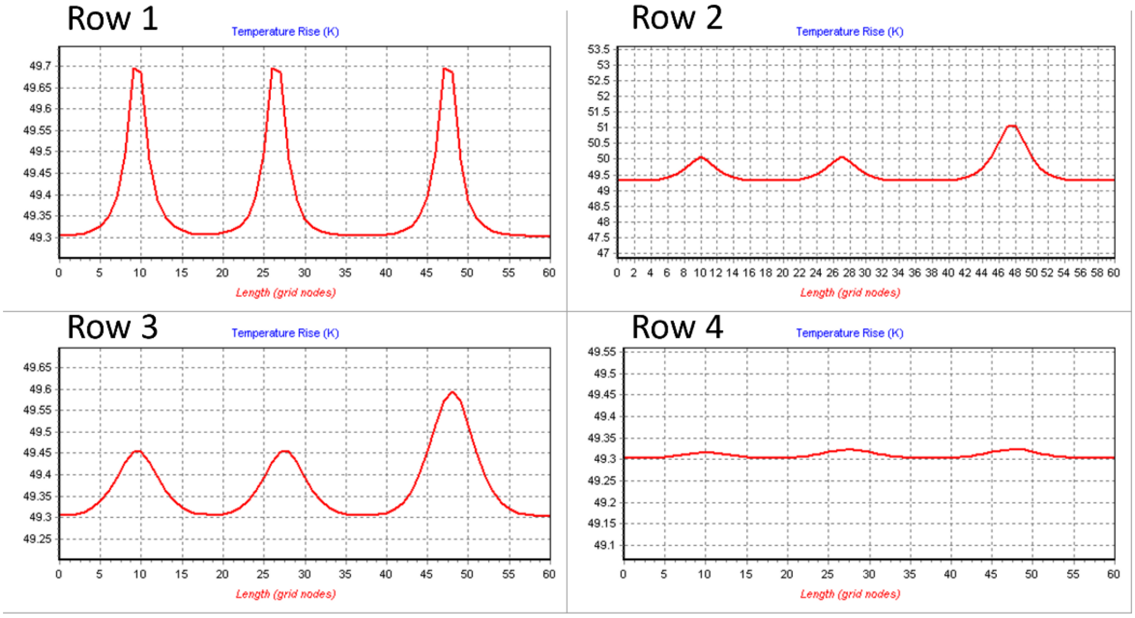

Graph 10 Delta T profiles for different rows of defects using optical lockin simulation ML12. Row#1 in blue, Row #2 in green, Row# 3 in Orange and Row#4 in red

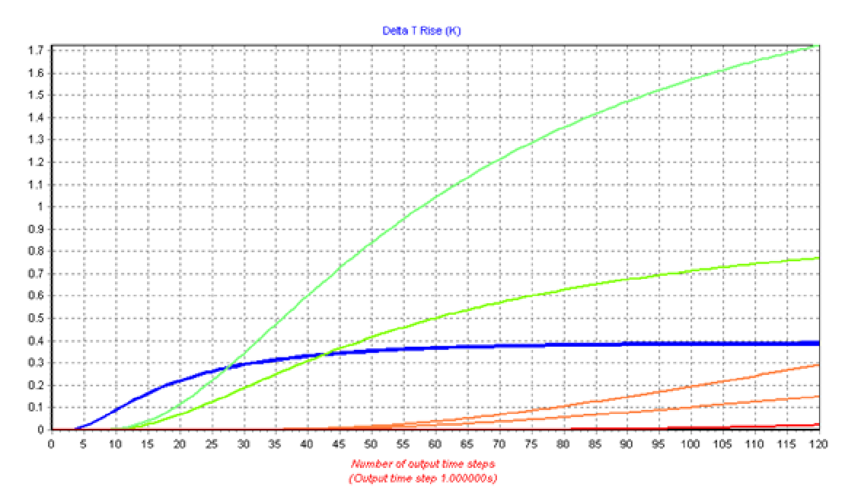

Graph 11 Delta T profiles for Row #3 and #4 of defects using optical lockin simulation ML12. Row# 3 in orange and Row#4 in red

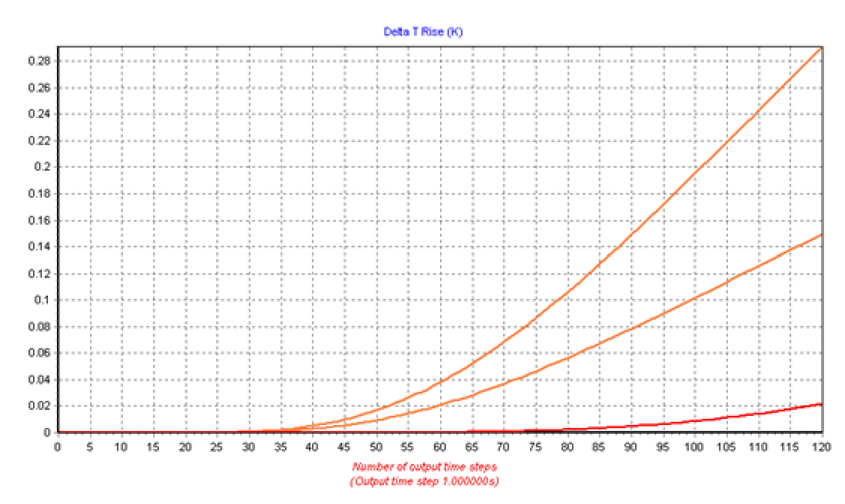

The next step of the experimentation was to increase once again the heating power density to 22222 W/m^2 which is equivalent to 2000W on the sample size. On simulation ML13-17 it has been decided to remain at 4 sec wave period and see what difference the total heating time would make. Therefore, values ranging from 20-120 sec were used. This was done based on the indications from the previous simulations and the fact that in order to start detecting Row #3 and #4 longer heating times were needed. Lower total heating time values did not reveal defects below 10mm depth. The main detection results came from 120s where all 4 rows for defects could be detected through their temperature signal. The results of simulation ML17 are shown below. Figure 25 shows that 3 rows of defects are detected using these settings. Graph 12 shows that all rows have been detected while using the space profile and Row #4 provides enough, although small, temperature signal to be detected.

Figure 25 Thermal image for simulation ML17 using Optical lockin: Heating density 22222W/m2, Wave period 4s, Total time 120s

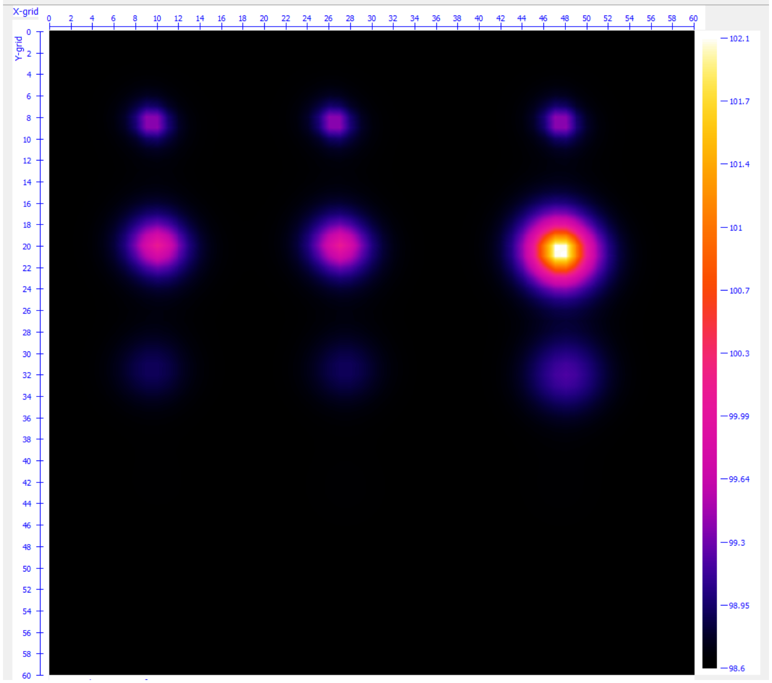

Graph 12 Space profiles of the different rows of defects using optical lockin simulation ML17 settings

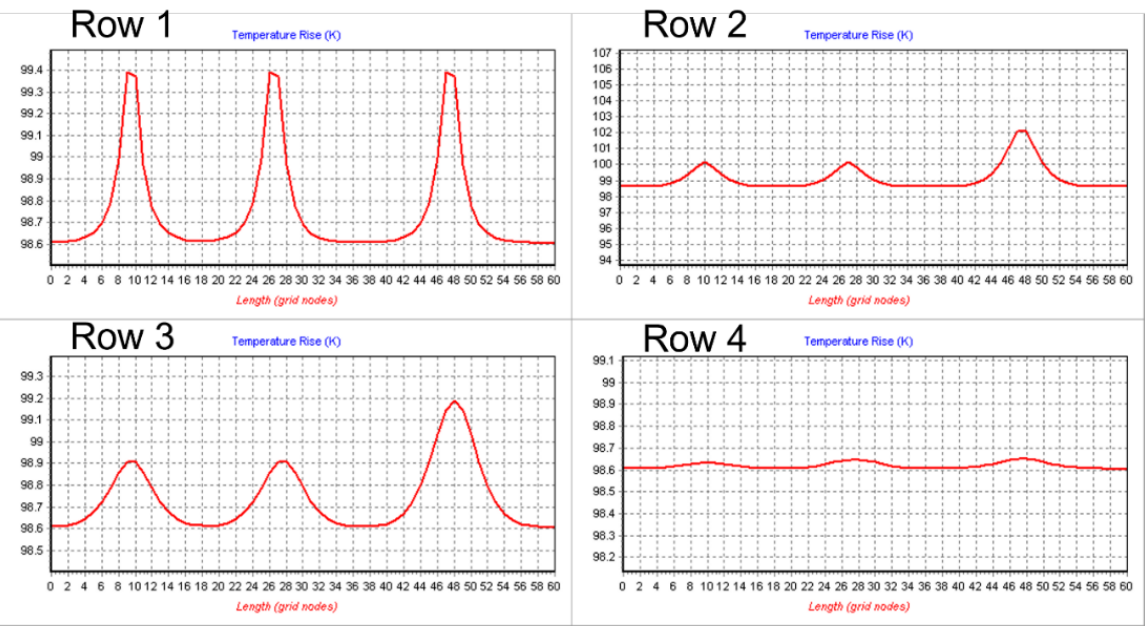

Graph 13 Delta T profiles for different rows of defects using optical lockin simulation ML17. Row#1 in blue, Row #2 in green, Row# 3 in Orange and Row#4 in red

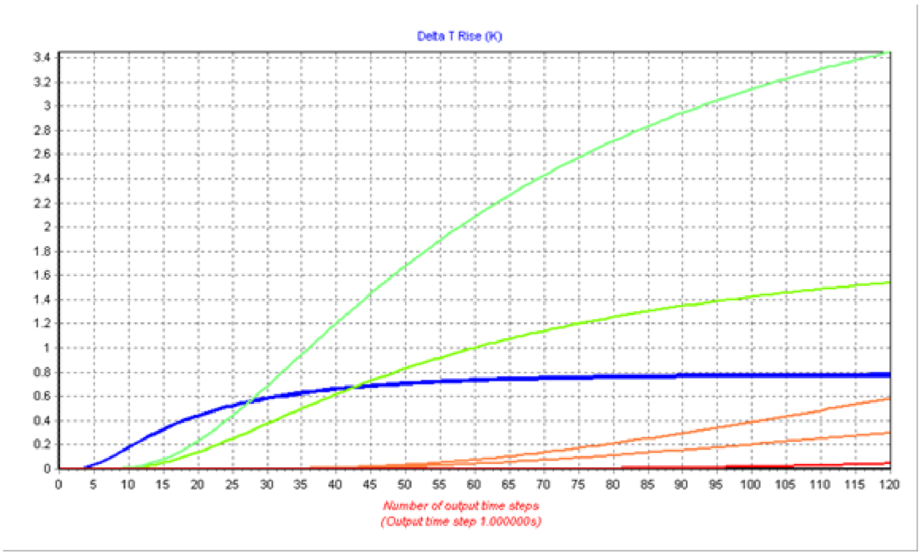

Graph 14 Delta T profiles for Row #3 and #4 of defects using optical lockin simulation ML17. Row# 3 in orange and Row#4 in red

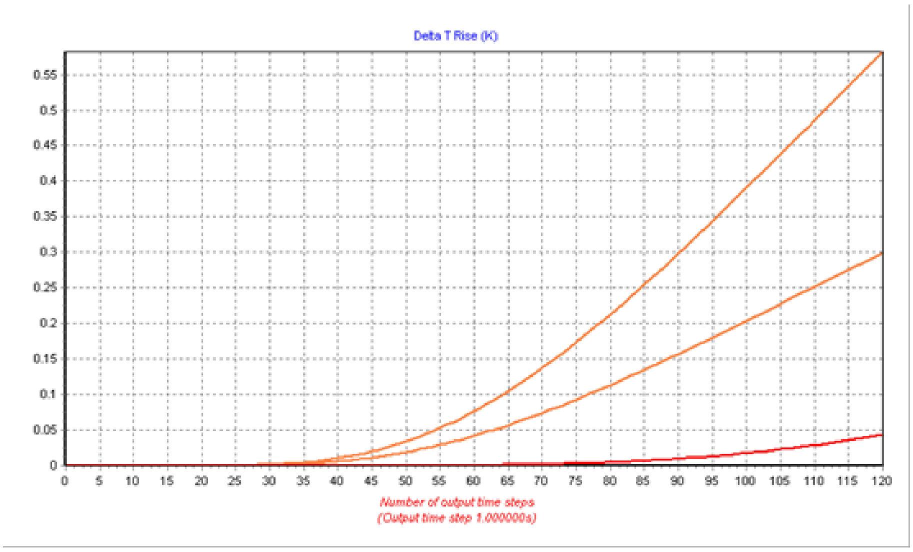

General conclusions from optical lockin simulation on monolithic CFRP sample

To conclude with the optical lockin simulations, it can be said that based on the experimentations, the most important factors for detecting deep defects in the 20mm monolithic CRFP sample are the following:

- Short wave period in the region of 4sec
- Long total heating time above 60sec up to 120 sec
- High heating power will increase the overall sample's temperature

The value of 120sec for the total time is quite long but probably proportional to the thickness, However, the monolithic component is expected to be located vertically between the windows section. This means that it will only cover small portions of the overall carbody shell.

At this stage some additional analysis could be suggested although it is not part of D 2.1 and mostly relevant to D 2.3- "Data processing and pattern recognition software". Although it has been established that under long heating time, deep defects can be detected using the simulated optical lockin technique, some defects remain visually undetected on the thermal image. To overcome this obstacle when experimenting in lab conditions, image processing techniques will be used. Thus, defects that are very faint in the thermal images will require further processing. ThermoCalC 3D already offers two commonly used methods such as PCA (Principal Component Analysis) and Fourier transform (FT). These methods have already been discussed in D 1.1 "Terms of Reference, Requirements and Specifications for Carbody Inspection Technology" as well as Ibarra-Castanedo et al. (2009). Figure 26 and Figure 27 shows how all rows of defects can be amplified using image and signal processing compared to the first thermal images.

Figure 26 PCA from simulation ML17 and ML12. Left 22222 W/m^2 and right 11111 W/m^2 at 120sec total heating time

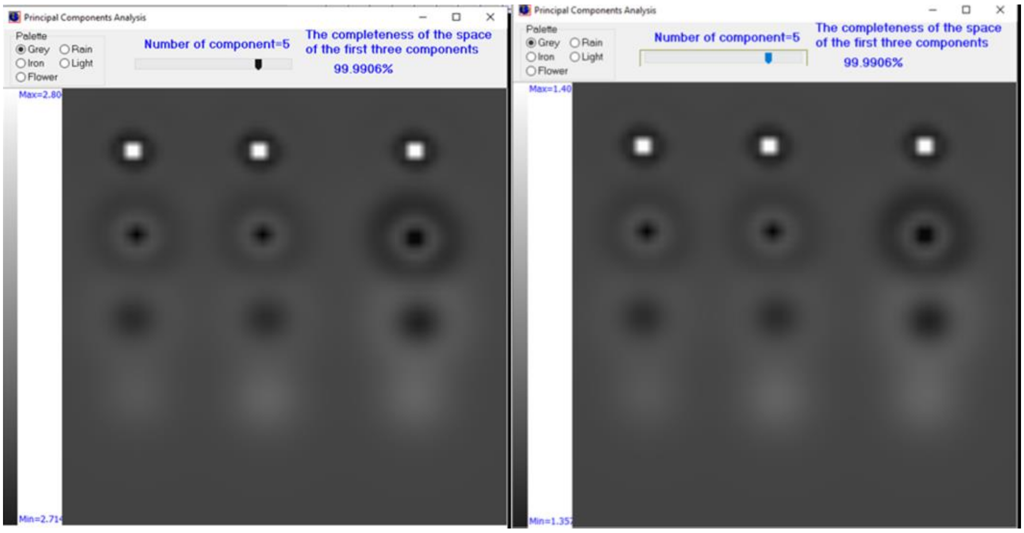

Figure 27 FT from simulation ML17 and ML12. Left 22222 W/m^2 and right 11111 W/m^2 at 120sec total heating

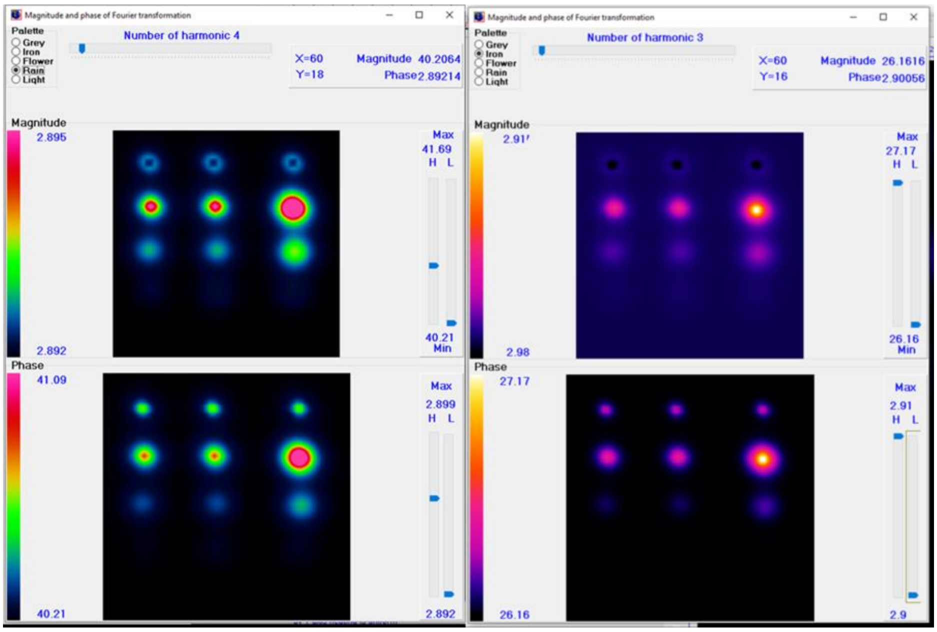

4.2.1.2 Pulsed thermography for monolithic CFRP component

Figure 28 Single square pulse heating function

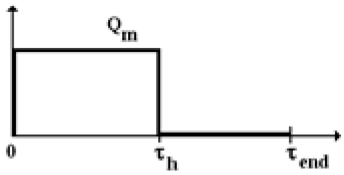

In order to carry out the pulsed thermography simulations the single square heating function was used, that is provided by the software. Compared to the optical locking this method uses a different heating function at shown on Figure 28.

Table 14 Settings for single square pulse simulations used on the monolithic CFRP sample and results

Simulation #	Heating density (W/m^2)	Heating time (s)	Total time (s)	Time step (s)	No. defects detected	Detection depth limit
MP1[12]	11111111	0.003	5	0.003	3/12	2.5 mm
MP2	11111111	0.003	10	0.003	6/12	5 mm
MP3	11111111	0.006	10	0.006	6/12	5 mm
MP4	1000000	0.05	10	0.05	6/12	5 mm
MP5	1000000	0.05	20	0.05	6/12	5 mm

[12] MP= Monolithic Pulsed

MP6	1000000	0.05	40	0.1	9/12	10 mm
MP7	1000000	0.05	60	0.1	9/12	10 mm
MP8	333000	0.1	20	0.2	6/12	5 mm
MP9	333000	0.1	40	0.2	9/12	10 mm
MP10	333000	0.1	60	0.2	9/12	10 mm
MP11	666000	0.1	20	0.2	6/12	5 mm
MP12	666000	0.1	40	0.2	9/12	10 mm

Heating density: Max heating power (Q_m see Figure 28) is the pulse amplitude and is expressed in the form of heating density in the ThermoCalc 3D software as already explained in section 4.2.2

Heating time: Heating time τ_h signifies the duration of the heating pulse used on the sample. Heating time for pulsed thermography is meant to be very small due to the amount of energy released on the sample.

Total time: Total time in the case of single square pulse is different from optical lockin and is shown by τ_{end}. In this case total time is the process time to stop computations which means that it includes the heating time and an observation time after the pulse has ended.

Time step: signifies the duration of the calculation steps. The time step is dependent on the heating time in order for the computations to be more accurate. Therefore, for heating time of a few ms the heating time will have to be of the same scale or up to 0.1-0.2s

Early simulation results with pulse thermography did not provide any satisfactory results. Typical values optical pulsed thermography values of 0.003s (3ms) that were used in the simulation provided limited detection of defects mainly between 2.5mm to 5mm. In order to obtain good accuracy in the calculations, time steps equivalent to the heating time were used. Consequently, such simulations can take up to 1hour even on PCs with high computing power. In addition, longer heating and observation times were used to compensate for the thickness of the sample. Experimentation stopped at 0.1 seconds heating time due to the fact that values above this figure are significantly long for pulsed thermography and are unrealistic.

Better detection results came from MP 4 simulation using heating time of 0.05 and total time 10s. In this simulation Rows #1 and # 2 were detected both visually and through their temperature signal. The next step was to use a longer observation time of 20s where much better results were given by the simulation with Row # 2 being more distinct. Thermal images from MP4 and MP5 simulations are shown below. Simulations MP6-MP7 established that detection of defects up to 10mm can easily be done with 0.05sec of heating. However, long observation times are required 40-60sec.

Figure 29 Thermal image for simulation MP4 (left) and MP5 (right) using single square pulse: Heating density 1000000 W/m2, Heating time 0.05s, Total time 10-20s

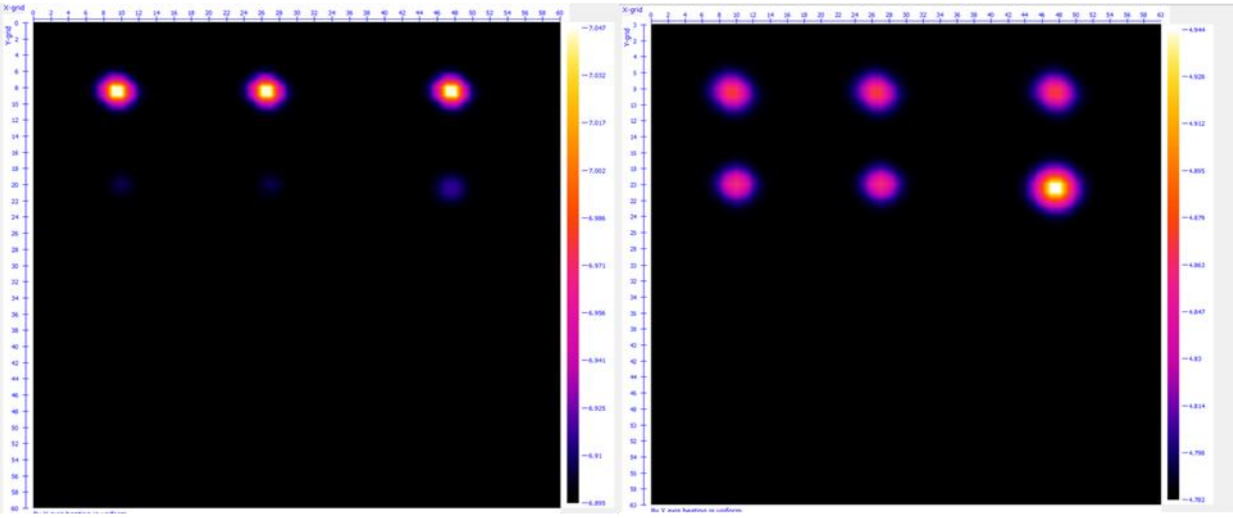

Graph 15 Space profiles of the different rows of defects using optical pulse simulation MP5 settings

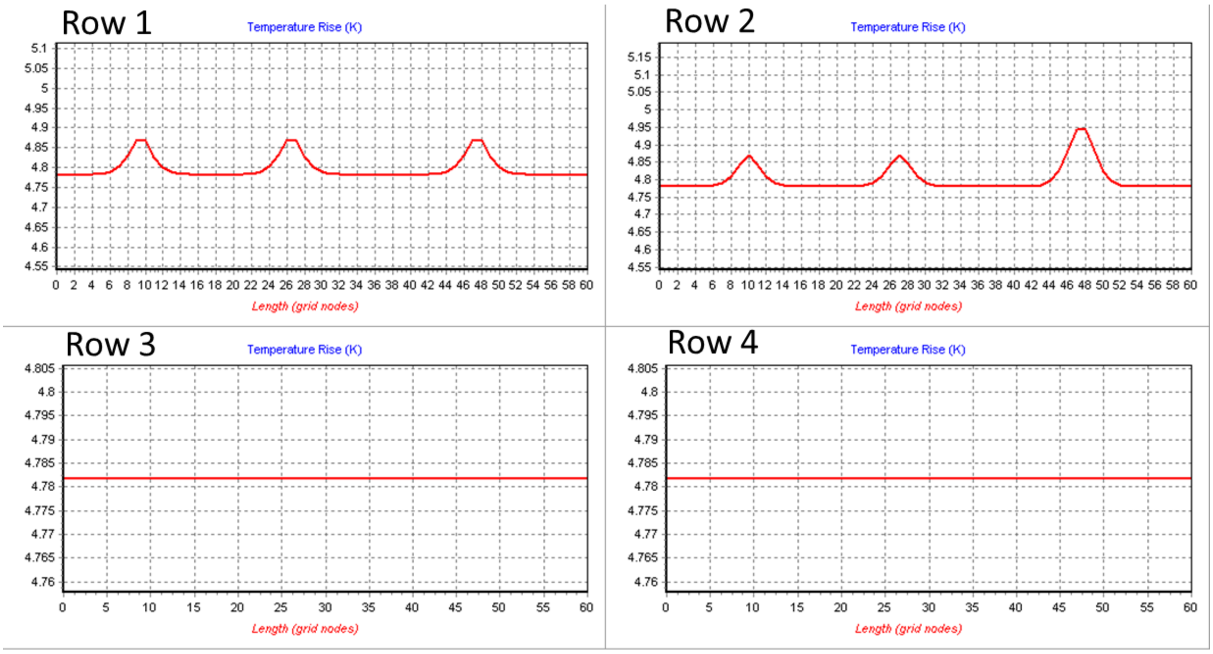

Graph 16 Delta T profiles for different rows of defects using optical pulse simulation MP5. Row#1 in blue, Row #2 in green, Row# 3 in Orange and Row#4 in red

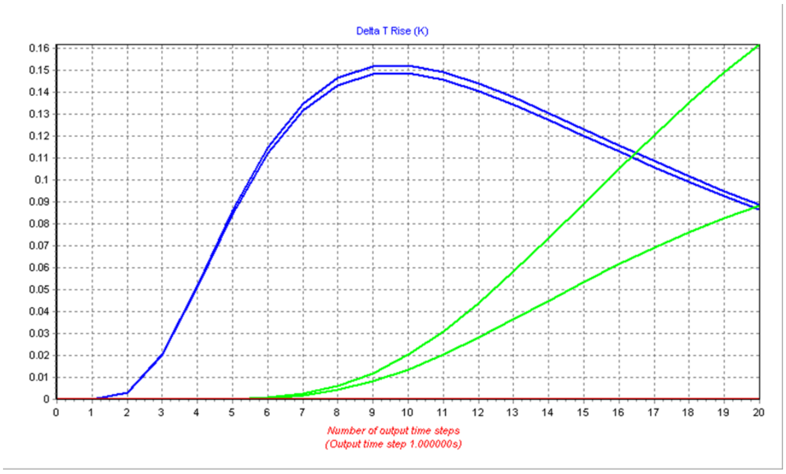

Thus, the next step was to begin aiming for detection of Row #3 of the defects. Detection occurred at MP6 at 0.05s heating time and using a long observation time of 60s. Row #3 was also visible at MP8 using 0.1 sec heating time and 40sec observation time. This means that due to the thickness of the component, heat requires long time to propagate and reach defects at 10mm.

Figure 30 Thermal image for simulation MP 8 using single square pulse: Heating density 33300W/m^2, Heating time 0.1s, Total time 40s

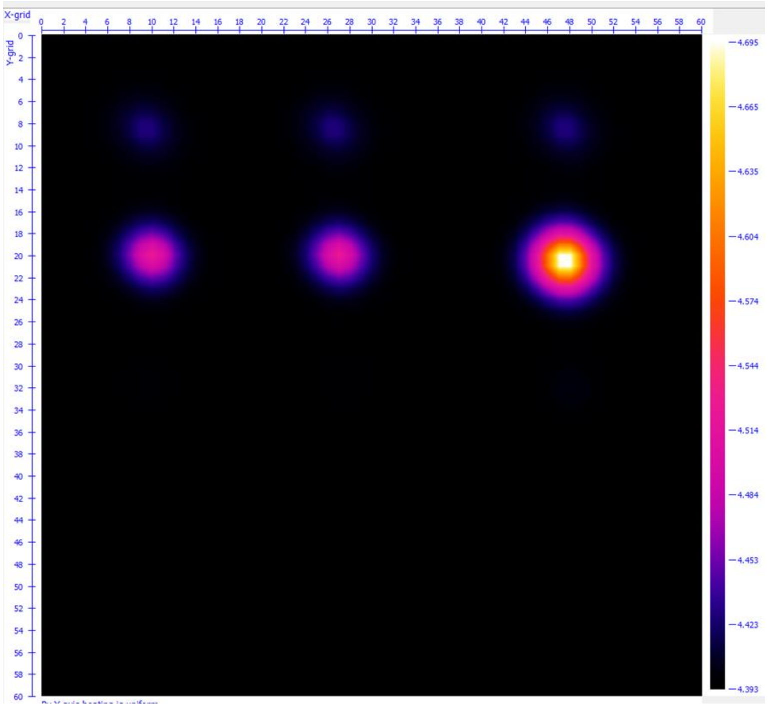

Graph 17 Space profiles of the different rows of defects using optical pulse simulation MP8 settings

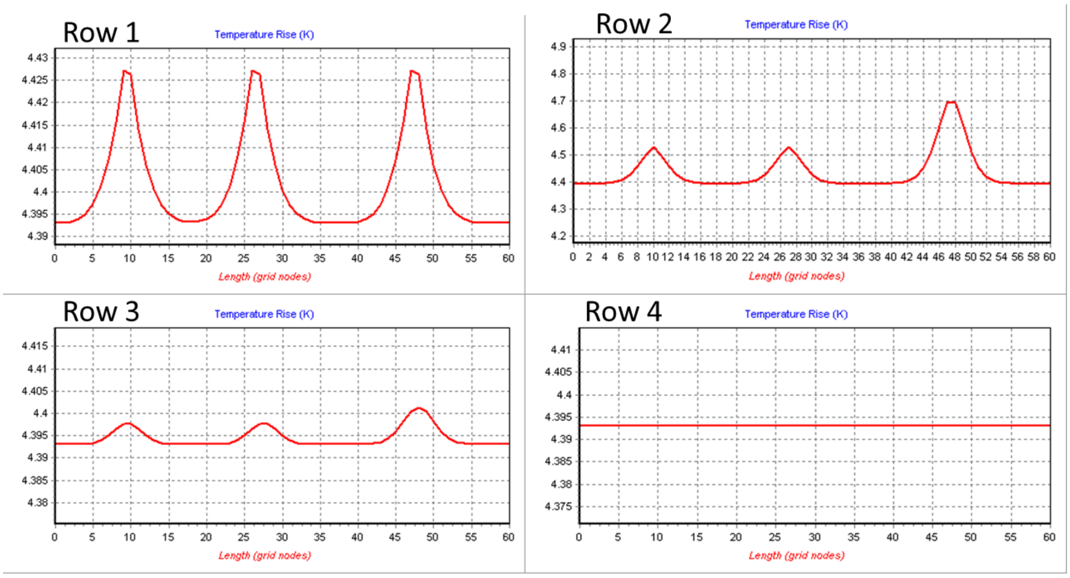

Graph 18 Delta T profiles for different rows of defects using optical pulse simulation MP8. Row#1 in blue, Row #2 in green, Row# 3 in Orange and Row#4 in red

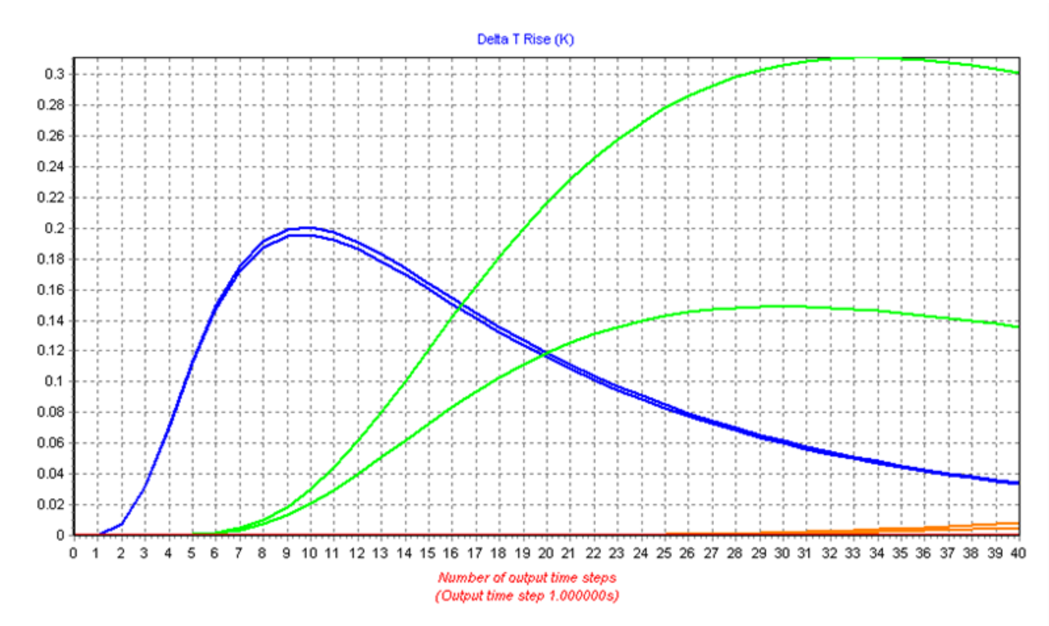

Graph 19 Delta T profiles for Row #3 and #4 of defects using optical pulse simulation MP8. Row# 3 in orange and Row#4 in red

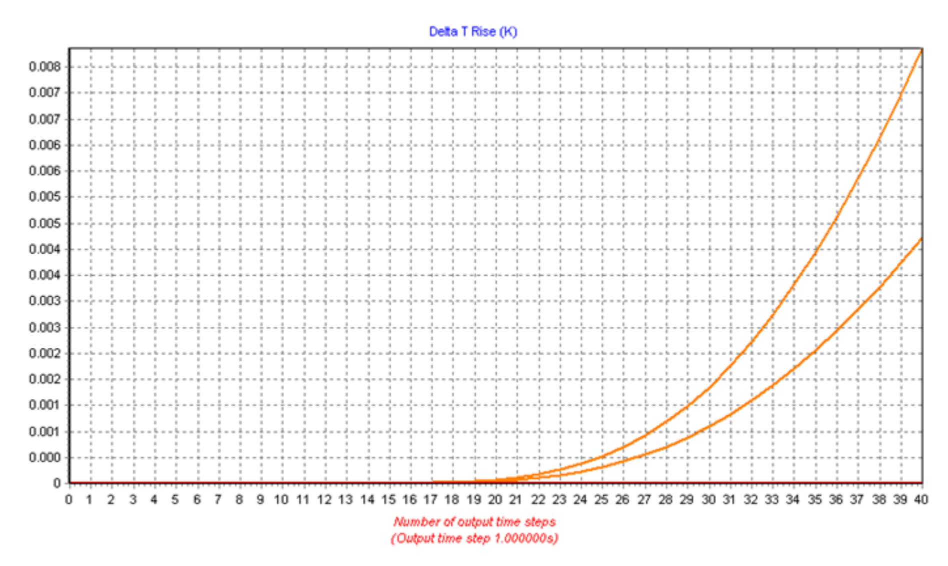

Results from the remaining simulations did not provide any better results in terms of Row# 4 detection. Only simulations MP11 and MP9 where 40-60sec observation time was used, picked up faint temperature signals from Row #4 that can be regarded negligible is the scale of 0.0001 °C.

General conclusions from the pulsed thermography simulation on the monolithic sample

- Pulsed thermography is more reliable for defects up to 5mm- 10mm with good temperature signals as it is intended to be used in real life
- Simulations using realistic heating times did not provide adequate results in the 20mm CFRP sample probably due to its extreme thickness
- Heating time of 0.1 sec was used mostly with heating pulse that was equivalent to 3-6 KJ on the sample area 0.09 m^2
- The long observation times (40-60sec) that were used were mainly in order to see how many rows of defects are detectable. Typically, pulsed thermography is very fast in progress and does not include such long observation.
- Additional image processing of short observation time simulations did not provide better detectability of row#3 or 4#. Therefore, the results from MP11 PCA and FT data processing are given below.

Figure 31 PCA processing from simulation MP11 using heat pulse density 666000 W/m^2, heating time 0.1 sec and 40sec total time

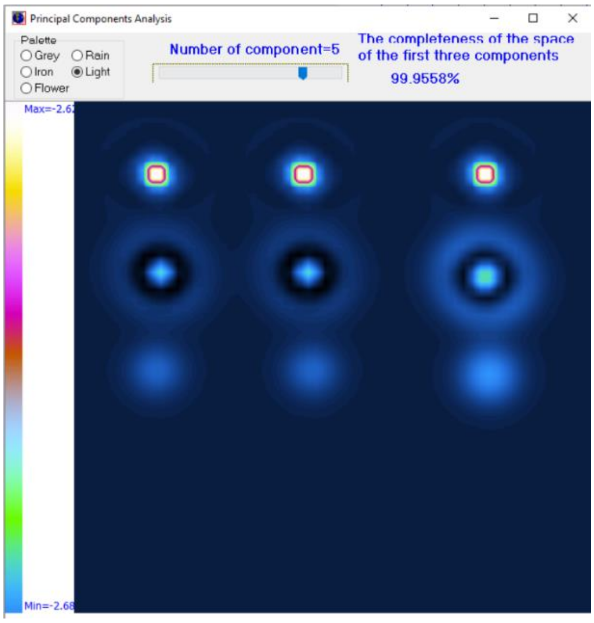

Figure 32 FT from simulation MP11 using heat pulse density 666000 W/m^2, heating time 0.1 sec and 40sec total time

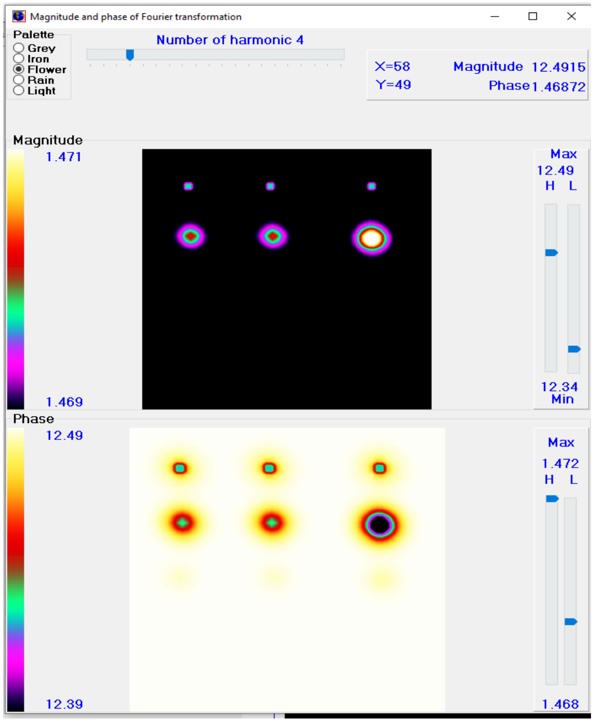

4.2.2 Sandwich CFRP-PET component modelling and simulations

In order to model the sandwich CF-PET-CF component, the same thermal properties and principles were used as for the CF monolithic sample. The only difference is the introduction of the PET foam core between the two CF skins. Skins are 5mm thick while the PET core thickness is 30mm. The thermal and mechanical properties that were used, can be found in Table 10. The subsurface defects that were introduced in the component are meant to simulate delaminations or disbonds between skins and core at the top and back surface.

Table 15 Dimensions of defects on the CF-PET-CF sample

Row #	Depth	Location	Defect size
1	1.25 mm	Top skin surface	3mm, 5mm,7mm (length & width), 1mm thickness
2	2.5 mm	Top skin	9mm,11mm,13mm (length & width), 1mm thickness
3	3.75 mm	Top skin	15mm,17mm,19mm (length & width), 1mm thickness
4	5 mm	Top skin and core	21mm, 23mm, 25mm (length & width), 1mm thickness
5	35 mm	Core-back skin	27mm, 29mm, 31mm (length & width), 1mm thickness

Figure 33 Sandwich CF-PET-CF component defects and dimensions

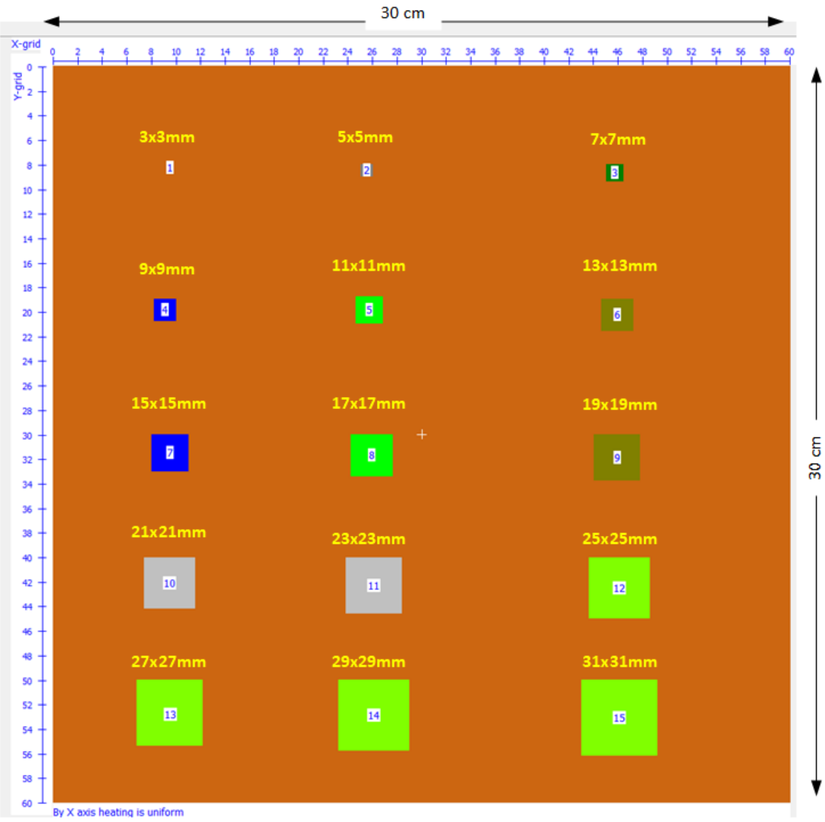

Figure 34 Top view of the CF-PET-CF sandwich and depth of defects

4.2.2.1 Optical lockin simulations for sandwich CFRP-PET component

The principles of using the thermal waves heating function in ThermoCalc 3D software have already been explained section 4.2.1.1. This section describes the optical lockin simulations that have been carried out on the CFRP-PET sandwich component. Table 16 presents the simulation settings and the detection results

Table 16. Settings for optical lockin simulation used on the sandwich CF-PET-CF sample and results

Simulation #	Heating density (W/m^2)	Wave period (s)	Total time (s)	Time step (s)	No. defects detected	Detection depth limit
SL1[13]	3000	3	30	0.5	12/15	5mm
SL2	6000	4	20	0.5	12/15	5mm
SL3	6000	4	30	0.5	12/15	5mm
SL4	6000	6	30	0.5	12/15	5mm
SL5	6000	4	60	0.5	12/15	5mm
SL6	6000	4	90	0.5	12/15	5mm
SL7	6000	4	120	0.5	12/15	5mm
SL8	11111	4	30	0.5	12/15	5mm
SL9	11111	4	60	0.5	12/15	5mm
SL10	11111	7	60	0.5	12/15	5mm
SL11	11111	4	90	0.5	12/15	5mm
SL12	11111	4	120	0.5	12/15	5mm
SL13	22222	4	30	0.5	12/15	5mm
SL14	22222	4	60	0.5	12/15	5mm
SL15	22222	4	90	0.5	12/15	5mm
SL16	22222	4	120	0.5	12/15	5mm

Results from the first simulations with low power density are very satisfactory. Defects up to 3.75mm are visually detectable with the thermal image, while row #4 defects can be detected through their temperature signal using space profile (Graph 20) and Delta T rise (Graph 21). Only Row #5, between the bottom CF skin and the core, remains undetected although it gives very small temperature signal below 0.001 °C.

[13] SL= sandwich lockin

Figure 35 Thermal image for simulation SL1 using Optical lockin: Heating density 3000W/m^2, Wave period 3s, Total time 30s

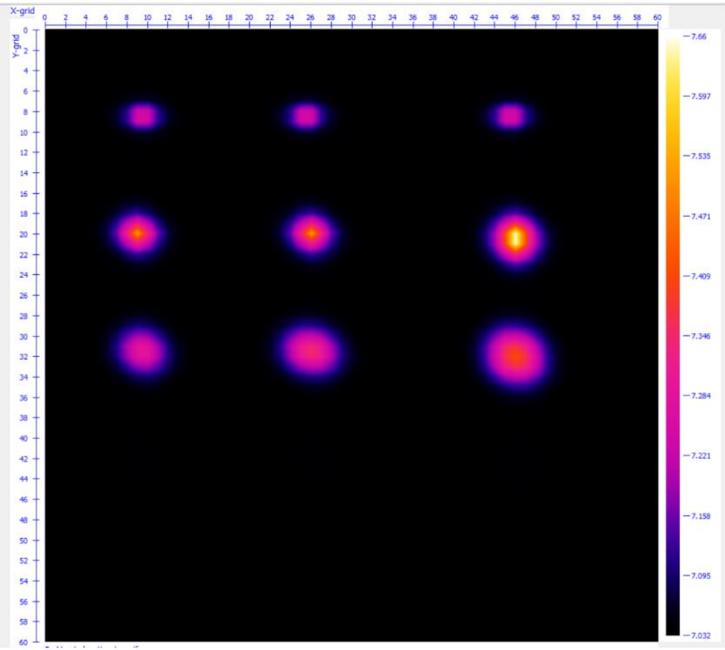

Graph 20 Space profiles of the different rows of defects using optical lockin simulation SL1 settings

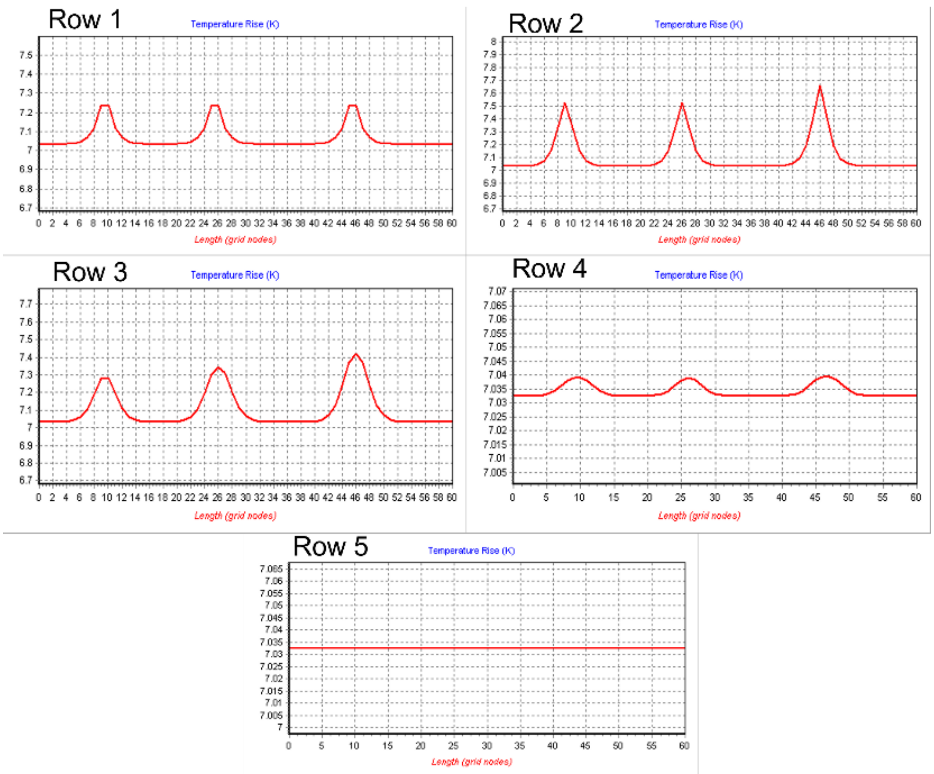

Graph 21 Delta T profiles for different rows of defects using optical lockin simulation SL1. Row#1 in blue, Row #2 in green, Row# 3 in Orange, Row# 4 yellow and Row #5 in red

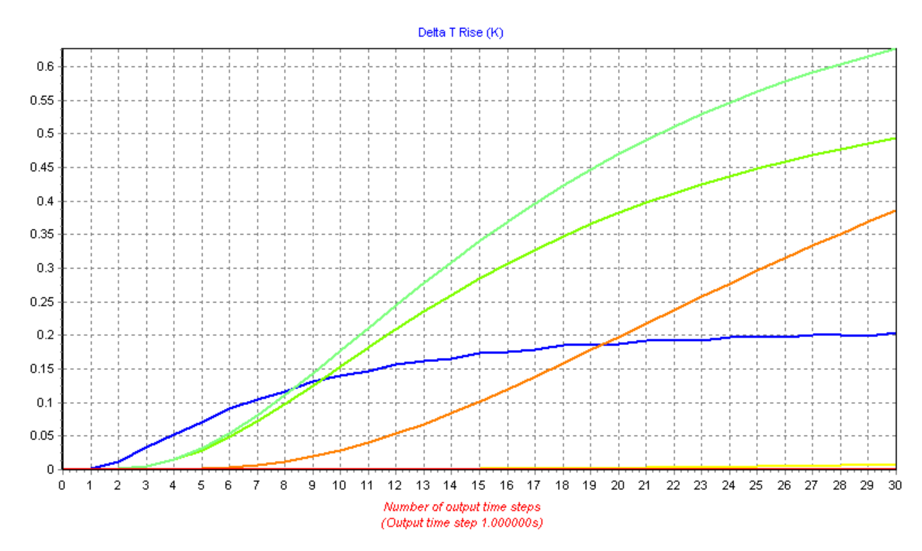

Graph 22 Delta T profiles for Row #4 and #5 of defects using optical lockin simulation SL1. Row# 4 in yellow and Row#4 in red

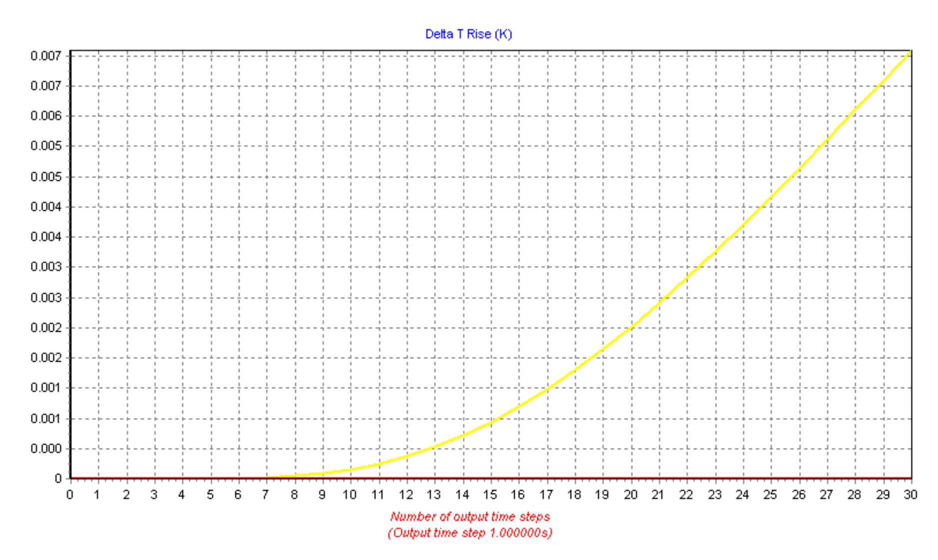

The main difference between simulations SL5- 7 was the duration of the total heating time. Attempts to increasing wave period time or decrease were not significant in revealing row #4 on the thermal image or improve the temperature signal for row #5. Therefore, the main difference at 6000 W/m^2 and wave period of 4sec, was mostly made by increasing the total heating duration from 60- 120sec. Results for simulation SL 7 at 120sec total heating time are shown below.

Figure 36 Thermal image for simulation SL7 using Optical lockin: Heating density 6000W/m^2, Wave period 4s, Total time 120s

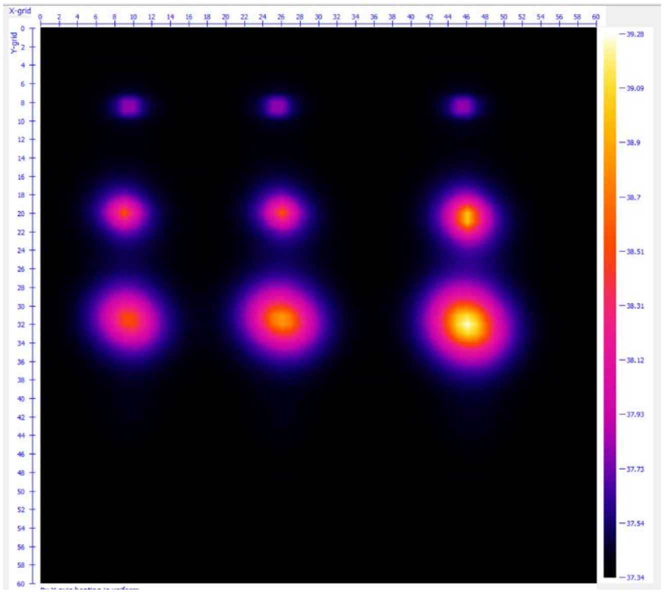

Graph 23 Space profiles of the different rows of defects using optical lockin simulation SL7 settings

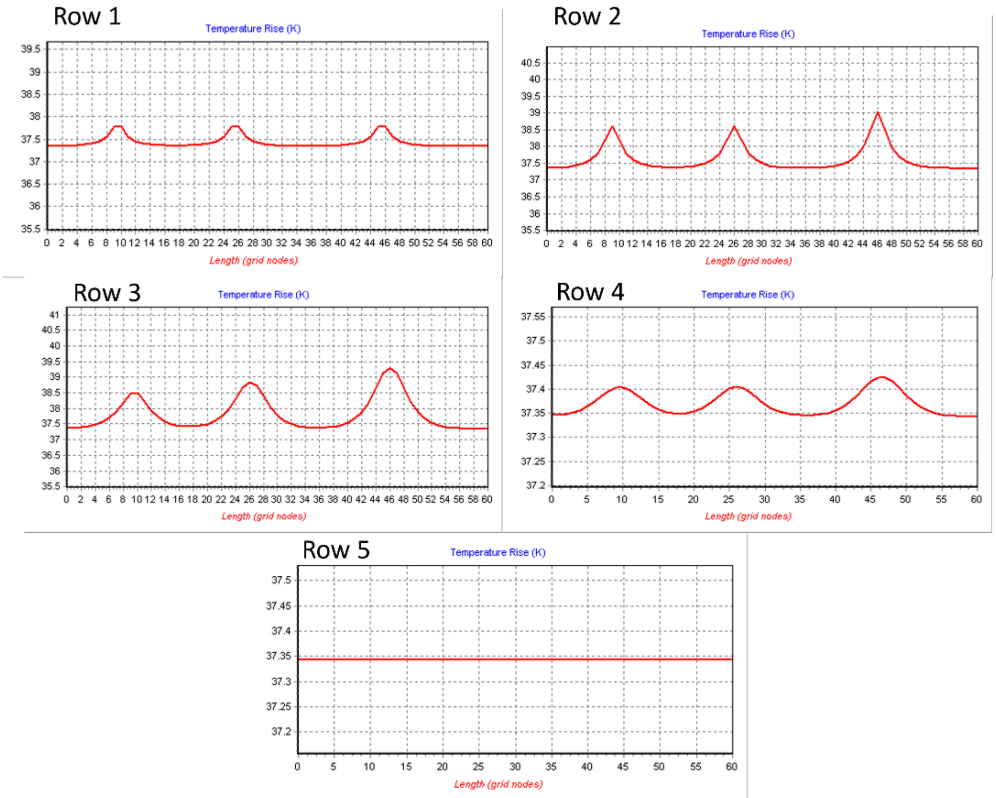

Graph 24 Delta T profiles for different rows of defects using optical lockin simulation SL7. Row#1 in blue, Row #2 in green, Row# 3 in Orange, Row# 4 yellow and Row #5 in red

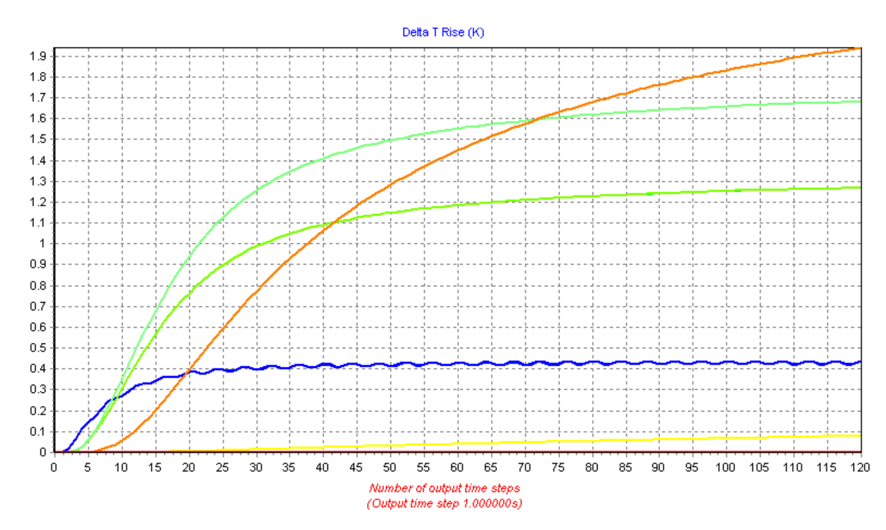

Graph 25 Delta T profiles for Row #4 and #5 of defects using optical lockin simulation SL7. Row# 4 in yellow and Row#4 in red

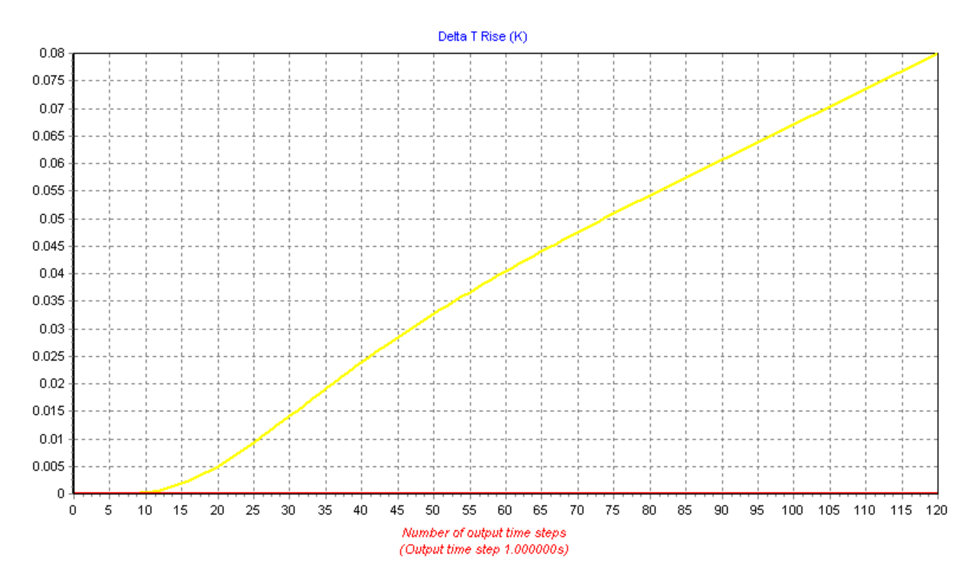

Increasing the heating density to 11111 W/m^2 did not provide significantly better results apart from when using long heating total time ranging from 60-120 sec. The difference between 90 and 120sec of heating time was mainly that the temperature signal for Row #4 become more distinct on the Delta T graphs. As expected this is the result of more heat being put into the sample. It is also important to note that Row #4 defects are located between the CF and the PET material. Which means that probably no better results will be extracted even with more heating power. In addition, Row #5 is still undetectable with the exception of some minute heating signal >0.00001 °C

Figure 37 Thermal image for simulation SL12 using Optical lockin: Heating density 11111W/m^2, Wave period 4s, Total time 120s

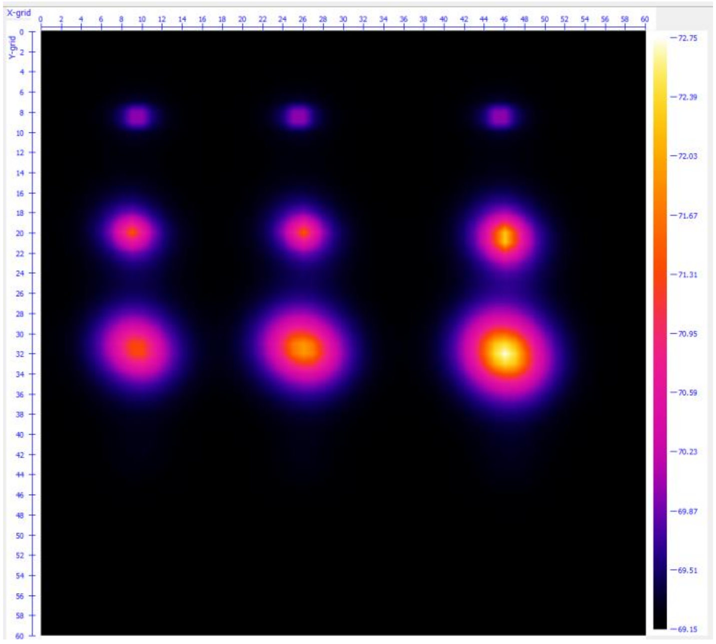

Graph 26 Space profiles of the different rows of defects using optical lockin simulation SL12 settings

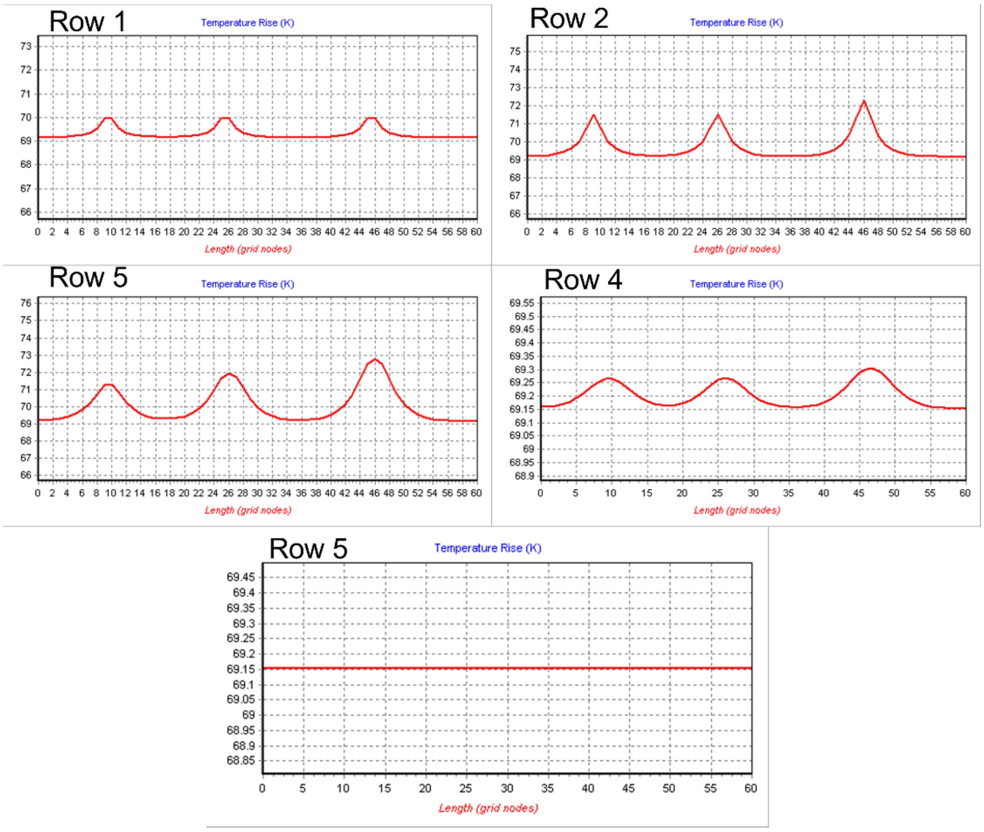

Graph 27 Delta T profiles for different rows of defects using optical lockin simulation SL12. Row#1 in blue, Row #2 in green, Row# 3 in Orange, Row# 4 yellow and Row #5 in red

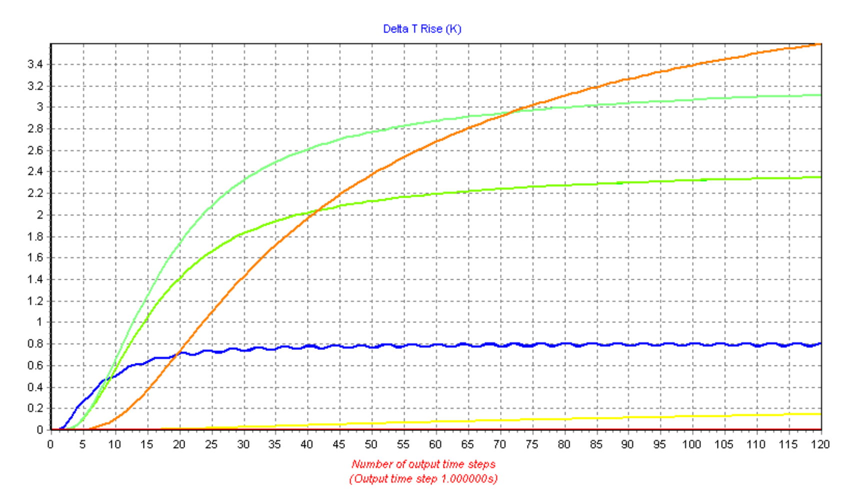

Graph 28 Delta T profiles for Row #4 and #5 of defects using optical lockin simulation SL12. Row# 4 in yellow and Row#4 in red

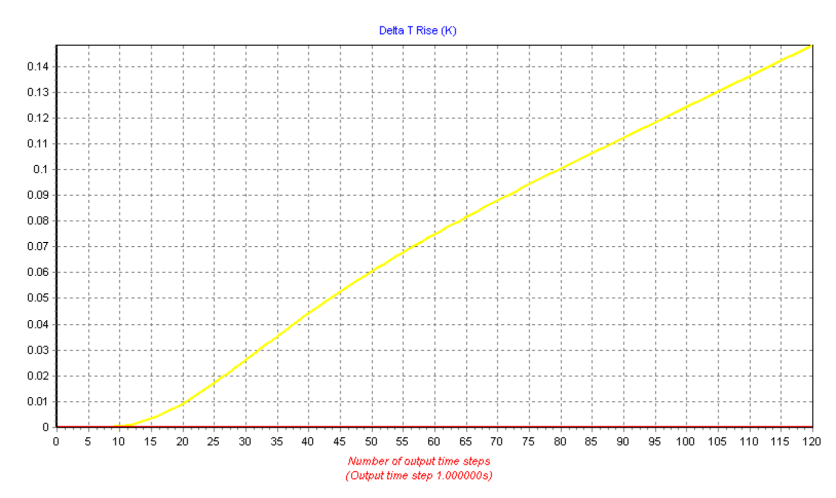

For the final simulations 22222W/m^2 heat density was used with variations of heating time. All simulations used a 4sec wave period since it has given consistent results throughout the experimentations. Simulation SL 16 is presented below with total heating time 120sec. Its thermal image (Figure 38), shows that rows 1-3 are visually detected while row #4, which is very faintly beginning to appear on the thermal image, is mostly detected through its temperature signal (Graph 29, Graph 31, Graph 30). Row #5 remains undetected using all types of analysis.

Figure 38 Thermal image for Simulation SL16 using Optical lockin: Heating density 22222W/m^2, Wave period 4s, Total time 120s

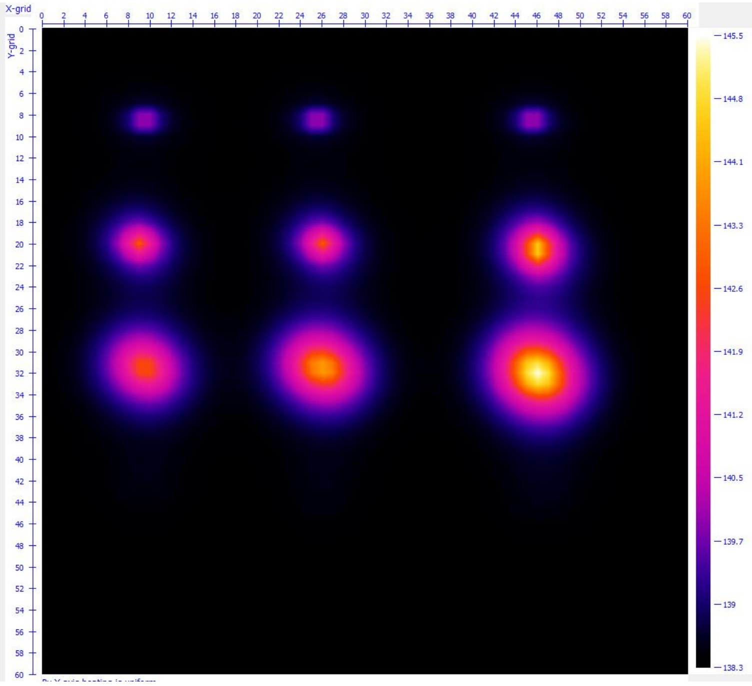

Graph 29 Space profiles of the different rows of defects using optical lockin simulation SL16.

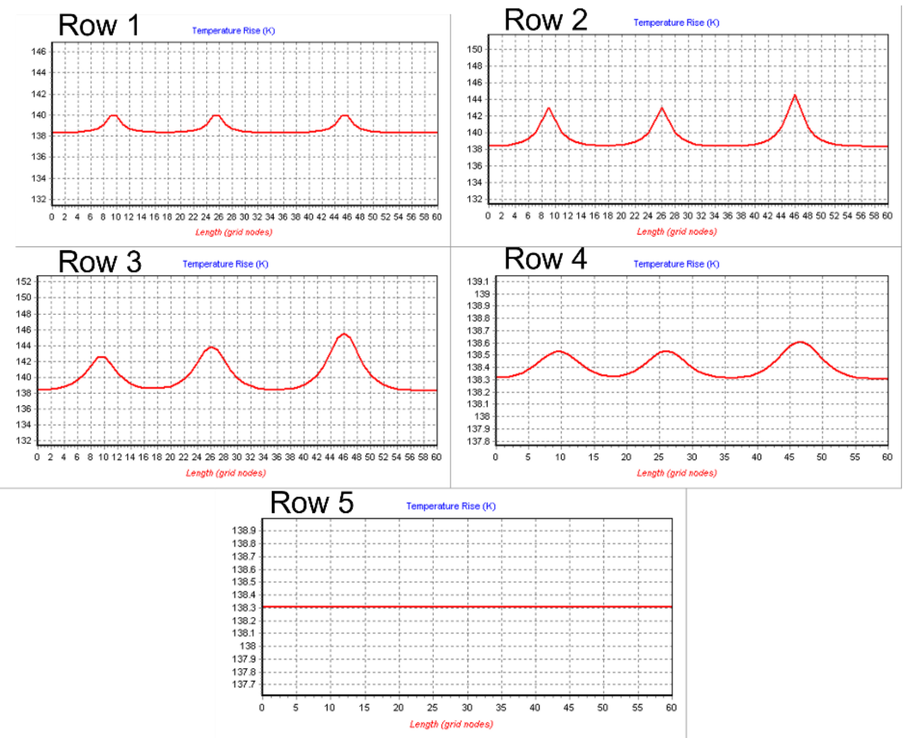

Graph 30 Delta T profiles for different rows of defects using optical lockin simulation SL16. Row#1 in blue, Row #2 in green, Row# 3 in Orange, Row# 4 yellow and Row #5 in red

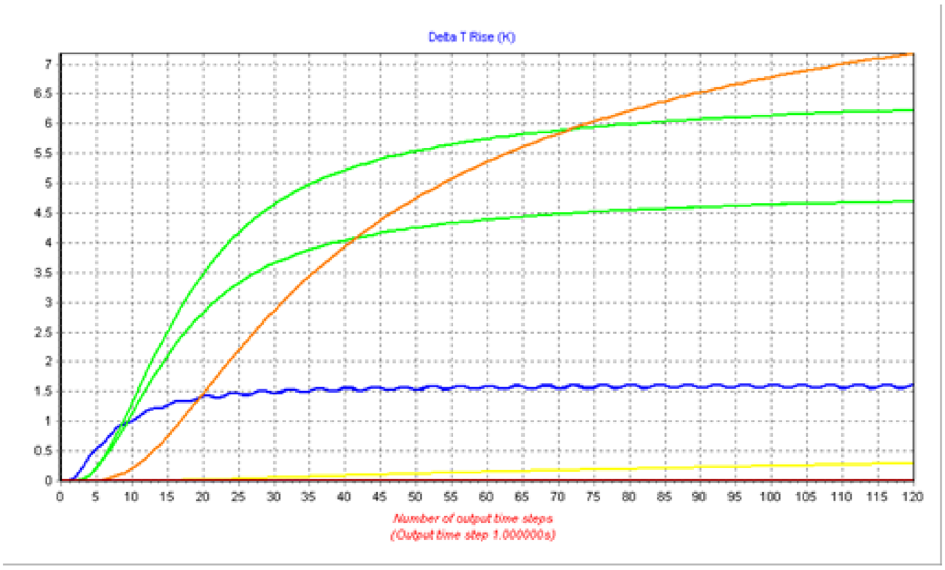

Graph 31 Delta T profiles for Row #4 and #5 of defects using optical lockin simulation SL16. Row# 4 in yellow and Row#4 in red

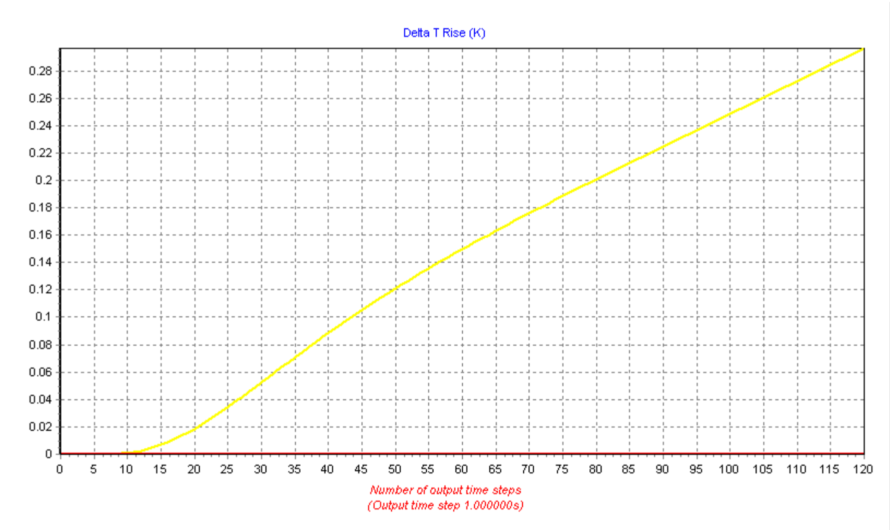

General conclusions for optical lockin simulations of the composite sandwich component, are the following:

- Most of the settings, even those with low level of heating power density, have been able to detect at least 3 rows of defects
- Row #4 was mainly being detected through its temperature signal

- Row #5 was undetected with every available setting and remains probably unclear whether it can be detected since it is at located at 35mm depth between the PET core and the back CF skin
- The PET core is most likely acting as a heat resistant material
- The component will heat up to 145 °C using the 22222W/m^2 settings

Finally, some further analysis using PCA and FT can reveal 4 rows of defects at both cases as seen on Figure 39

Figure 39 FT from simulation ML16 and ML12. Left 22222 W/m2 and right 11111 W/m2 at 120sec total heating

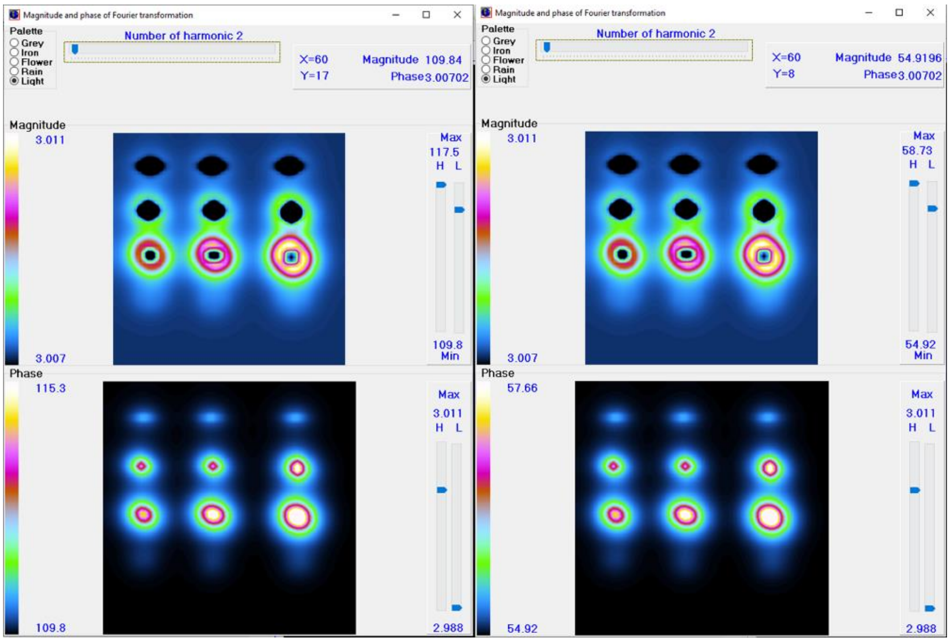

Figure 40 PCA from simulation ML16 and ML12. Left 22222 W/m2 and right 11111 W/m2 at 120sec total heating

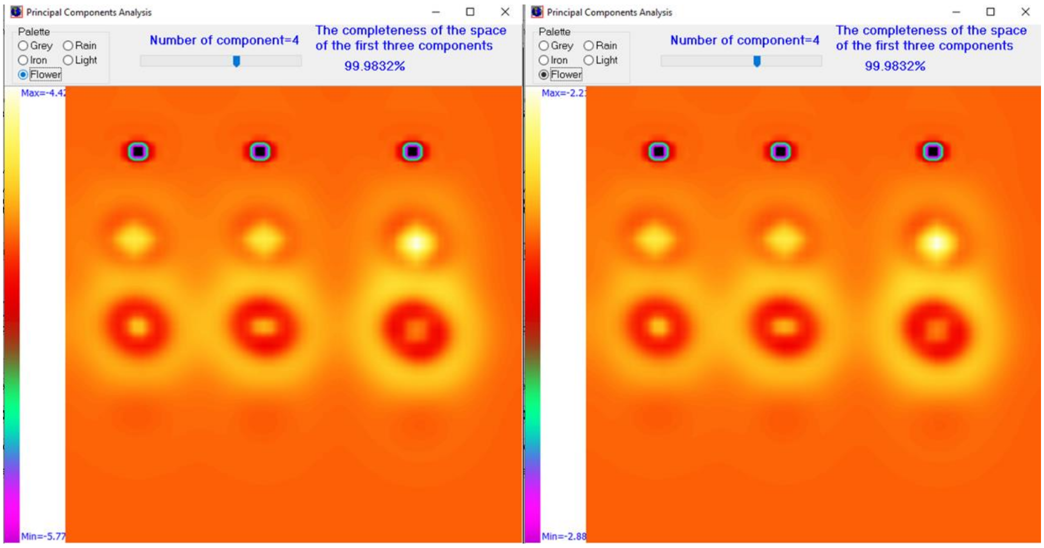

4.2.2.2 Pulsed thermography simulations for sandwich CFRP-PET component

Table 17 presents the settings that were used on the ThermoCalc 3D simulations for pulsed thermography on the sandwich CFRP-PET component. The simulations for pulsed thermography were based on similar settings with the monolithic component.

Table 17 Settings for pulsed thermography simulation used on the sandwich CF-PET-CF sample and results

Simulation #	Heating density (W/m^2)	Heating time (s)	Total time (s)	Time step (s)	No. defects detected	Detection depth limit
SP1[14]	11,111,111	0.003	5	0.003	9/15	3.75 mm
SP2	11,111,111	0.003	10	0.003	9/15	3.75 mm
SP3	11,111,111	0.006	10	0.006	9/15	3.75 mm
SP4	1,000,000	0.05	10	0.05	9/15	3.75 mm
SP5	1,000,000	0.05	20	0.05	12/15	5 mm
SP6	1,000,000	0.05	40	0.1	12/15	5 mm
SP7	1,000,000	0.05	60	0.1	12/15	5 mm
SP8	333,000	0.1	20	0.2	12/15	5 mm
SP9	333,000	0.1	40	0.2	12/15	5 mm
SP10	333,000	0.1	60	0.2	12/15	5 mm
SP11	666,000	0.1	20	0.2	12/15	5 mm
SP12	666,000	0.1	40	0.2	12/15	5 mm

[14] Sandwich Pulsed

Simulations SP1-3, where a very quick 3-6ms heating burst was used, provided defect detection up to 3.75mm. The heating densities that were used in all simulations, simulated 3-6kJ over time on the sample area. Results from SP3 are presented in below where heating time of 0.006 sec was used and observation time of 10sec. Graph 32 presents that apart from Row 1-3, Row #4 is also giving a faint temperature signal (0.003°C of Delta T). This means that overall Rows 1-3 can easily be detected using short or long times of heating or observations. Like with previous simulation experiments, the observation time was increased up to 40 sec in SP6 to reveal defects on Row 4. Simulations with long observation time were carried out mostly in order to increase the temperature signal of Row #4.

However, long observation times are not in line with how pulsed thermography should be used. Therefore, heating time was increased with shorter observation time. In this case, at simulation SP8, Row #4 begun to have a stronger temperature signal using 0.1 sec heating time and 20 sec observation time. Results from SP11 offer a good balance between temperature signal from Row#4 and observation time. These results are presented at Figure 42, Graph 35, Graph 36. Detection of Row#4 defects is very important in order to detect disbonds between the core and the front skins.

Figure 41 Thermal image for simulation SP 3 using single square pulse: Heating density 1,000,000 W/m^2, Heating time 0.05s, Total time 10s

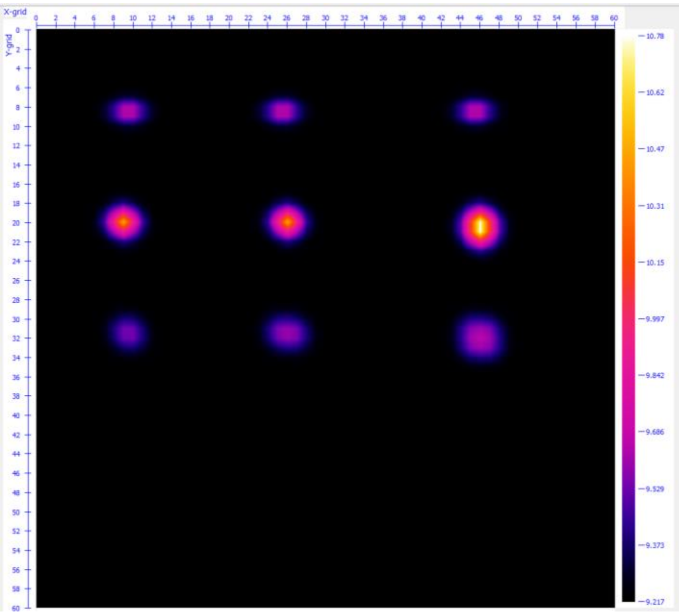

Graph 32 Space profiles of the different rows of defects using optical pulse simulation SP3 settings

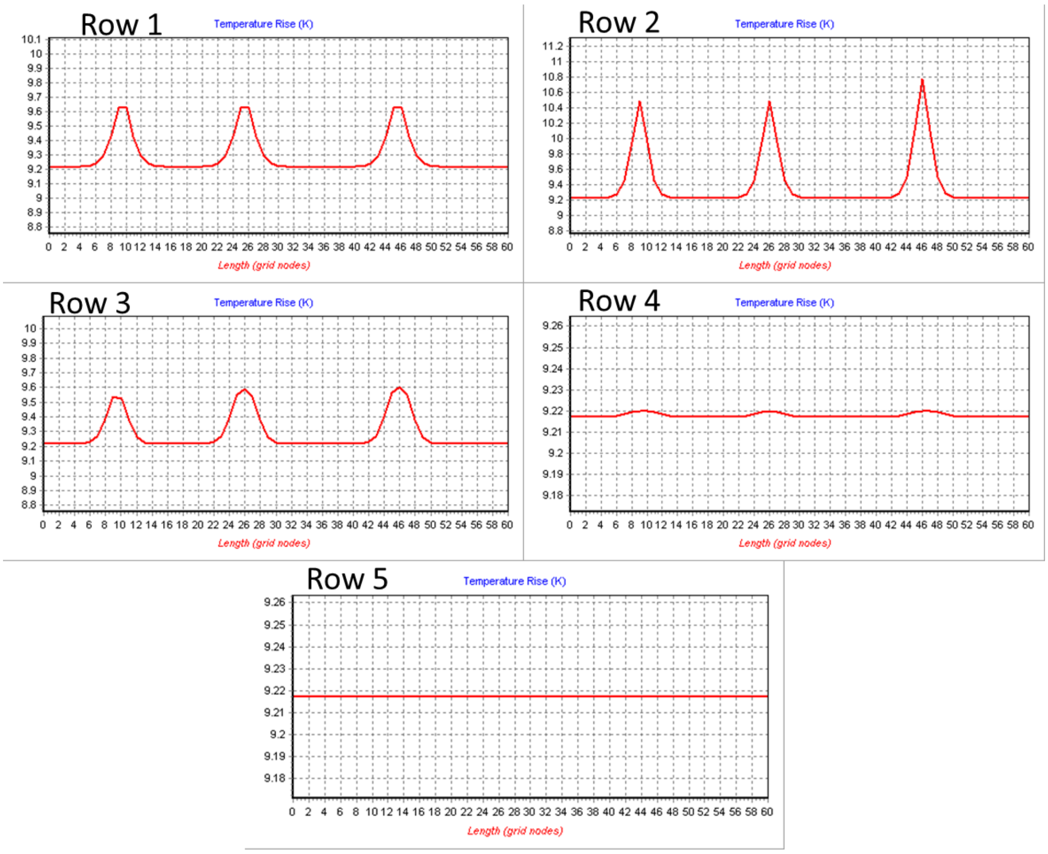

Graph 33 Delta T profiles for different rows of defects using optical pulsed thermography simulation SP3. Row#1 in blue, Row #2 in green, Row# 3 in Orange, Row# 4 yellow and Row #5 in red

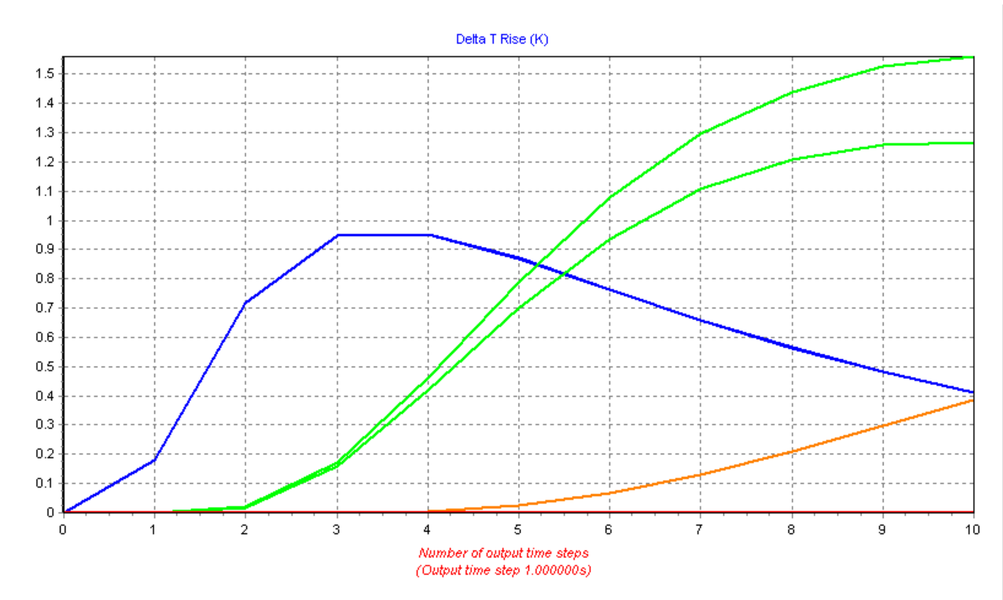

Figure 42 Thermal image for simulation SP11 using single square pulse: Heating density 666,000 W/m^2, Heating time 0.1s, Total time 20s

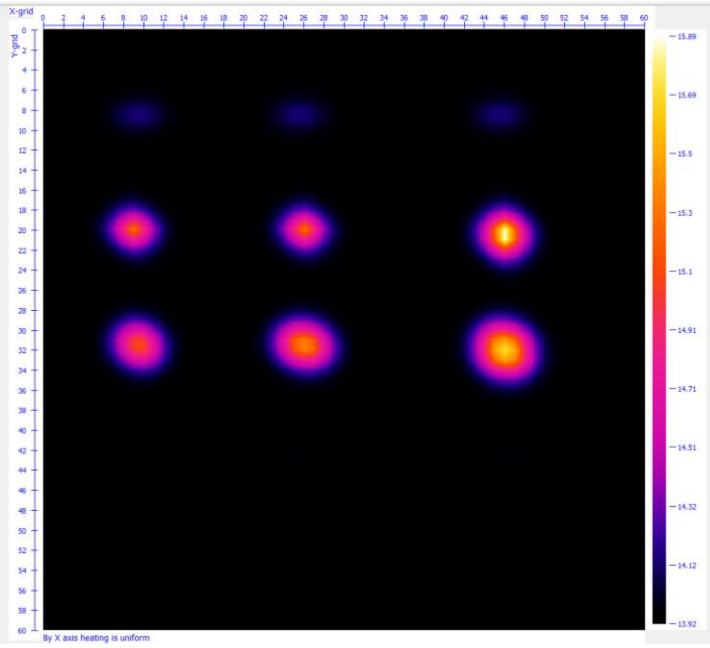

Graph 34 Space profiles of the different rows of defects using optical pulse simulation SP11 settings

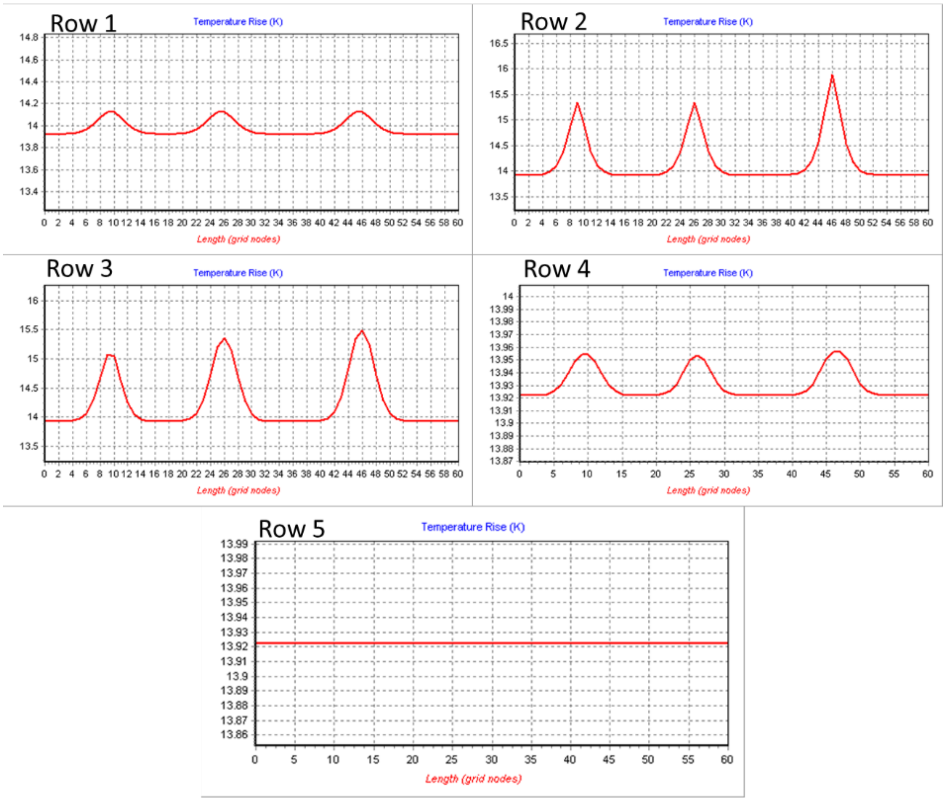

Graph 35 Delta T profiles for different rows of defects using optical pulsed thermography simulation SP11. Row#1 in blue, Row #2 in green, Row# 3 in Orange, Row# 4 yellow and Row #5 in red

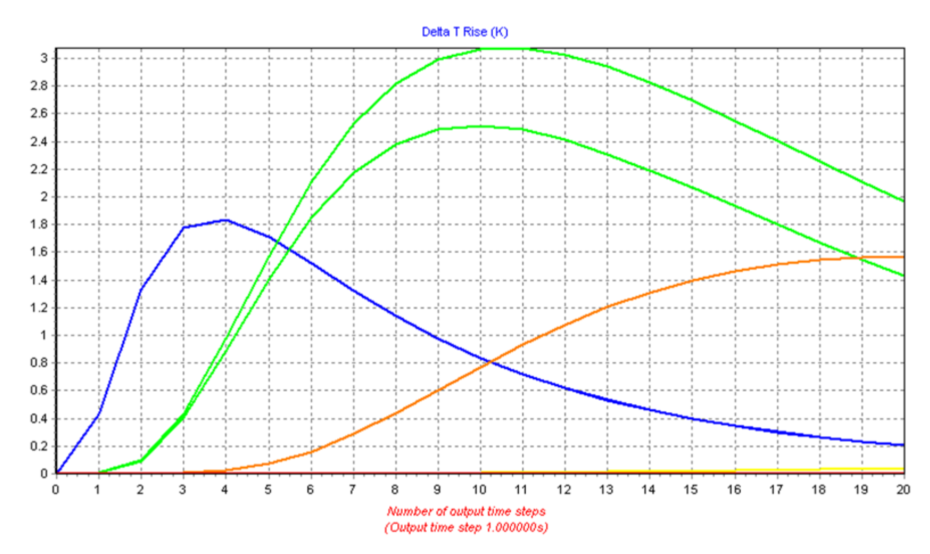

Graph 36 Delta T profiles for Row #4 and #5 of defects using optical lockin simulation SP11. Row# 4 in yellow and Row#4 in red

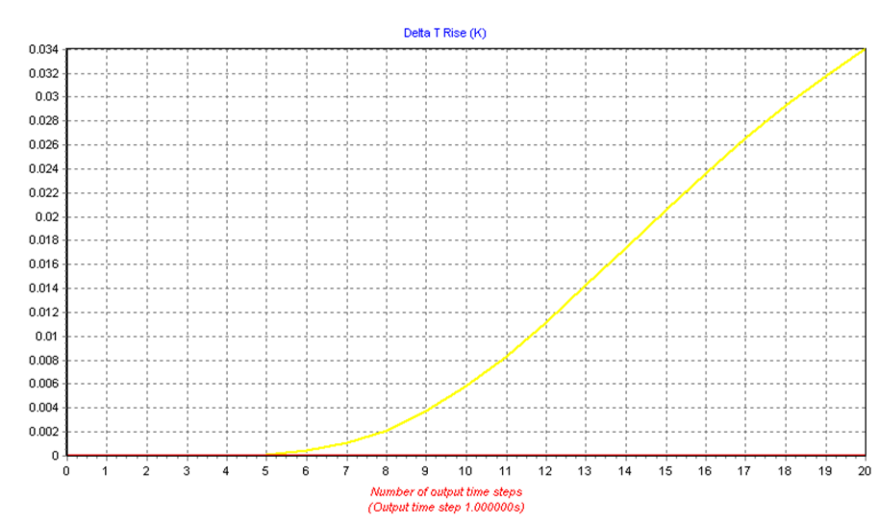

General conclusions from the pulsed thermography simulation on the sandwich component

- Pulsed thermography is more reliable for defects up to 5mm- 10mm max with good temperature signals as it is intended to be used in real life
- Simulations using realistic heating times provide adequate results in the 40mm CFRP-PET-CFRP sandwich component. However, any defects below the 5mm skin depth and behind the core were not visible.

- Heating time of 0.1 sec was used mostly with heating pulse that was equivalent to 3-6 KJ on the sample area 0.09 m^2
- The long observation times (40-60sec) that were used were mainly in order to see how many rows of defects are detectable. Typically, pulsed thermography is very fast in progress and does not include such long observation.
- Row #5 remained undetected
- Additional image processing of short observation time simulations did not provide better detectability of row#3 or 4#. Therefore, the results from SP11 PCA and FT data processing are given below.

Figure 43 PCA processing from simulation SP11 using heat pulse density 666000 W/m^2, heating time 0.1 sec and 20sec total time

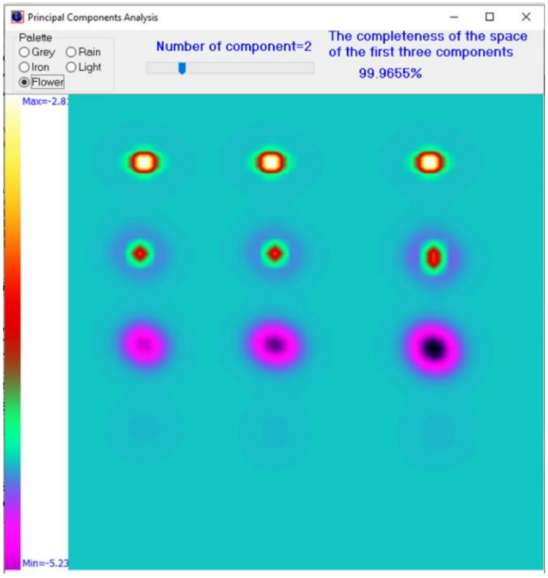

Figure 44 FT from simulation SP11 using heat pulse density 666000 W/m^2, heating time 0.1 sec and 20sec total time

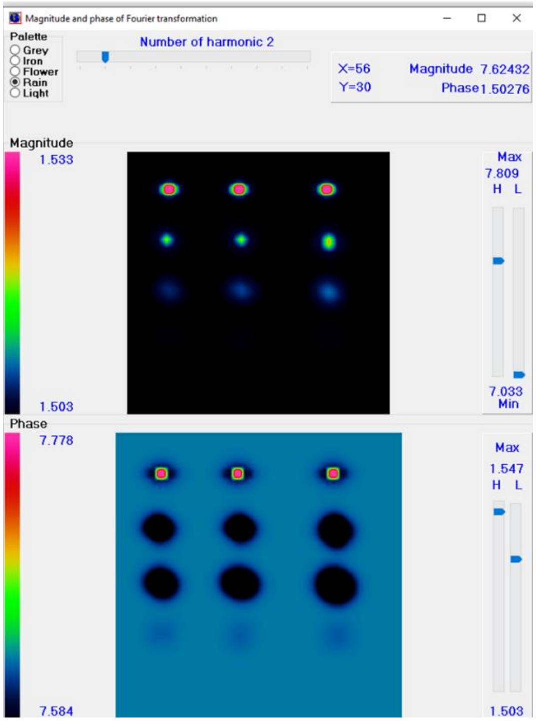

4.3 Ultrasonic testing modelling, simulations and results

The following section contains the principles that were used in the ultrasonic modelling and simulations

Finite Element Method (FEM) in Composite plates

Comsol 5.6 software was used to carry out the FEM simulations the has been used. In general, FEM methods were developed as an alternative for solving Partial Differences Equations (PDE). The idea of FEM tools is to discretize PDE problems to be solved by algebraic equation system (AES).

The PDE that are presented in many fields of physics and engineering, have spatial derivates of second order and time derivates of a second and first order (hyperbolical and parabolic equations), except for the elliptic case where only spatial second order derivates are used. This way of presentation of many laws of physics could be expressed as ***strong formulation.*** Although, Comsol presents a view of these equations, the software does not use them in this form. Instead, the Galerkin Methods is used where the PDE is transformed in an integral version named ***weak formulation***. This weak formulation has only spatial derivatives of the first order which it is a great advantage because it can use function base to approximate the solutions that cannot be used under the strong form. For this Galerkin method, piecewise polynomial functions such as Lagrange polynomials are employed.

For the case of time derivate, the same strategy is not available in Comsol. For this case a finite difference method is used with several algorithms that were developed from the actualization of Comsol version. The last case is the Discontinuous Galerkin method, which is a very efficient algorithm that is used in this report for the case of the solution of the acoustic wave equations.

As mentioned before, Comsol considered that the solution is expressed as a linear combination of special base functions that are introduced in the weak formulation. In this process a mesh of the dominium is developed based on the defined size of the approximate expansion on these base functions. From this process, the AES is obtained from the linear combination which must be solved using the algebraic lineal method.

The AES has a matrix whose size depends on the domain and the order of the polynomial base. In the case of Galerkin method used in Comsol, the piecewise polynomial base has an interesting property: it is localized in geometrical space which means that every base function has a value equal to one on the mesh associated point and decreases to zero in the point close to it. This makes that the matrix A is sparse, which means that have many zeros on it. This is very convenient for software tools and for the memory used by the software.

In order to solve the AES, Comsol introduces two methods from lineal algebra: the Direct Method and the iterative method, the first one is used for 1D and 2D cases while the second in cases where the size of the matrix A is large. The current simulations used the Direct Method.

Figure 45 shows the principal screen of the Comsol software. The model builder is located on the left side, where the user defines the processes involved in FEM: geometry, material, physical model, mesh. The middle part shows details of the settings while the right side shows the geometry and the results according to the model created.

Figure 45 Comsol software

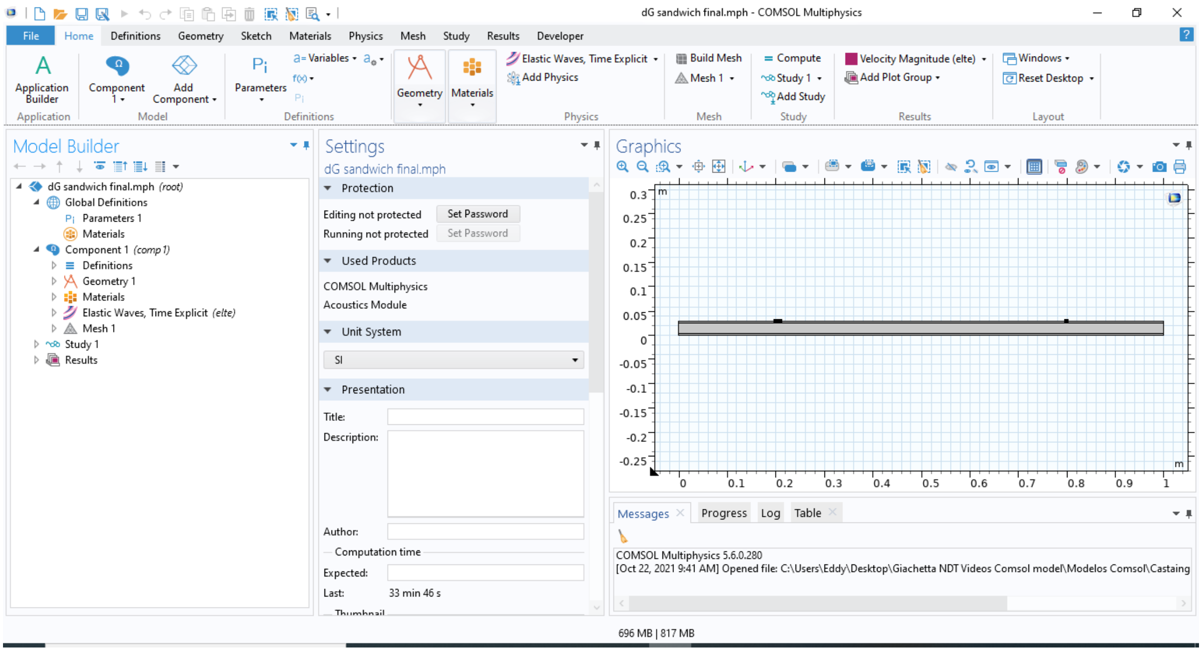

Source: Comsol own software

In the case of wave propagation in composite materials the *Elastic Wave, Time Explicit (elte)* model has been used. This is a novel model incorporated after the 5.5 version of Comsol. It incorporates what is called the Discontinuous Galerkin Method or dG. With this model, it is possible to describe the pulse propagation in several conditions including orthotropic material.

Two configurations were studied: the monolithic CFRP composite and the sandwich composed of two layers of CFRP with a PET foam core. A total of six FEM models were developed and are presented below.

A secondary software was used to carry out some additional simulations using the pulse echo ultrasonic technique on the monolithic component. To carry out this task, the SimNDT software was used, which is an open source UT simulation software. Figure 46 shows the SimNDT software environment. The left side shows the user defined parameters of the specimen that is modelled, while the right side shows the specimen with a 10x1mm (width, height) defect. The SimNDT software offers simplicity where the user can define some material properties and create defects with certain material properties. The defect that was modelled in this case was an air gap in order to simulate a delamination. Hence, the user can define the transducers size that will be used in the simulations, the type of pulse to be used, amplitude and frequency.

Figure 46 SimNDT software environment

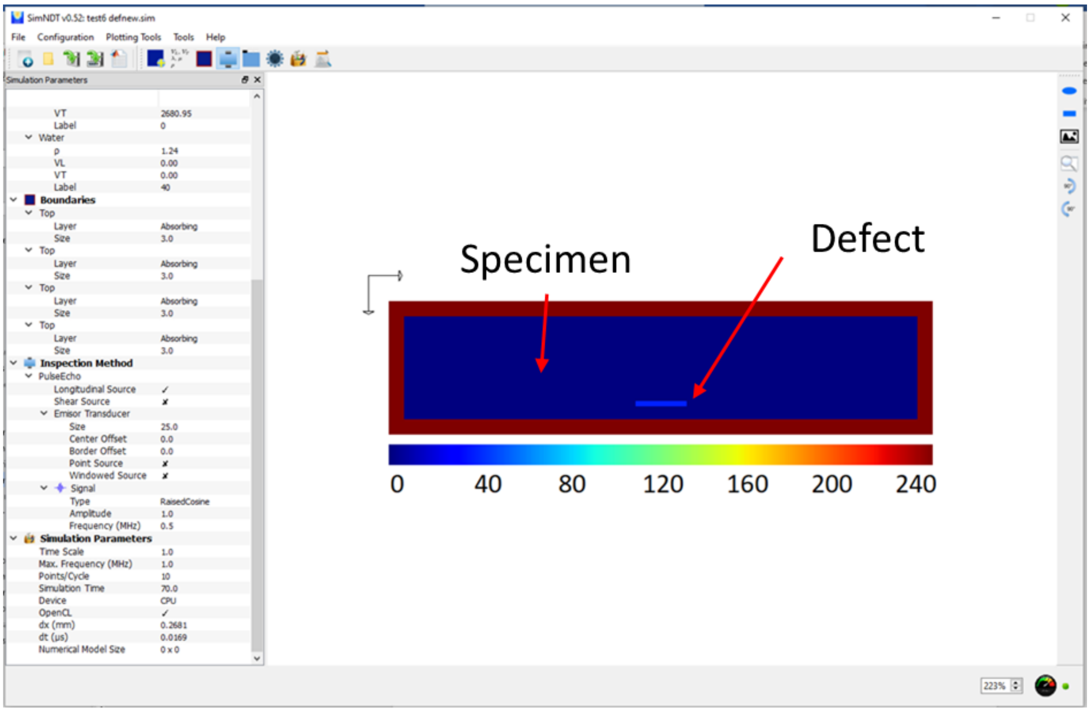

Source: SimNDT own software

4.3.1 Ultrasonic testing of CFRP monolithic material

In this case an orthotropic model was developed in Comsol 5.6 using the ***Elastic Wave, Time Explicit (elte)*** model, which is based on the discontinuous Galerkin method. The following table shows the material values.

Table 18 Elastic and density for CFRP in Voigt notation.

Density [Kg/m^3]	C_{11} [GPa]	C_{12} [GPa]	C_{22} [GPa]	C_{66} [GPa]
1600	250	9	12	5

Source: Castaings (2001), Hosten (2001)

For the case of a plate with a 1 mm thickness the following dispersion curves were obtained (Graph 37).

Graph 37 Dispersion curve for phase and group velocity of CFRP of 1 mm thickness obtained in Matlab

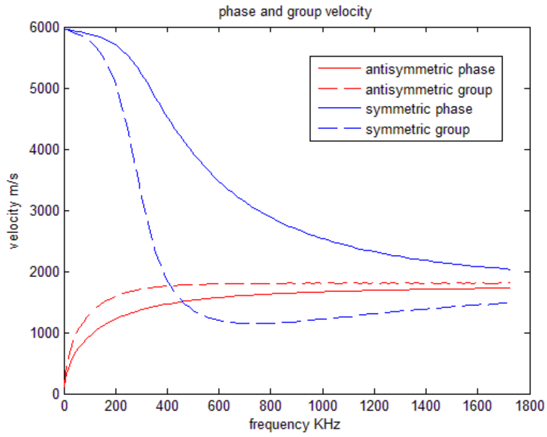

According to the previous curves it was decided to use an excitation pulse of 500 KHz.

Graph 38 shows the pulse form applied as excitation Tx with its spectral frequency.

Graph 38 Pulse of excitation for 500 KHz simulation experiment from Matlab (Left). Frequency spectral of the pulse from Comsol (Right)

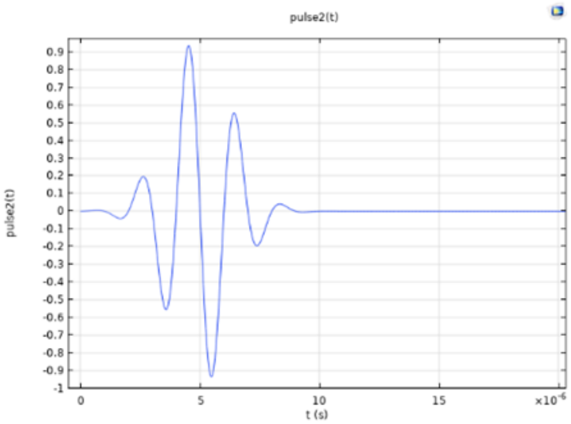

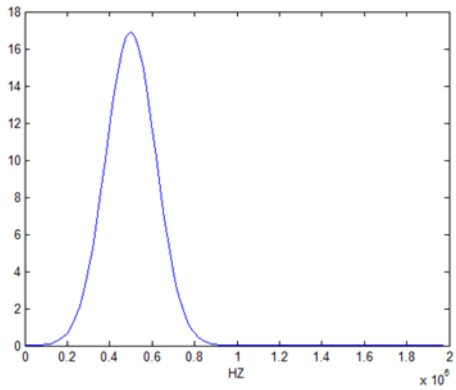

Figure 47 shows the geometry considerations used for the monolithic CFRP sample. The excitation pulse was applied in longitudinal and shear directions as shown by the blue arrows in Figure 47. The red arrow shows the reception position. The idea is to produce the S_0 and A_0 modes simultaneously in order to test the model.

Figure 47 Geometry considerations. Blue arrows show the two ways excitations at the same time. Red arrow shows the reception point. Thickness 2mm

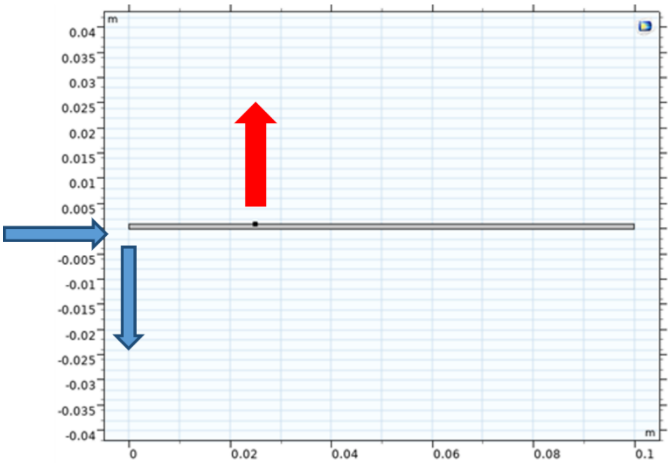

Source: own elaboration

Graph 39 shows the signal at the reception point of two velocity components. The longitudinal and the shear component. In both graphics the first signal corresponds to the symmetric mode and the second signal to the antisymmetric mode. As expressed above the idea is to check the first FEM model. The symmetric mode arrives first according to the dispersion curve because this mode has a higher value of group velocity. Also, the relative amplitudes of the signal agree the ultrasonic wave physics for both models (Martincek, 1975). Then it is possible to assume the validity of the model.

Graph 39 Left- Shear velocity component at reception. Right-Longitudinal velocity component at reception

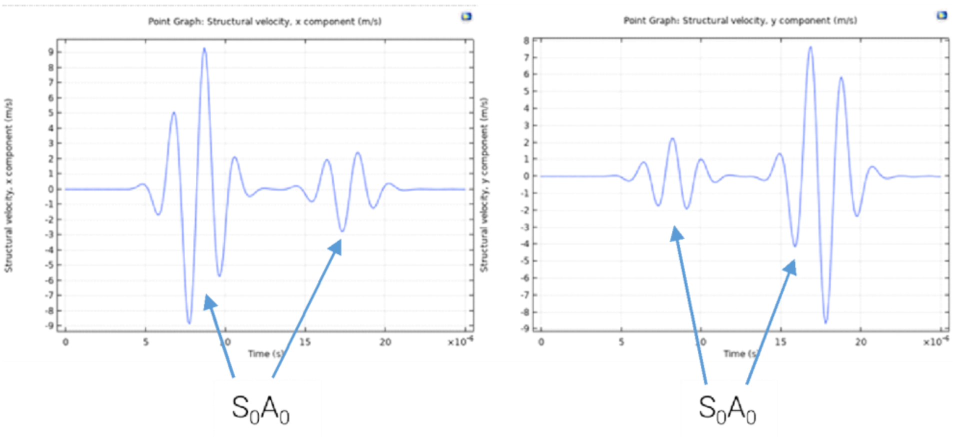

Source: own elaboration

Finally, Figure 48 shows the surface image of the two modes at 15 μseg, which is typical for the propagation of these two modes. Although this kind of excitation is not possible from the application point of view, it helps in the correct evaluation of the orthotropic FEM model.

Figure 48 Surface velocity at 15 µseg. It is shown the symmetric (right) and antisymmetric mode (left)

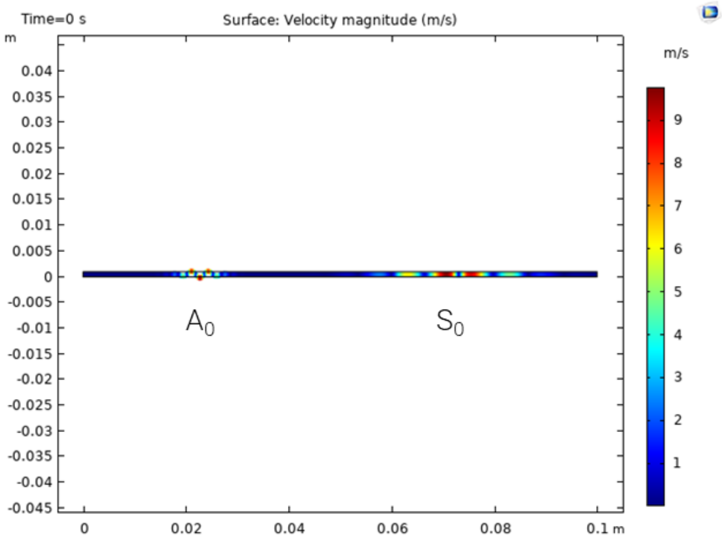

Source: own elaboration

In addition to the Lamb waves simulations as mentioned is section 3.3, additional pulse echo simulations were made on the 20mm monolithic CFRP specimen. Information on pulse echo method can be found on de Oliveira et al. (2021) and Tian et al. (2019).

A defect was introduced at a depth of 17mm, in order to test defects at depths that were beyond what was tested with IRT. The defect dimensions were 10mm x 1mm in order to be comparable to those used in the IRT models. An initial simulation was carried out without any defect in order to gain the pulse signal without any interference. A 25 mm transducer and a raised cosine pulse with amplitude of 1V and frequency of 0.5 Hz were used in both cases.

Figure 49. 20mm CFRP monolithic specimen with 10x1mm defect at 17 mm depth

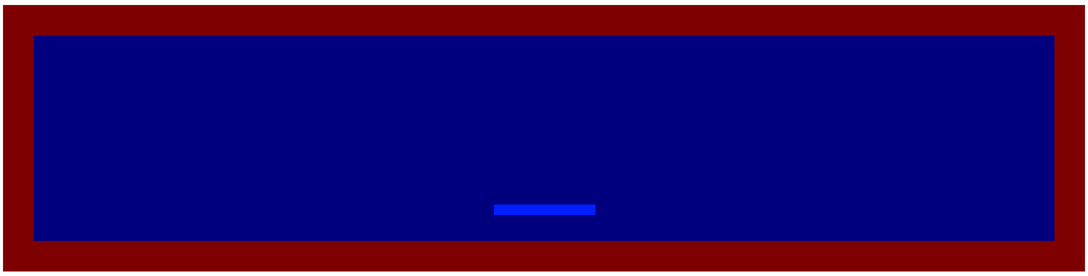

The results from the pulse echo simulation show that the defect is detectable. However, its location and size at the depth of 17mm causes energy to reflect back and forth between the transducer and the defect. This can be identified on both Figure 50 and Figure 51. On Figure 50, the left image shows the attenuation effect of the signal where there is no reflection from any defect. Figure 51 shows the C scans of the monolithic component taken from the simulations with and without defect. Figure 51-e shows the initial pulse energy reaching the defect, causing reflection of the energy back to the transducer (Figure 51-f and

g) while a portion passes through it.

Figure 50 Pulse echo receiver plot for cosine signal without defect (left) and with defect (right)

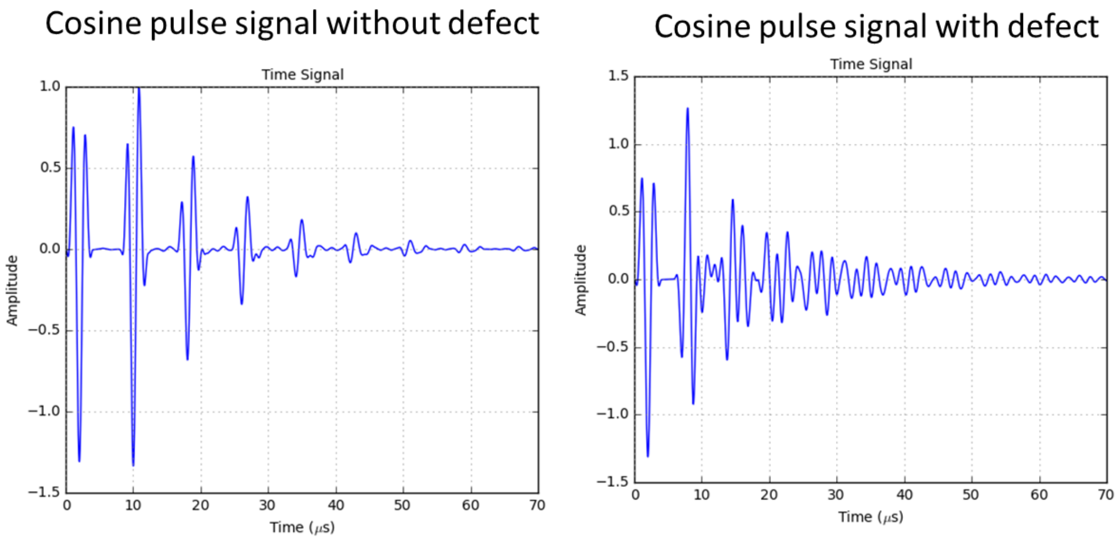

Figure 51 Pulse echo C scans during different moments of the simulation on the CFRP monolithic component. A-D C scans without defect, E-H with defect

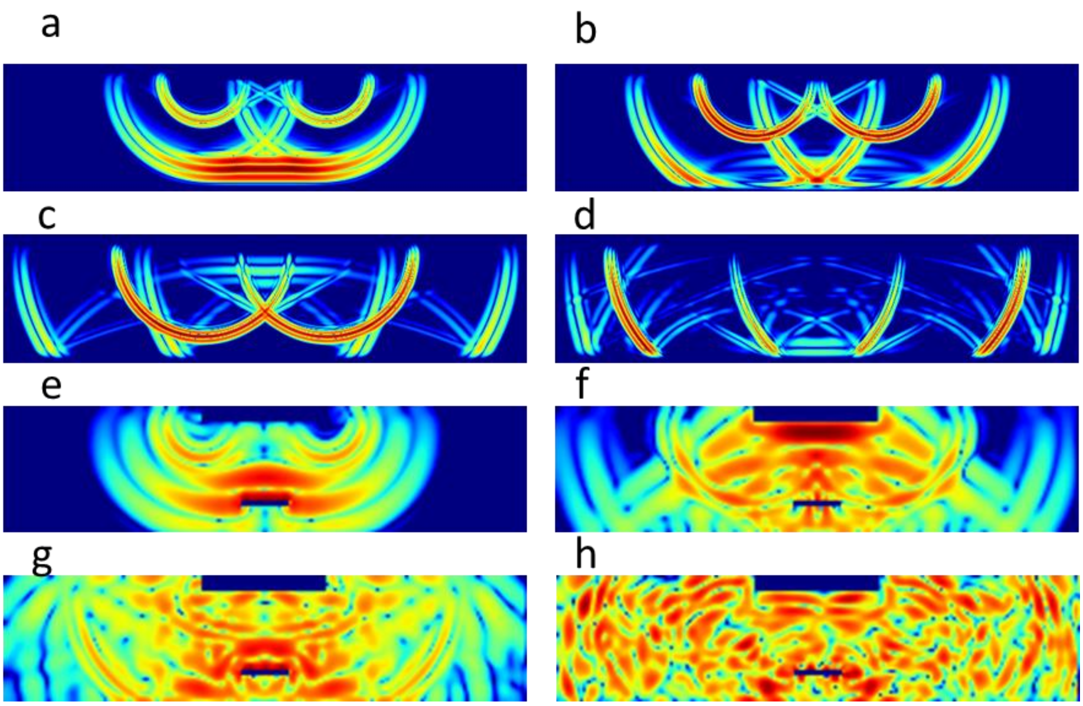

4.3.2 Ultrasonic testing of CFRP-PET-CFRP sandwich component

Case 1- Thin sandwich

Figure 52 shows a general geometric for a first sandwich model with 12 mm total thickness. The dimension was adopted according to samples that were offered by the European market to Dasel. The idea is to develop first the simulation and compare it with future experiments. The sandwich sample is composed by two layers of CFRP at the top and bottom and a core layer of PET foam. For the CFRP, it has been assumed to have orthotropic properties according as shown on Table 18. Table 19 shows the PET foam isotropic properties that were used in the model. Figure 52 also shows the configuration of the two transducers: the transmitter Tx that actuates the signal and the receiver Rx. Figure 53 shows a zoom version with the delamination that was modelled. The flaws observed in the sequence show two kinds of delamination models for the sandwich plate (SP) developed. SP with 10 mm of delamination in the upper boundary CFRP/PET, SP with 50 mm delamination in the same upper boundary CFRP/PET and SP with 50 mm delamination in the lower boundary CFRP/PET. All these cases represent the simulation work plan as it will be described below. One final detail, the Tx and Rx boundaries are delimitated each of them by two points. The distance between these two points is adjusted according to the frequency used by Zhongqing (2006).

Figure 52 Sandwich structure. Tx is the transmitter and Rx receiver. CFRP thickness=1 mm each. PET foam core thickness 10 mm

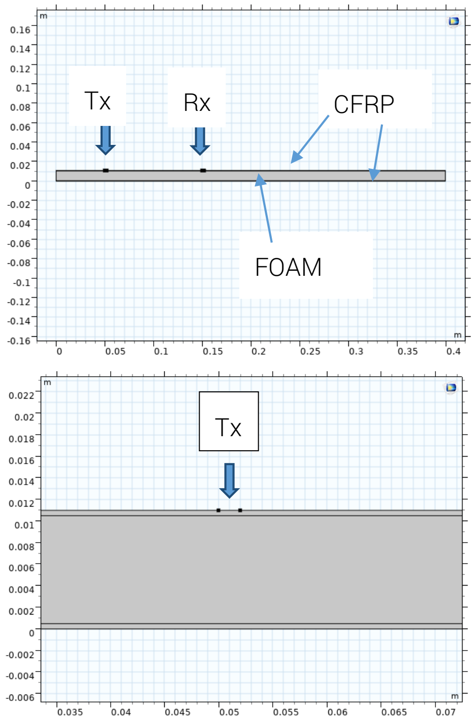

Source: Own elaboration

Figure 53 Delamination flaws analysed in the model developed.

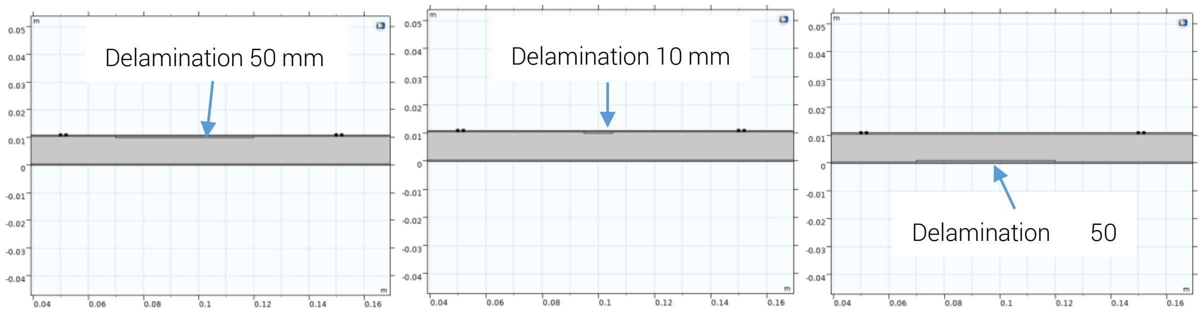

Source: Own elaboration

Table 19 PET foam core material mechanical properties

Density (kg/m^3)	Young Modulus (MPa)	Poisson ratio (μ)
60	100	0.35

Source: Vries (2009)

PET properties in Table 19 shows an acoustic situation where the material has a very low acoustic impedance relative to the CFRP. Graph 40 shows the dispersion curves associated to this material which reflect the fact of a relative low velocity/frequency modes compared with the CFRP layer material.

Graph 40 Dispersion curves of phase velocity for PET foam (blue curve-symmetric Lamb waves mode and red curve-antisymmetric Lamb waves mode) . Component thickness 10 mm.

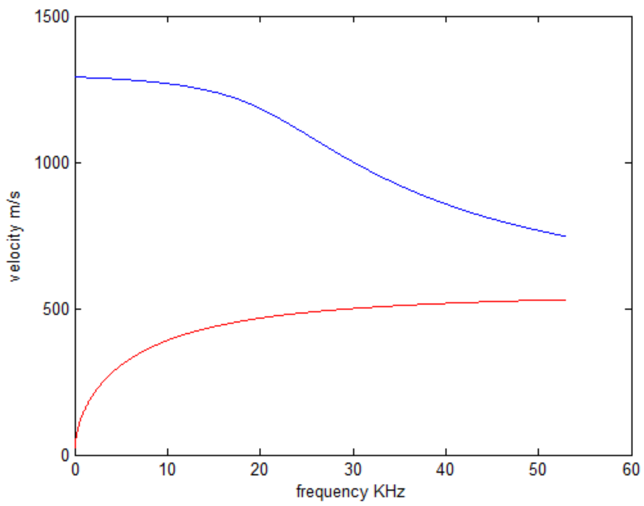

Two simulation frequency strategies were adopted for the geometrical configuration of Figure 52 and Figure 53. The first is to use a low frequency around few KHz (15 KHz) in order to produce low frequency Lamb modes, (the term "*Low frequency sandwich modes*" is used). In this case, it is expected that the Lamb waves propagate through all the plate body. The second is to use a higher frequency around hundreds of KHz (200 KHz) in order to produce ***Leakage Lamb waves*** (the term "*High frequency sandwich modes*" is used), similar to the previous case of monolithic CFRP. This second experiment should produce only Lamb waves at the top (or the bottom) layer with the leakage phenomena which is known as Generalized Lamb Waves (Martincek, 1975; Mason, 1958). The idea is to compare, these two ways of diagnostic for the sandwich component, in order to evaluate a better practical implementation from the point of view of ultrasonic technology.

For both simulation strategies, Graph 41 describes an example of the excitation pulses of approximately 8 cycles that were used. Only the fundamental frequency will be changed for each case.

Graph 41 Excitation pulse at Tx

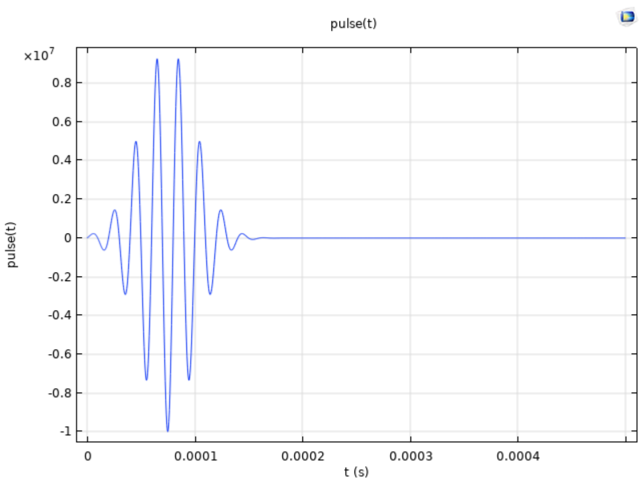

Case 2- Low frequency in thin sandwich

Figure 54 presents the two Repetitive Frequency (RF) signals that are excited at the time of 10 μseg traveling to both, left and right directions (blue arrows). The image shows the magnitude of velocity in a deformation view. At this low 15 KHz frequency, it can be observed that the plate moves as a whole, which includes the CFRP layers and the foam core.

Figure 54 Surface velocity at 10µseg. Frequency 15 KHz. No defects were considered on this first simulation. Red arrow represents the pulse excitation. The blue arrows the two signals emerged from this point.

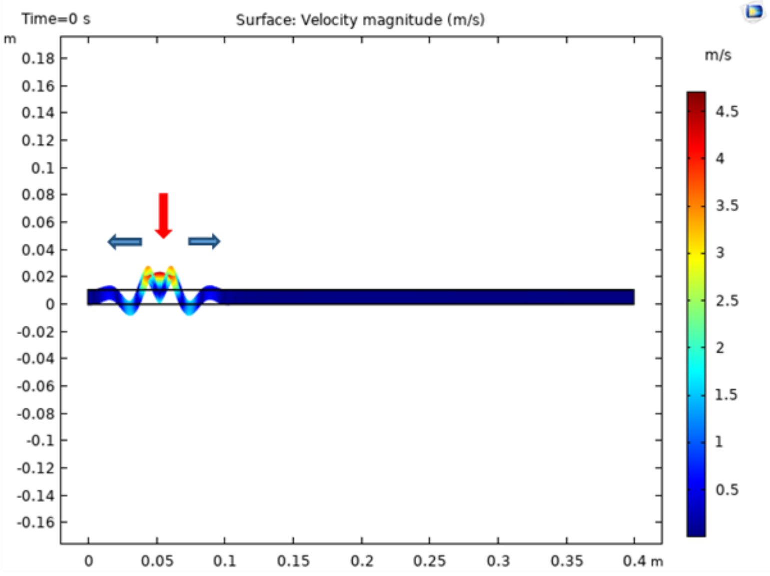

Graph 42 compares the flawless signal with delamination signals situated above (two length 10 and 50 mm) and below (only one length 50 mm) as shown in Figure 53.

Graph 42 RF signal obtained at the receiver position Rx. Left shows the flawless case with the delamination above at two length sizes. Right shows the same flawless case compare with one delamination below.

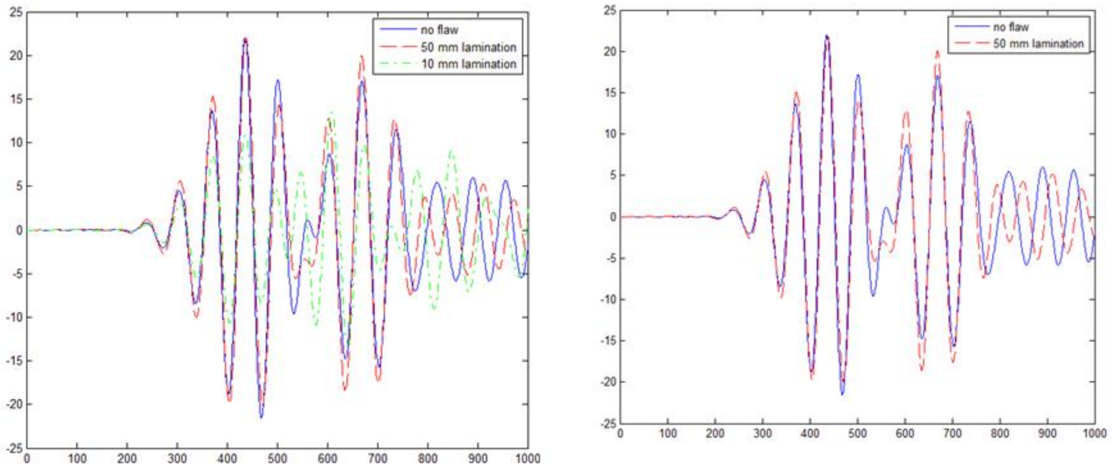

Some changes relative to amplitude and time shift can be observed from the graph. The blue case could be considered as a fingerprint of the plate at good conditions. An algorithm could be developed in order to compare signals and several flaw conditions. Nevertheless, it is not easy to determine the flaw size from this low frequency method. In any case the model could help in a future frequency study for this geometry and others with several flaw conditions.

Case 3-High frequency thin sandwich

Figure 55 shows a similar condition as in Figure 54. The main difference is the high frequency used for this case. In fact both modes, the low and high frequency, are similar from the FEM point of view. Of course, the mesh is adapted according to the frequency value.

Figure 56 displays an interesting wave propagation phenomena phenomenon. In this case there is an A_0 Lamb waves that propagate only at the surface given by the CFRP layer. As it can be seen in Figure 55 the Lamb mode leakage part of its energy to the rest of the plate fundamentally made by the foam material. Up to this simulation case there is no deformation of the lower CFRP layer.

There is another detail and it is the attenuation produced by the leakage. It is greater than the previous low frequency case.

Figure 55 Upper left surface velocity at 40 μseg. Frequency 200 KHz. Left zoom of the previous graphic. No flaws are considered yet on these simulations

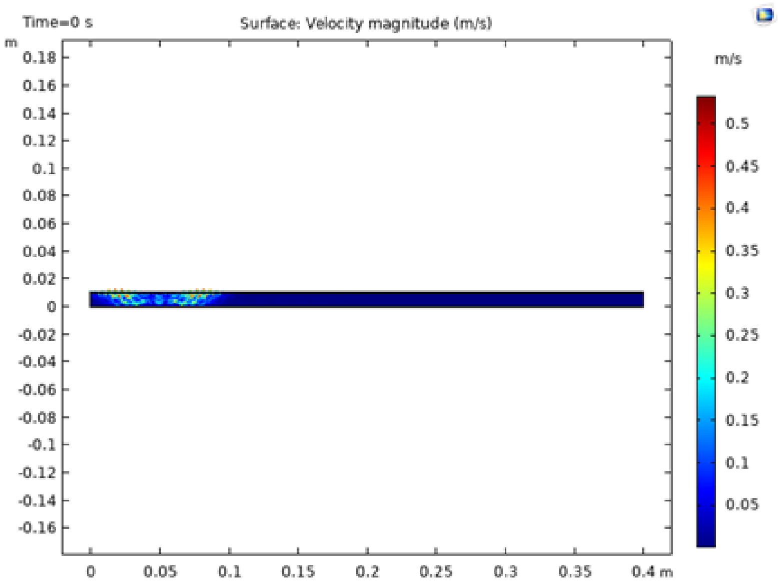

Source: own elaboration

Figure 56 Magnification of the propagation on the 50 mm of delamination

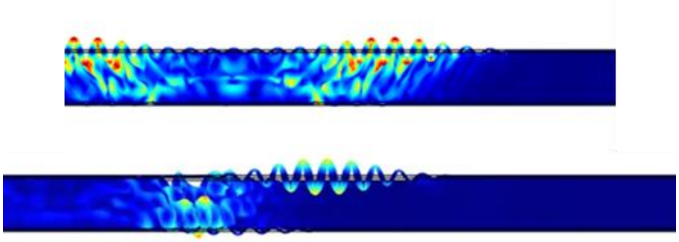

Source: own elaboration

However, in Figure 56 an interesting case of wave propagation for the 50 mm of delamination can be observed. There is a second A_0 Lamb wave mode that propagate on the lower layer of CFRP. It also should be noted that for the case of delamination the attenuation is lower than for the case of flawless case.

Graph 43, compares three situations of flawless and delamination in the upper CFRP layer. In this frequency range it seems to have a better resolution compared with the previous low frequency case. For the lower delamination, Graph 44 shows a similar situation compared with the previous case. In both graphs it is clear that the delamination increases the amplitude of the signal. This is a consequence of the fact that in the plate there is no leakage when a delamination is present.

Graph 43 Top CFRP skin 50mm delamination in CFRP-PET foam sandwich component

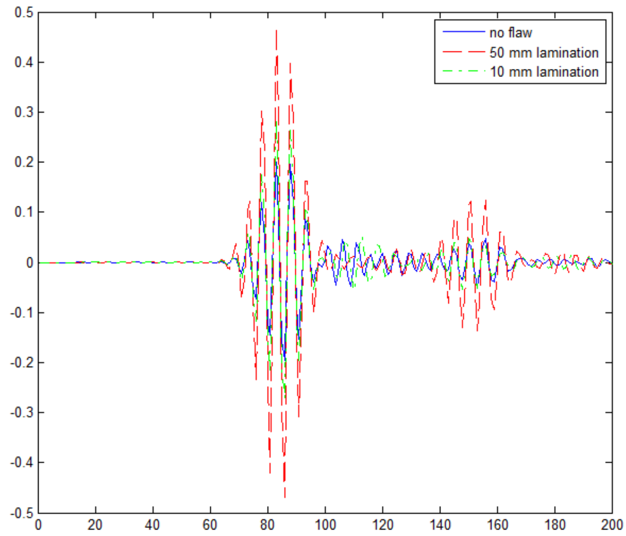

Graph 44 Bottom skin 50mm delamination in CFRP-PET foam sandwich component

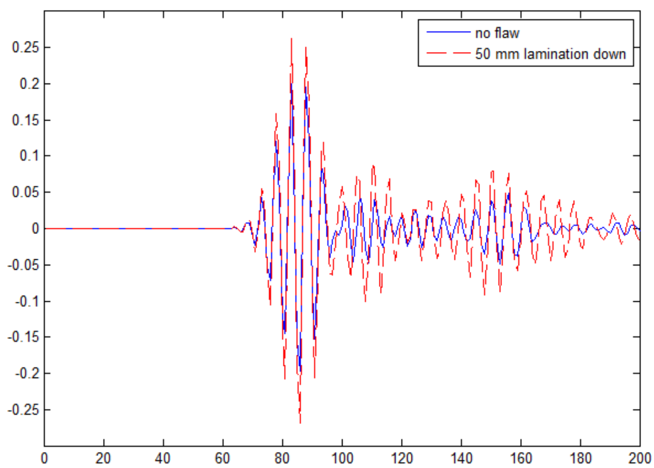

Case 4- High frequency thick sandwich

The last simulations were based on the PIVOT2 material specification which are much thicker that what has been tested so far. Therefore, simulations have been also performed in this kind of samples. Figure 57 shows this new case where the thickness of the sandwich component increased to 40 mm, using two CFRP skins with 5mm thickness and a 30 mm foam core.

In this case similar results as the case above were expected, with a shift of the possible ultrasonic frequency that could be used. In this case four reception points were added compared to one in the previous case. In this manner, it is possible to obtain a measurement of the phase velocity according to the frequency imposed.

Frequencies ranging from 100 to 200 KHz were used in the simulation. It is important to note that 200 KHz is preferred according to the air transducers that could be used in experimental testing during this project.

Figure 58 shows the first results on the excitation for this last frequency on the point Tx on the surface. Similar to the previous case, two signals are generated on both sides of the sample. The zoomed version however shows another characteristic. In this case there is an S_0 mode generated joint with the A_0 mode. This is a consequence of the fact that this sample is thicker that the first examples. Of course, this is not a good situation for time measurements because there are two modes mixed in the sample.

Figure 57 Case 4 simulation sample, 5 mm CFRP skins and 30 mm foam core. Total thickness= 40 mm. Right picture shows a magnification from the reception region.

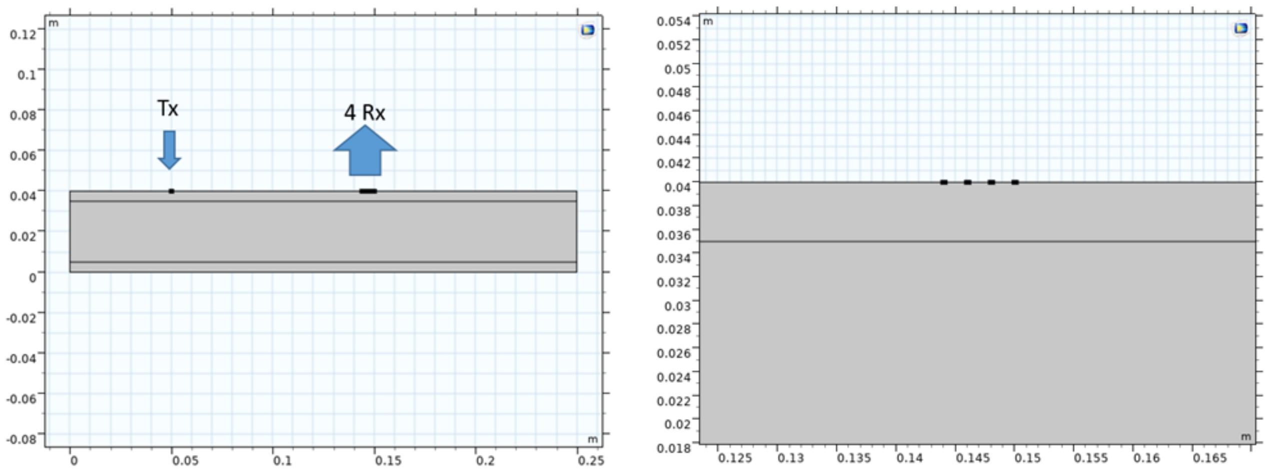

Source: own elaboration

Figure 58 Results at 200 KHz of the emission of Lamb waves at the initial moment. The perpendicular arrow (left) shows the Tx point

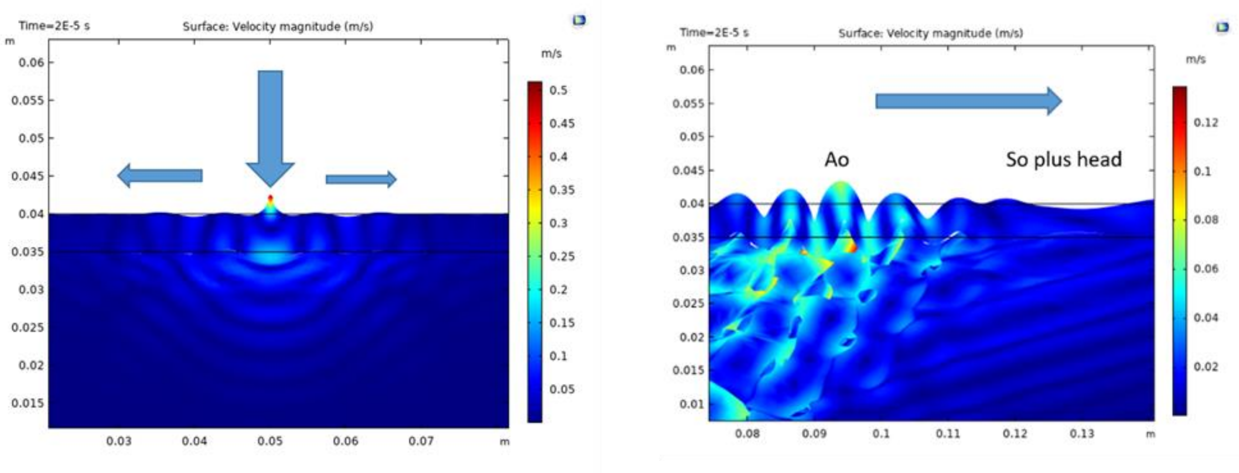

Source: own elaboration

Graph 45 shows the displacement of the four reception point in both x and y axes for 200 KHz frequency. As we can see the influence of the S_0 is very strong with a high interference of the A_0 mode. However, from the first cycles of the A_0 mode, a velocity around 1610 m/s has been obtained. This of course correspond only to the CFRP layer, because as we shown in the thinner case at this frequency it is only possible to test the upper CFRP layer.

Graph 45. Displacement of the 4 points at reception. Frequency 200 KHz. The circle shows the region for the phase velocity method.

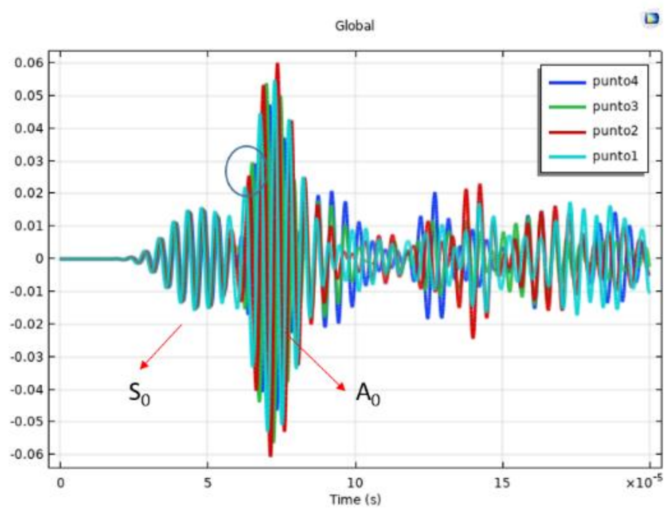

Similar experiments were performed at 100 KHz. Graph 46 shows similar results compared with the previous case. But in this case the amplitude of the S_0 mode is lower than the 200 KHz case. A velocity around 1500 m/s was obtained, which is lower than the previous case as expected for this A_0 mode.

Graph 46 Displacement of the 4 points at reception. Frequency 100 KHz. The circle shows the region for the phase velocity method

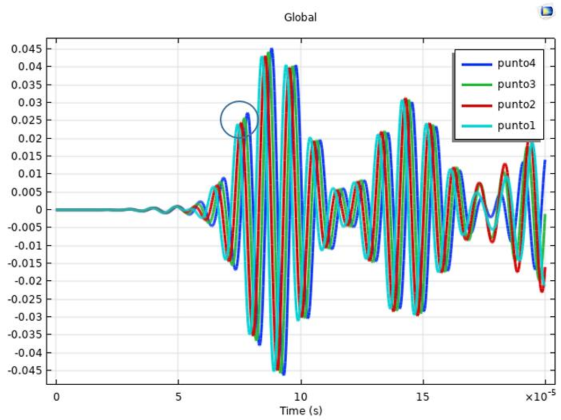

Delaminations of 50 mm and 150 mm were simulated according to the graphic displayed on Figure 59. With these examples several experiments were performed in order to obtain the velocity for all these cases. However, the results show no velocity differences from these samples. This is a consequence of the fact that the foam has a low impedance compared with the CFRP layer, so practically it could be considered as a free boundary load to this layer.

Figure 59 Delaminations samples simulated; Left 50 mm delamination. Right 150 mm delamination

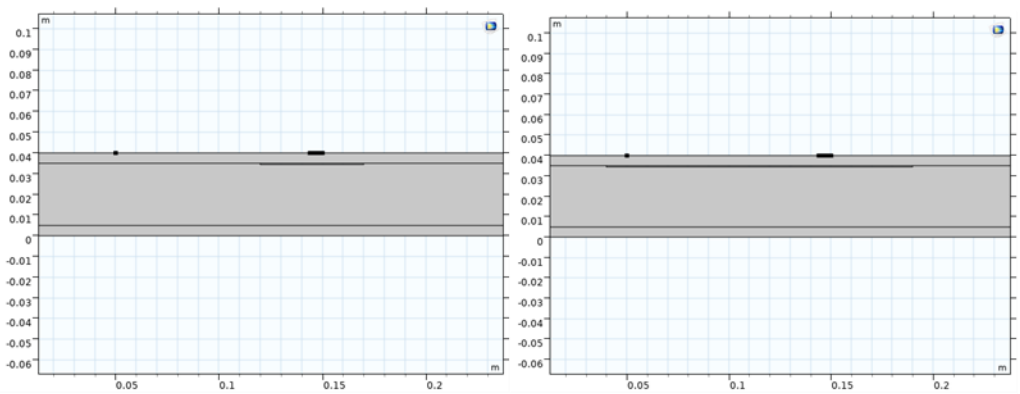

Source: own elaboration

Finally, Graph 47 shows, the results of the amplitude difference for no flaws and delamination cases for frequencies of 100 and 200 KHz. In both cases there is an influence on amplitude parameter. Only the 200 KHz case shows the additional S_0 signal at the beginning of the pulse. Therefore, it is expected that the amplitude parameter could be used for delamination detection, like in the thinner previous case.

Graph 47 Influence of the delamination on the signal's amplitude at last reception point. 100 KHz left and 200 KHz right

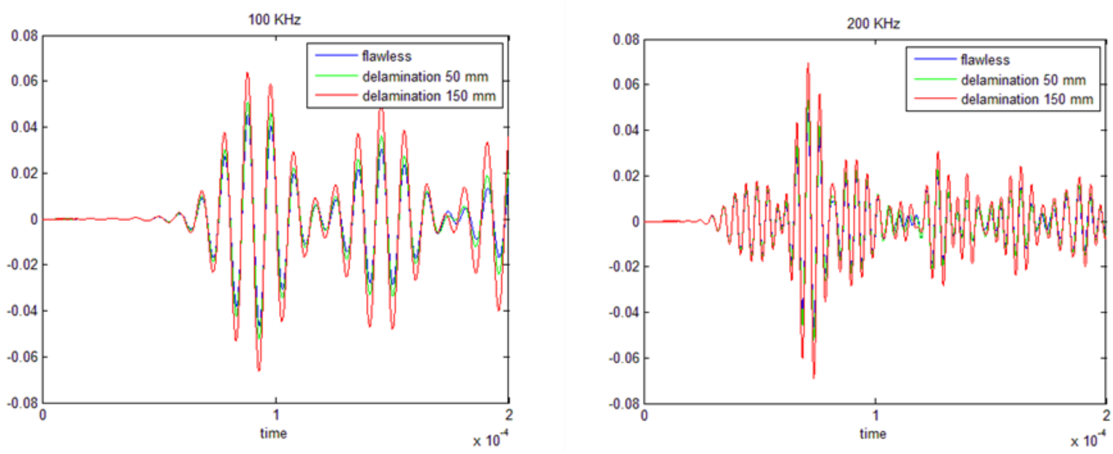

It is important to note that lower frequency methods have not been simulated because it is expected because they are very low for ultrasonic technology use.

5 Conclusions

Based on the potential NDT methods that were reviewed in D1.1."Terms of Reference, Requirements and Specifications for Carbody Inspection Technology" the current deliverable D 2.1 aimed to explore further the suitability of active thermography and ultrasonic testing techniques for the inspection of composites components that will be used in the PIVOT2 composite carbody shell. To carry out this task, finite difference and finite element analysis software such as ThermoCalc 3D, Comsol and SimNDT were used for modelling and simulating these NDT methods.

D2.1 created models of the composite components that were based partially on dimensional specifications (thickness of the components) from PIVOT2 as well as thermal and mechanical properties from literature. This fact alone means that the actual PIVOT2 prototype could differ, thus making the simulations mostly a tool to test the ability of IRT and UT techniques in detecting defects in these defined specimens.

A monolithic CFRP component of 20mm thickness and a sandwich component of CFRP with a PET foam core of 40mm thickness were modelled. Delaminations of various sizes were introduced in the components to simulate potential damage or defects. The dimensions of the defects/damages aimed to test the capability of the inspection methods to detect even small defects.

Optical pulsed and lockin thermography were simulated using heating functions that ThermoCalc 3D offers. Both thermography techniques showed that the components are extremely thick and that they will require extensive heat and observation time in order to detect deep defects.

In the case of the monolithic component, defects up to 15 mm of depth were detected. However, these were only identified using optical lockin thermography with fast heating wave period and long overall heating process of 2 minutes. This is probably due to the component thickness and the thermal conductivity that were used in the sample. On the other hand, pulsed thermography was only able to detect defects/damage up to 10mm depth and was simulated with long heating pulses compared to real life experimental practise.

For the sandwich component the results were in line with those from the monolithic specimen. The fact that the CFRP skins were 5 mm thick made the task easier. Defects up to 5mm were detectable with both pulsed and lockin thermography methods. Any efforts to detect deeper defects between the back CF skin and the core were unsuccessful. In fact, PET foam is an insulating material so it would be difficult for heat to propagate through and reach the back side.

Although simulations are a good tool for testing whether specific settings or techniques will work, they remain a theoretical tool. In addition, IRT simulations did not have any noise. This means that detection of defects with very low temperature signal would have not been detectable in real life. Also, the assessment of how many defects an IRT simulation could detect was mostly qualitative i.e. 6/12. This means that, as long as the simulation gave some detection of a temperature signal (at least above 0.01), the defect was considered as detected. In actual lab experiments, a very low temperature signals of 0.03 °C or even less, as it was observed in many cases during the simulations especially for deeper defects, would mean that they are undetectable by the IR camera, unless the IR camera had a very low NETD (Noise Equivalent Temperature Difference) of less than 30 mk. Even with a low NETD IR camera, noise of ± NETD/2 would make many of these defects undetectable. What can be concluded from the IRT simulations is that further experimentation is required in a lab environment in order to test further the capabilities of the aforementioned IRT methods with such thick composites. This work will be described in D 2.2 "Development of inspection approaches" that will include the lab experimentation based on actual samples that will be fabricated with defects and inspected using optical pulsed and lockin thermography. As already mentioned, data processing using algorithmic processing is also meant to be applied during the lab experiments and will help improve detection of the defects/damage in the actual samples.

In terms of the ultrasonic testing simulations, the work that was carried out in Comsol and SimNDT gave some promising results for both composite components. Six FEM models were presented. Two were for the monolithic CFRP, while the remaining models were for the sandwich structure. The UT simulations focused on the use of Lamb waves and presented their usage for the detection of delaminations. Since the UT simulation results rely on theoretical material properties from literature, they can only be taken as a theoretical demonstration of the capabilities that these UT techniques will have on the actual PIVOT2 carbody prototype. The most important, the models are already done for studying other cases which could include several flaw considerations. The novel FEM method of discontinuous Galerkin is good enough for this purpose.

Expected values for low frequency Lamb is less than 15 KHz which is far from the ultrasonic technology. Hence it is expected that only high frequency values above 100 KHz could be used in the actual ultrasonic technology. However, the simulations showed that only the top skin of the CFRP sandwich could be tested. The low impedance of PET foam creates a challenge for the possible use of contactless air transducer. Finally, other methods, such as phase array or pulse echo technique, cannot be used on the composite sandwich component. Instead, the pulse echo method was used on the monolithic component to prove that this technique can detect deep defects.

It is also important to understand that the NDT techniques will supplement each other in the field. Thus, the defects that are undetectable with one method will be easier to be detected with another. This will be the work of D 2.2 "Development of inspection approaches" and WP3 "Development of prototype equipment for inspection of carbody shell"

6 References

Ameen M., Xiaochan W, Yaseen M, Umair M., Yousaf K., Yang Z., Soomro S.A., (2018), Performance Evaluation of Root Zone Heating System Developed with Sustainable Materials for Application in Low Temperatures, Sustainability 2018, 10(11), 4130 doi:10.3390/su10114130

Armacell (2021), Technical Data ArmaPET struct, https://local.armacell.com/fileadmin/cms/pet-foams/ArmaPET_website/Product_Flyer/ArmaPET_Struct_GR.pdf

Avdelidis N.P., Almond D.P., (2004), Through skin sensing assessment of aircraft structures

using pulsed thermography, NDT&E International 37, pp. 353–359

Castaings M., Hosten B., (2001), Lamb and SH waves generated and detected by air-coupled ultrasonic transducers in composite material plates, NDT&E International 34 249±258 Elsevier.

Castaings M., Predoi M.V., Hosten B., (2005), Ultrasound propagation in viscoelastic material guides. Proceedings of the COMSOL Multiphysics User's Conference 2005 Paris.

De Oliveira B.C.F, Marció B.S, Flesch C.C. R (2021), Measurement, Vol 167, 108445

Design Academy (2021), https://www.designtechcadacademy.com/index

Diab (2021), Divinycell PNbrochure, https://www.diabgroup.com/media/dyblo00w/diab-divinycell-pn-september-2021-rev13-si.pdf

Dib G., Larche, R.M., Prowant S., M., Jacob E.R., Ramuhalli P., Diaz A.A., (2018), Ultrasound Modelling and Simulation: Status Update, U.S. Department of Energy, https://www.nrc.gov/docs/ML1901/ML19010A072.pdf

Diamanti K., Hodgkinson J. M. and Soutis C., (2004), Detection of Low-velocity Impact Damage in Composite Plates using Lamb Waves. DOI: 10.1177/1475921704041869. *Structural Health Monitoring,* 3: 33.

Diamanti K., Soutis C., Hodgkinson J.M. ,(2005), A Non-destructive inspection of sandwich and repaired composite laminated structures. Composites Science and Technology 65 2059–2067.

Diamanti K., Soutis C., Hodgkinson J.M., (2007) Composites: Part A 38 1121–1130. Elsevier.

Diamanti K., C.Soutis., (2010), Structural health monitoring techniques for aircraft composite structures, Progress in Aerospace Sciences 46, 342–352 Elsevier.

Ibarra-Castanedo C. , Piau J.M, Guilbert S., Avdelidis N., Genest M., Bendada A. (2009), Comparative Study of Active Thermography Techniques for the Non-destructive Evaluation of Honeycomb Structures, Research in Non-destructive Evaluation 2009; 20(1):1–31.

Kazys R., Demcenko A., Zukauskas E., Mazeika L., (2006), Air-coupled ultrasonic investigation of multi-layered composite materials Ultrasonics 44, p819–p822.

Kalogiannakis G., Van Hemelrijck D., Longuemart S., Ravi J., Okasha A., Glorieux C., (2006), Thermal characterization of anisotropic media in photothermal point, line, and grating configuration, Journal Of Applied Physics, Vol. 100, pp 063521- 12

Kim J.S, Jeong J.C, (2006), Natural frequency evaluation of a composite train carbody with length of 23 m, Composites Science and Technology 66, pp. 2272–2283

Martincek G., (1975), Theory and methods of dynamic non-destructive testing of plane elements (in Slovak), Brastislava: Veda,

Mason W. Physical Acoustic and the Properties of Solids. D. Van Nostrand Company. Princeton, New Jersey, 1958

Moreno E., Galarza N., Rubio B., Otero J. A. (2015), Phase velocity method for guided wave measurements in composite plates. 43rd Annual Symposium of the Ultrasonic Industry Association, UIA Symposium 2014. Physics Procedia 63 54 – 60. Elsevier

Mustapha S., Ye L., Wang D., Ye Lu., (2011), Assessment of debonding in sandwich CF/EP composite beams using A0 Lamb wave at low frequency, Composite Structures, Volume 93, Issue 2, January 2011, p. 483-491

Petrov K. V, Muravieva O. V, and Gabbasova M. A., (2017), Mathematical Modelling of the Acoustic Wave Propagation Generated by the Through-type Transducer in a Cylindrical Object, International Conference on Information Technologies in Business and Industry 2016, *IOP Conf. Series: Journal of Physics*, Vol.803, 012114, doi:10.1088/1742-6596/803/1/012114.

Roll2Rail (2016), D 3.4 New Dependable Rolling Stock For A More Sustainable, Intelligent And Comfortable Rail Transport In Europe, http://www.roll2rail.eu/Page.aspx?CAT=DELIVERABLES&IdPage=45291e18-8d8f-4fd6-99f8-5d4b7a519b9c

S2R, (2019), Multi-Annual Action Plan, https://shift2rail.org/wp-content/uploads/2020/09/MAAP-Part-A-and-B.pdf accessed online 8/04/2020

Simscale (2021), https://www.simscale.com/

ThermoCalc 3D (2018), ThermoCalC 3D: Operation Manual- The software for computing 3D dynamic temperature distributions in anisotropic layered solids with subsurface defects.

Tian F., Hao Y., Zou Z., Zheng Y., He W., Yang L., and Li L. (2019), An Ultrasonic Pulse-Echo Method to Detect Internal Defects in Epoxy Composite Insulation, Energies, 12 (24), pp 4804, doi:10.3390/en12244804

Umar M.Z, Ahmad I., Vavilov V., Swiderski W., Hamzah Ab, R, Wan Abdullah W.S., (2008), Developing methodology of pulsed thermal NDT of materials: Step-by-step analysis of reference samples, NDT.net - The e-Journal of Nondestructive Testing, (May)

Vavilov V., Burleigh D. (2020) Infrared Thermography and Thermal Nondestructive Testing. Springer, https://doi.org/10.1007/978-3-030-48002-8_9

Vavilov V., Marinetti S., Pan Y., Chulkov A., (2016), Detecting water ingress in aviation honeycomb panels: Qualitative and quantitative aspects, Polymer Testing, Issue 54, p 270-280

Viktorov I., (1967), Rayleigh and Lamb Waves. Physical and Theoretical Applications. Plenum Press New York

Vries D. (2009), Characterizations of polymeric foams. Eindnoven Uniersity of Technology. Department of Mechanical Engineering. Mechanics of Materials. July

Watkins R., Jha R., (2012), A modified time reversal method for Lamb wave based diagnostics of composite structures, Volume 31, August, p345-354

Zhongqing S., Ye L., Lu Y.. (2006), Guided Lamb waves for identification of damage in composite structures: A review. Journal of Sound and Vibration, 295 753–780.

7 Appendix 1 Thermography simulations results for monolithic CFRP component

7.1 Optical lockin thermography- monolithic component

ML 1

Figure 60 Thermal image for simulation ML1 using Optical lockin: Heating density 3000W/m^2, Wave period 3s, Total time 30s

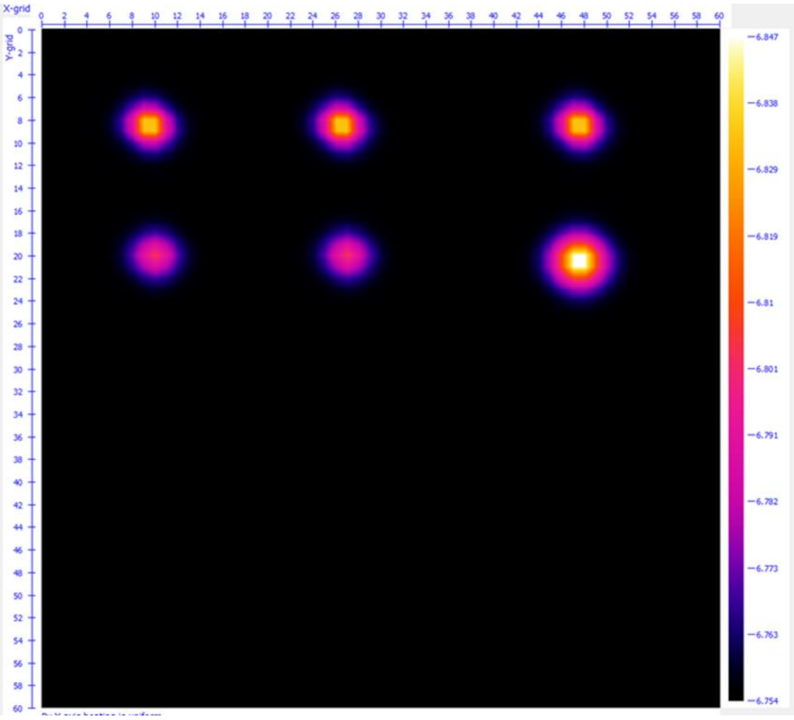

Graph 48 Space profiles of the different rows of defects using optical lockin simulation ML1 settings

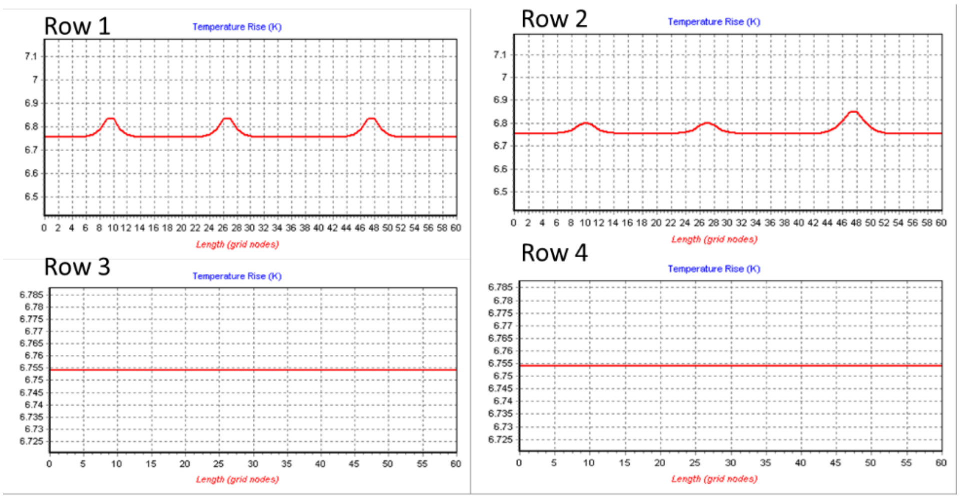

Graph 49 Delta T profiles for different rows of defects using optical lockin simulation ML1 settings. Row#1 in blue, Row #2 in green, Row# 3 in Orange and Row#4 in red

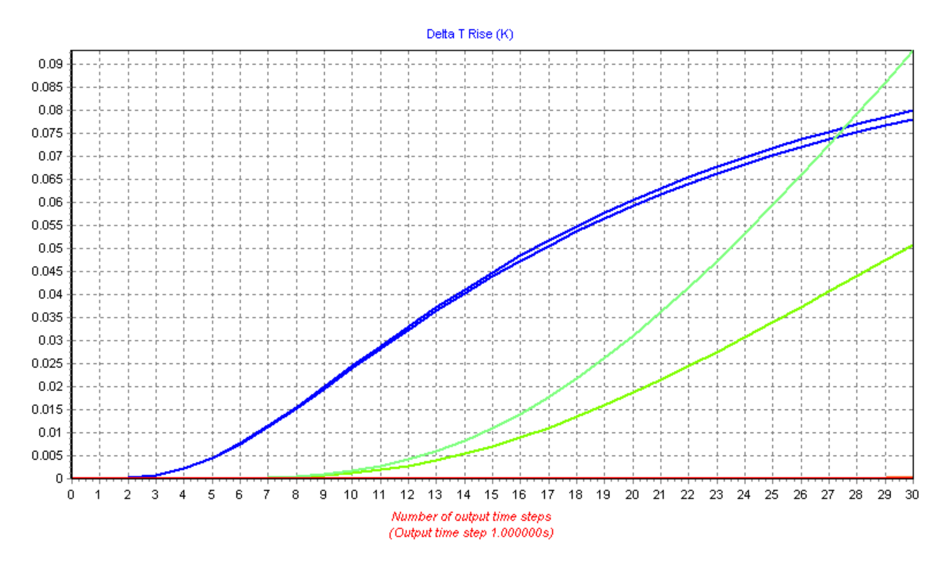

ML2

Figure 61 Thermal image for simulation ML2 using Optical lockin: Heating density 3000W/m^2, Wave period 3s, Total time 25s

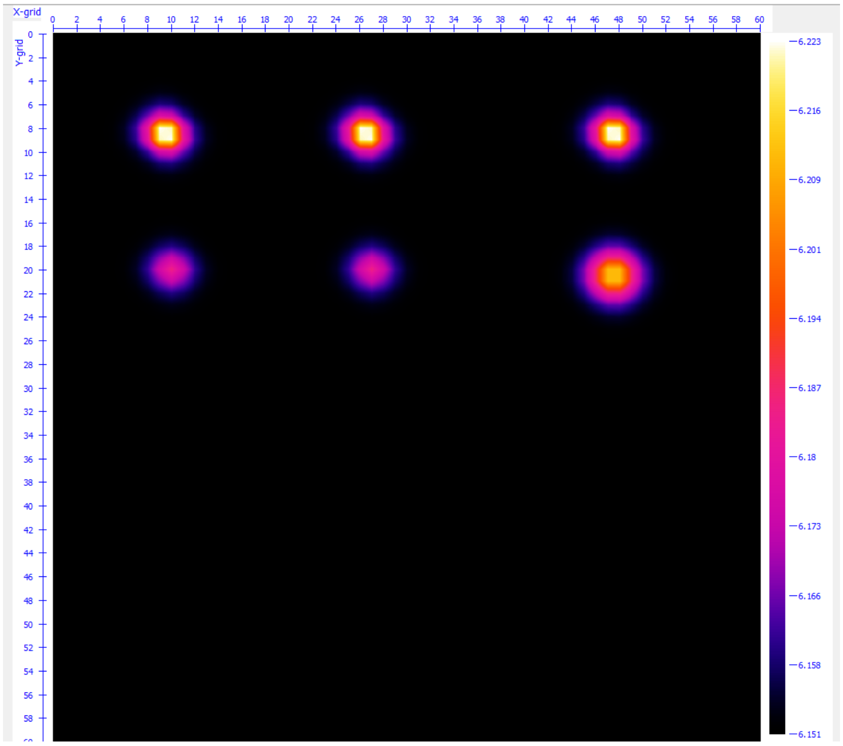

Graph 50 Space profiles of the different rows of defects using optical lockin simulation ML2 settings

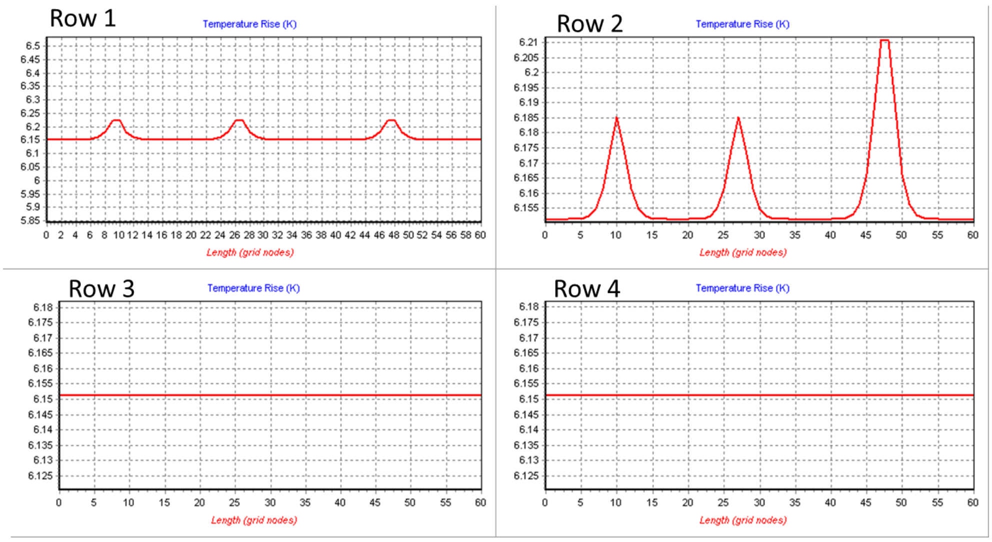

Graph 51 Delta T profiles for different rows of defects using optical lockin simulation ML2 settings. Row#1 in blue, Row #2 in green, Row# 3 in Orange and Row#4 in red

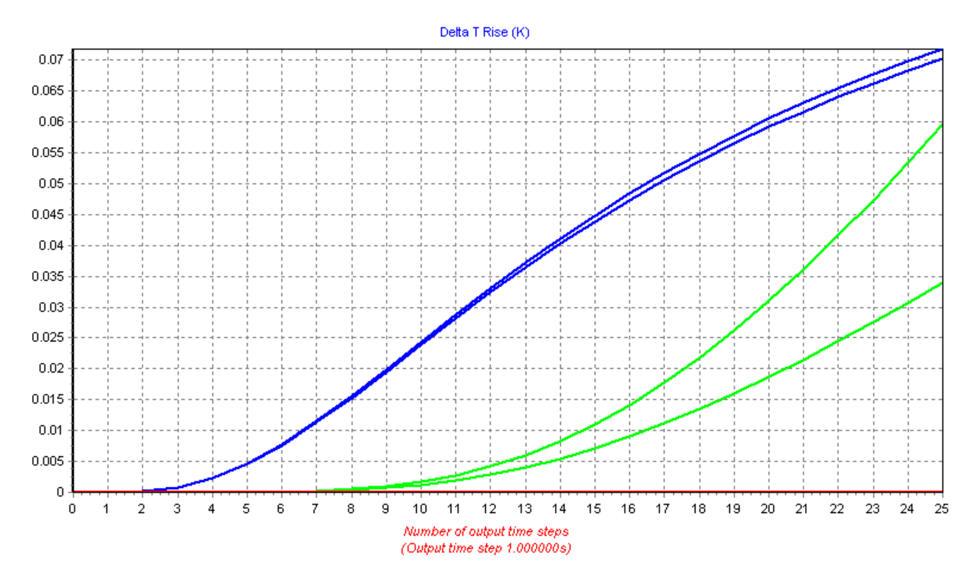

ML3

Figure 62 Thermal image for simulation ML3 using Optical lockin: Heating density 6000W/m^2, Wave period 5s, Total time 20s

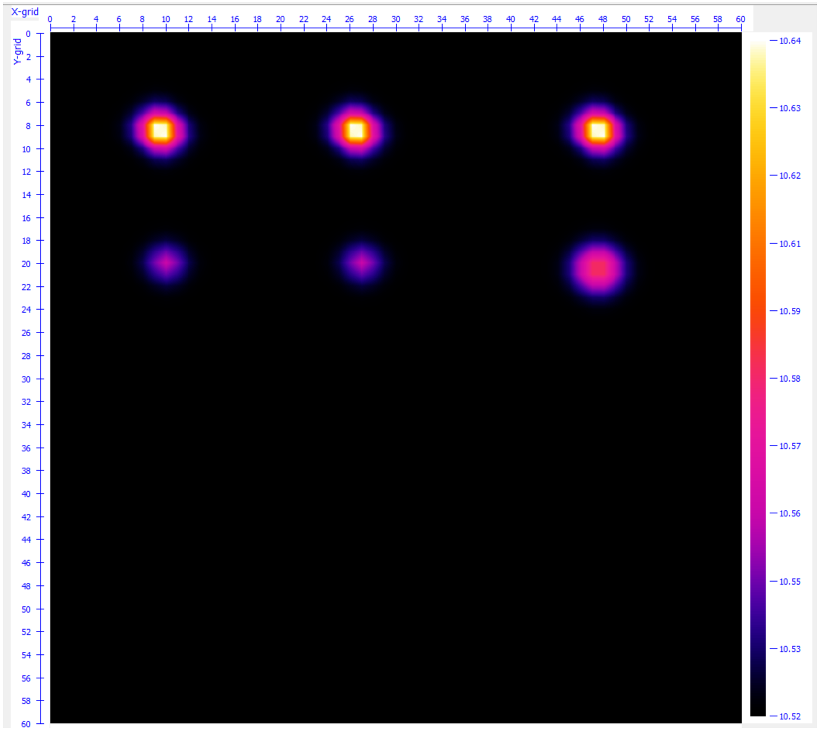

Graph 52 Space profiles of the different rows of defects using optical lockin simulation ML3 settings

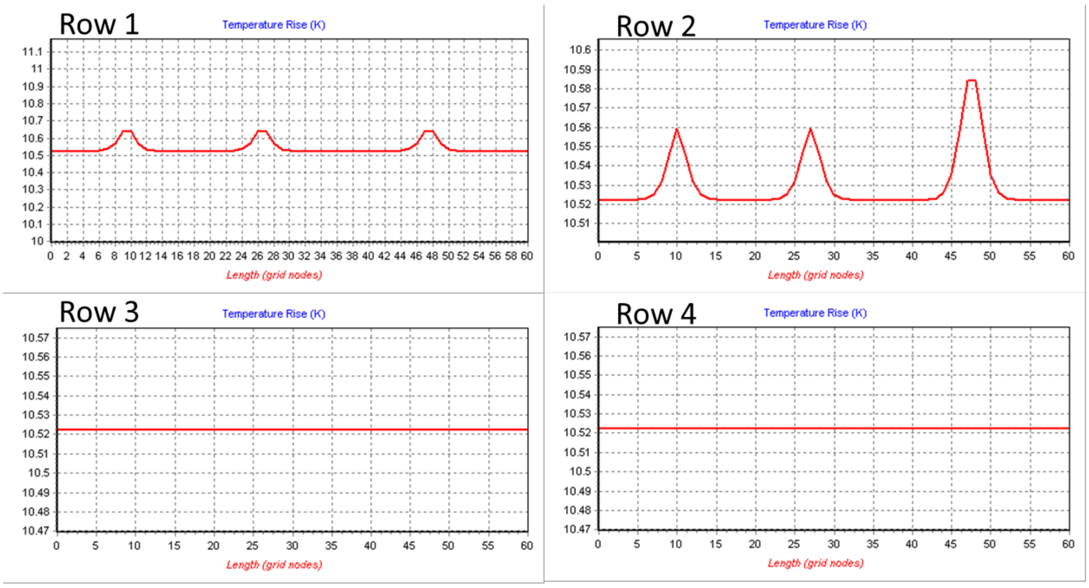

Graph 53 Delta T profiles for different rows of defects using optical lockin simulation ML3 settings. Row#1 in blue, Row #2 in green, Row# 3 in Orange and Row#4 in red

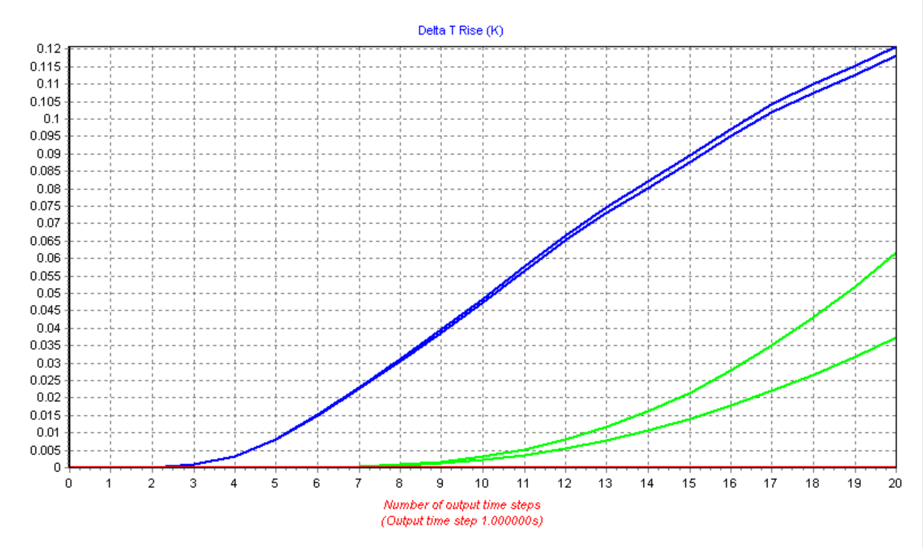

ML4

Figure 63 Thermal image for simulation ML4 using Optical lockin: Heating density 6000W/m^2, Wave period 7s, Total time 20s

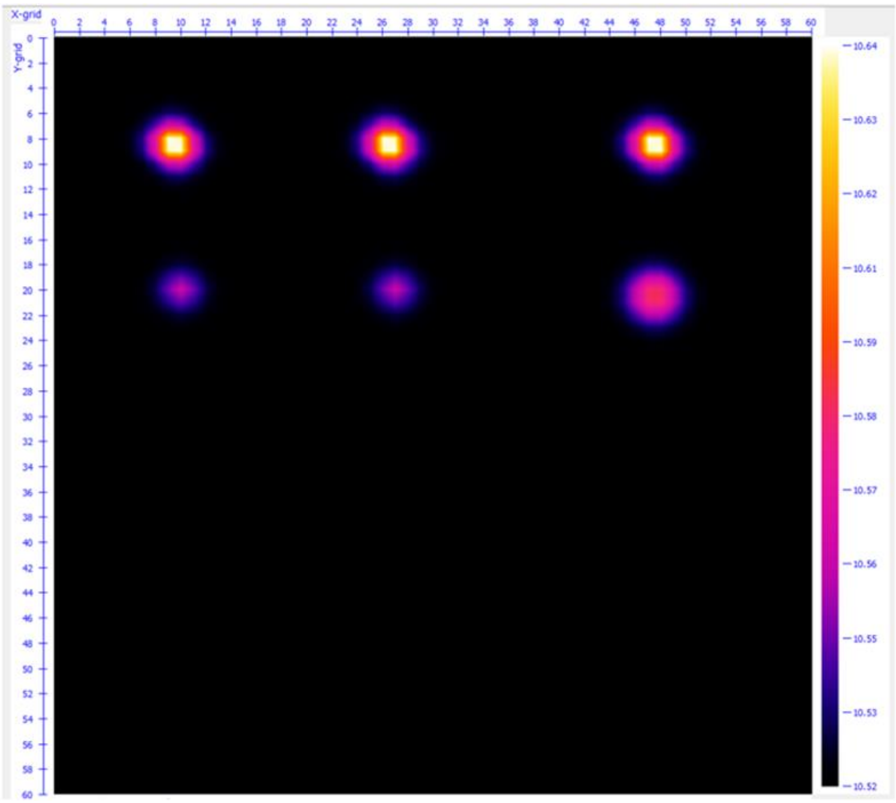

Graph 54 Space profiles of the different rows of defects using optical lockin simulation ML4 settings

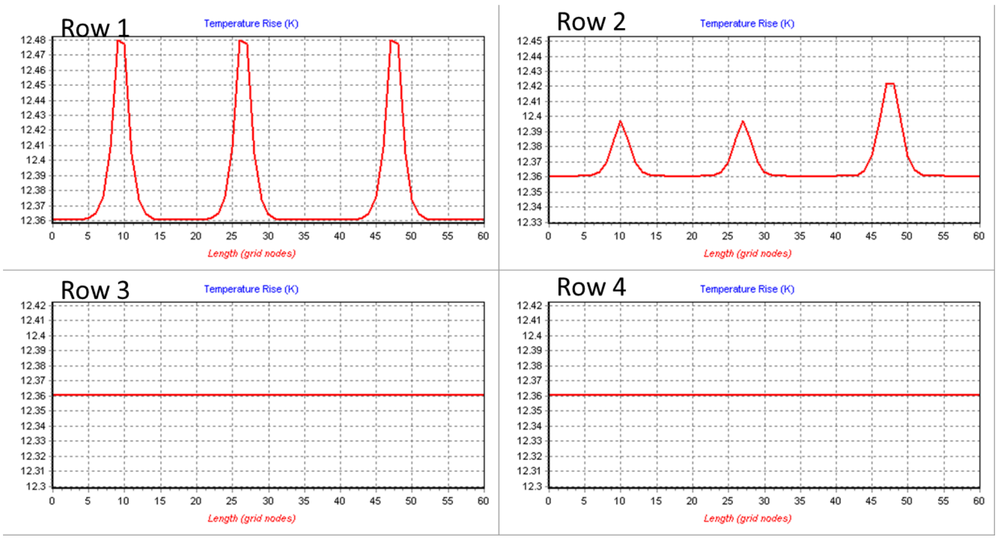

Graph 55 Delta T profiles for different rows of defects using optical lockin simulation ML4 settings. Row#1 in blue, Row #2 in green, Row# 3 in Orange and Row#4 in red

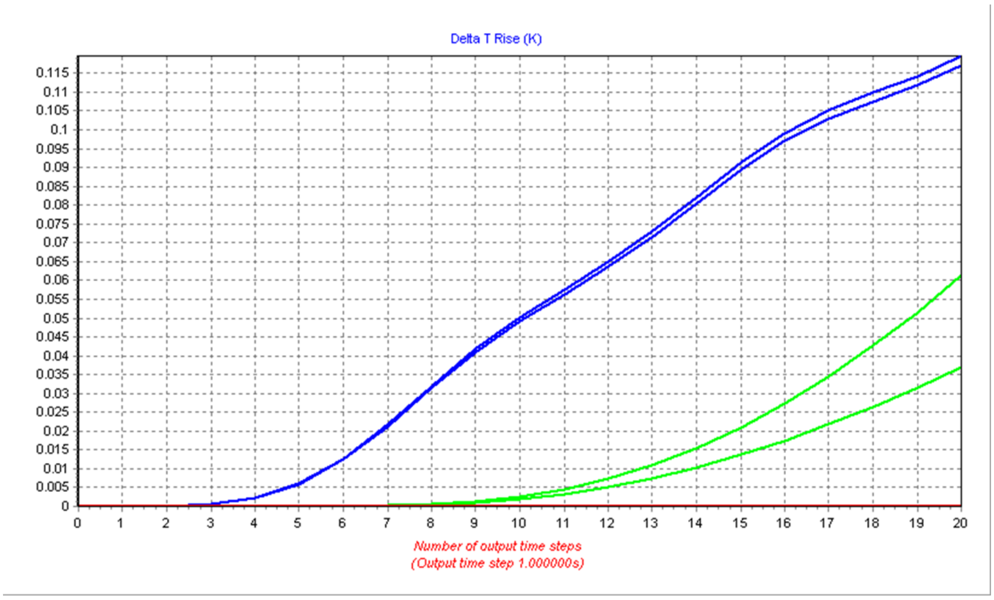

ML5

Figure 64 Thermal image for simulation ML5 using Optical lockin: Heating density 6000W/m^2, Wave period 3s, Total time 30s

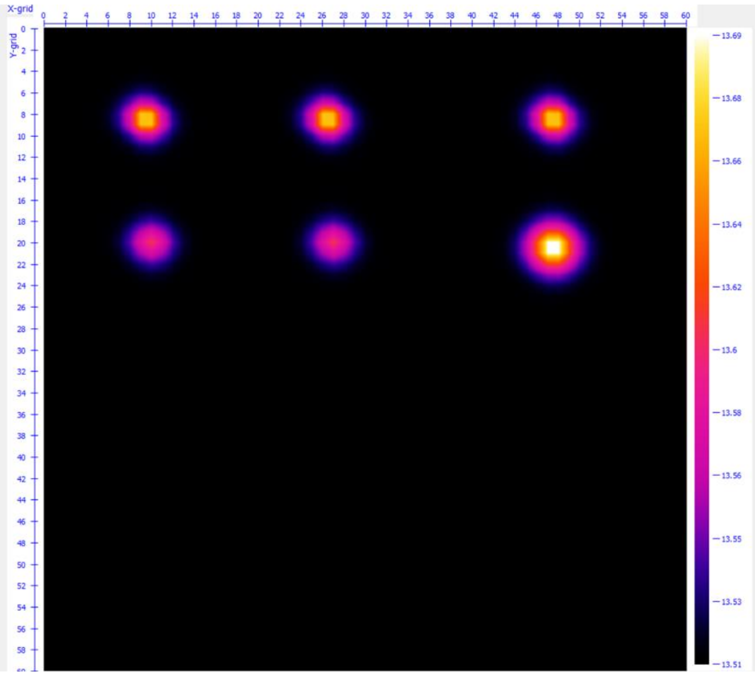

Graph 56 Space profiles of the different rows of defects using optical lockin simulation ML5 settings

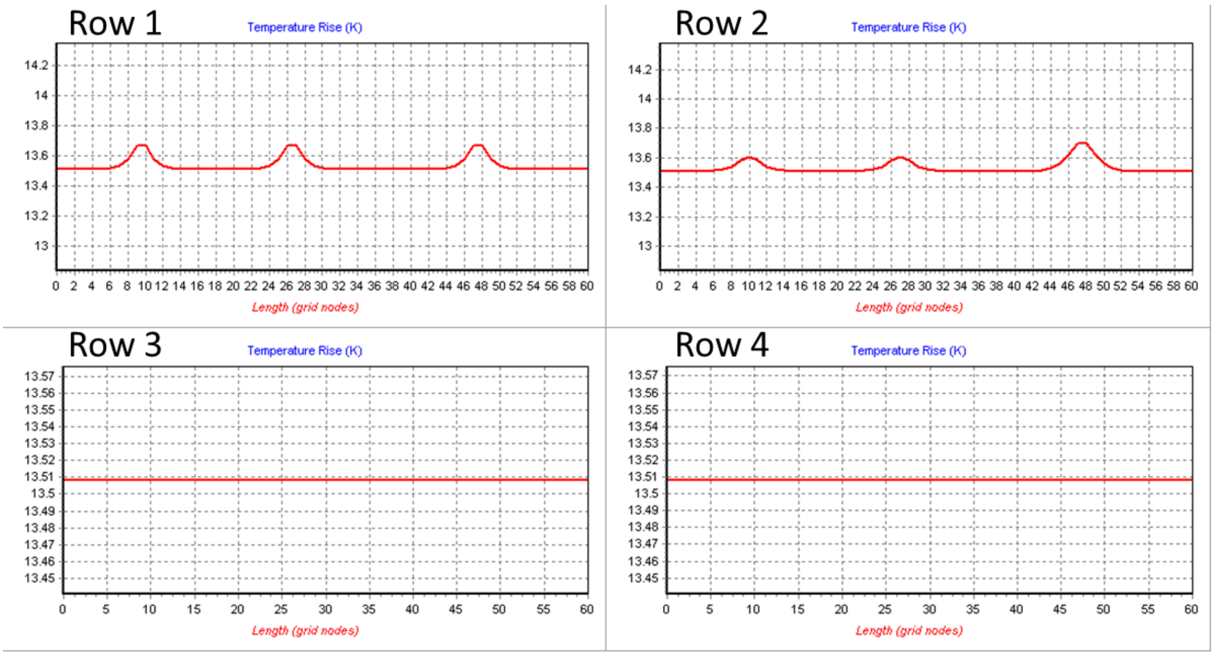

Graph 57 Delta T profiles for different rows of defects using optical lockin simulation ML5 settings. Row#1 in blue, Row #2 in green, Row# 3 in Orange and Row#4 in red

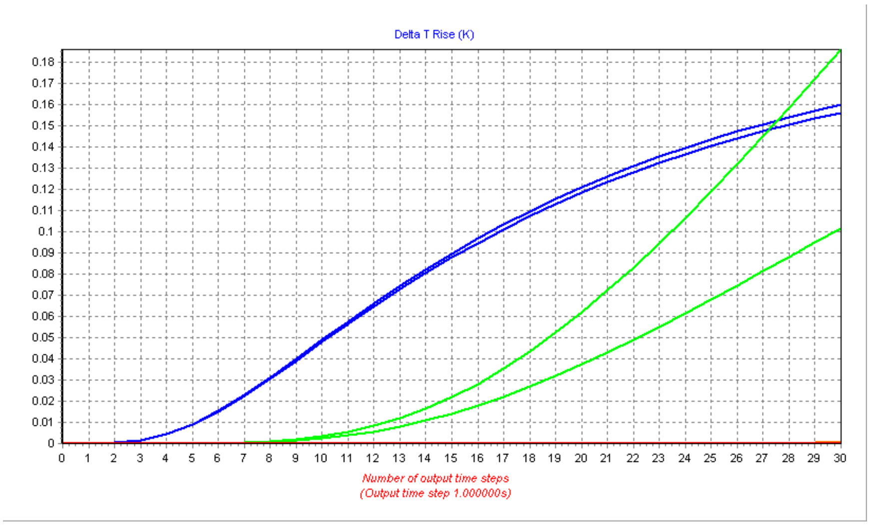

ML6

Figure 65 Thermal image for simulation ML6 using Optical lockin: Heating density 6000W/m^2, Wave period 4s, Total time 40s

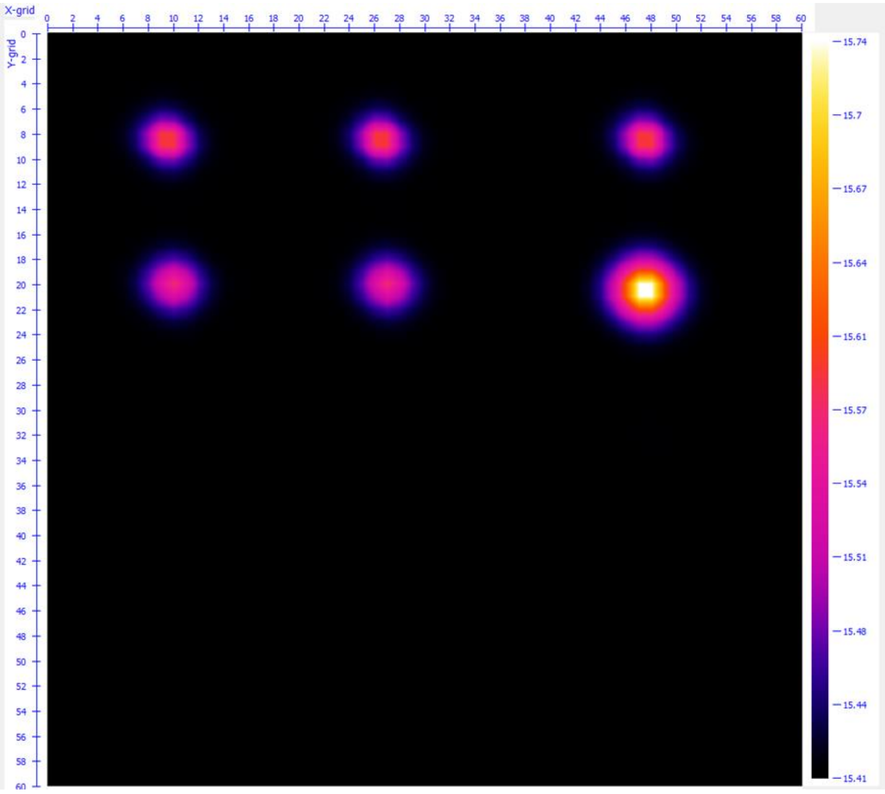

Graph 58 Space profiles of the different rows of defects using optical lockin simulation ML6 settings

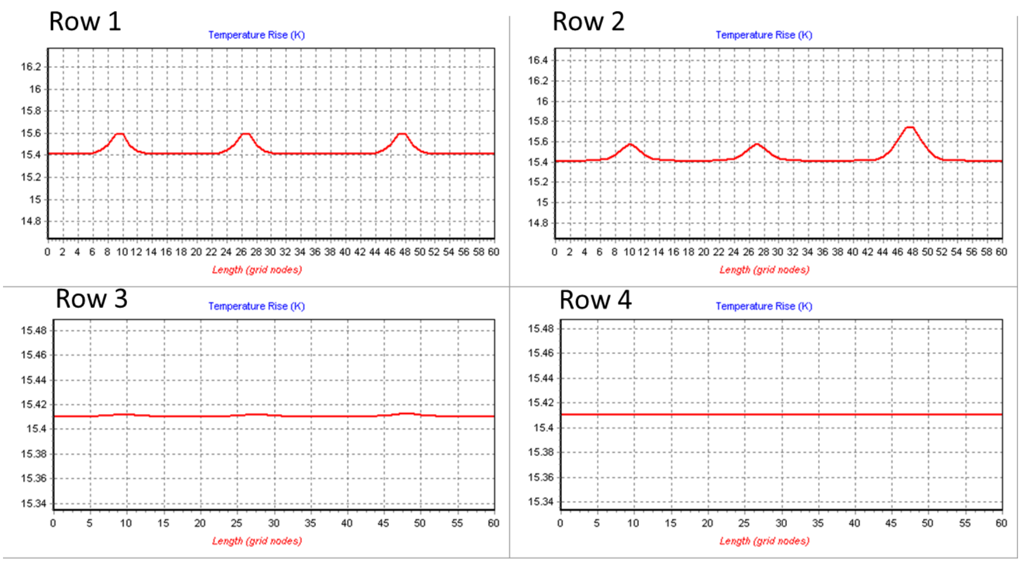

Graph 59 Delta T profiles for different rows of defects using optical lockin simulation ML6 settings. Row#1 in blue, Row #2 in green, Row# 3 in Orange and Row#4 in red

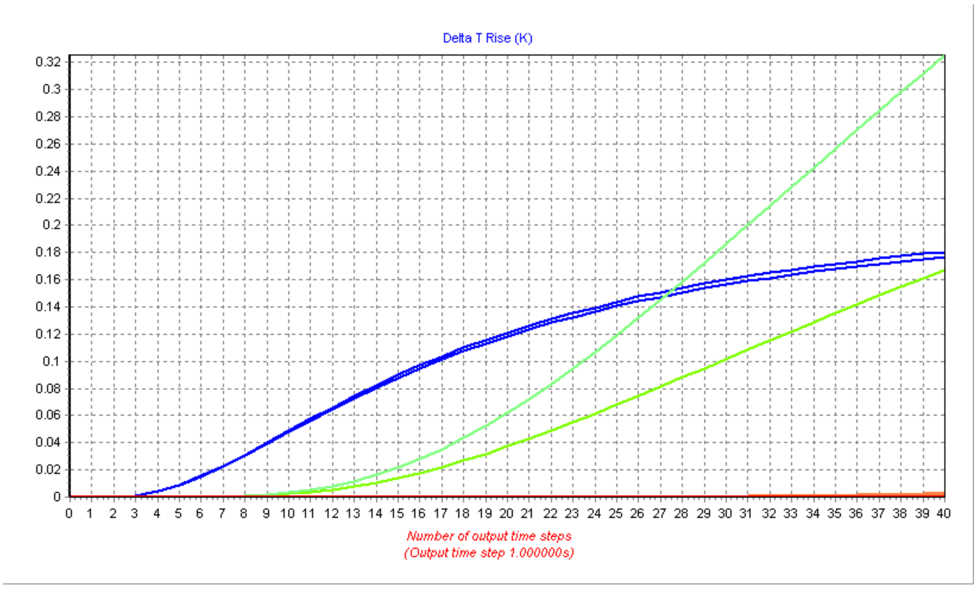

Graph 60 Delta T profiles for Row #3 and #4 of defects using optical lockin simulation ML6. Row# 3 in orange and Row#4 in red

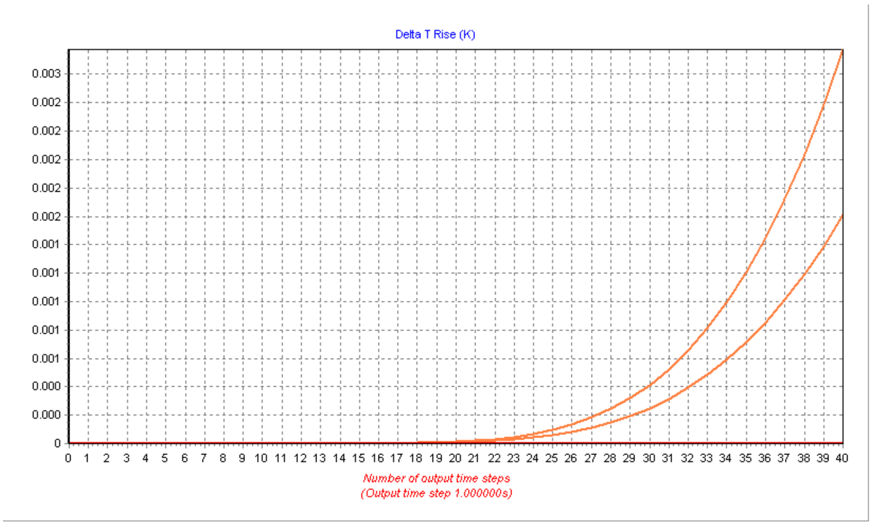

ML7

Figure 66 Thermal image for simulation ML7 using Optical lockin: Heating density 6000W/m^2, Wave period 4s, Total time 60s

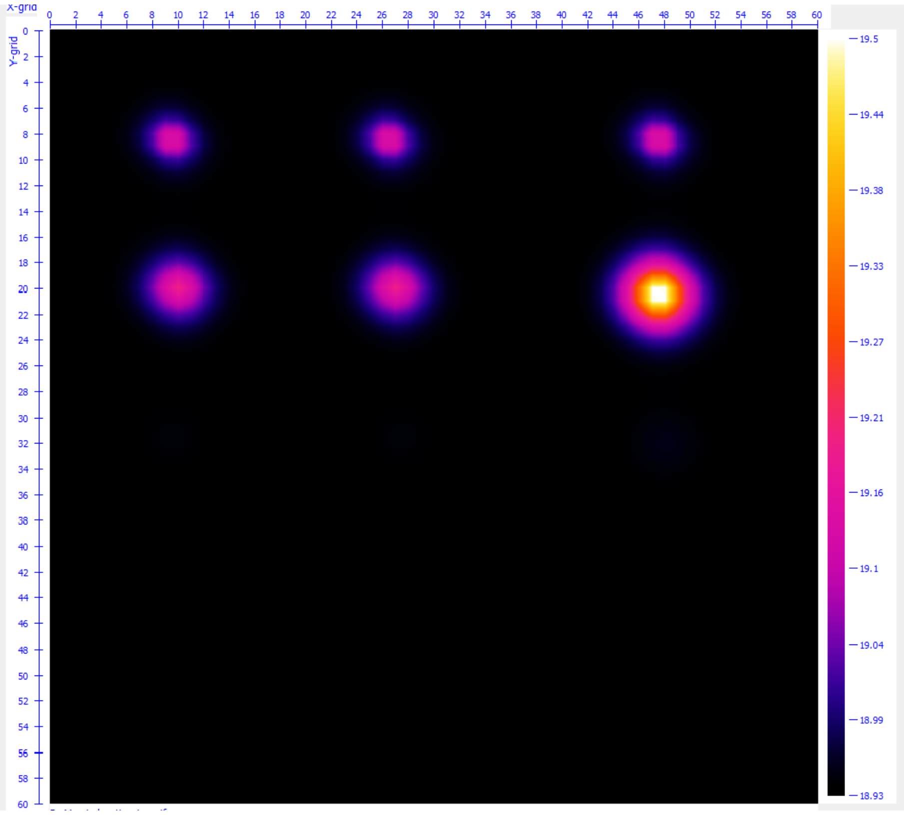

Graph 61 Space profiles of the different rows of defects using optical lockin simulation ML7 settings

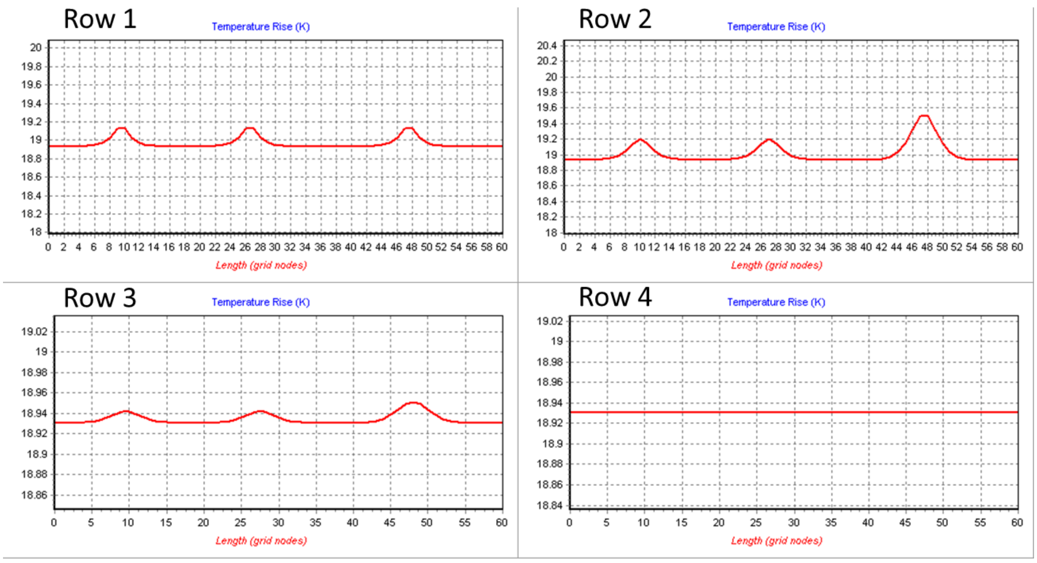

Graph 62 Delta T profiles for different rows of defects using optical lockin simulation ML7 settings. Row#1 in blue, Row #2 in green, Row# 3 in Orange and Row#4 in red

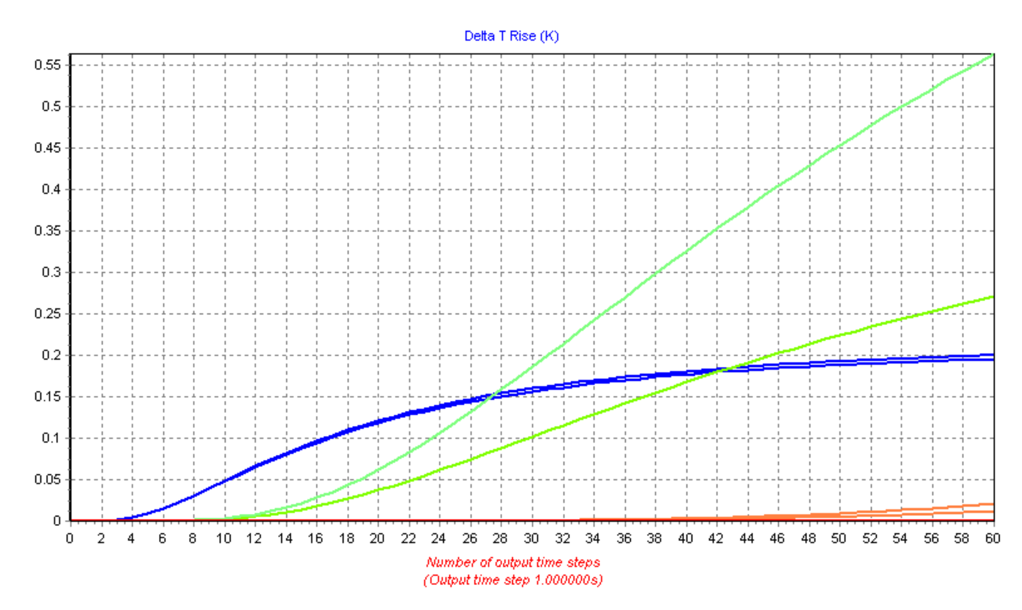

Graph 63 Delta T profiles for Row #3 and #4 of defects using optical lockin simulation ML7. Row# 3 in orange and Row#4 in red

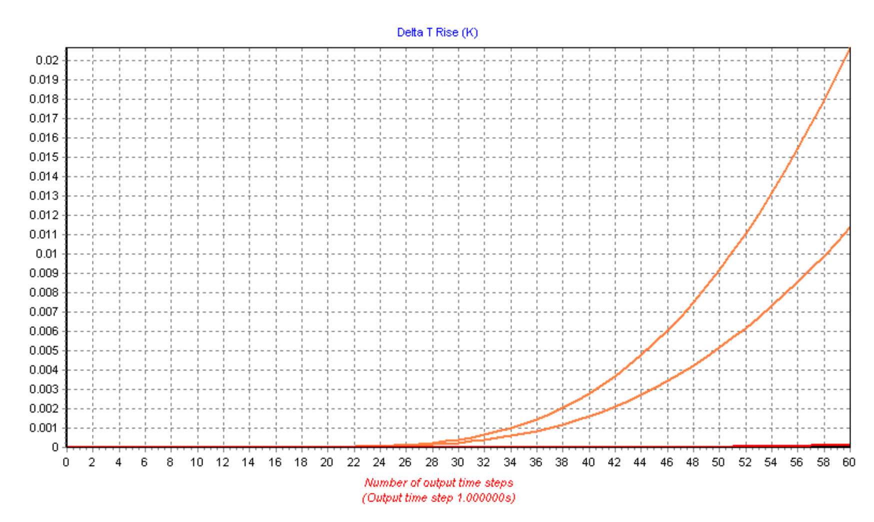

ML8

Figure 67 Thermal image for simulation ML8 using Optical lockin: Heating density 11111W/m^2, Wave period 3s, Total time 60s

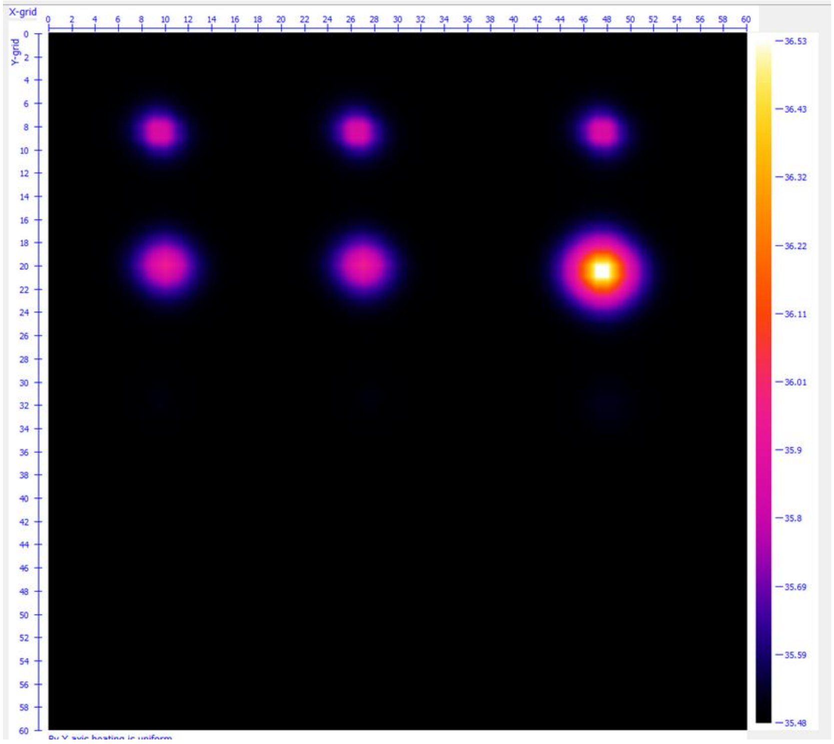

Graph 64 Space profiles of the different rows of defects using optical lockin simulation ML8 settings

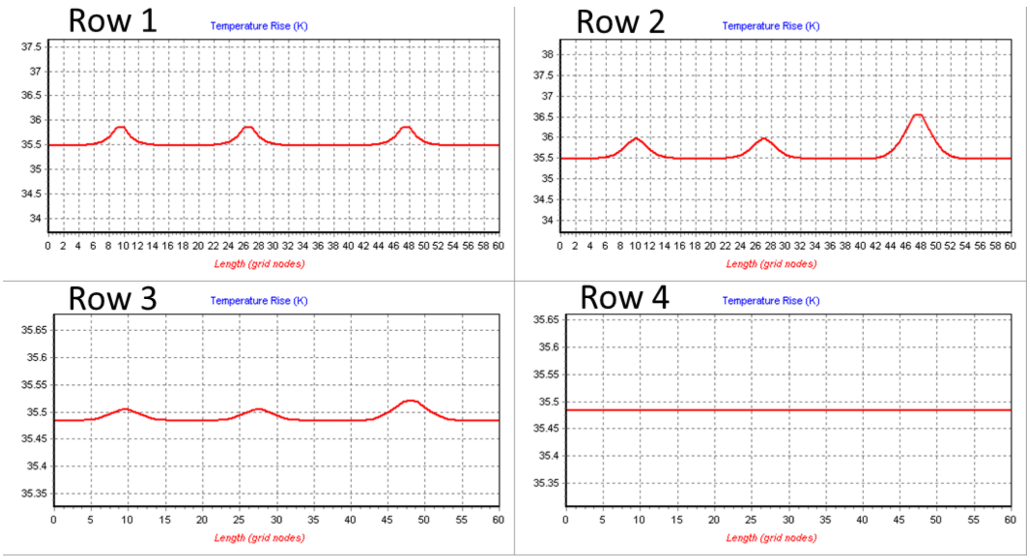

Graph 65 Delta T profiles for different rows of defects using optical lockin simulation ML8 settings. Row#1 in blue, Row #2 in green, Row# 3 in Orange and Row#4 in red

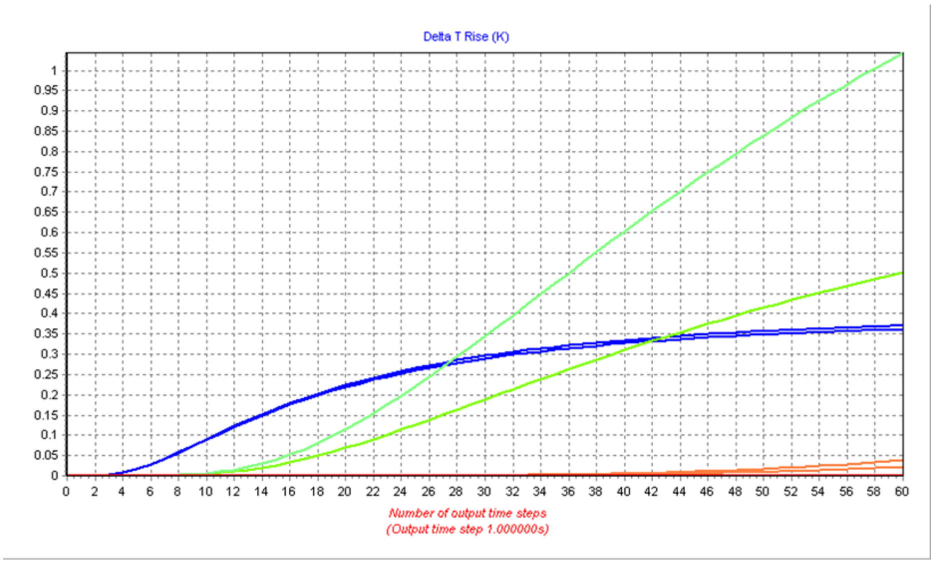

Graph 66 Delta T profiles for Row #3 and #4 of defects using optical lockin simulation ML8. Row# 3 in orange and Row#4 in red

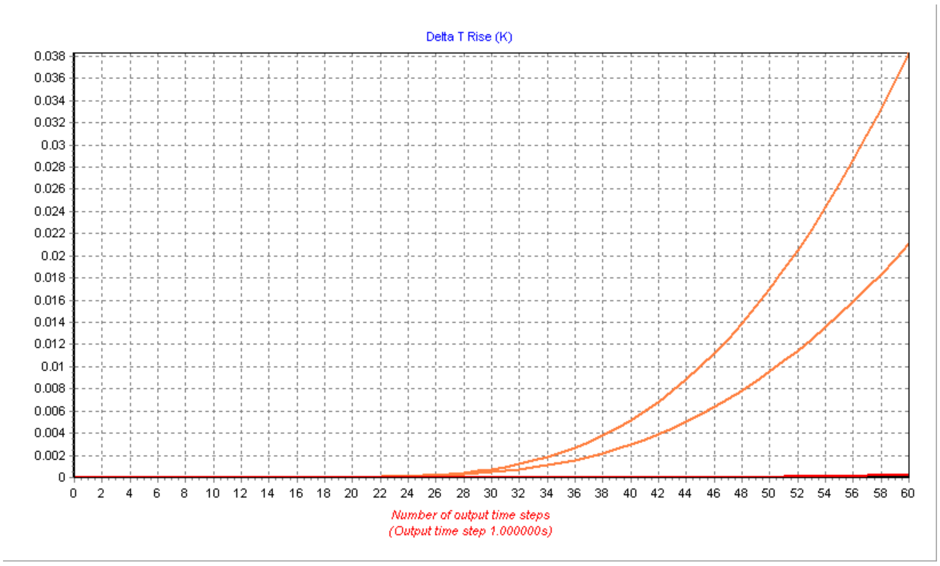

ML9

Figure 68 Thermal image for simulation ML9 using Optical lockin: Heating density 11111W/m^2, Wave period 4s, Total time 60s

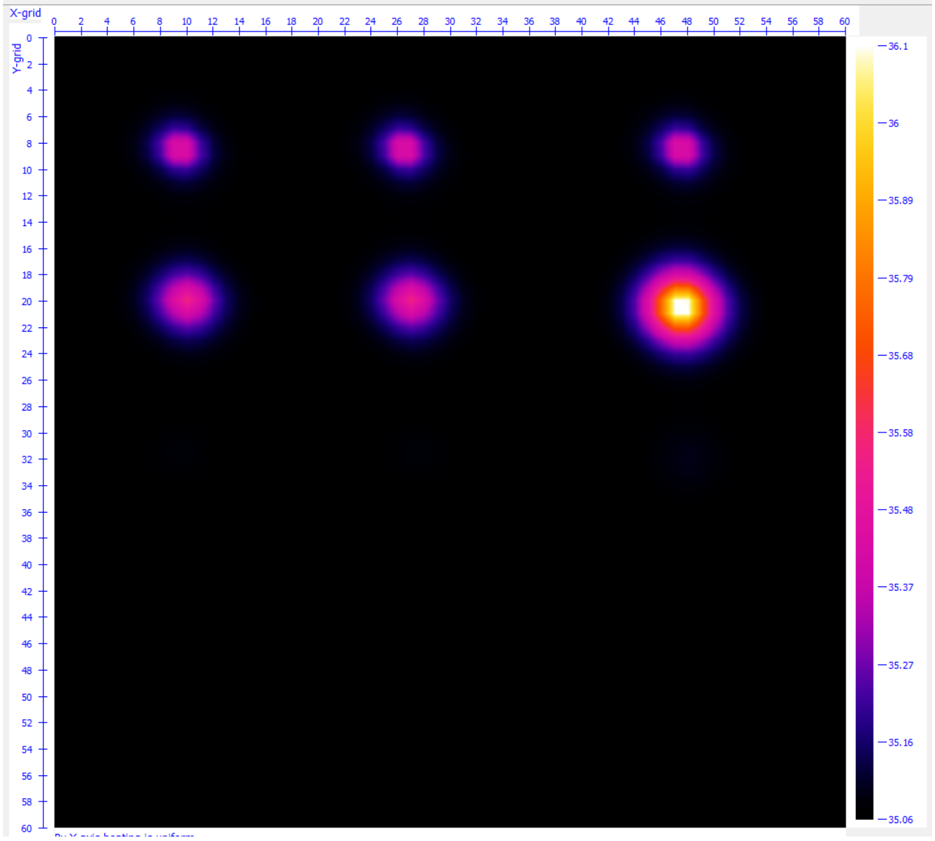

Graph 67 Space profiles of the different rows of defects using optical lockin simulation ML9 settings

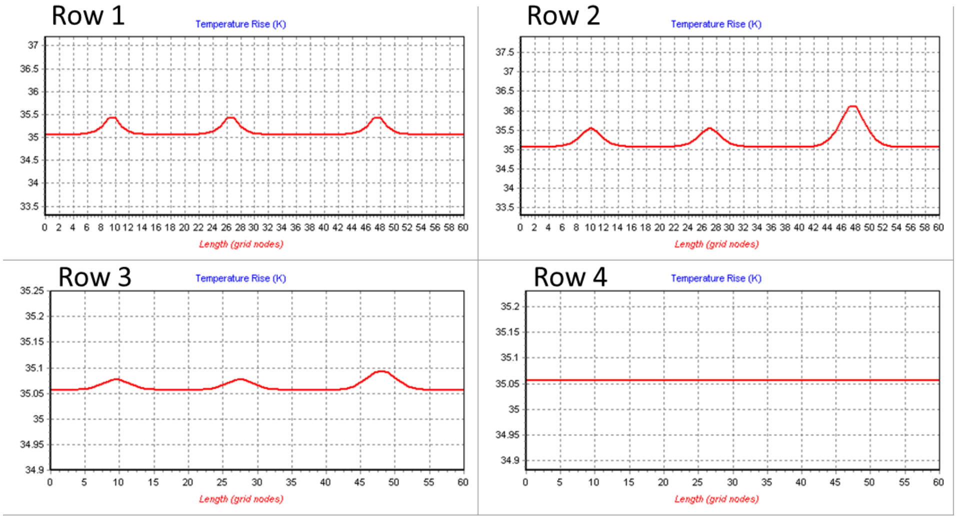

Graph 68 Delta T profiles for different rows of defects using optical lockin simulation ML9 settings. Row#1 in blue, Row #2 in green, Row# 3 in Orange and Row#4 in red

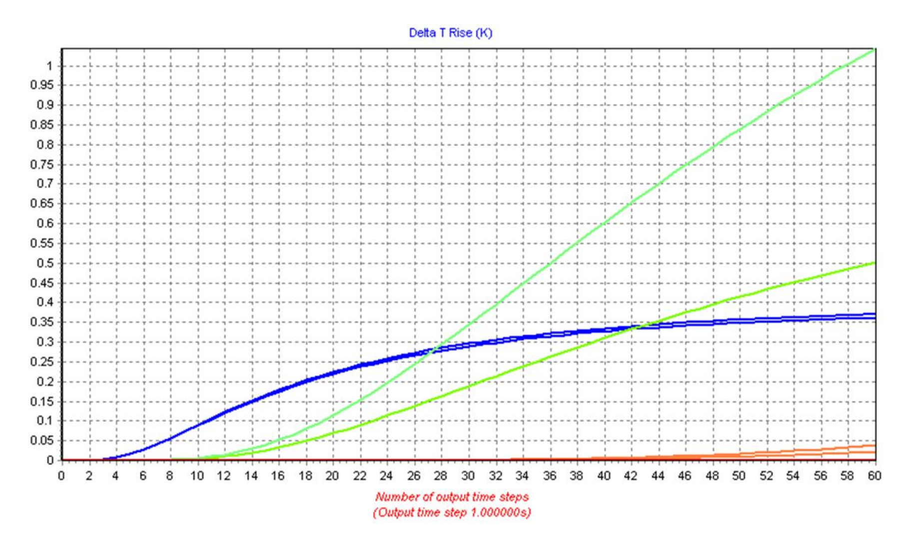

Graph 69 Delta T profiles for Row #3 and #4 of defects using optical lockin simulation ML9. Row# 3 in orange and Row#4 in red

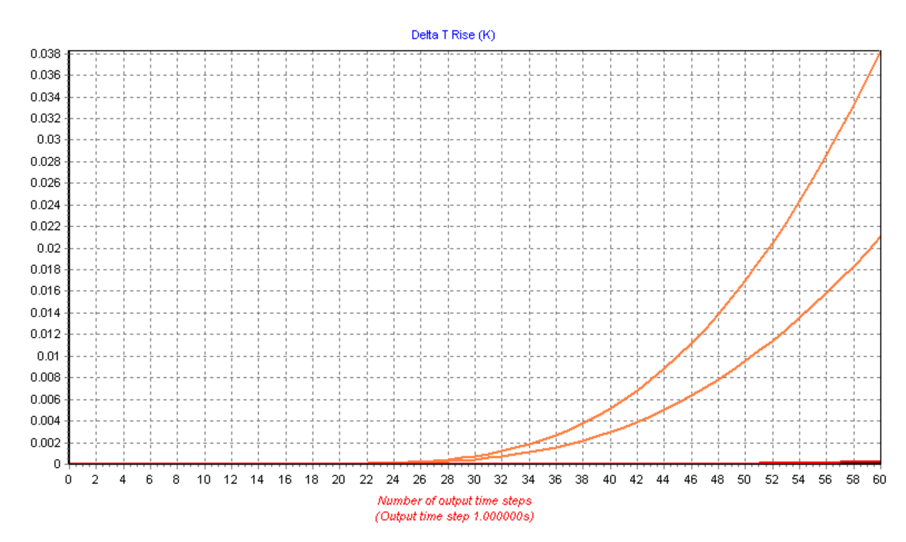

ML10

Figure 69 Thermal image for simulation ML10 using Optical lockin: Heating density 11111 W/m^2, Wave period 7s, Total time 60s

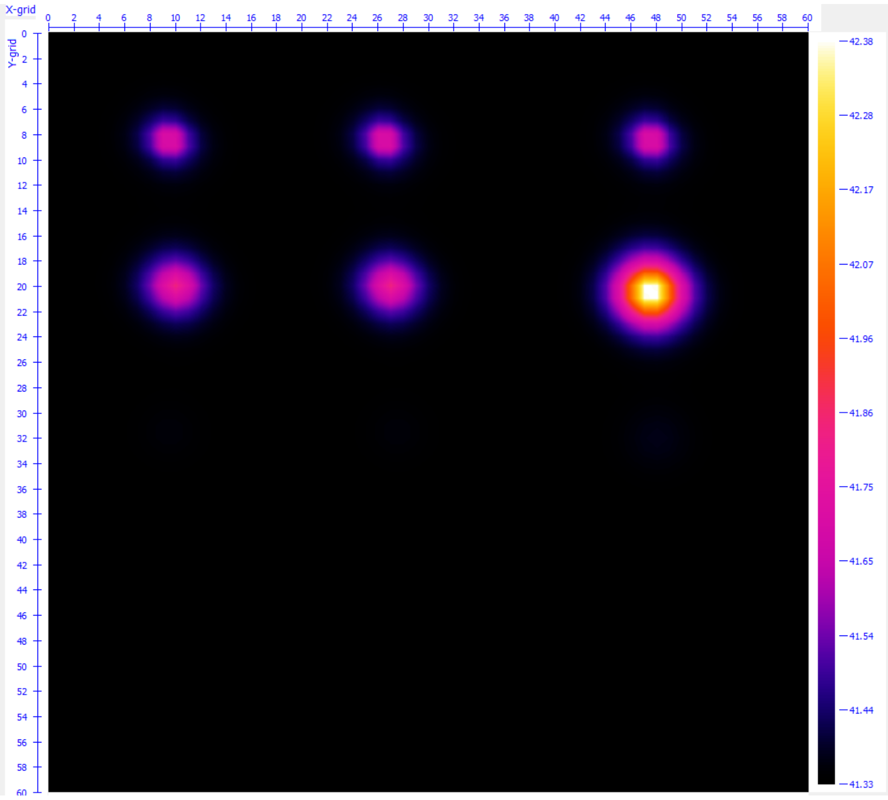

Graph 70 Space profiles of the different rows of defects using optical lockin simulation ML10 settings

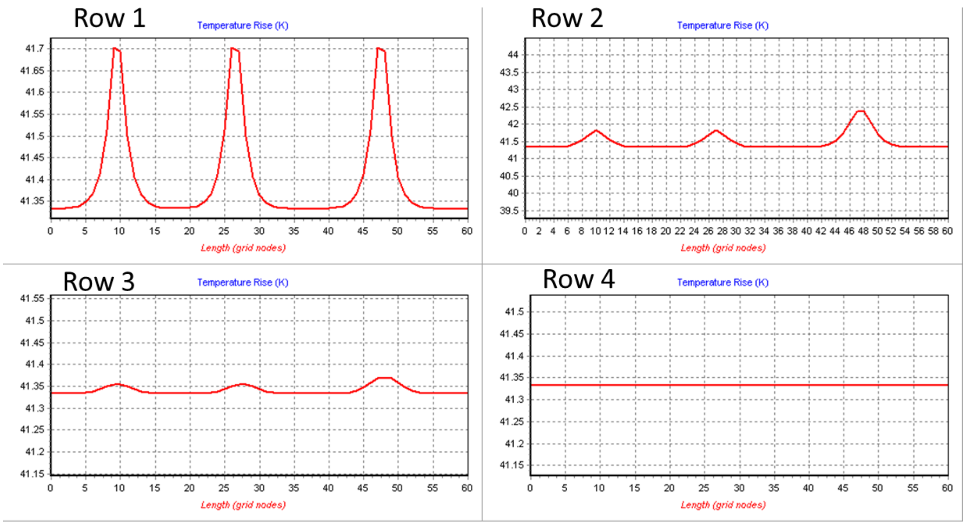

Graph 71 Delta T profiles for different rows of defects using optical lockin simulation ML10 settings. Row#1 in blue, Row #2 in green, Row# 3 in Orange and Row#4 in red

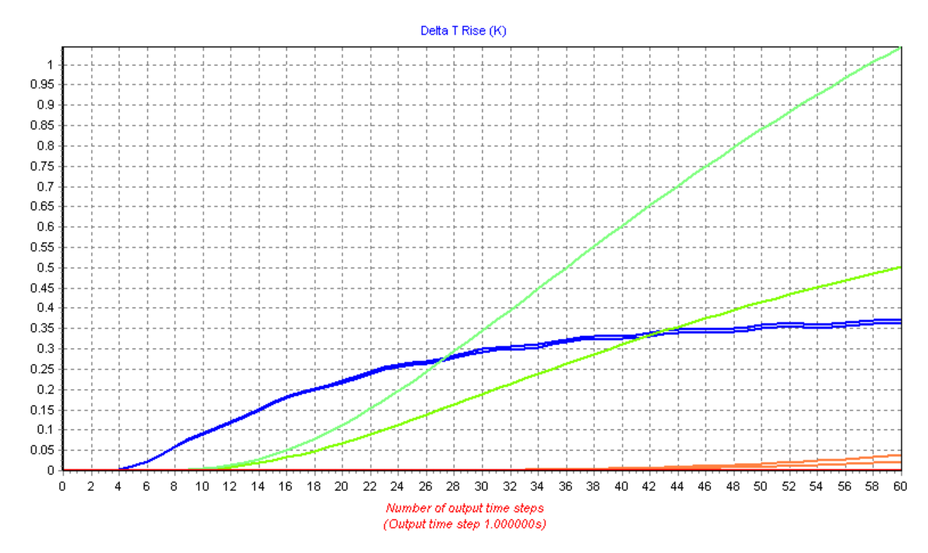

Graph 72 Delta T profiles for Row #3 and #4 of defects using optical lockin simulation ML10. Row# 3 in orange and Row#4 in red

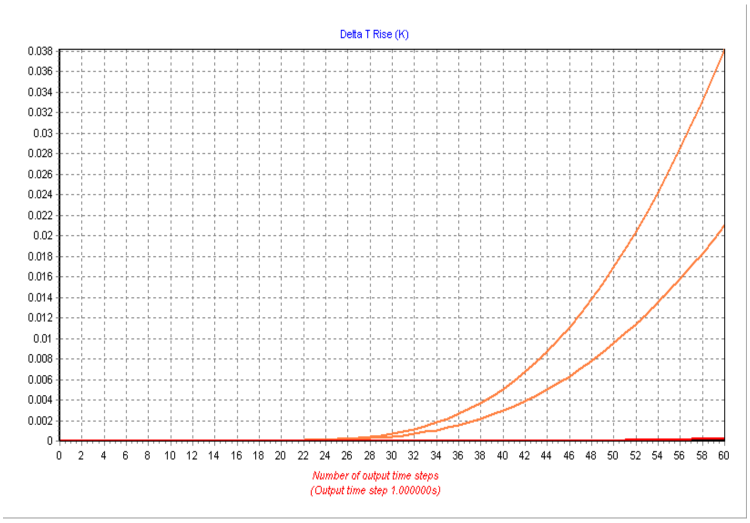

ML11

Figure 70 Thermal image for simulation ML11 using Optical lockin: Heating density 11111 W/m^2, Wave period 4s, Total time 90s

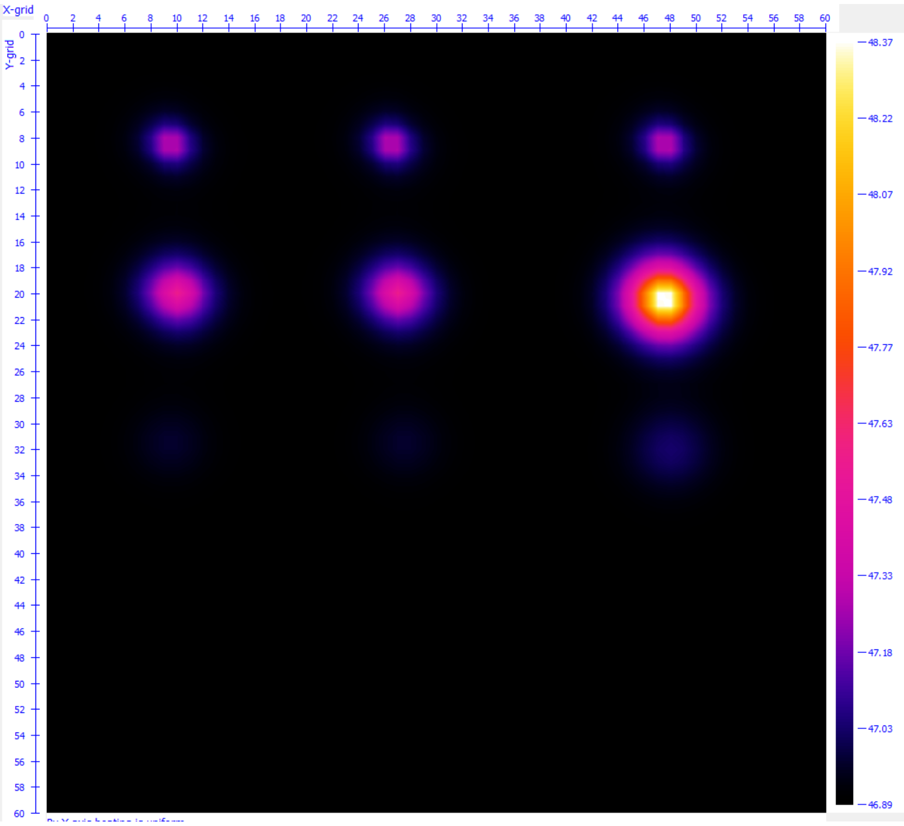

Graph 73 Space profiles of the different rows of defects using optical lockin simulation ML11 settings

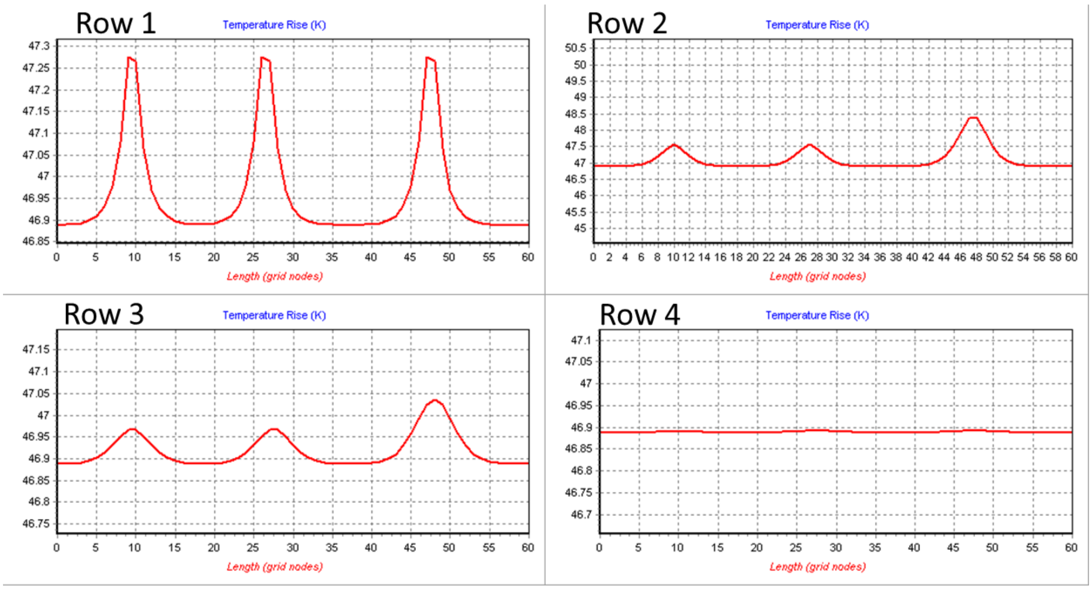

Graph 74 Delta T profiles for different rows of defects using optical lockin simulation ML11 settings. Row#1 in blue, Row #2 in green, Row# 3 in Orange and Row#4 in red

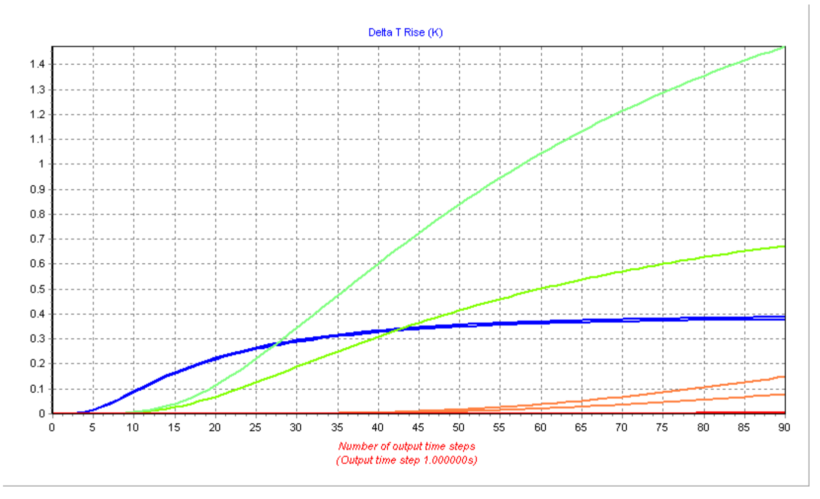

Graph 75 Delta T profiles for Row #3 and #4 of defects using optical lockin simulation ML11. Row# 3 in orange and Row#4 in red

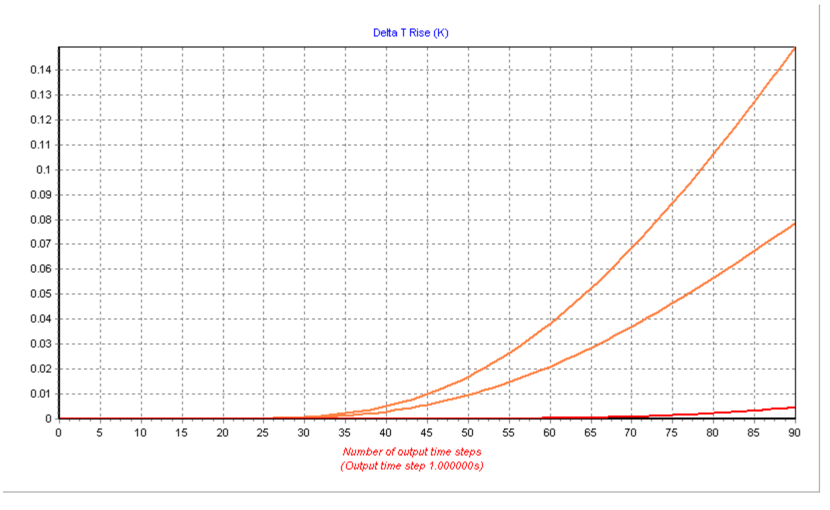

ML12

Figure 71 Thermal image for simulation ML12 using Optical lockin: Heating density 11111 W/m^2, Wave period 4s, Total time 120s

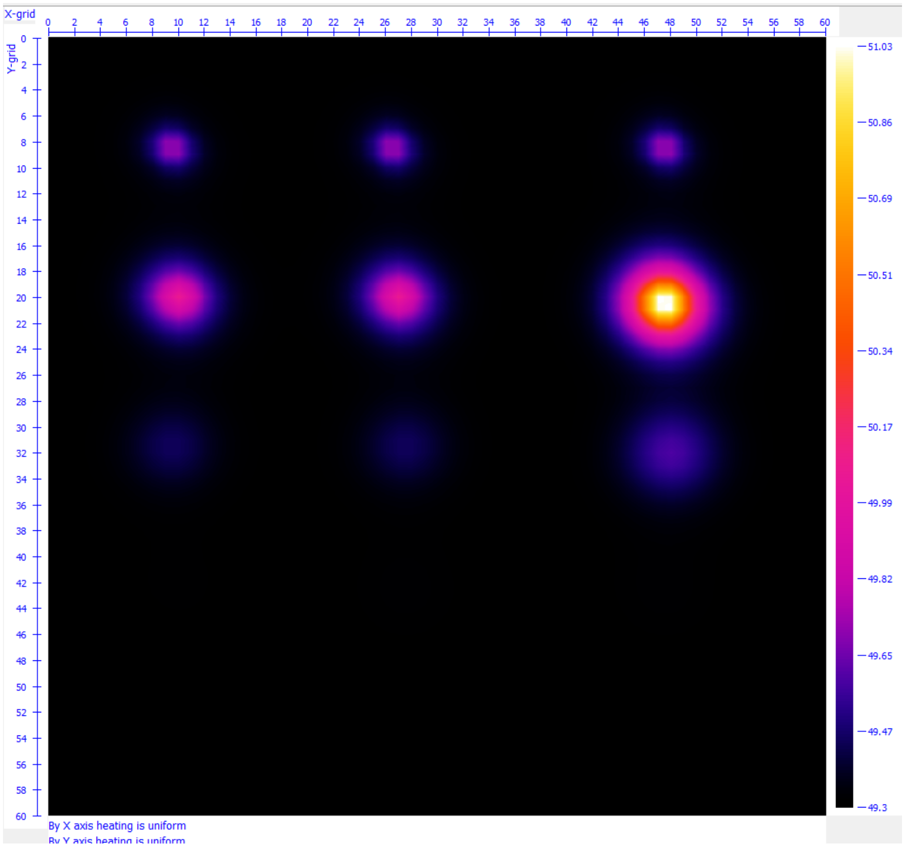

Graph 76 Space profiles of the different rows of defects using optical lockin simulation ML12 settings

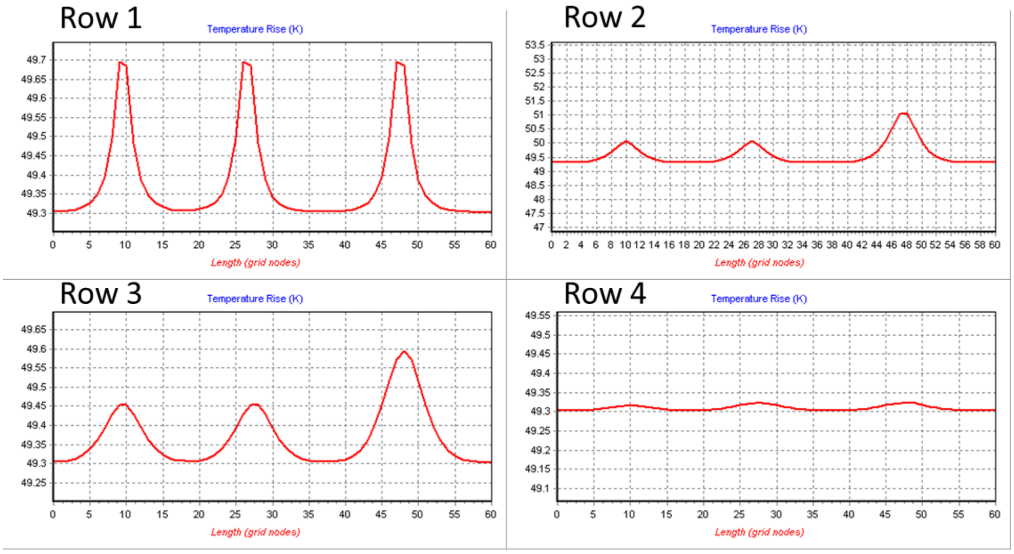

Graph 77 Delta T profiles for different rows of defects using optical lockin simulation ML12 settings. Row#1 in blue, Row #2 in green, Row# 3 in Orange and Row#4 in red

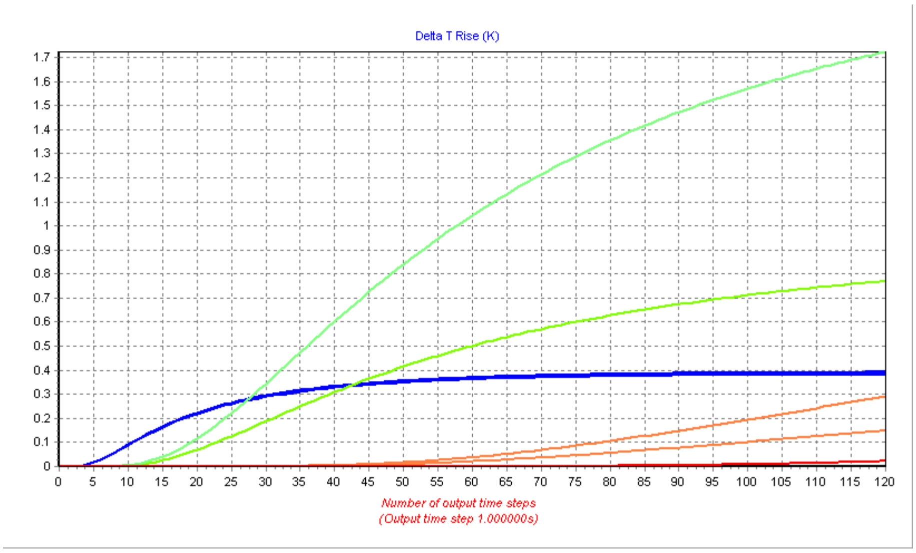

Graph 78 Delta T profiles for Row #3 and #4 of defects using optical lockin simulation ML12. Row# 3 in orange and Row#4 in red

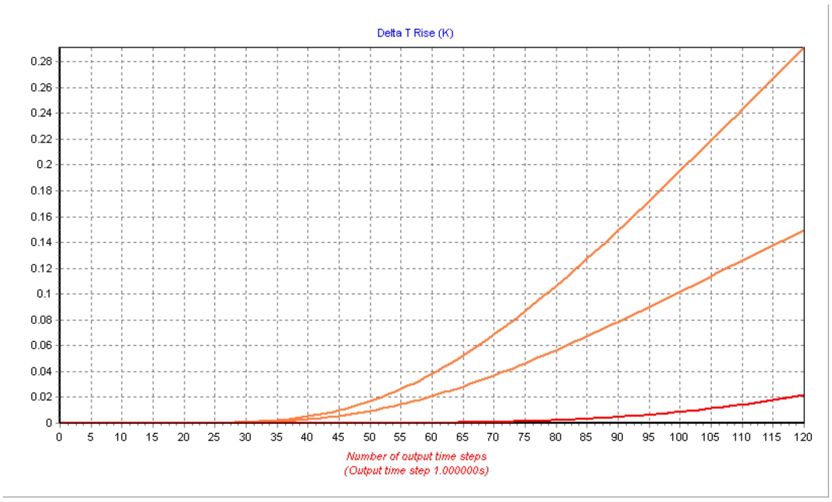

ML 13

Figure 72 Thermal image for simulation ML13 using Optical lockin: Heating density 22222 W/m^2, Wave period 4s, Total time 20s

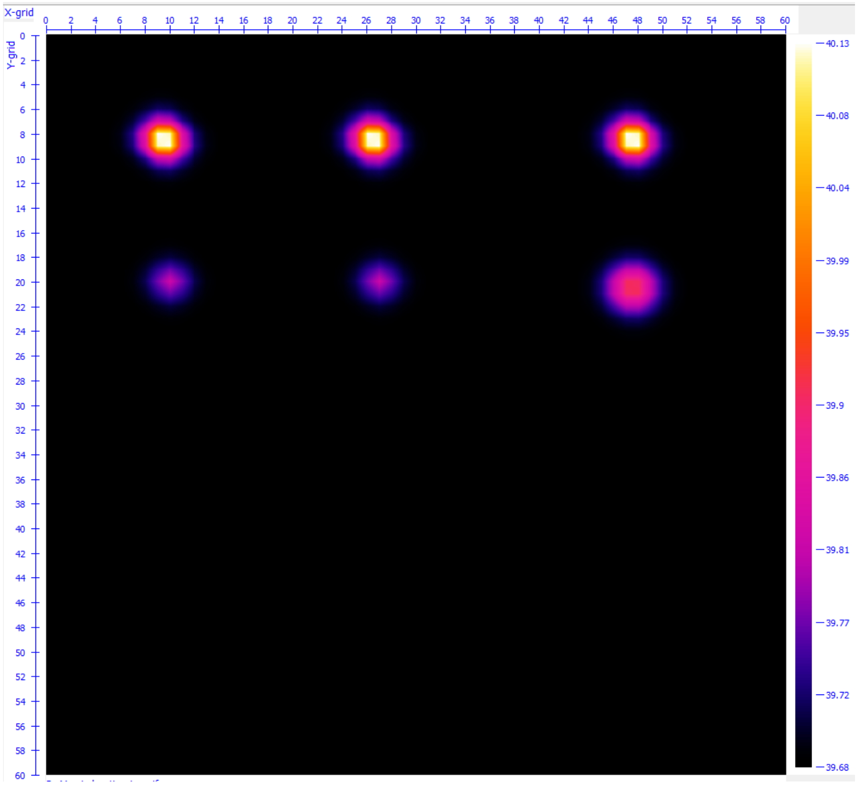

Graph 79 Space profiles of the different rows of defects using optical lockin simulation ML13 settings

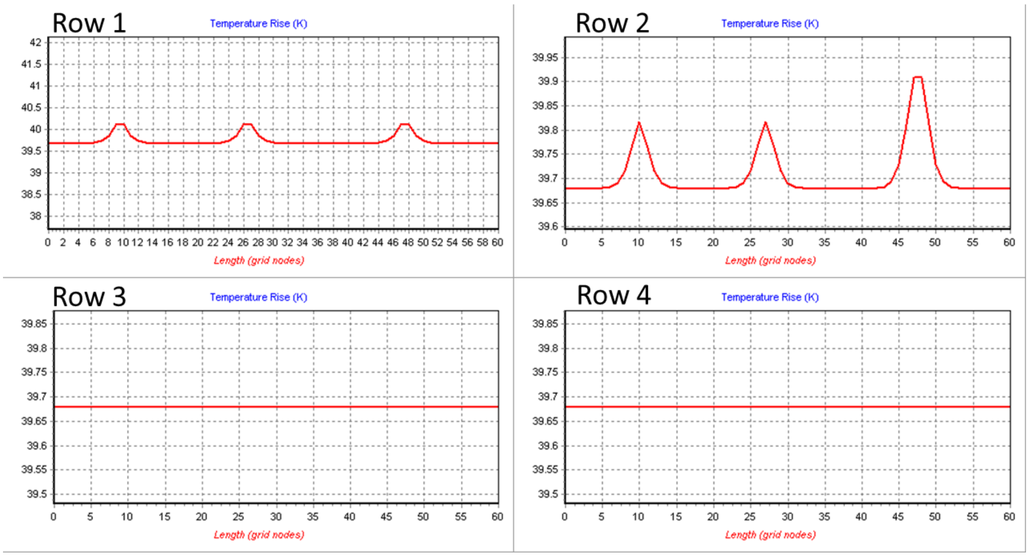

Graph 80 Delta T profiles for different rows of defects using optical lockin simulation ML13 settings. Row#1 in blue, Row #2 in green, Row# 3 in Orange and Row#4 in red

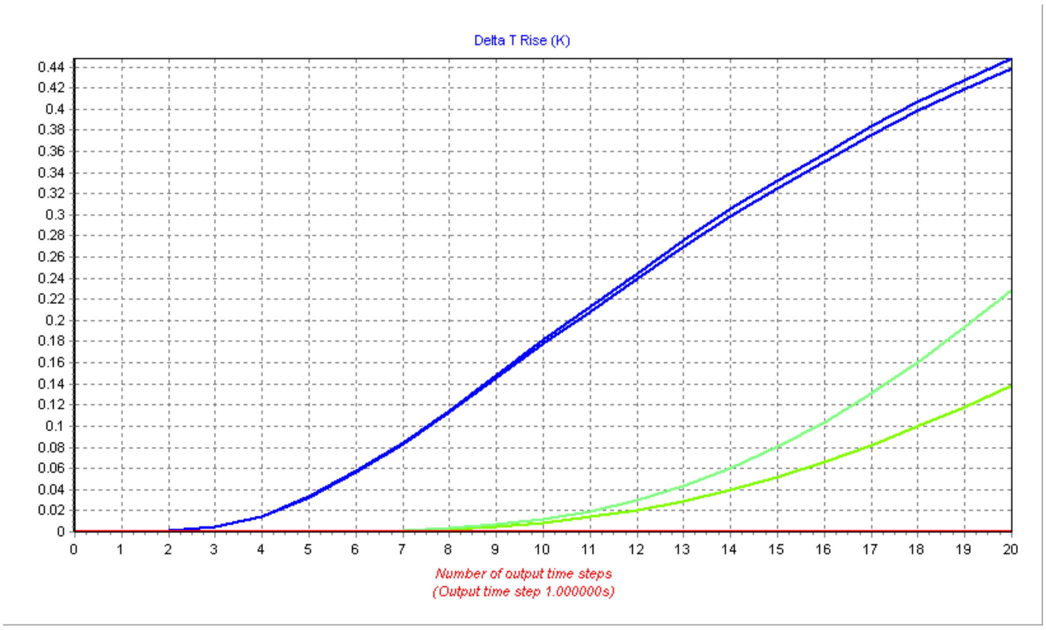

ML14

Figure 73 Thermal image for simulation ML14 using Optical lockin: Heating density 22222 W/m^2, Wave period 4s, Total time 30s

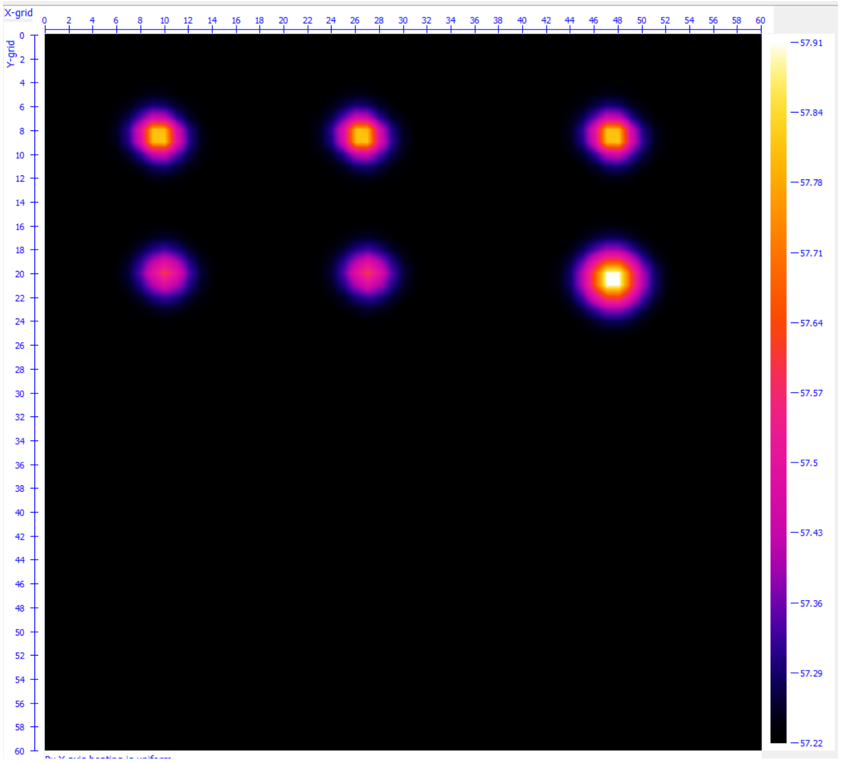

Graph 81 Space profiles of the different rows of defects using optical lockin simulation ML14 settings

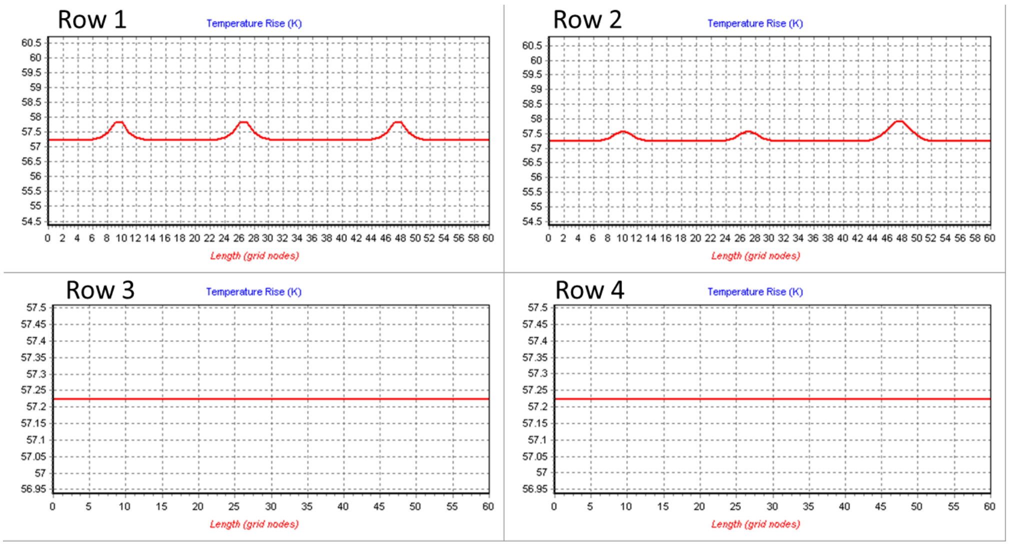

Graph 82 Delta T profiles for different rows of defects using optical lockin simulation ML14 settings. Row#1 in blue, Row #2 in green, Row# 3 in Orange and Row#4 in red

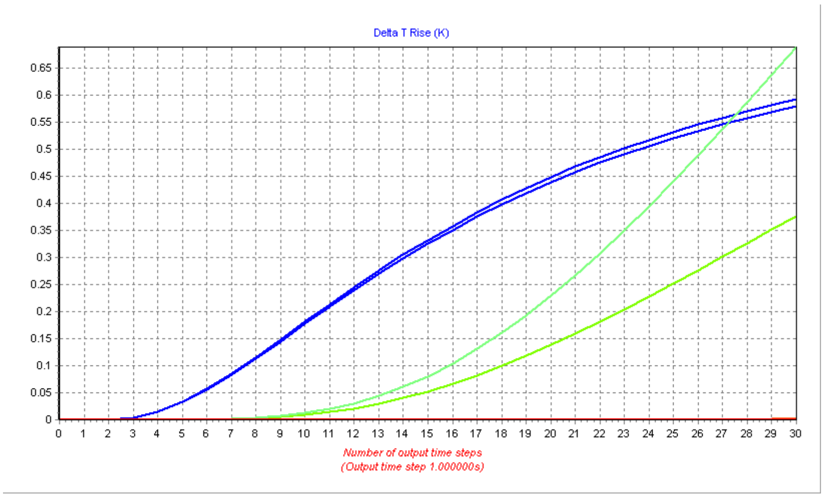

ML15

Figure 74 Thermal image for simulation ML15 using Optical lockin: Heating density 22222 W/m^2, Wave period 4s, Total time 600s

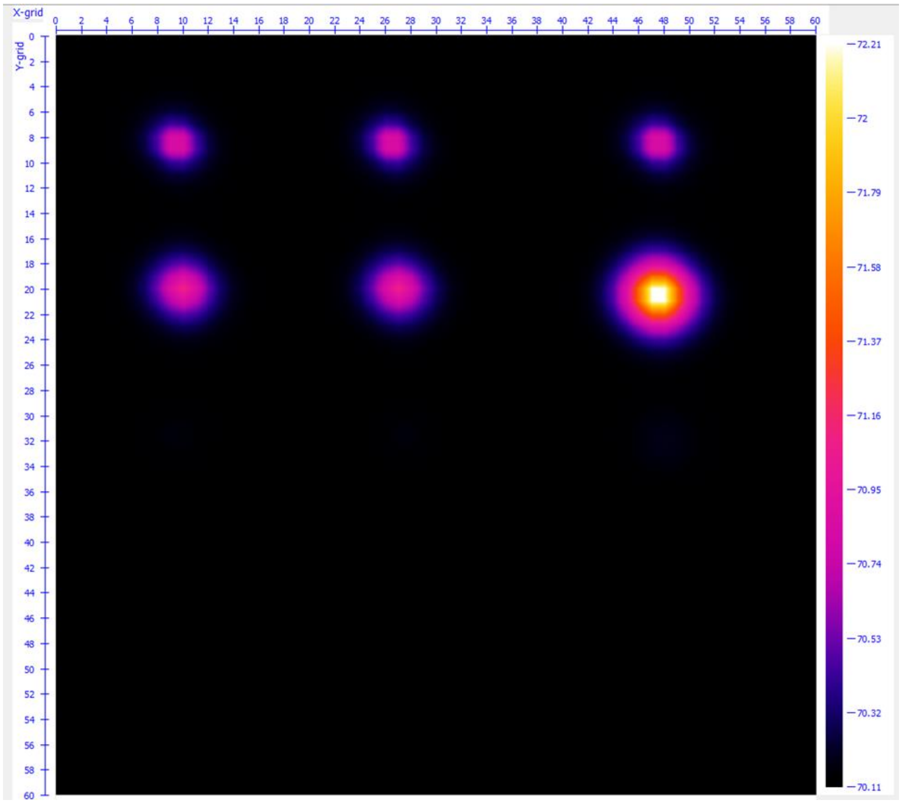

Graph 83 Space profiles of the different rows of defects using optical lockin simulation ML15 settings

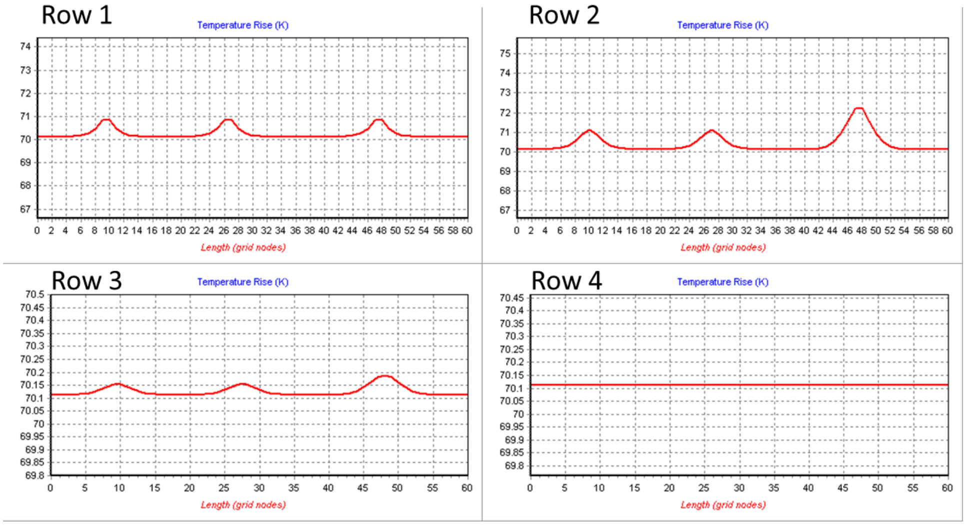

Graph 84 Delta T profiles for different rows of defects using optical lockin simulation ML15 settings. Row#1 in blue, Row #2 in green, Row# 3 in Orange and Row#4 in red

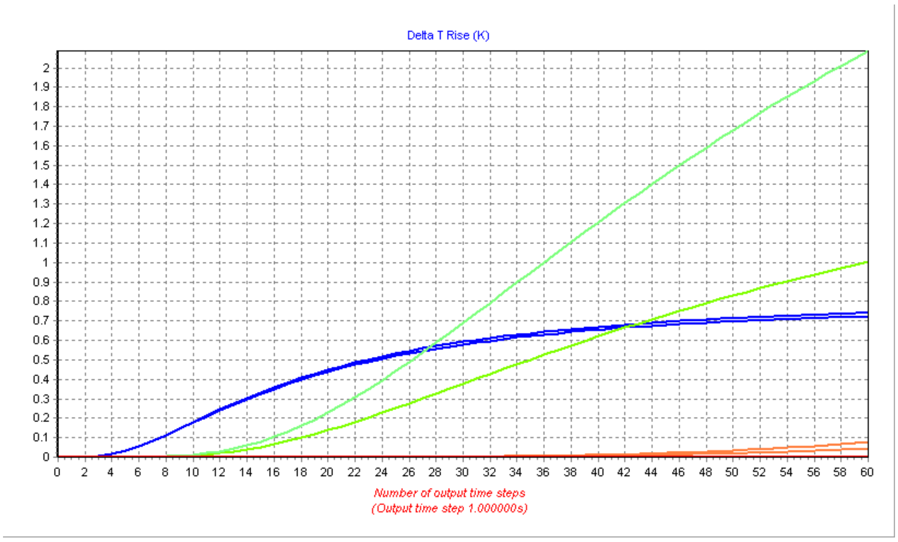

Graph 85 Delta T profiles for Row #3 and #4 of defects using optical lockin simulation ML15. Row# 3 in orange and Row#4 in red

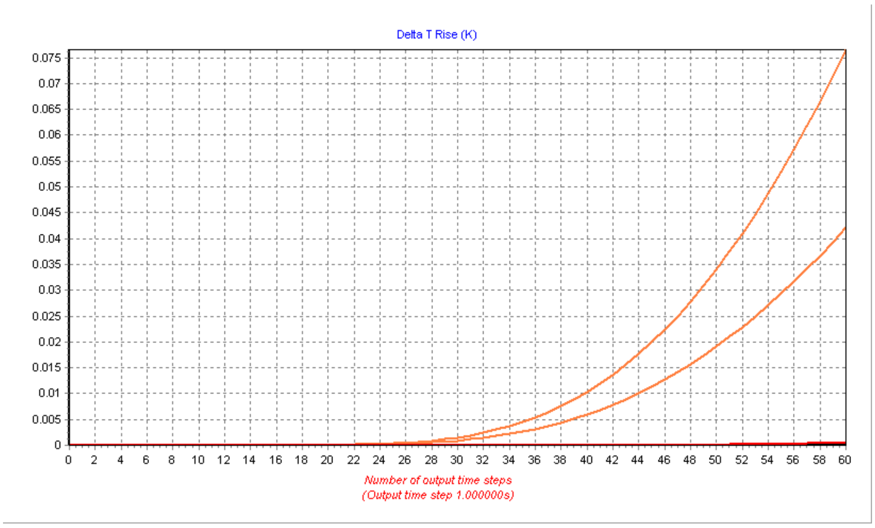

ML 16

Figure 75 Thermal image for simulation ML16 using Optical lockin: Heating density 22222 W/m^2, Wave period 4s, Total time 90s

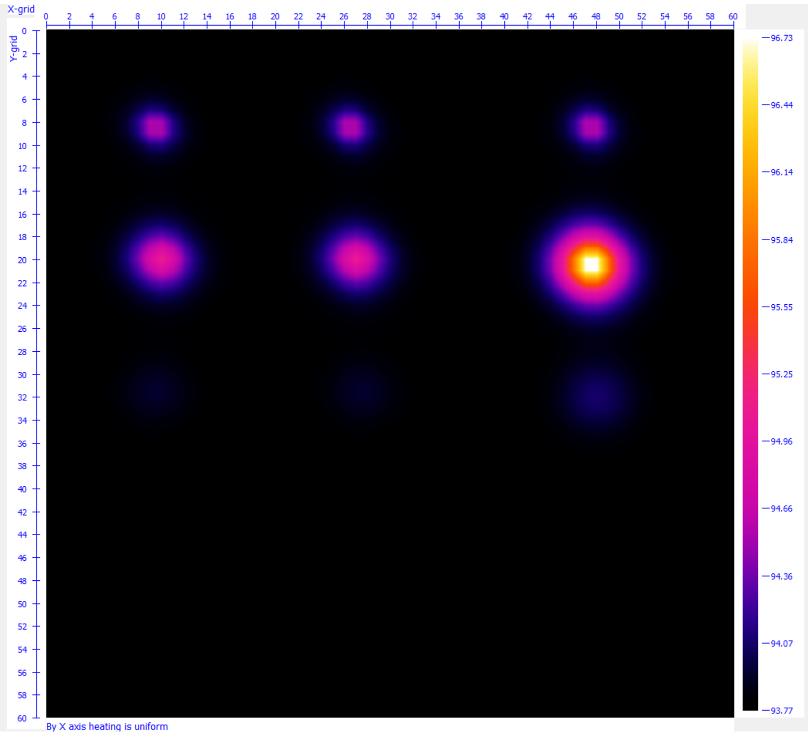

Graph 86 Space profiles of the different rows of defects using optical lockin simulation ML16 settings

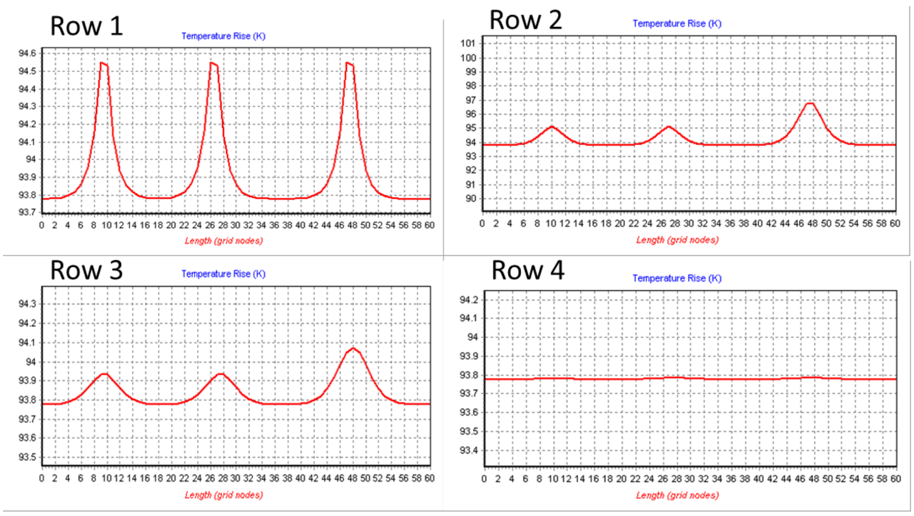

Graph 87 Delta T profiles for different rows of defects using optical lockin simulation ML16 settings. Row#1 in blue, Row #2 in green, Row# 3 in Orange and Row#4 in red

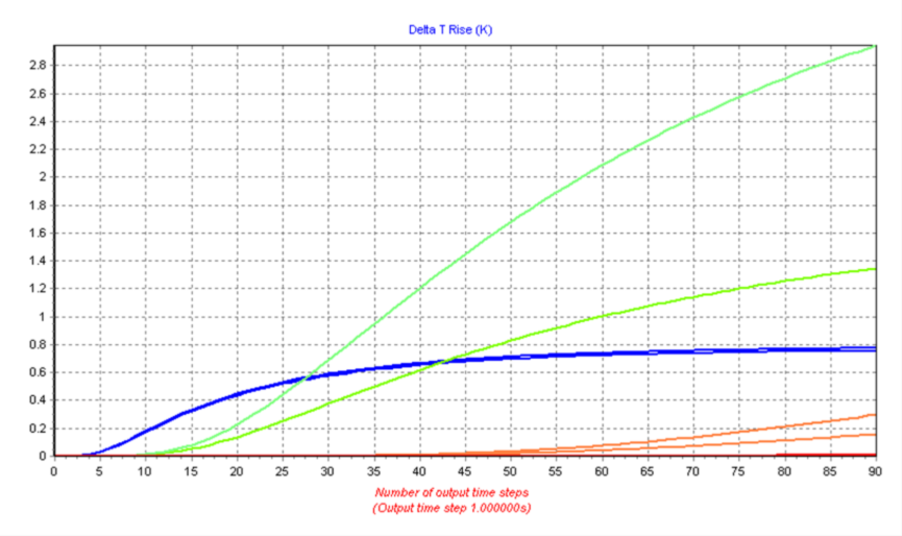

Graph 88 Delta T profiles for Row #3 and #4 of defects using optical lockin simulation ML16. Row# 3 in orange and Row#4 in red

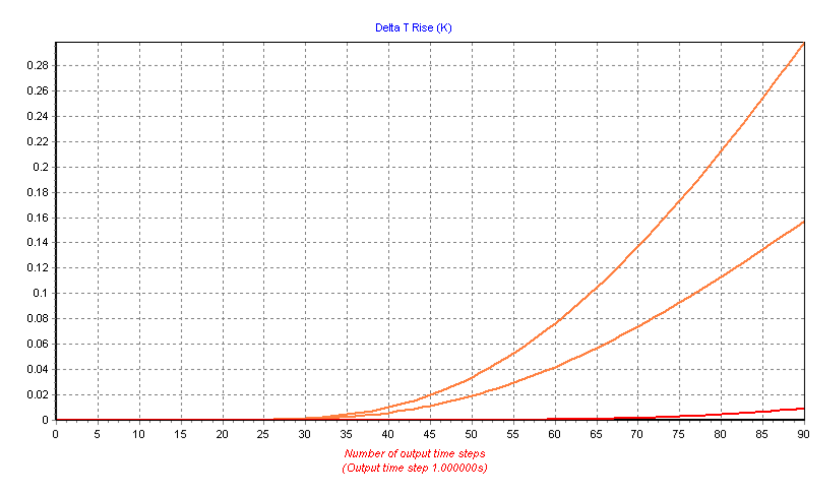

ML 17

Figure 76 Thermal image for simulation ML17 using Optical lockin: Heating density 22222 W/m^2, Wave period 4s, Total time 120s

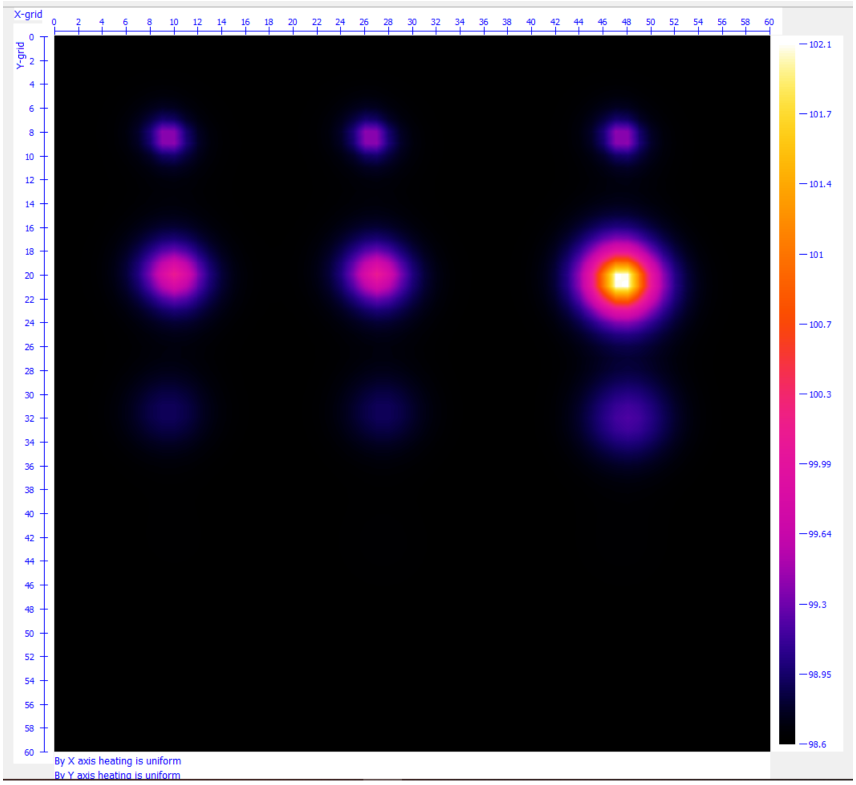

Graph 89 Space profiles of the different rows of defects using optical lockin simulation ML17 settings

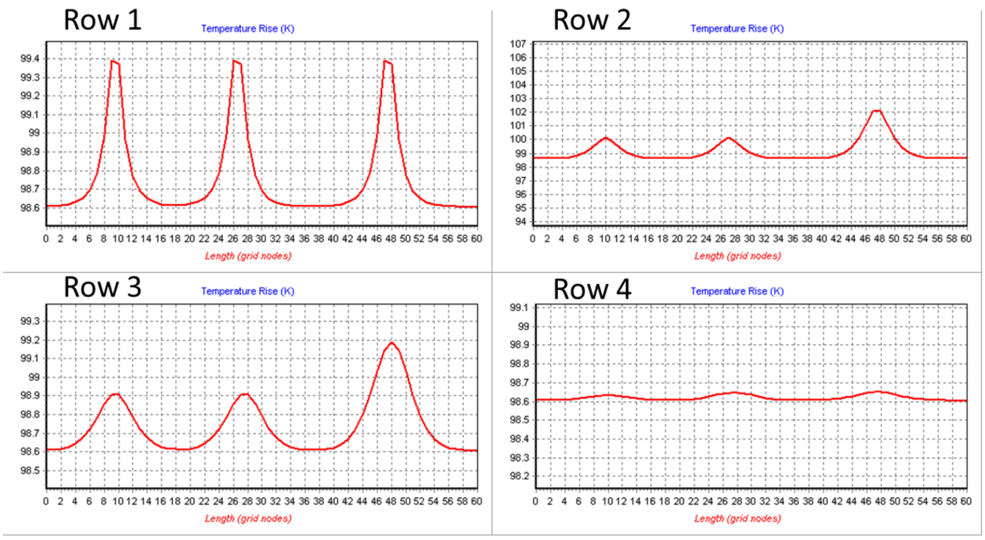

Graph 90 Delta T profiles for different rows of defects using optical lockin simulation ML17 settings. Row#1 in blue, Row #2 in green, Row# 3 in Orange and Row#4 in red

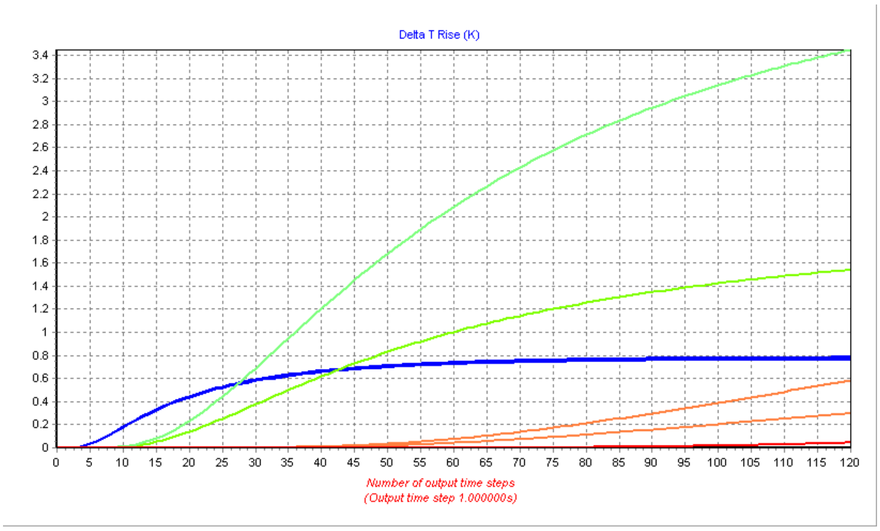

Graph 91 Delta T profiles for Row #3 and #4 of defects using optical lockin simulation ML17. Row# 3 in orange and Row#4 in red

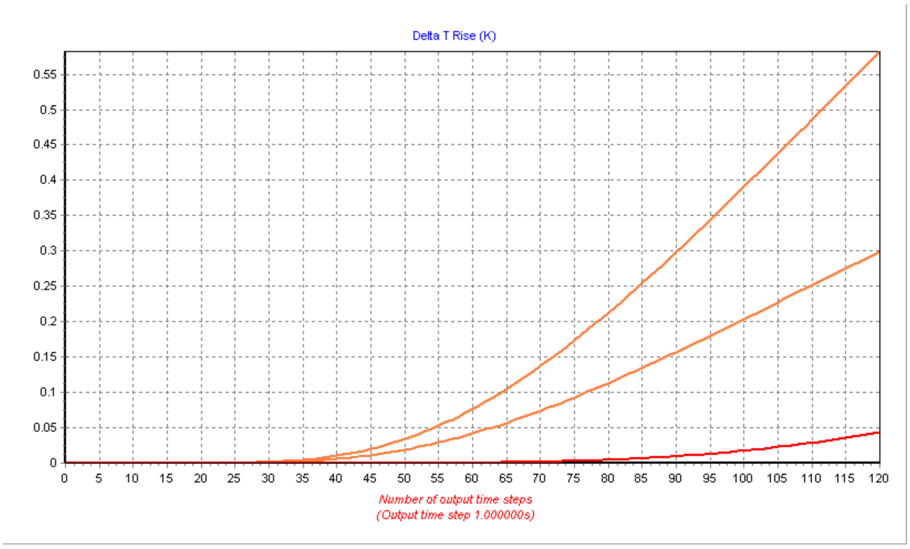

7.2 Optical pulsed thermography- monolithic component

MP1

Figure 77 Thermal image for simulation MP 1 using single square pulse: Heating density 11,111,111W/m^2, Heating time 0.003s, Total time 5s

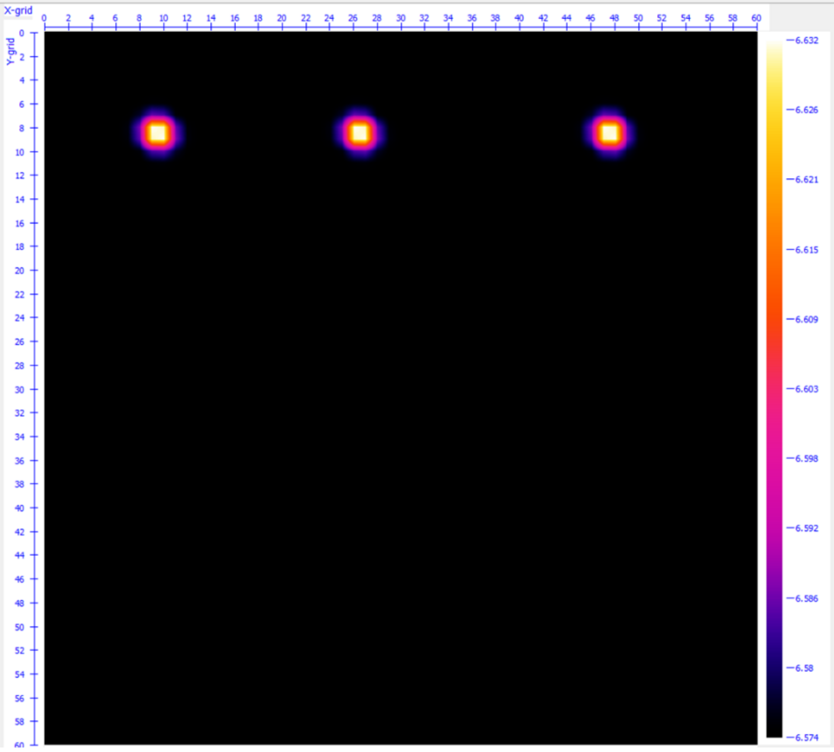

Graph 92 Space profiles of the different rows of defects using optical pulse simulation MP1 settings

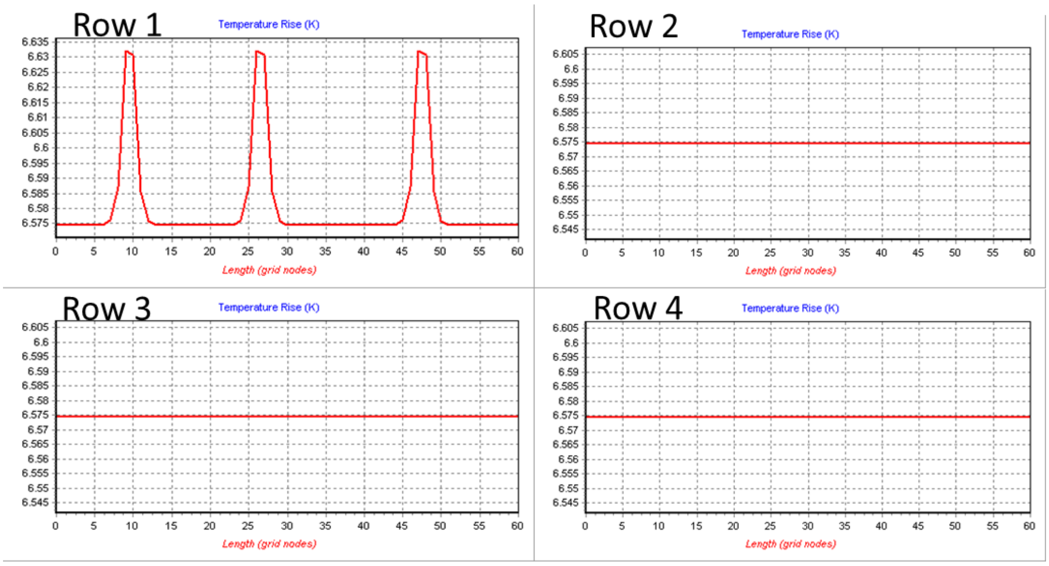

Graph 93 Delta T profiles for different rows of defects using optical pulse simulation MP1. Row#1 in blue, Row #2 in green, Row# 3 in Orange and Row#4 in red

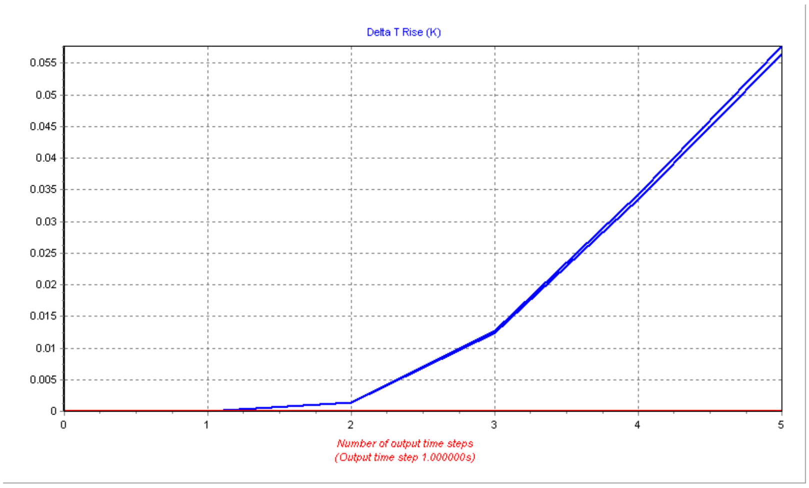

MP2

Figure 78 Thermal image for simulation MP 2 using single square pulse: Heating density 11,111,111 W/m^2, Heating time 0.003s, Total time 10s

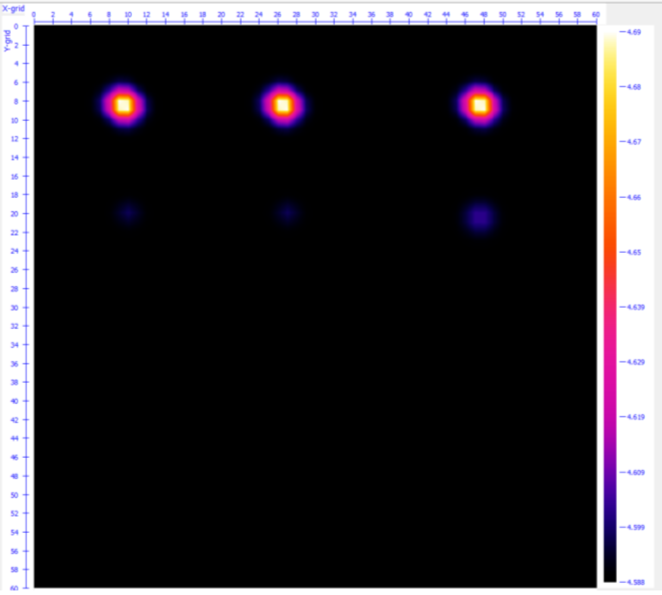

Graph 94 Space profiles of the different rows of defects using optical pulse simulation MP2 settings

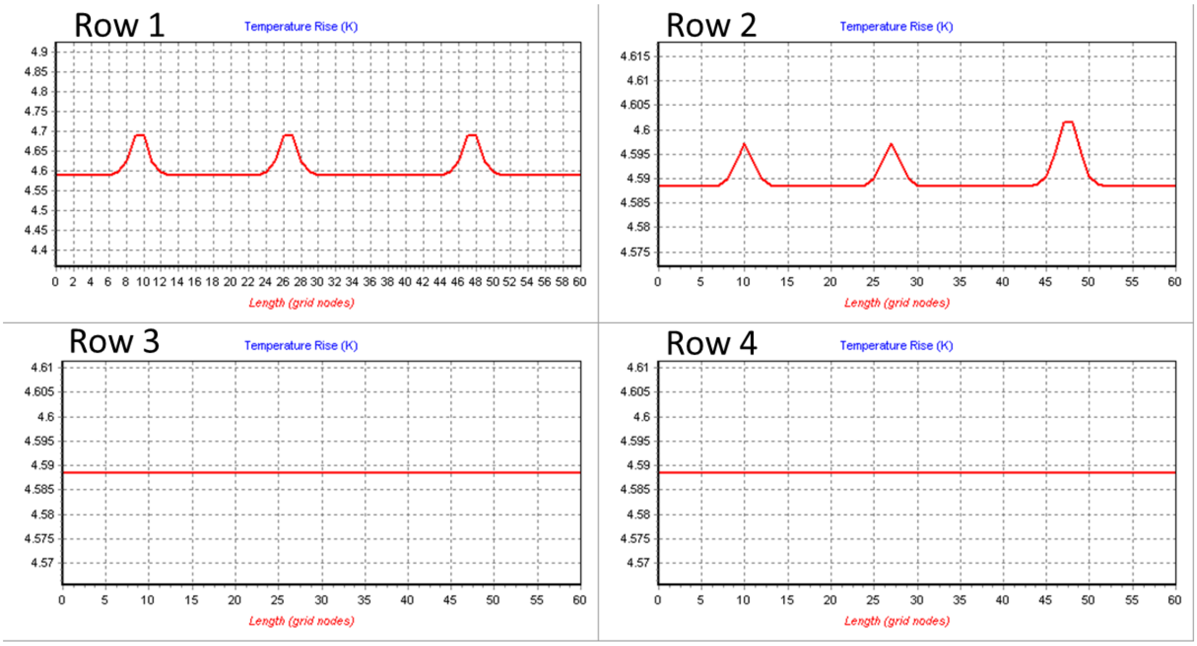

Graph 95 Delta T profiles for different rows of defects using optical pulse simulation MP2. Row#1 in blue, Row #2 in green, Row# 3 in Orange and Row#4 in red

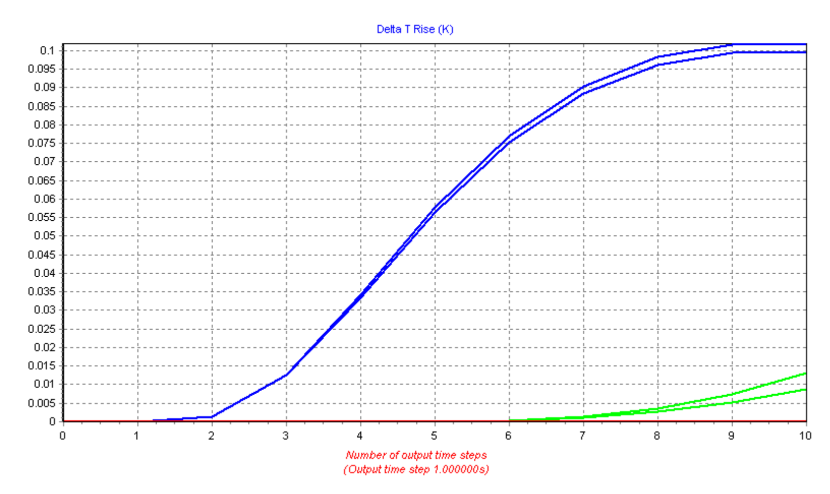

MP3

Figure 79 Thermal image for simulation MP 3 using single square pulse: Heating density 11,111,111 W/m^2, Heating time 0.006s, Total time 10s

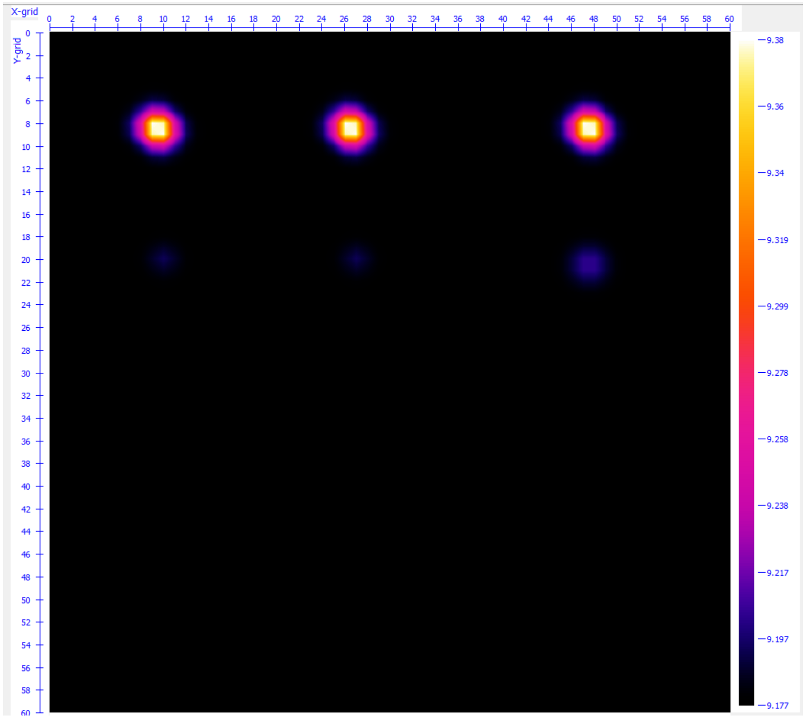

Graph 96 Space profiles of the different rows of defects using optical pulse simulation MP3 settings

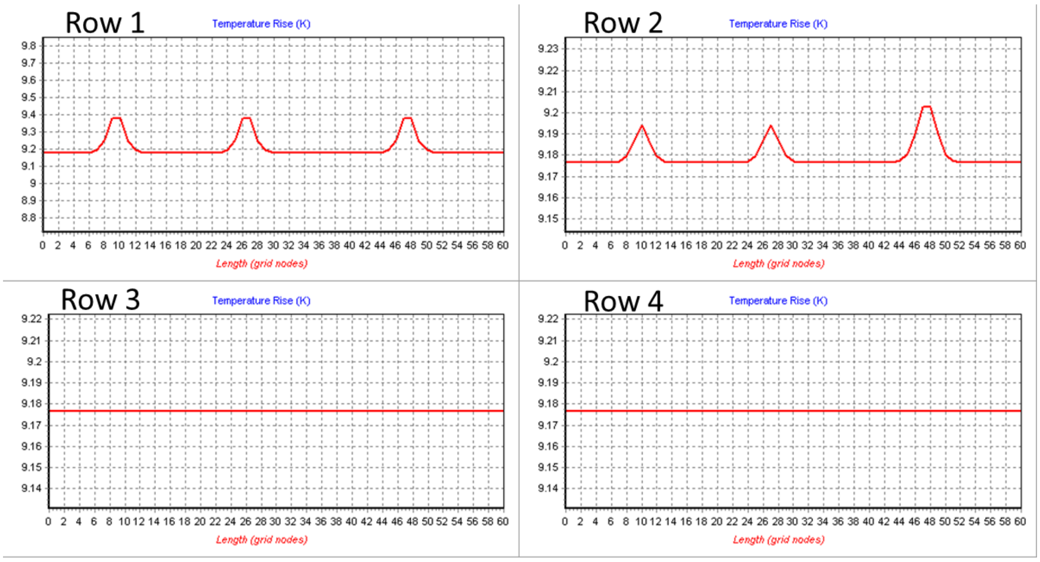

Graph 97 Delta T profiles for different rows of defects using optical pulse simulation MP2. Row#1 in blue, Row #2 in green, Row# 3 in Orange and Row#4 in red

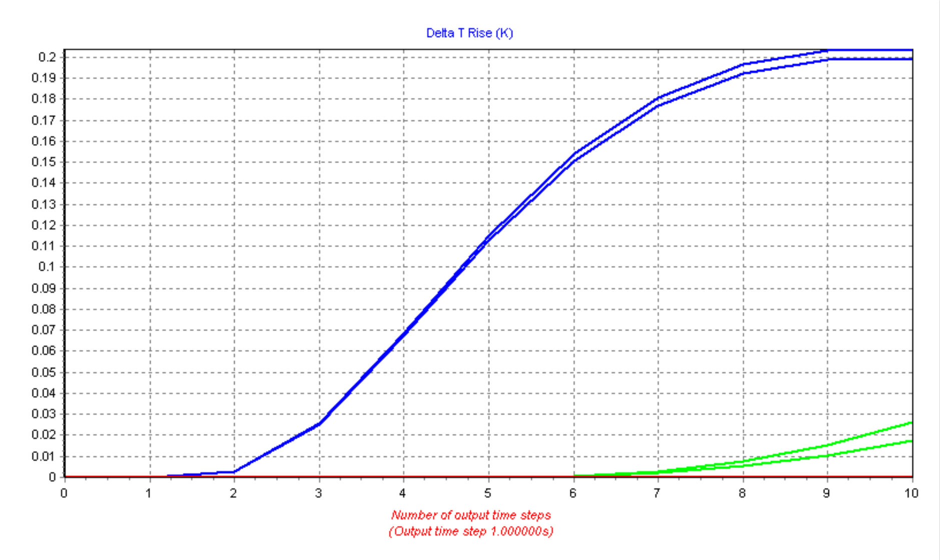

MP4

Figure 80 Thermal image for simulation MP 4 using single square pulse: Heating density 1,000,000W/m^2, Heating time 0.05s, Total time 10s

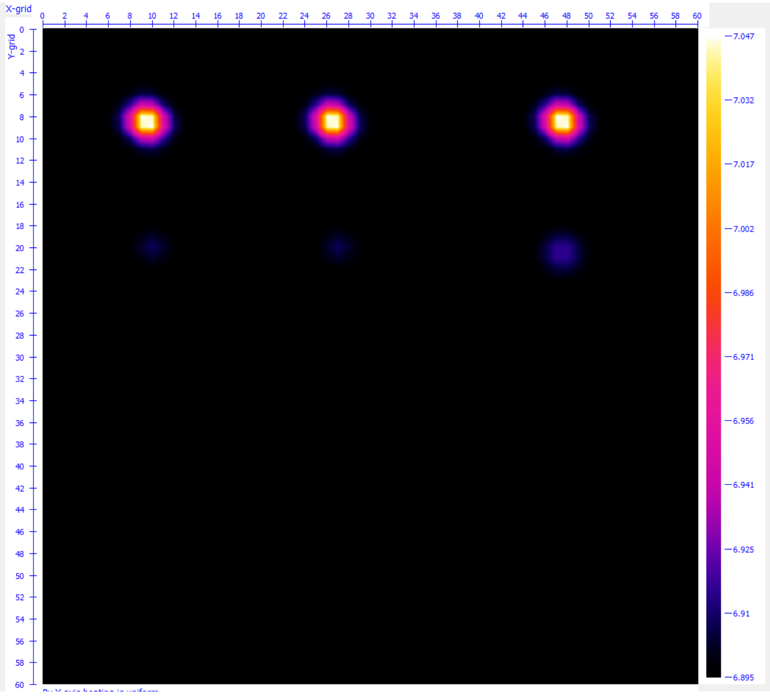

Graph 98 Space profiles of the different rows of defects using optical pulse simulation MP4 settings

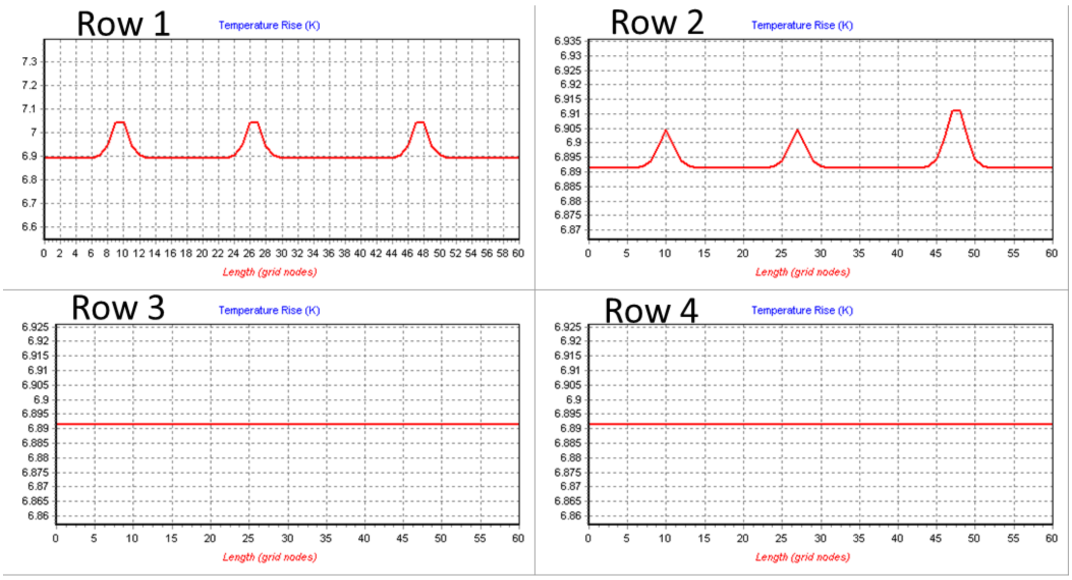

Graph 99 Delta T profiles for different rows of defects using optical pulse simulation MP4. Row#1 in blue, Row #2 in green, Row# 3 in Orange and Row#4 in red

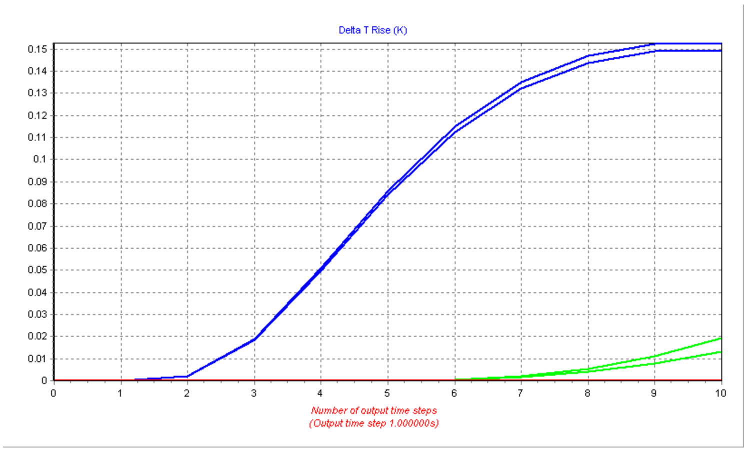

P5

Figure 81 Thermal image for simulation MP 5 using single square pulse: Heating density 1,000,000W/m^2, Heating time 0.05s, Total time 20s

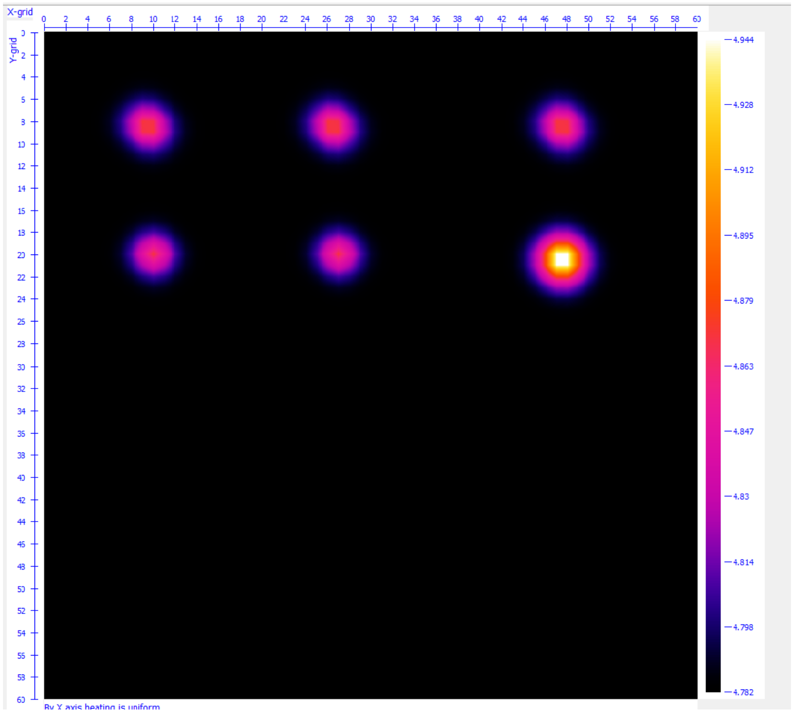

Graph 100 Space profiles of the different rows of defects using optical pulse simulation MP5 settings

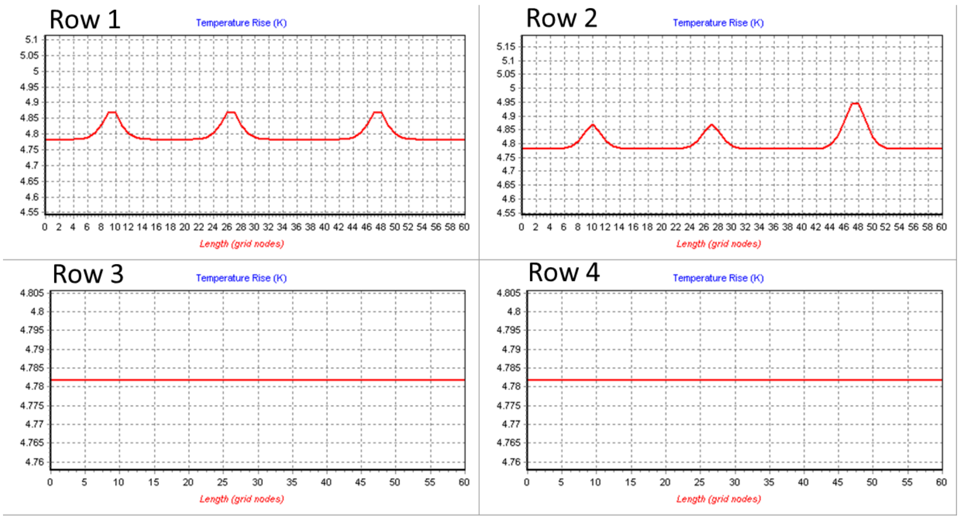

Graph 101 Delta T profiles for different rows of defects using optical pulse simulation MP5. Row#1 in blue, Row #2 in green, Row# 3 in Orange and Row#4 in red

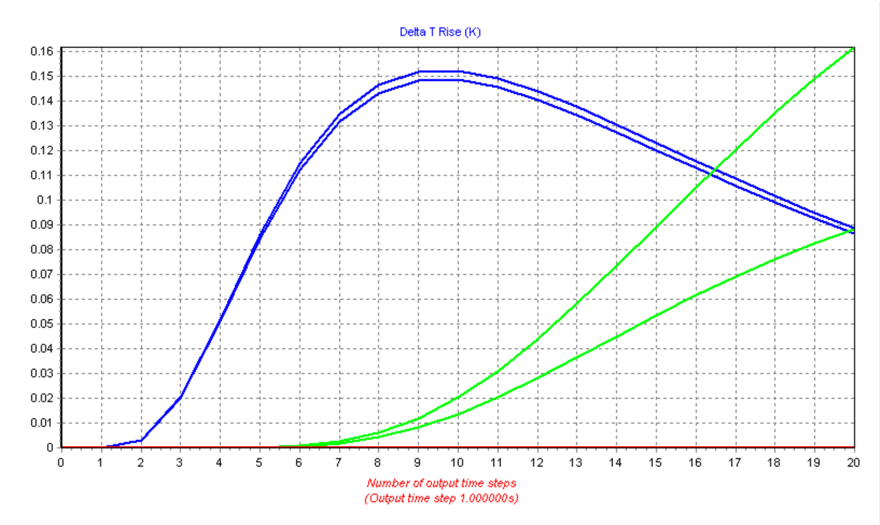

MP6

Figure 82 Thermal image for simulation MP 6 using single square pulse: Heating density 1,000,000W/m^2, Heating time 0.05s, Total time 40s

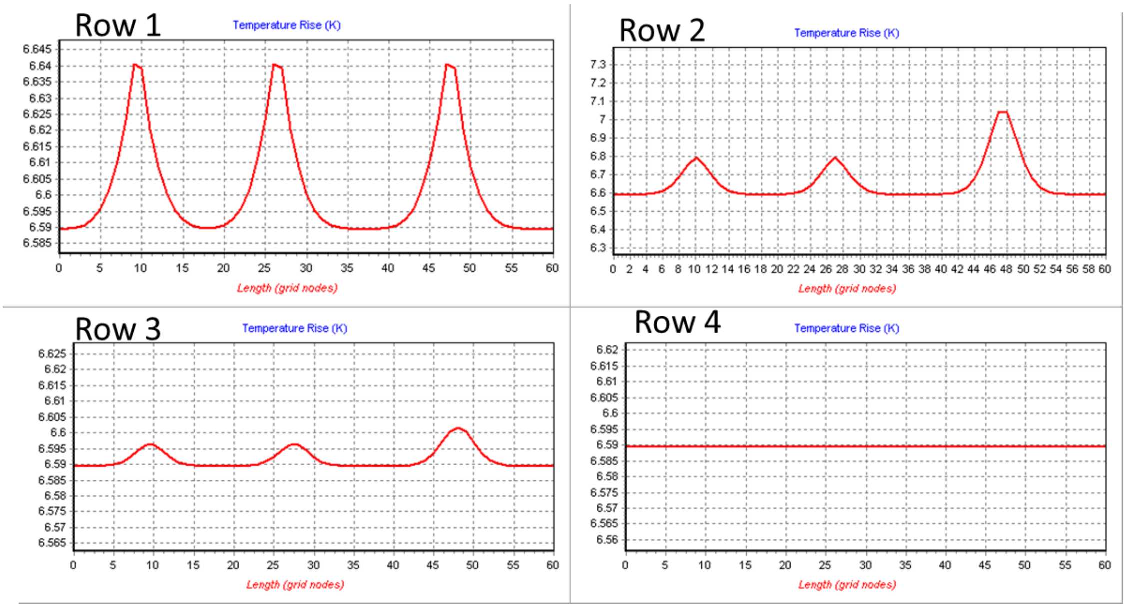

Graph 102 Delta T profiles for different rows of defects using optical pulse simulation MP6. Row#1 in blue, Row #2 in green, Row# 3 in Orange and Row#4 in red

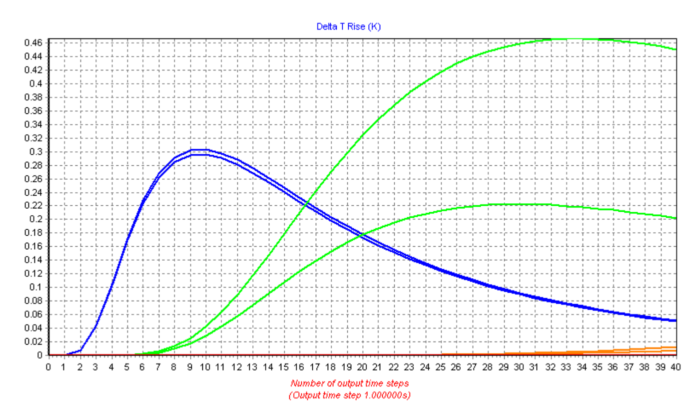

Graph 103 Delta T profiles for Row #3 and #4 of defects using optical pulse simulation MP6. Row# 3 in orange and Row#4 in red

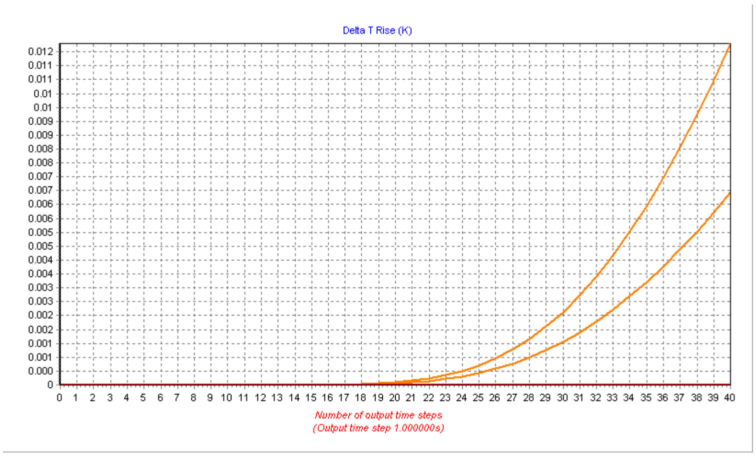

MP7

Figure 83 Thermal image for simulation MP 7 using single square pulse: Heating density 1,000,000W/m^2, Heating time 0.05s, Total time 60s

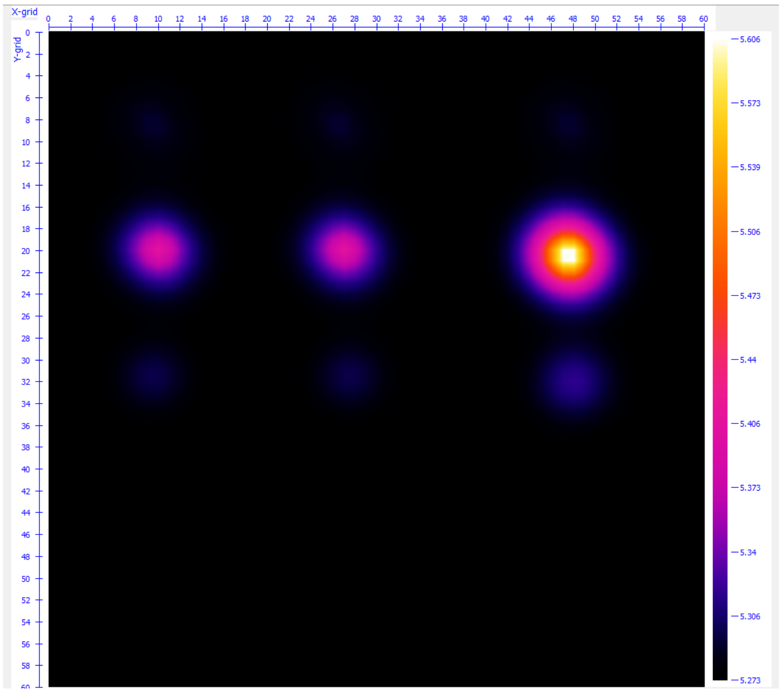

Graph 104 Space profiles of the different rows of defects using optical pulse simulation MP7 settings

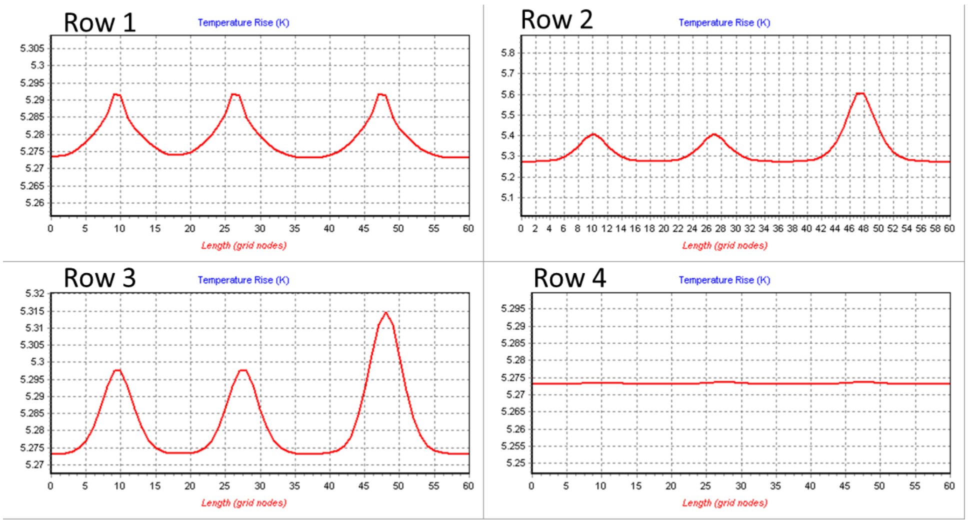

Graph 105 Delta T profiles for different rows of defects using optical pulse simulation MP7. Row#1 in blue, Row #2 in green, Row# 3 in Orange and Row#4 in red

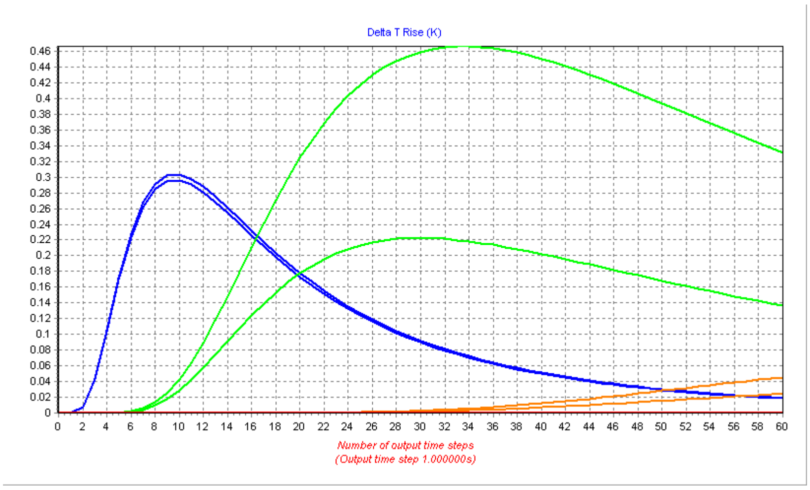

Graph 106 Delta T profiles for Row #3 and #4 of defects using optical pulse simulation MP7. Row# 3 in orange and Row#4 in red

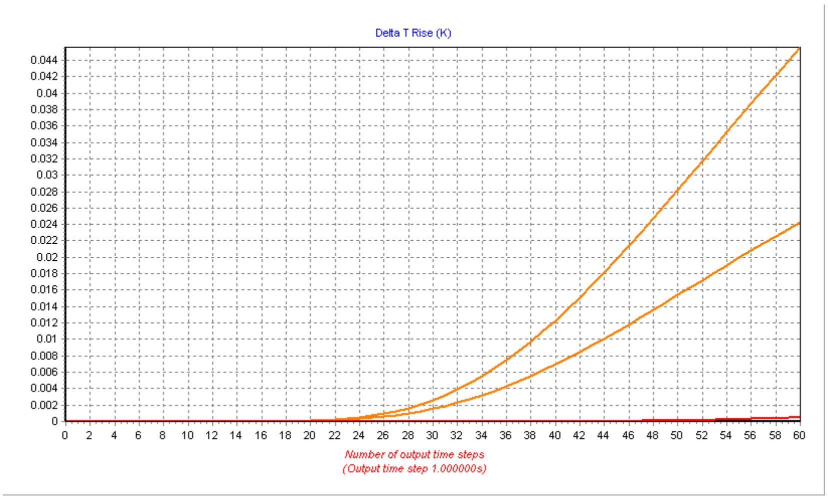

MP8

Figure 84 Thermal image for simulation MP 8 using single square pulse: Heating density 333000 W/m^2, Heating time 0.1s, Total time 20s

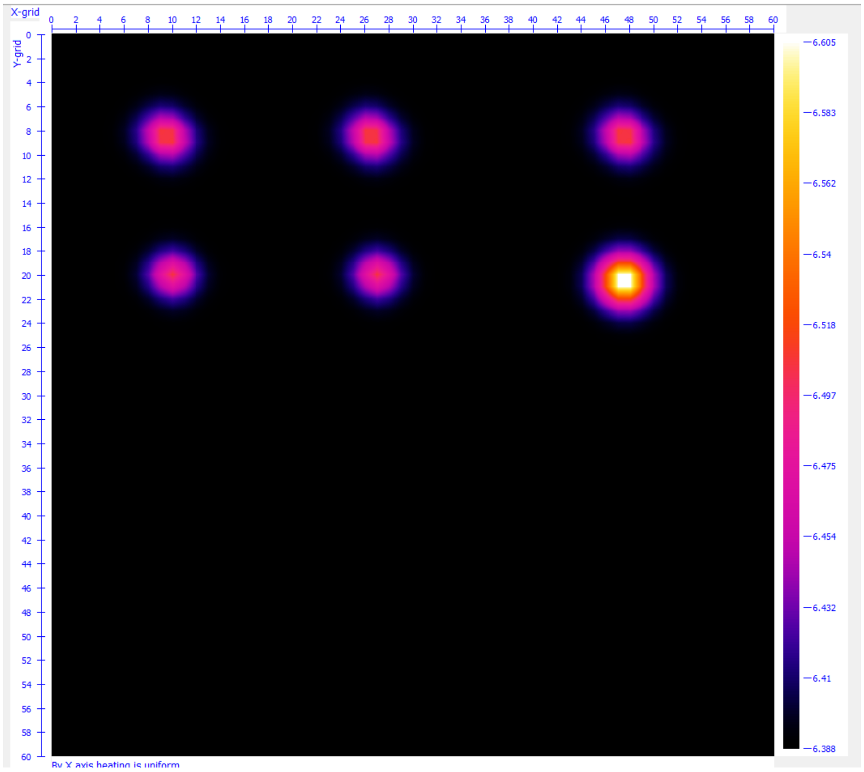

Graph 107 Space profiles of the different rows of defects using optical pulse simulation MP8 settings

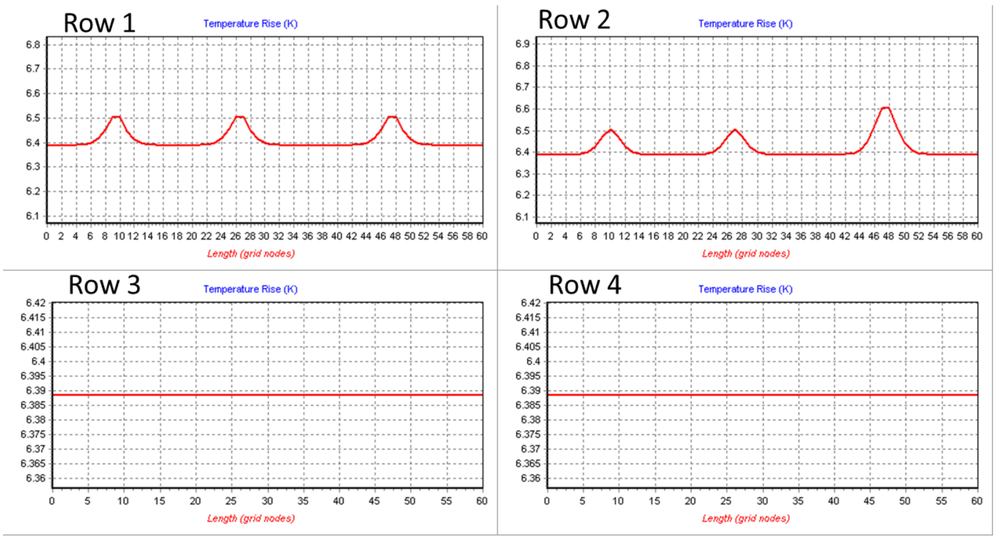

Graph 108 Delta T profiles for different rows of defects using optical pulse simulation MP7. Row#1 in blue, Row #2 in green, Row# 3 in Orange and Row#4 in red

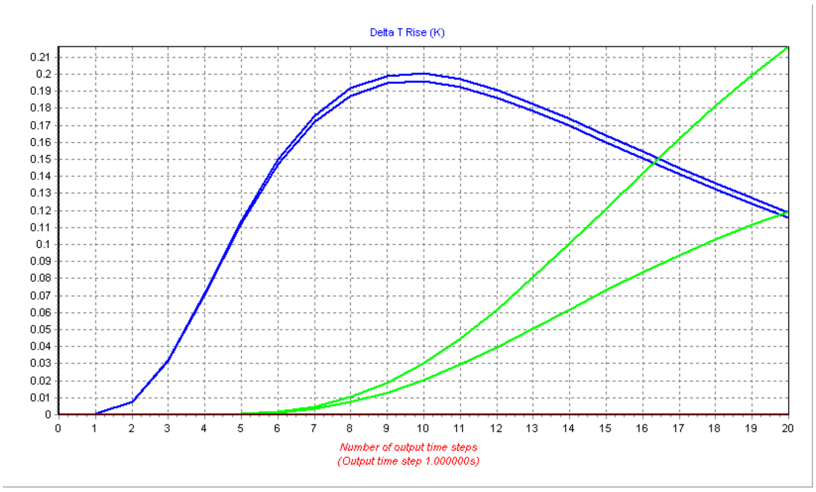

MP9

Figure 85 Thermal image for simulation MP 9 using single square pulse: Heating density 333000 W/m^2, Heating time 0.1s, Total time 40s

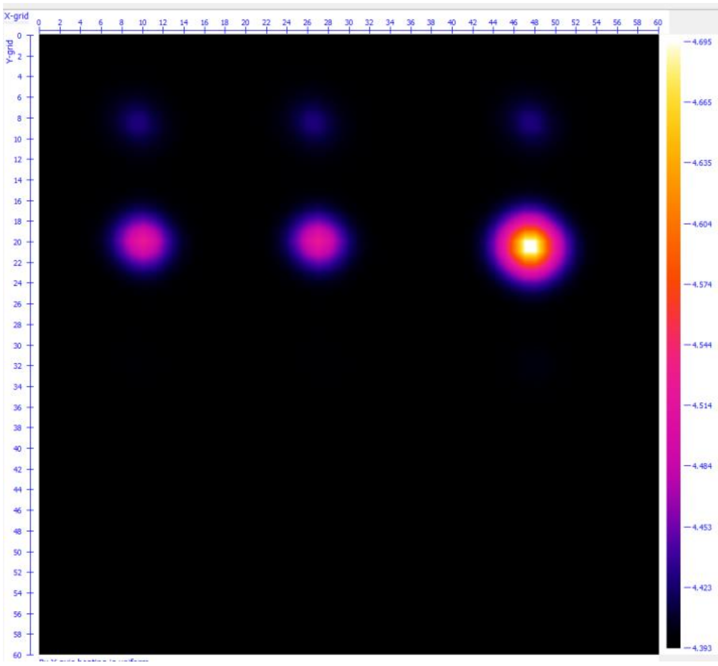

Figure 86 Space profiles of the different rows of defects using optical pulse simulation MP9 settings

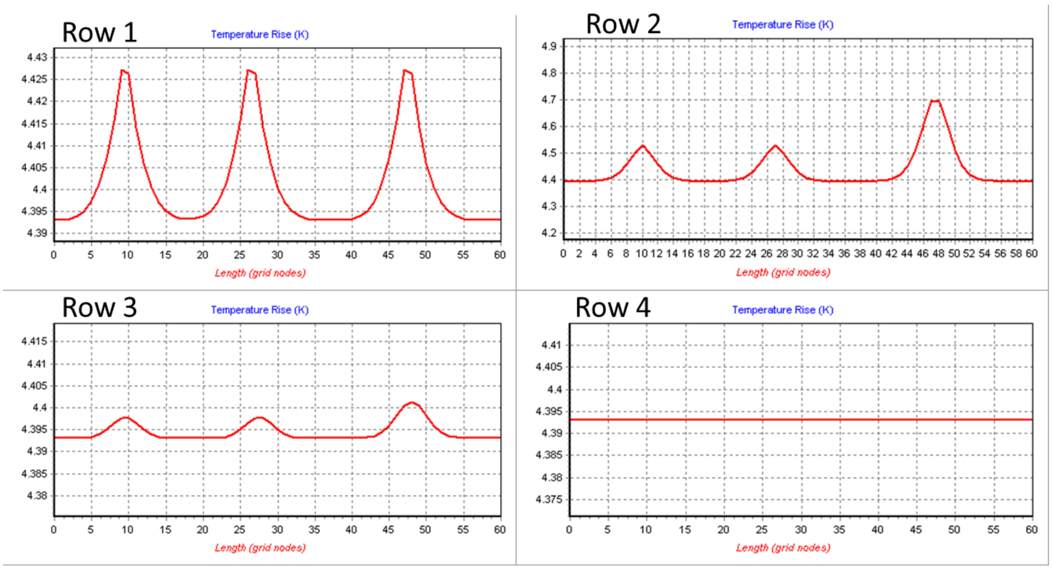

Graph 109 Delta T profiles for different rows of defects using optical pulse simulation MP9. Row#1 in blue, Row #2 in green, Row# 3 in Orange and Row#4 in red

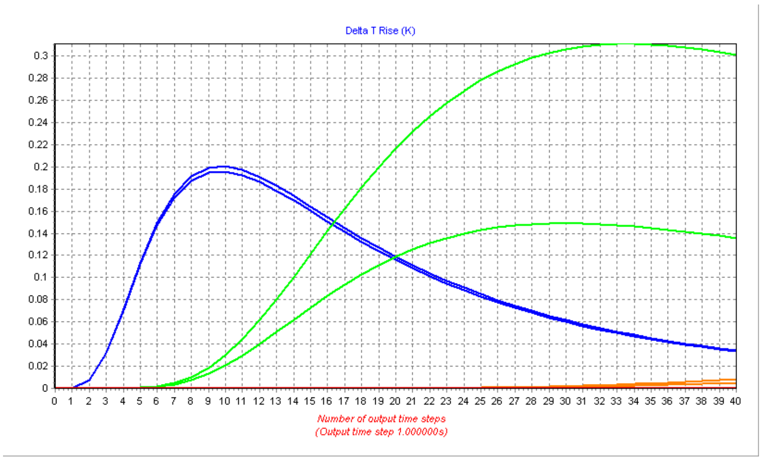

MP10

Figure 87 Thermal image for simulation MP 10 using single square pulse: Heating density 333000 W/m^2, Heating time 0.1s, Total time 60s

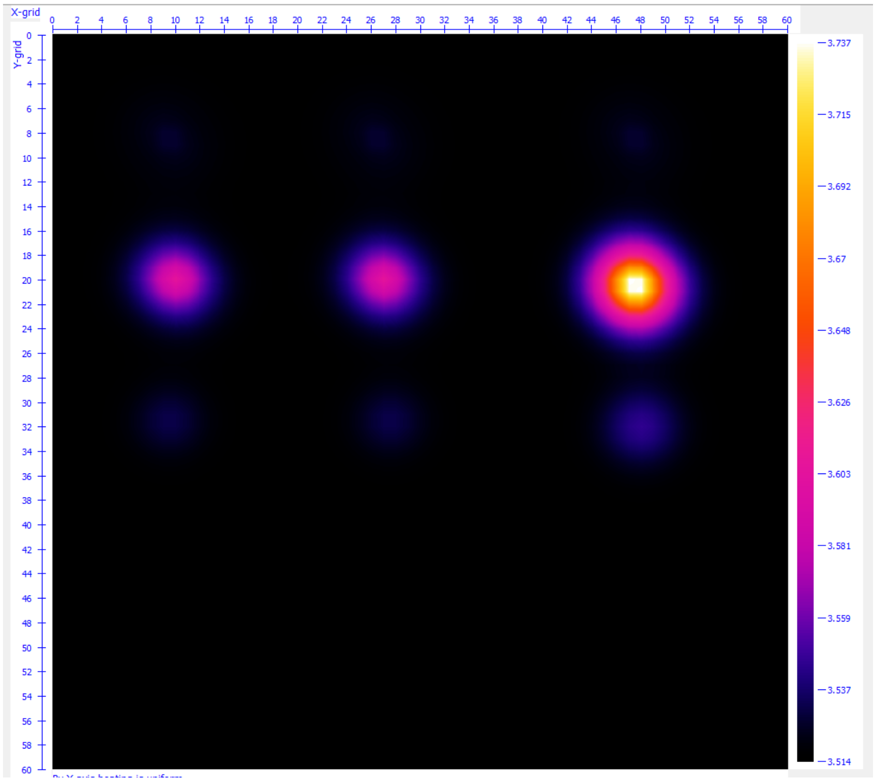

Graph 110 Space profiles of the different rows of defects using optical pulse simulation MP10 settings

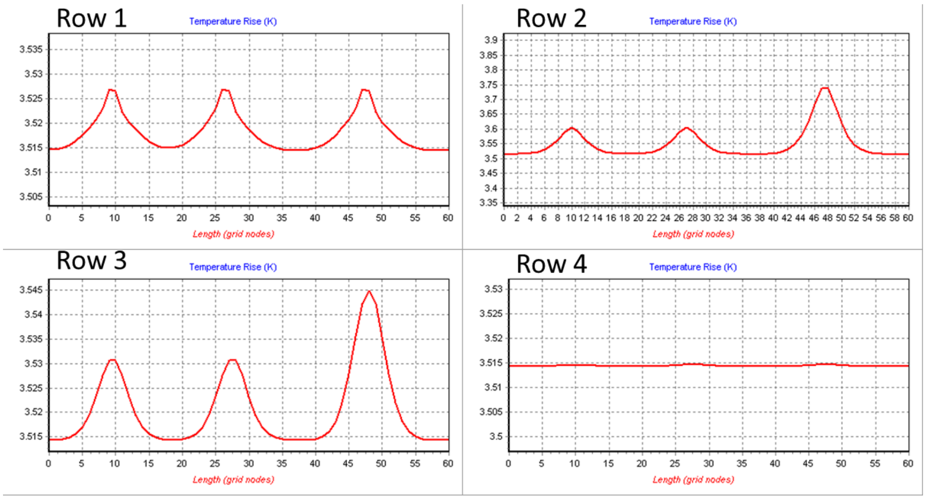

Graph 111 Delta T profiles for different rows of defects using optical pulse simulation MP10. Row#1 in blue, Row #2 in green, Row# 3 in Orange and Row#4 in red

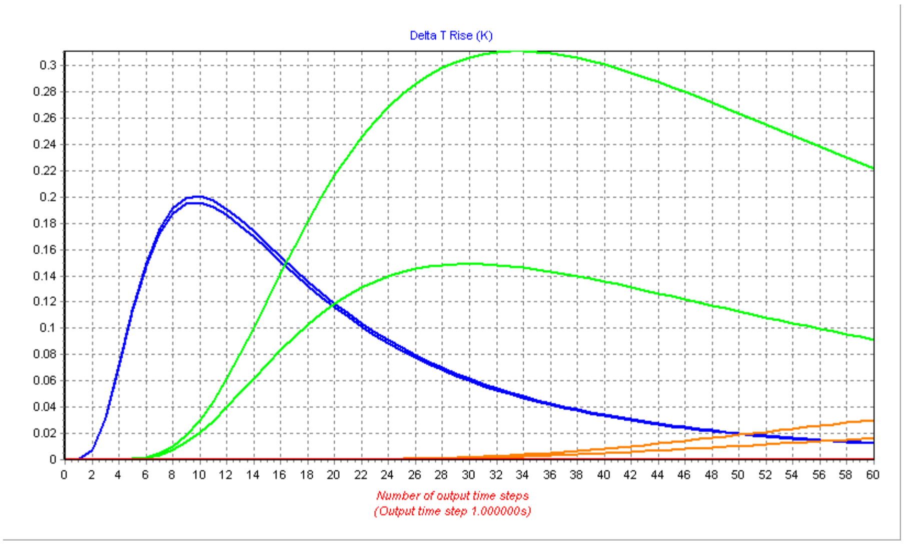

Graph 112 Delta T profiles for Row #3 and #4 of defects using optical pulse simulation MP10. Row# 3 in orange and Row#4 in red

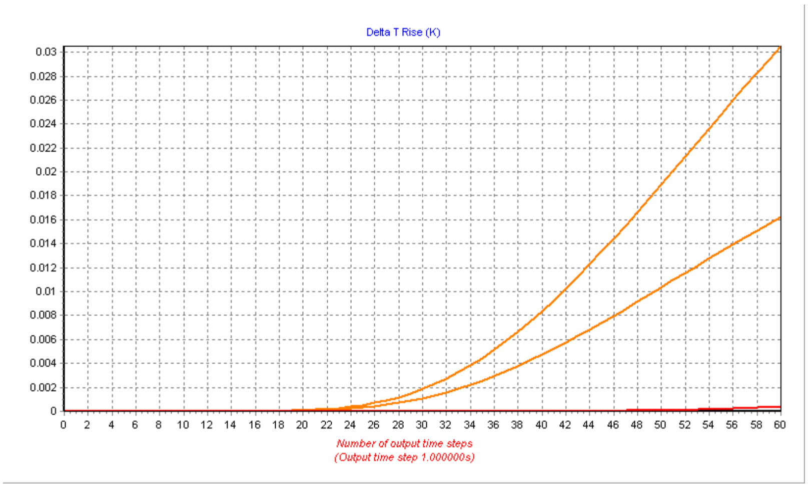

MP11

Figure 88 Thermal image for simulation MP 11 using single square pulse: Heating density 666000 W/m^2, Heating time 0.1s, Total time 20s

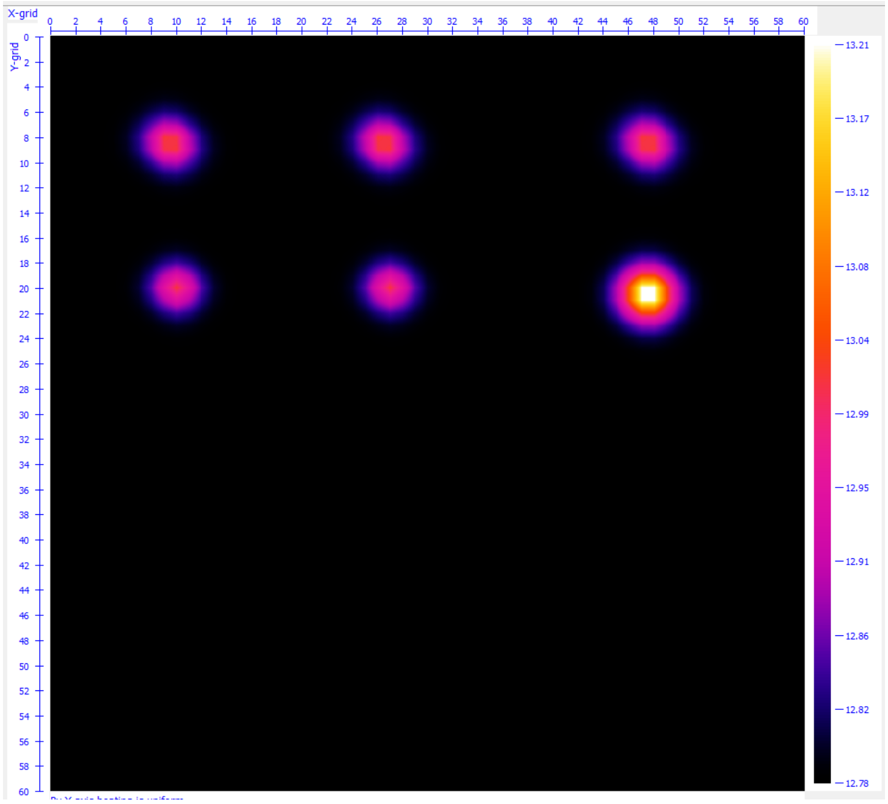

Graph 113 Space profiles of the different rows of defects using optical pulse simulation MP11 settings

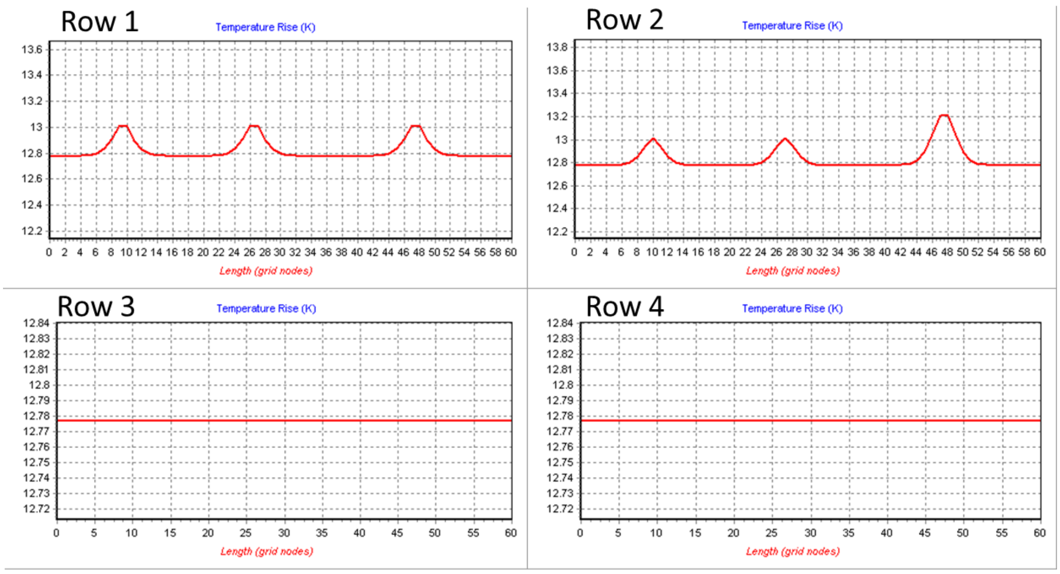

Graph 114 Delta T profiles for different rows of defects using optical pulse simulation MP11. Row#1 in blue, Row #2 in green, Row# 3 in Orange and Row#4 in red

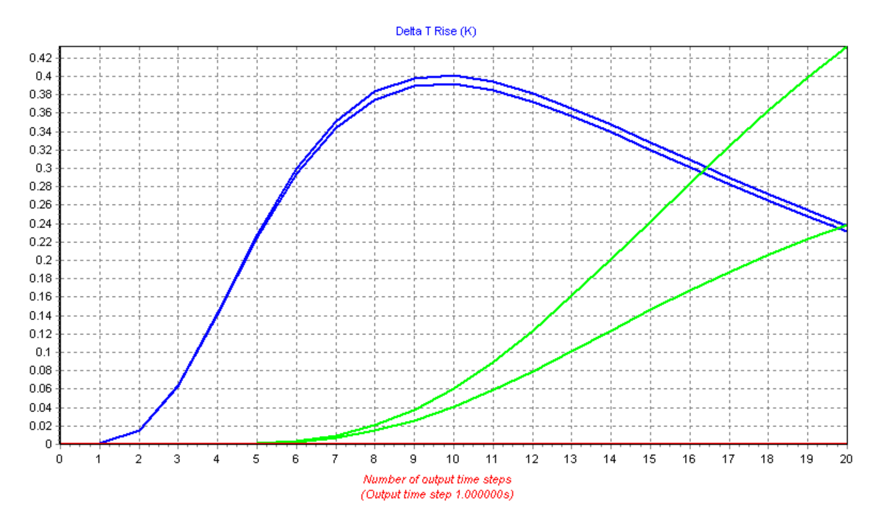

MP12

Figure 89 Thermal image for simulation MP 12 using single square pulse: Heating density 666000 W/m^2, Heating time 0.1s, Total time 40s

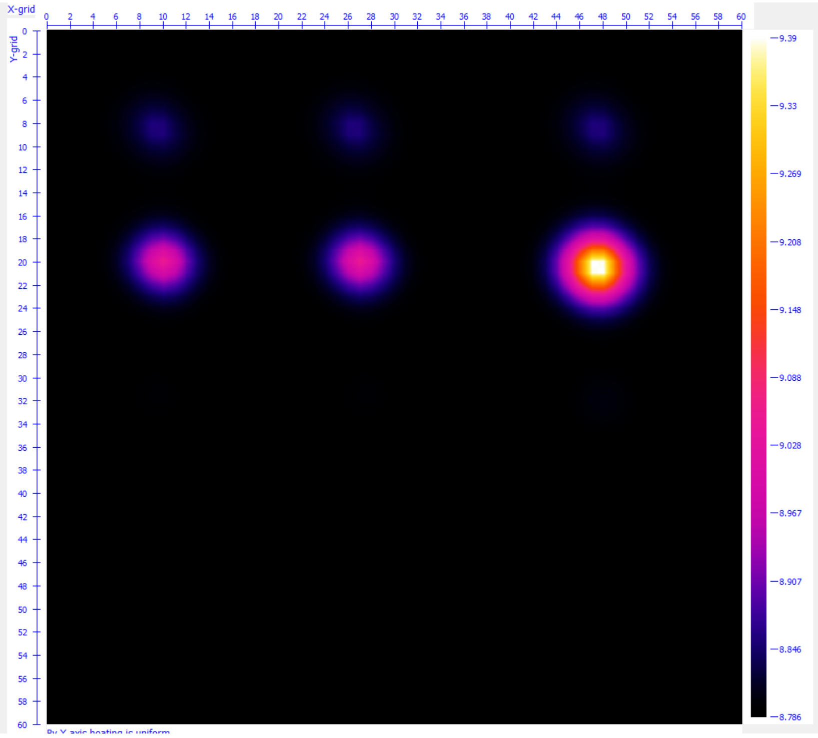

Graph 115 Space profiles of the different rows of defects using optical pulse simulation MP12 settings

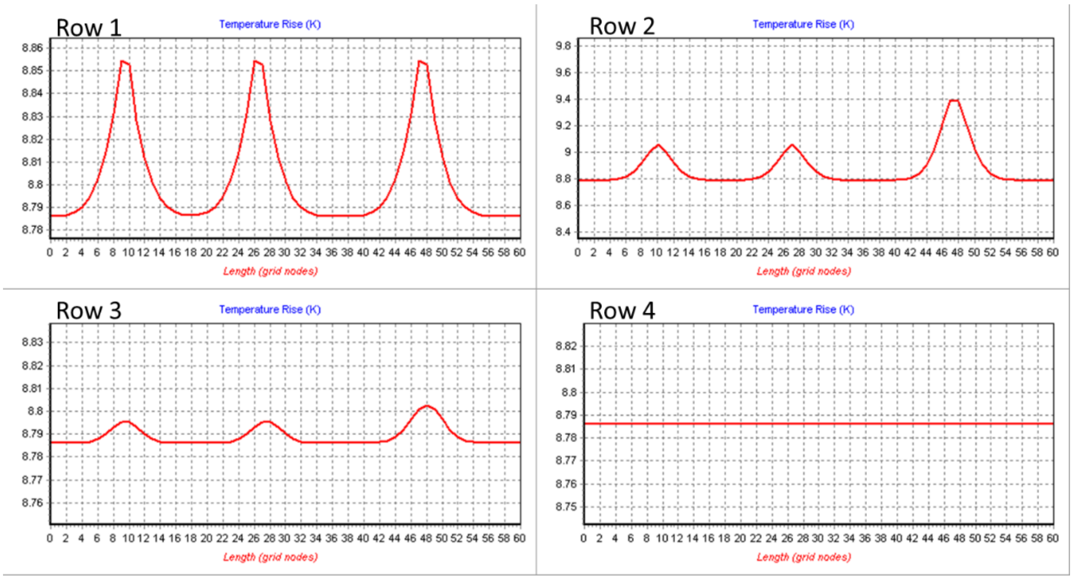

Graph 116 Delta T profiles for different rows of defects using optical pulse simulation MP11. Row#1 in blue, Row #2 in green, Row# 3 in Orange and Row#4 in red

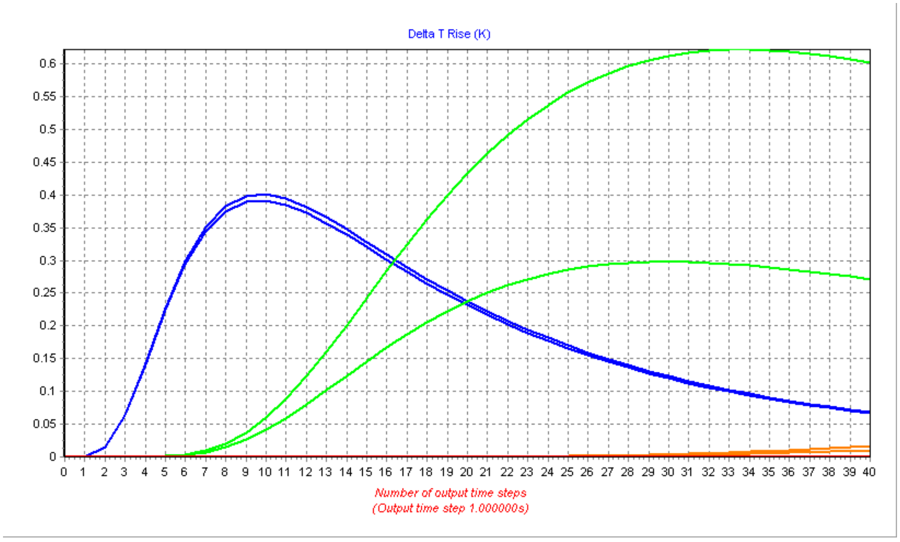

Graph 117 Delta T profiles for Row #3 and #4 of defects using optical pulse simulation MP12. Row# 3 in orange and Row#4 in red

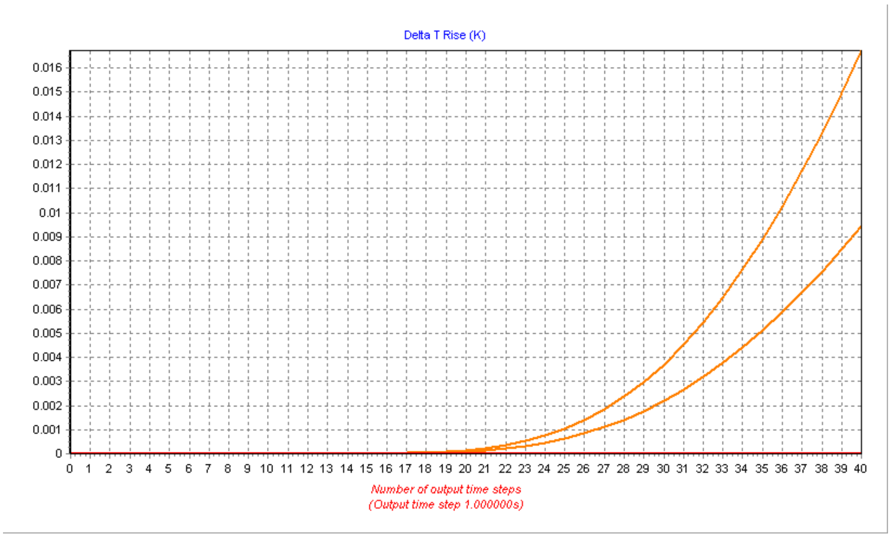

8 Appendix 2 Thermography simulation for CFRP-PET foam component

8.1 Optical lockin thermography- sandwich component

SL1

Figure 90 Thermal image for simulation SL1 using optical lockin: Heating density 3000 W/m^2, wave period 3s, Total time 30s

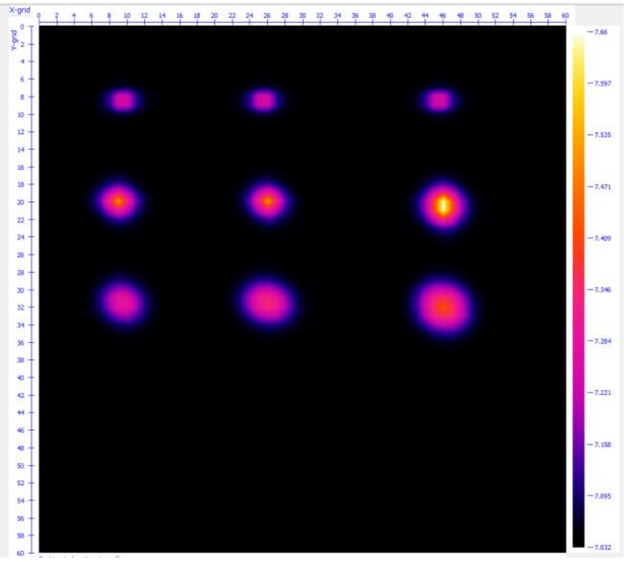

Graph 118 Space profiles of the different rows of defects using optical lockin simulation SL1 settings

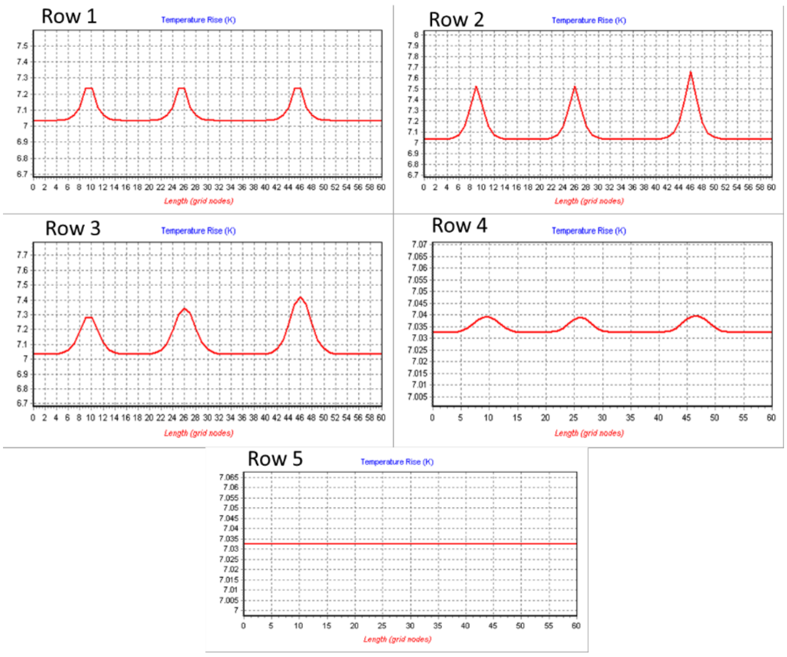

Graph 119 Delta T profiles for different rows of defects using optical pulsed thermography simulation SL1. Row#1 in blue, Row #2 in green, Row# 3 in Orange, Row# 4 yellow and Row #5 in red

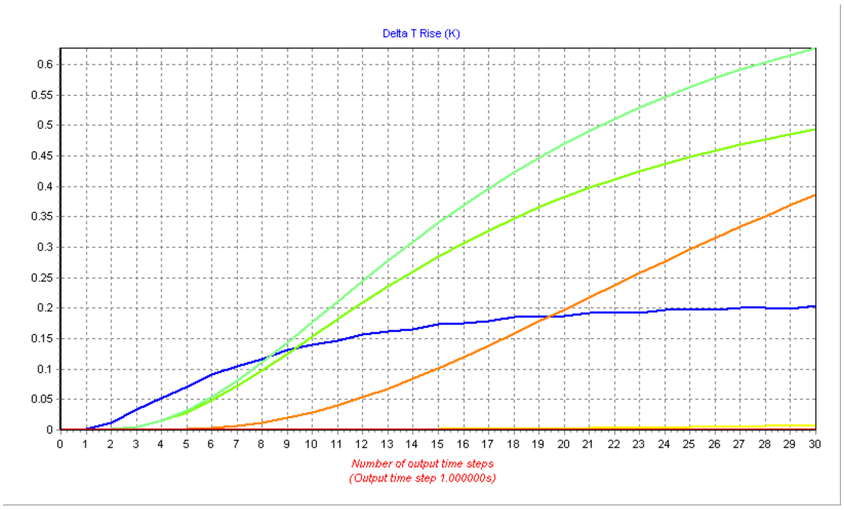

Graph 120 Delta T profiles for Row #4 and #5 of defects using optical lockin simulation SL1. Row# 4 in yellow and Row#4 in red

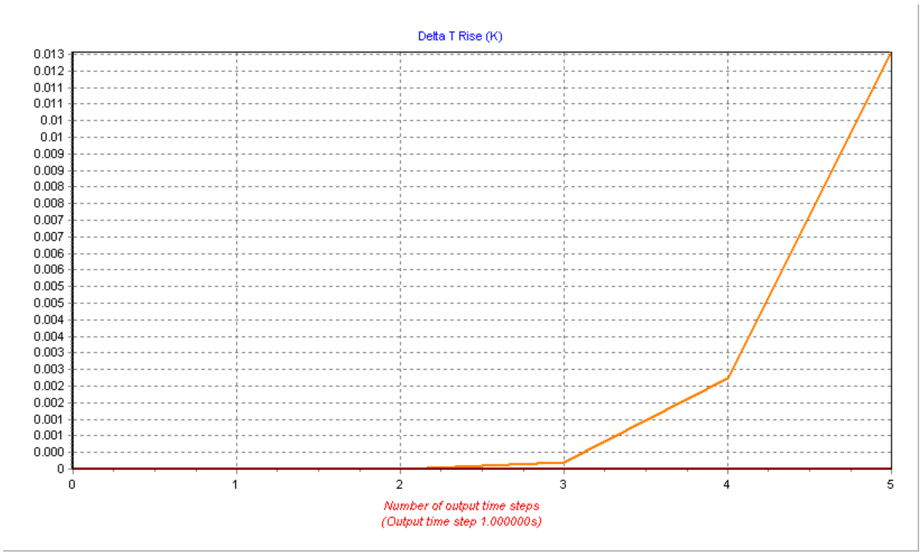

SL2

Figure 91 Thermal image for simulation SL2 using optical lockin: Heating density 6000 W/m^2, wave period 4s, Total time 20s

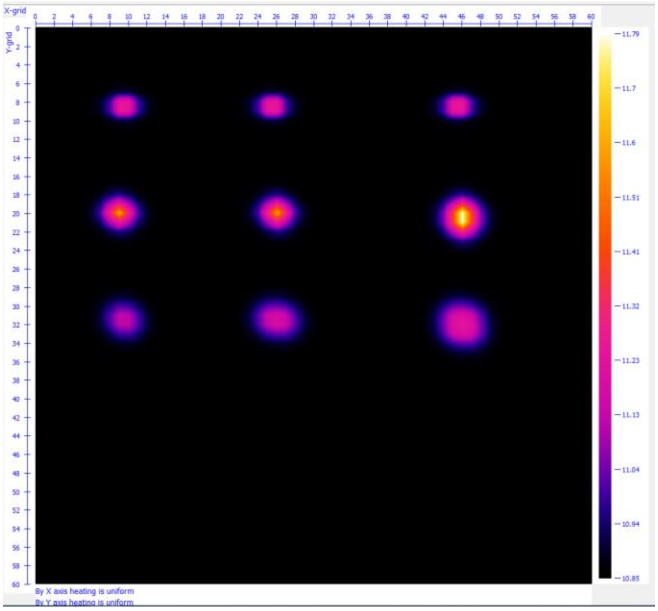

Graph 121 Space profiles of the different rows of defects using optical lockin simulation SL2 settings

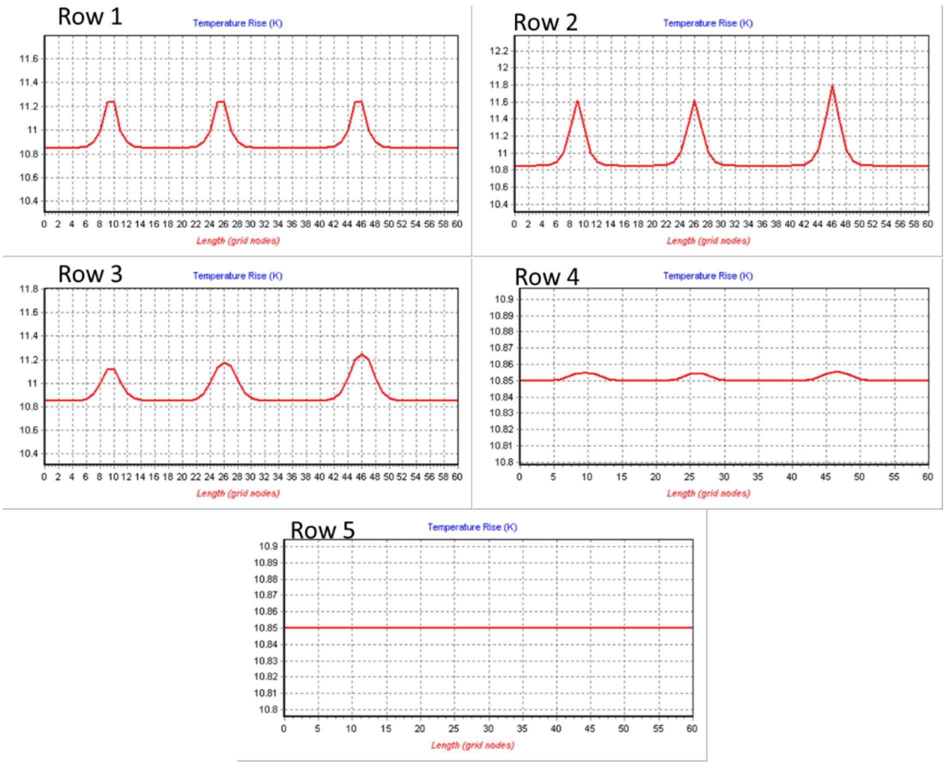

Graph 122 Delta T profiles for different rows of defects using optical pulsed thermography simulation SL2. Row#1 in blue, Row #2 in green, Row# 3 in Orange, Row# 4 yellow and Row #5 in red

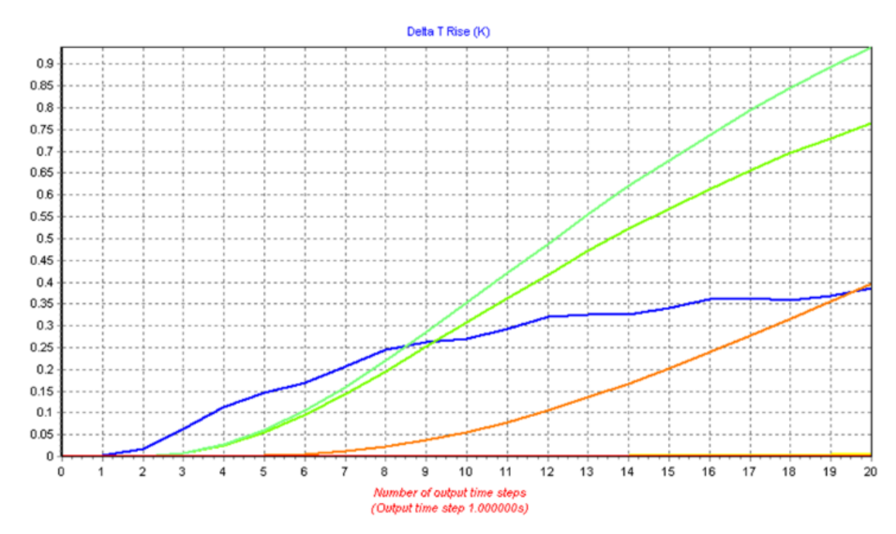

Graph 123 Delta T profiles for Row #4 and #5 of defects using optical lockin simulation SL2. Row# 4 in yellow and Row#4 in red

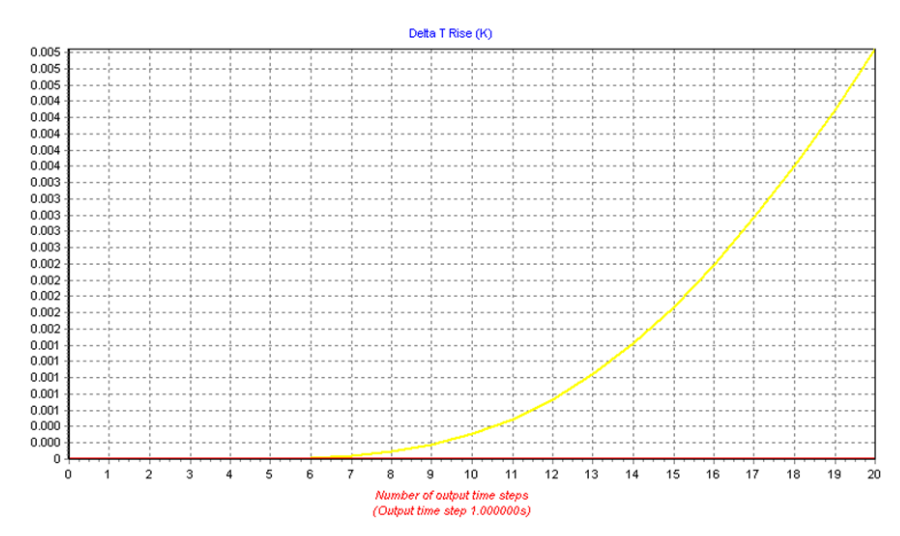

SL3

Figure 92 Thermal image for simulation SL3 using optical lockin: Heating density 6000 W/m^2, wave period 4s, Total time 30s

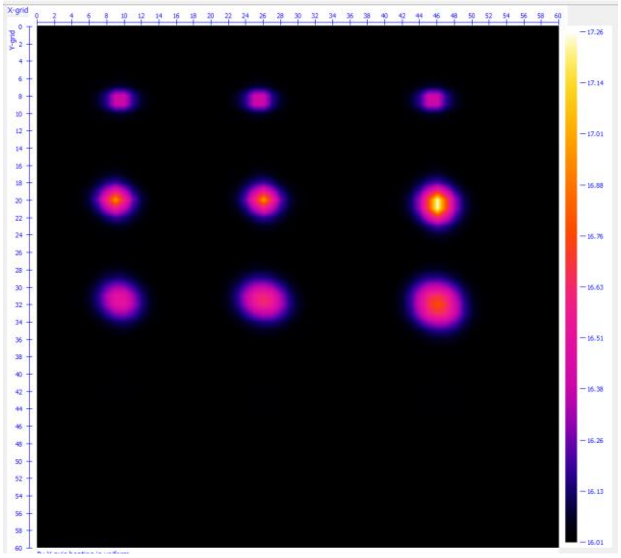

Graph 124 Space profiles of the different rows of defects using optical lockin simulation SL3 settings

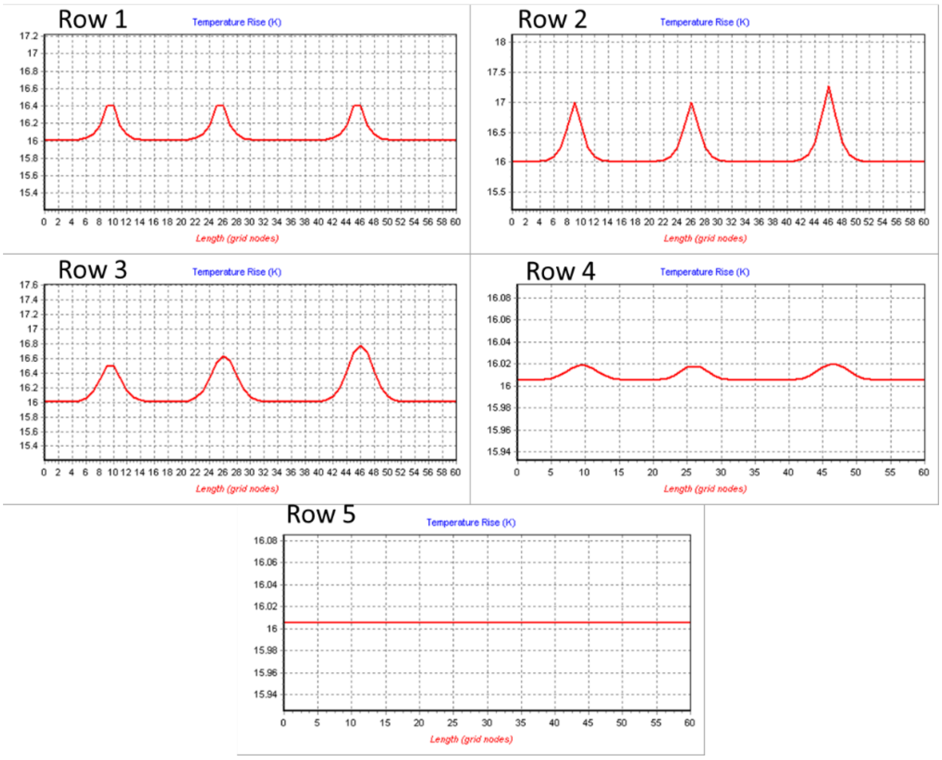

Graph 125 Delta T profiles for Row #4 and #5 of defects using optical lockin simulation SL3. Row# 4 in yellow and Row#4 in red

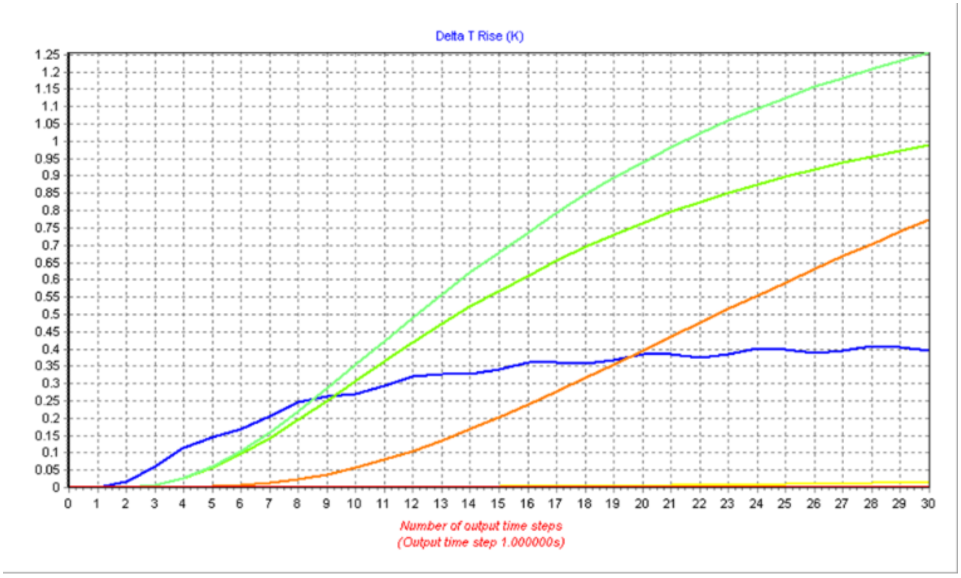

Graph 126 Delta T profiles for Row #4 and #5 of defects using optical lockin simulation SL3. Row# 4 in yellow and Row#4 in red

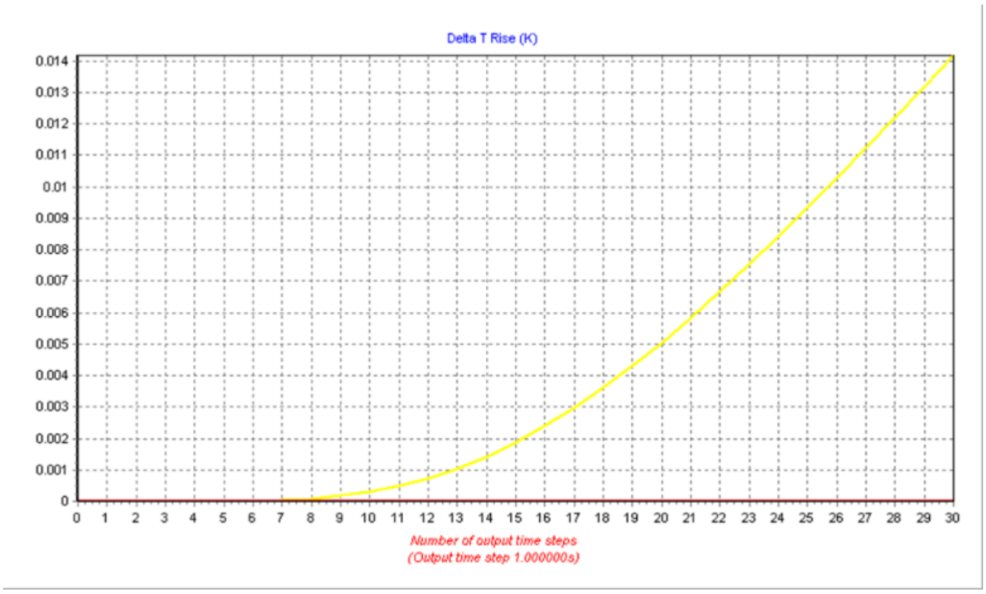

SL4

Figure 93 Thermal image for simulation SL2 using optical lockin: Heating density 6000 W/m^2, wave period 6s, Total time 30s

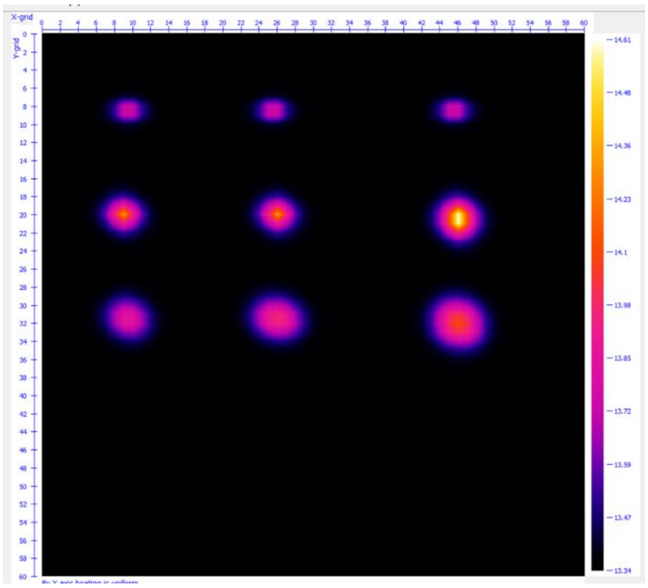

Graph 127 Space profiles of the different rows of defects using optical lockin simulation SL4 settings

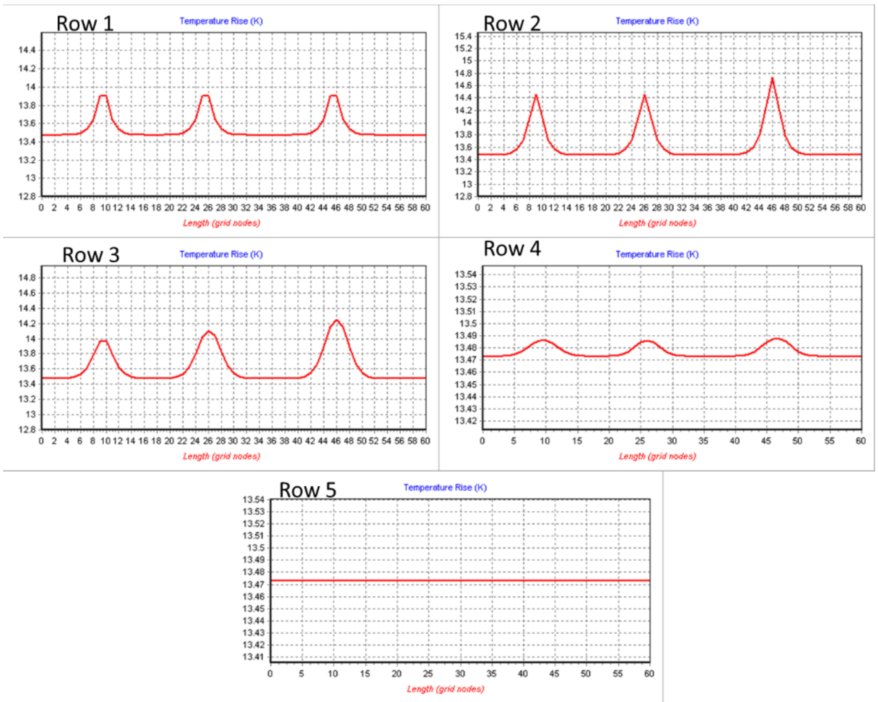

Graph 128 Delta T profiles for different rows of defects using optical pulsed thermography simulation SL4. Row#1 in blue, Row #2 in green, Row# 3 in Orange, Row# 4 yellow and Row #5 in red

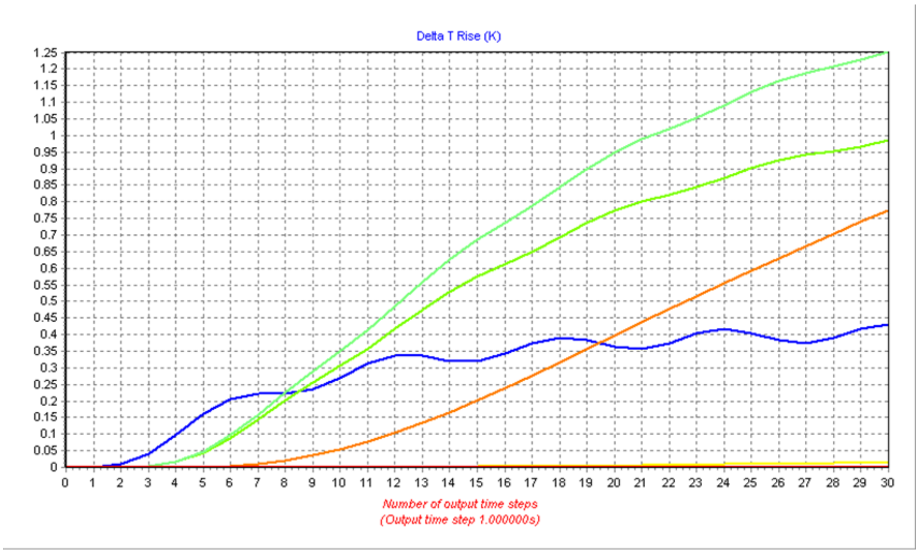

Graph 129 Delta T profiles for Row #4 and #5 of defects using optical lockin simulation SL4. Row# 4 in yellow and Row#4 in red

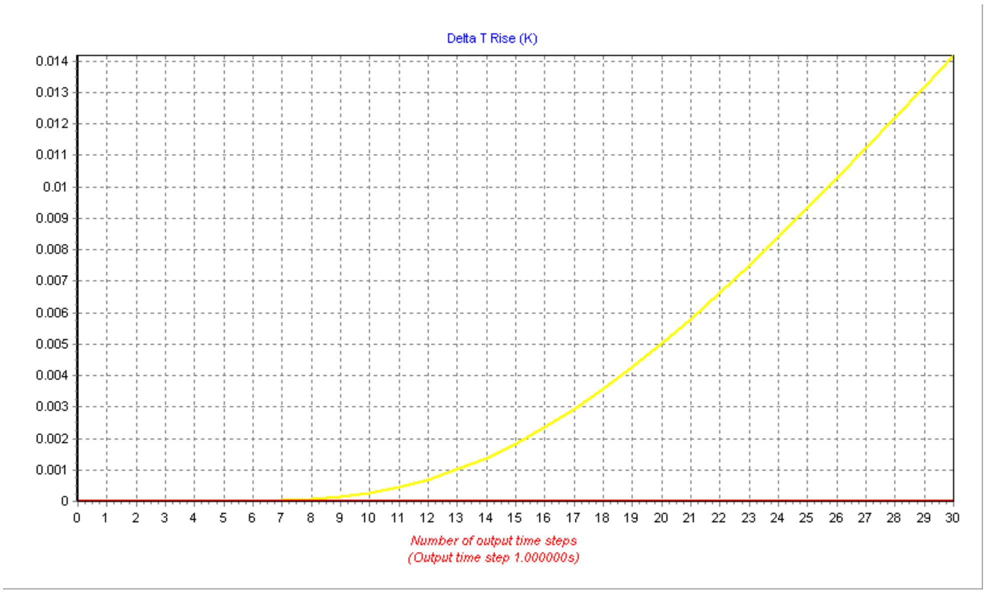

SL5

Figure 94 Thermal image for simulation SL5 using optical lockin: Heating density 6000 W/m^2, wave period 4s, Total time 60s

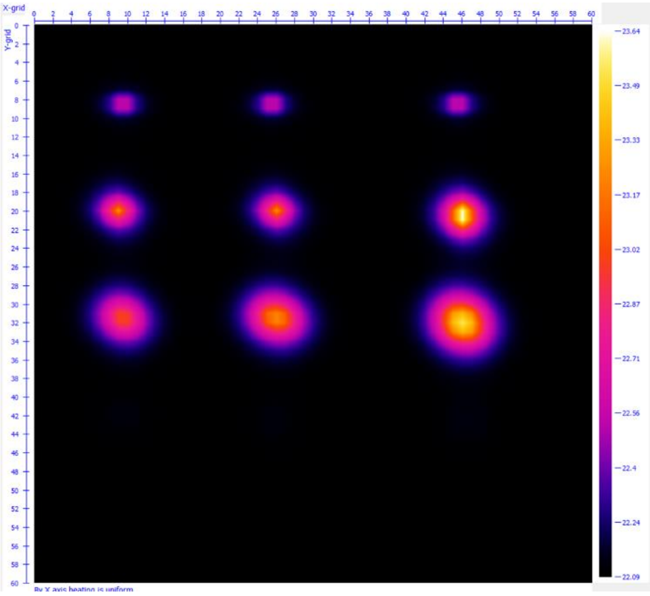

Graph 130 Space profiles of the different rows of defects using optical lockin simulation SL5 settings

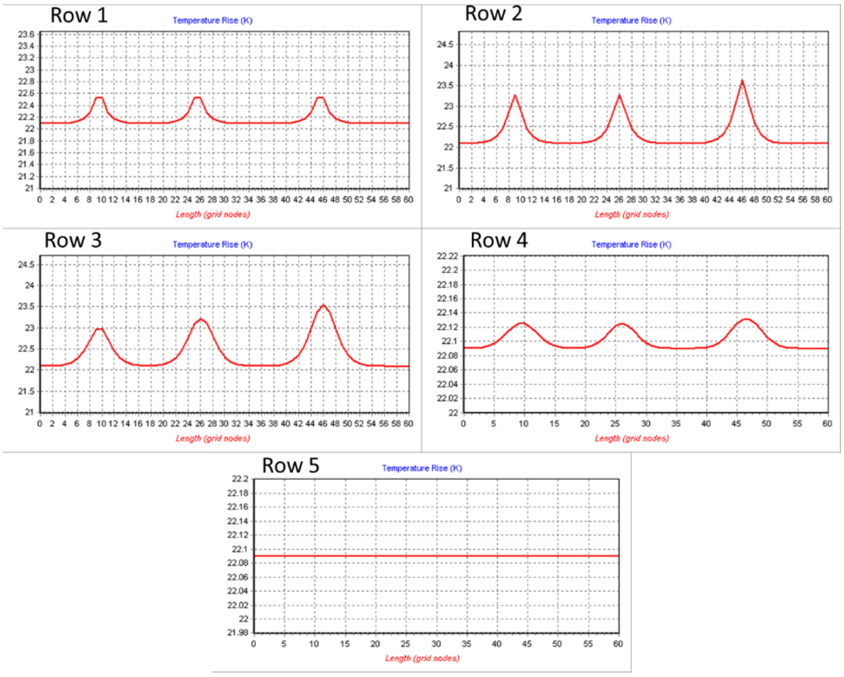

Graph 131 Delta T profiles for different rows of defects using optical pulsed thermography simulation SL5. Row#1 in blue, Row #2 in green, Row# 3 in Orange, Row# 4 yellow and Row #5 in red

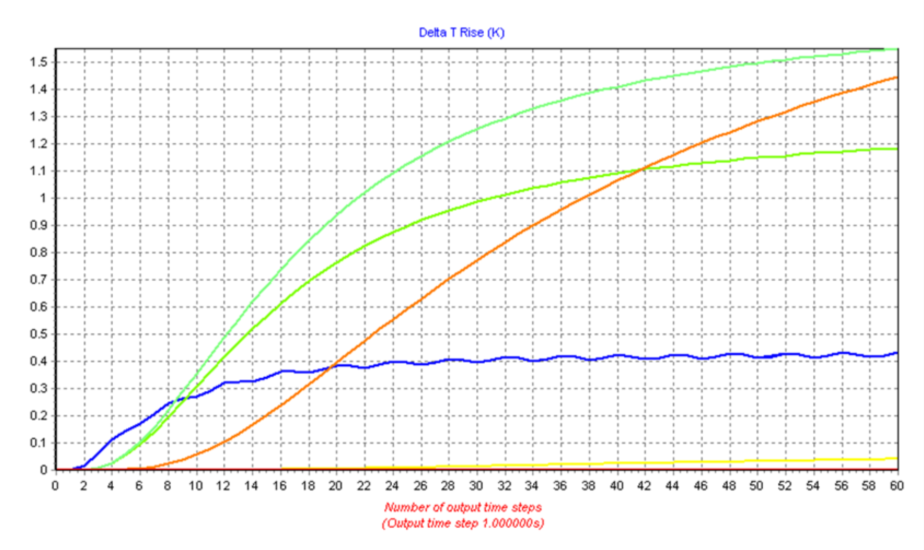

Graph 132 Delta T profiles for Row #4 and #5 of defects using optical lockin simulation SL5. Row# 4 in yellow and Row#4 in red

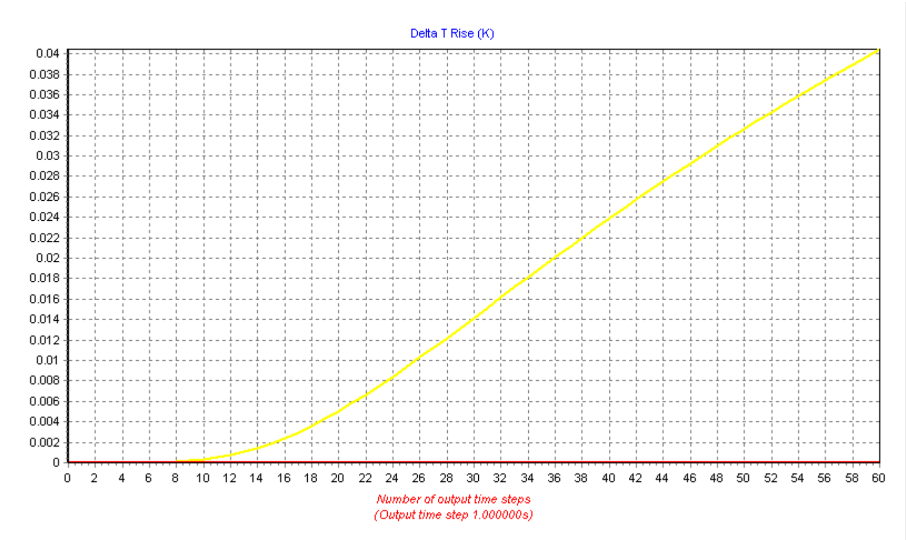

SL6

Figure 95 Thermal image for simulation SL6 using optical lockin: Heating density 6000 W/m^2, wave period 4s, Total time 90s

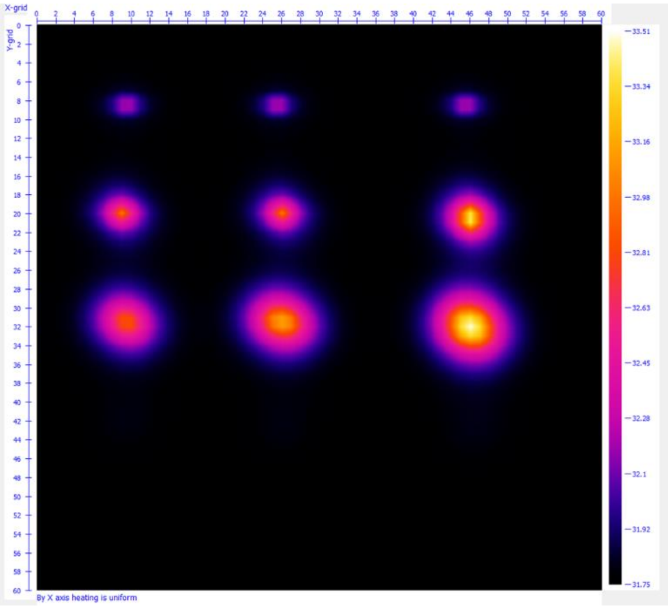

Graph 133 Space profiles of the different rows of defects using optical lockin simulation SL6 settings

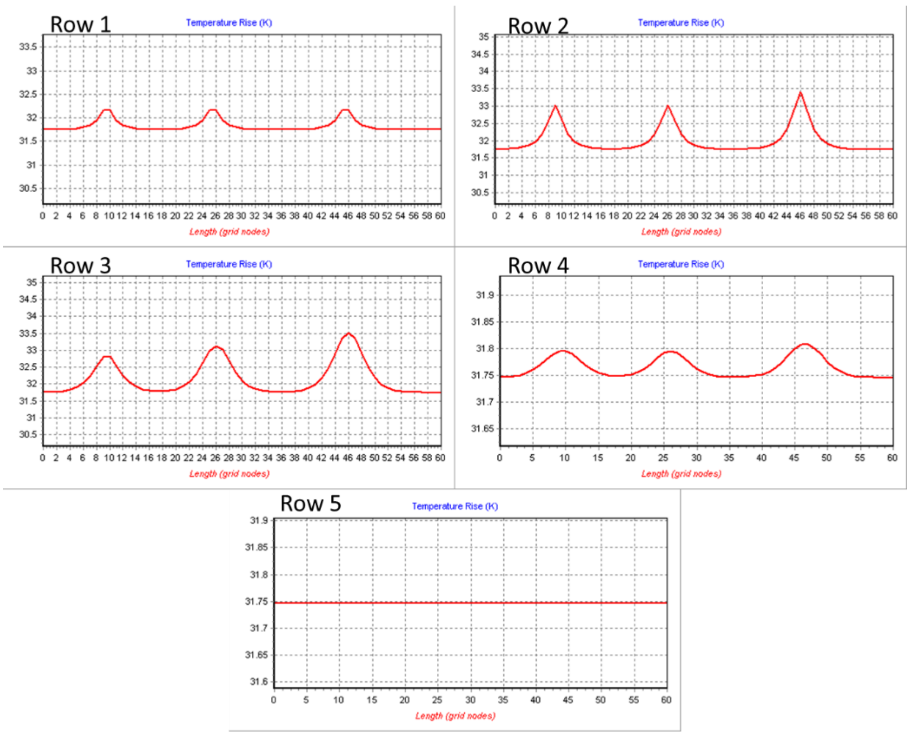

Graph 134 Delta T profiles for different rows of defects using optical pulsed thermography simulation SL6. Row#1 in blue, Row #2 in green, Row# 3 in Orange, Row# 4 yellow and Row #5 in red

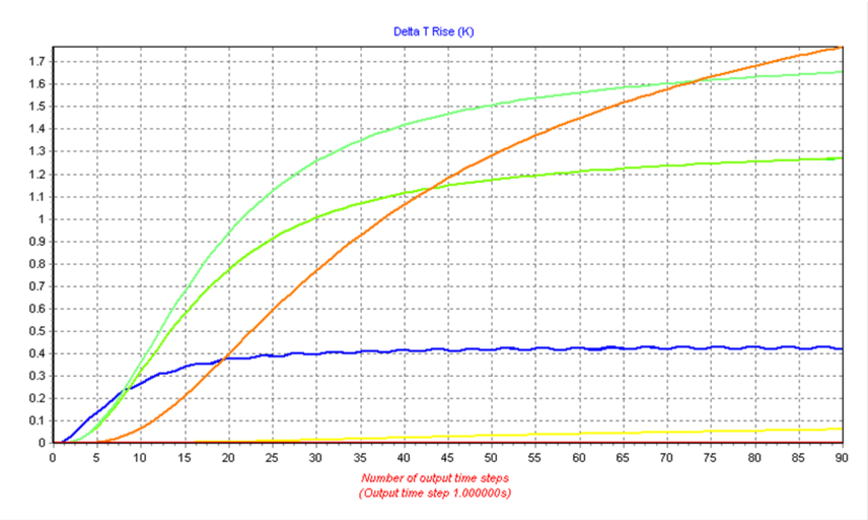

Graph 135 Delta T profiles for Row #4 and #5 of defects using optical lockin simulation SL6. Row# 4 in yellow and Row#4 in red

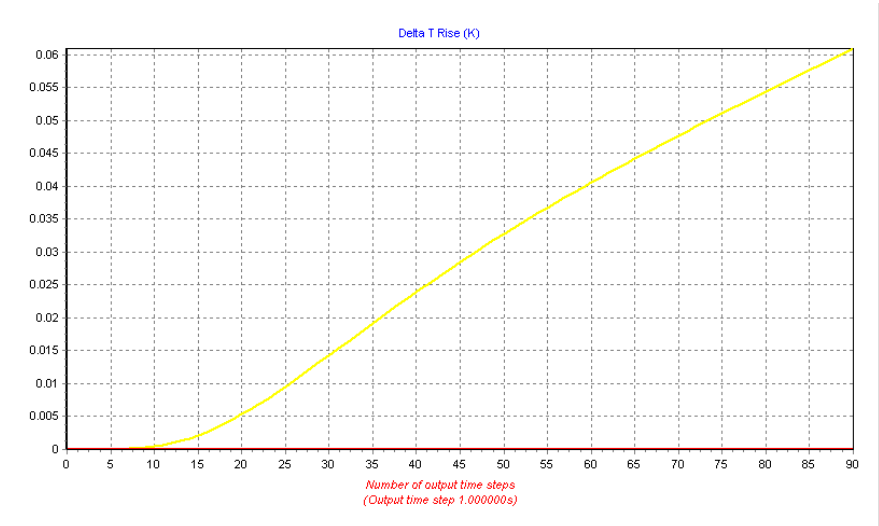

SL7

Figure 96 Thermal image for simulation SL7 using optical lockin: Heating density 6000 W/m^2, wave period 4s, Total time 120s

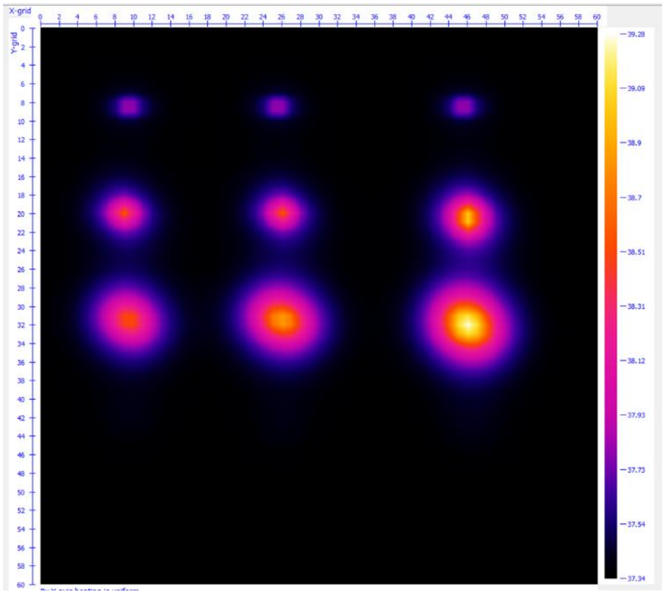

Graph 136 Space profiles of the different rows of defects using optical lockin simulation SL7 settings

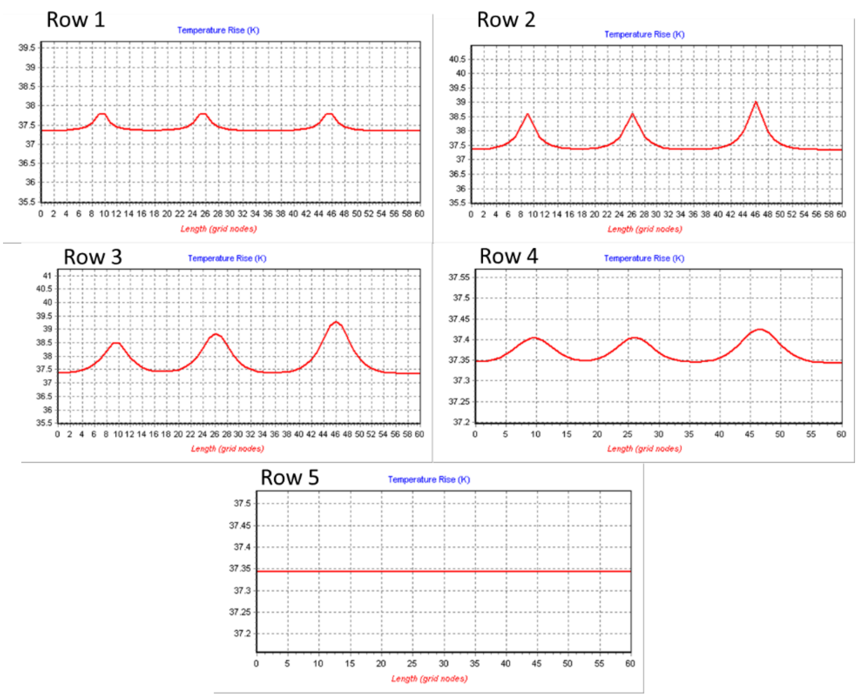

Graph 137 Delta T profiles for different rows of defects using optical pulsed thermography simulation SL7. Row#1 in blue, Row #2 in green, Row# 3 in Orange, Row# 4 yellow and Row #5 in red

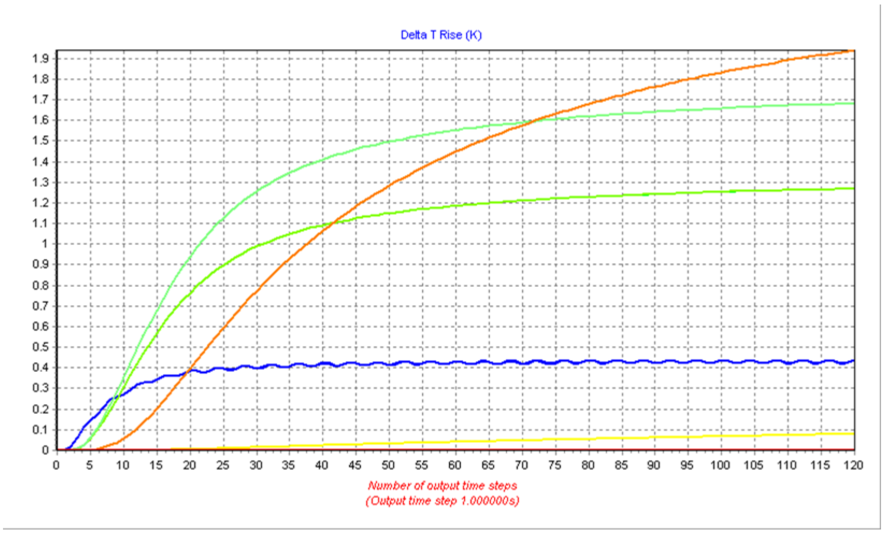

Graph 138 Delta T profiles for Row #4 and #5 of defects using optical lockin simulation SL7. Row# 4 in yellow and Row#4 in red

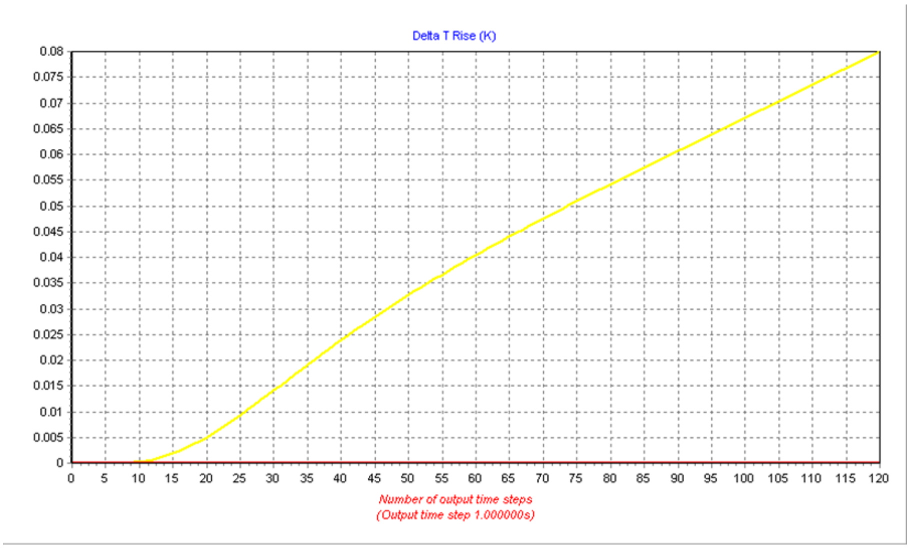

SL8

Figure 97 Thermal image for simulation SL8 using optical lockin: Heating density 11111 W/m^2, wave period 4s, Total time 30s

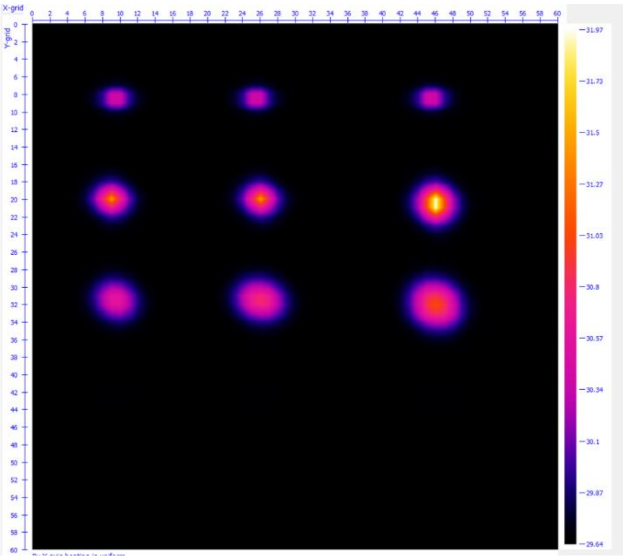

Graph 139 Space profiles of the different rows of defects using optical lockin simulation SL8 settings

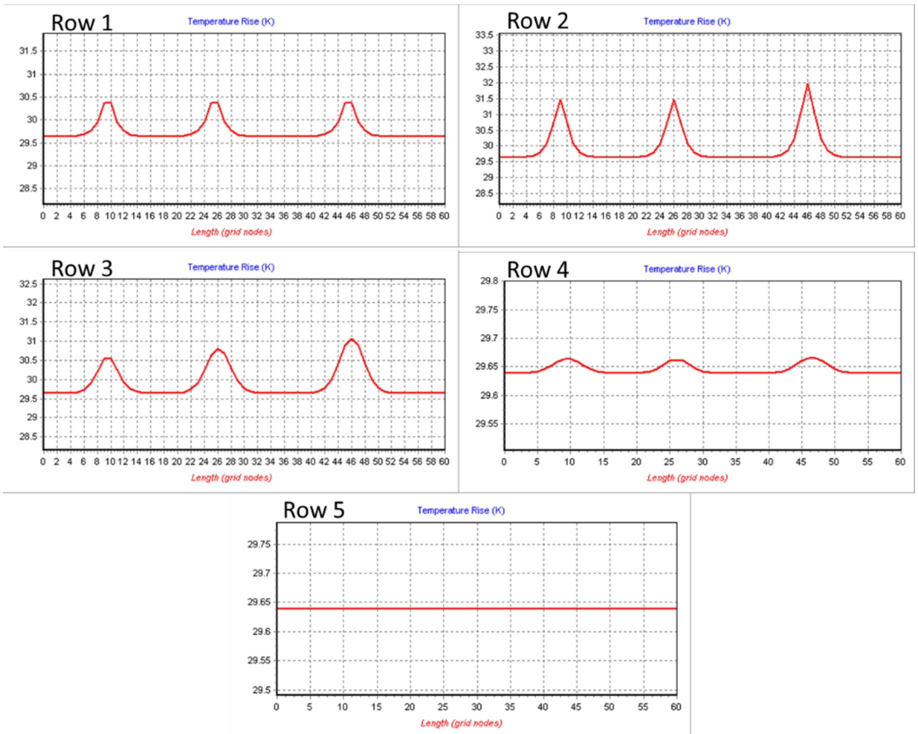

Graph 140 Delta T profiles for different rows of defects using optical pulsed thermography simulation SL8. Row#1 in blue, Row #2 in green, Row# 3 in Orange, Row# 4 yellow and Row #5 in red

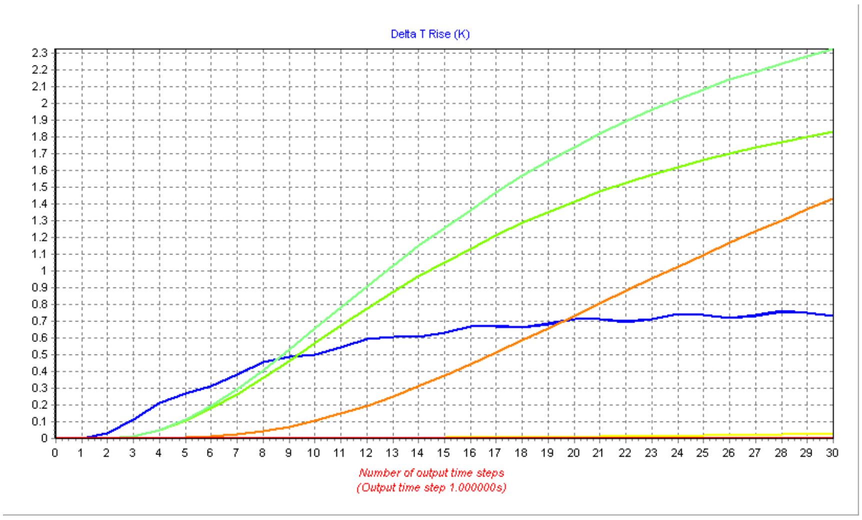

Graph 141 Delta T profiles for Row #4 and #5 of defects using optical lockin simulation SL8. Row# 4 in yellow and Row#4 in red

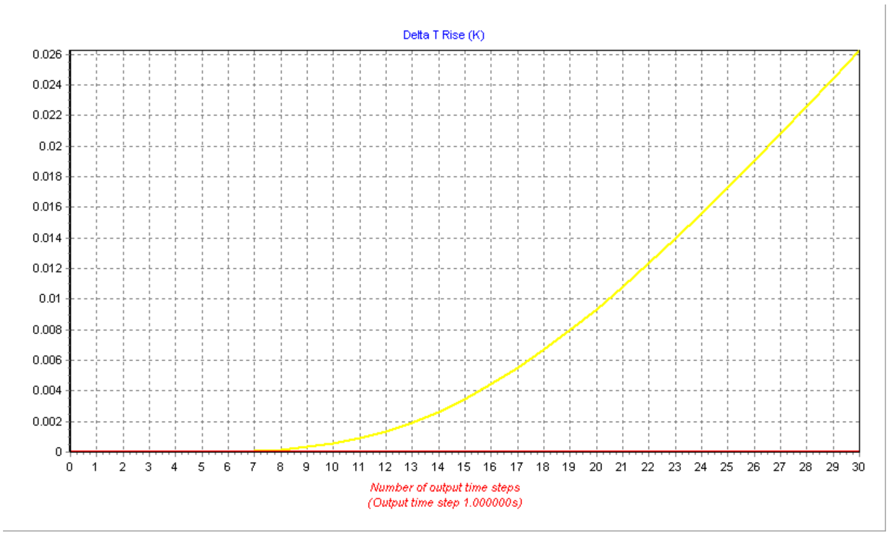

SL9

Figure 98 Thermal image for simulation SL9 using optical lockin: Heating density 11111 W/m^2, wave period 4s, Total time 60s

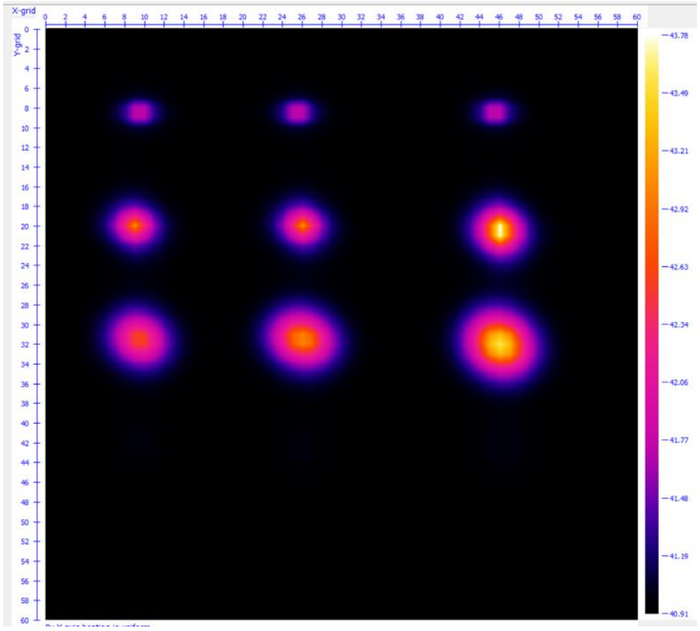

Graph 142 Space profiles of the different rows of defects using optical lockin simulation SL9 settings

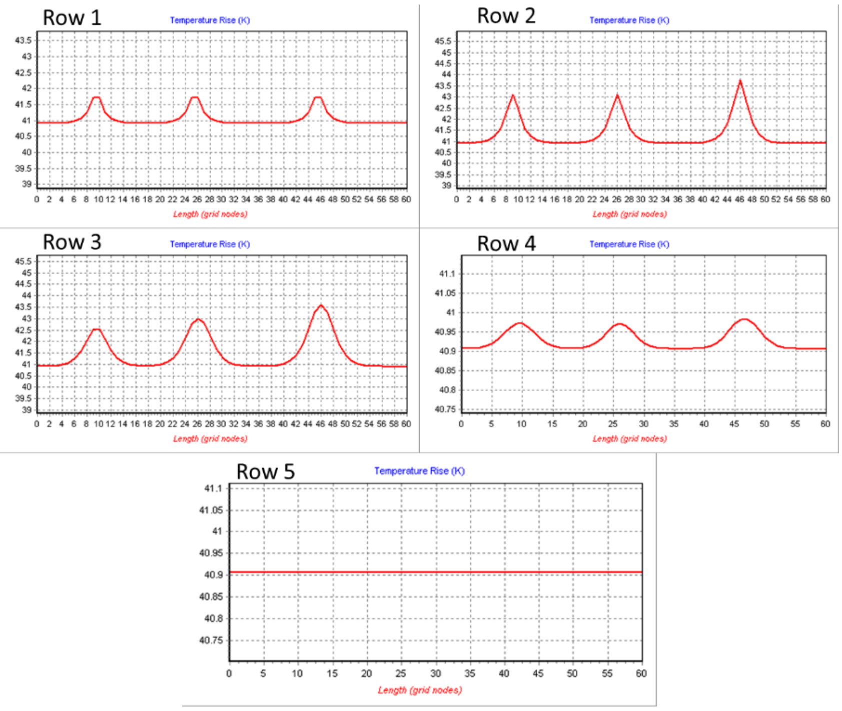

Graph 143 Delta T profiles for different rows of defects using optical pulsed thermography simulation SL9. Row#1 in blue, Row #2 in green, Row# 3 in Orange, Row# 4 yellow and Row #5 in red

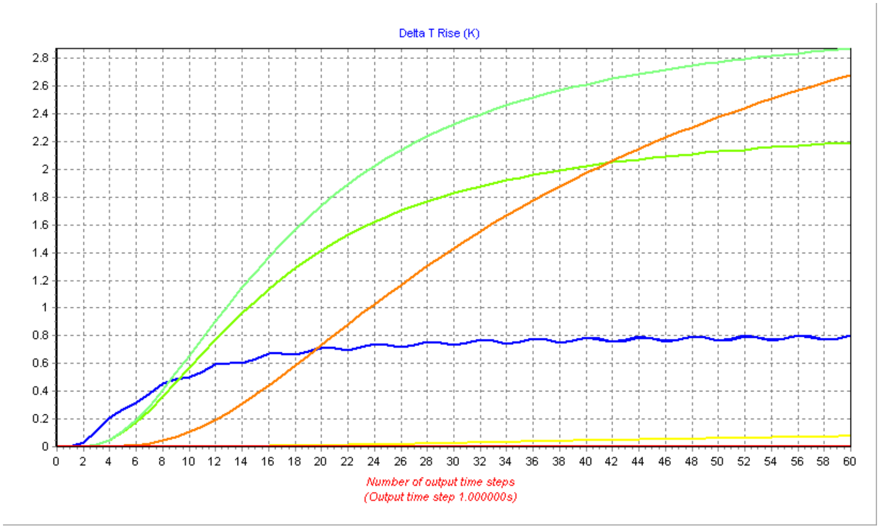

Graph 144 Delta T profiles for Row #4 and #5 of defects using optical lockin simulation SL9. Row# 4 in yellow and Row#4 in red

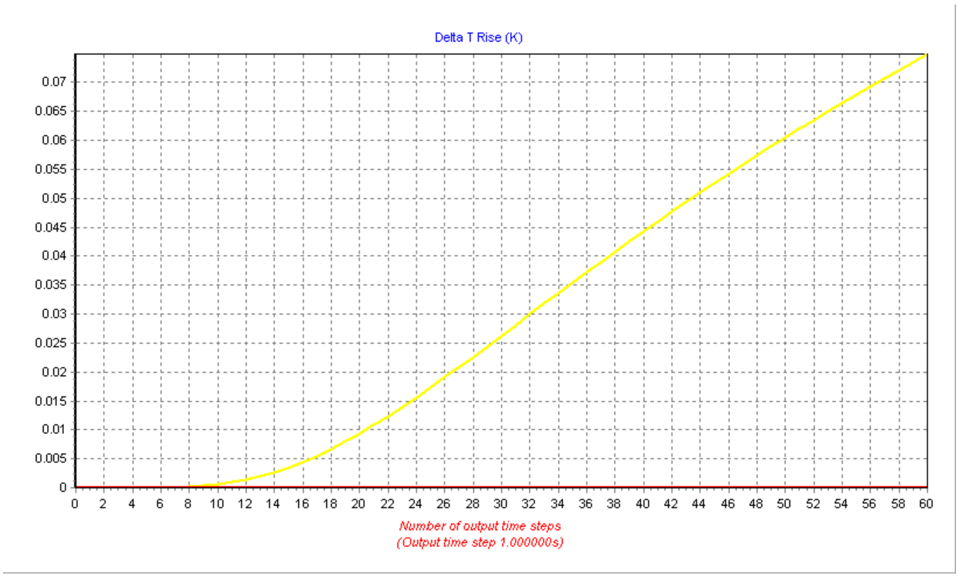

SL10

Figure 99 Thermal image for simulation SL10 using optical lockin: Heating density 11111 W/m^2, wave period 7s, Total time 60s

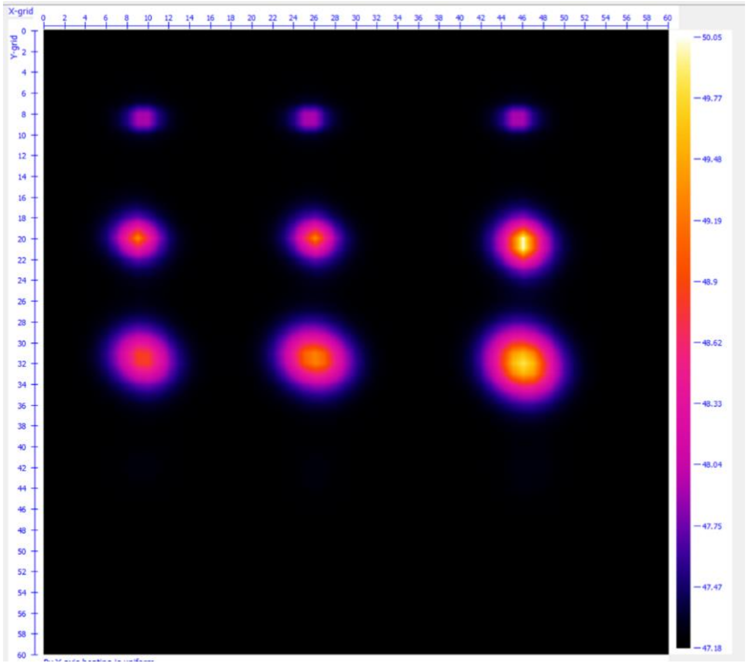

Graph 145 Space profiles of the different rows of defects using optical lockin simulation SL10 settings

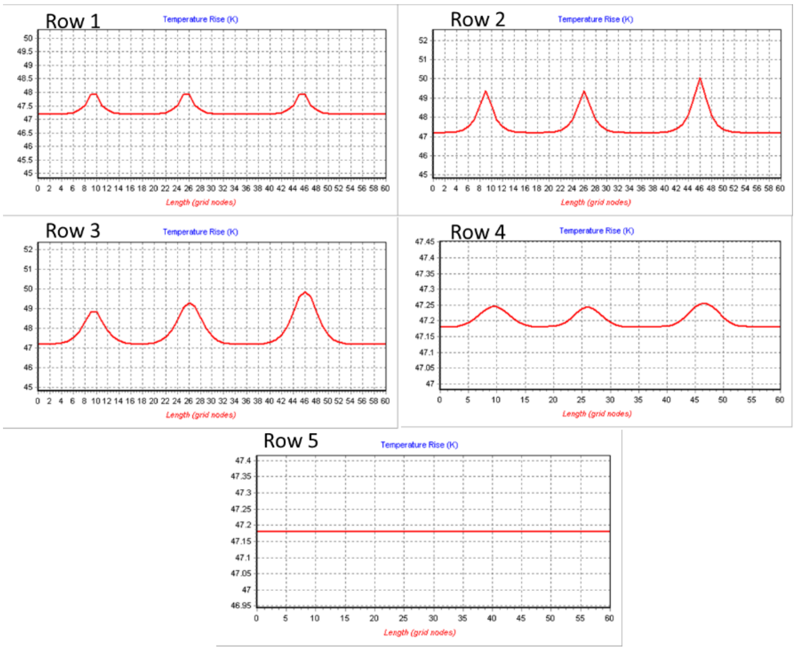

Graph 146 Delta T profiles for different rows of defects using optical pulsed thermography simulation SL10. Row#1 in blue, Row #2 in green, Row# 3 in Orange, Row# 4 yellow and Row #5 in red

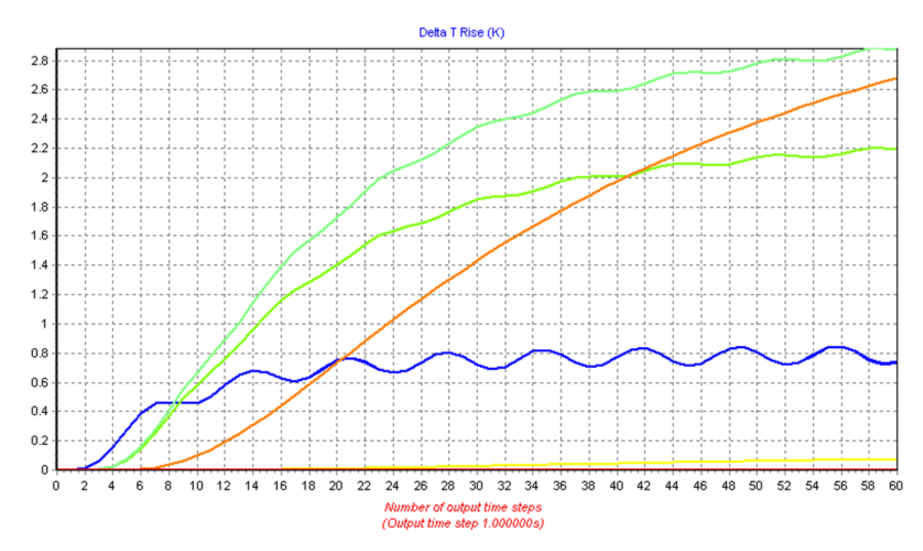

Graph 147 Delta T profiles for Row #4 and #5 of defects using optical lockin simulation SL10. Row# 4 in yellow and Row#4 in red

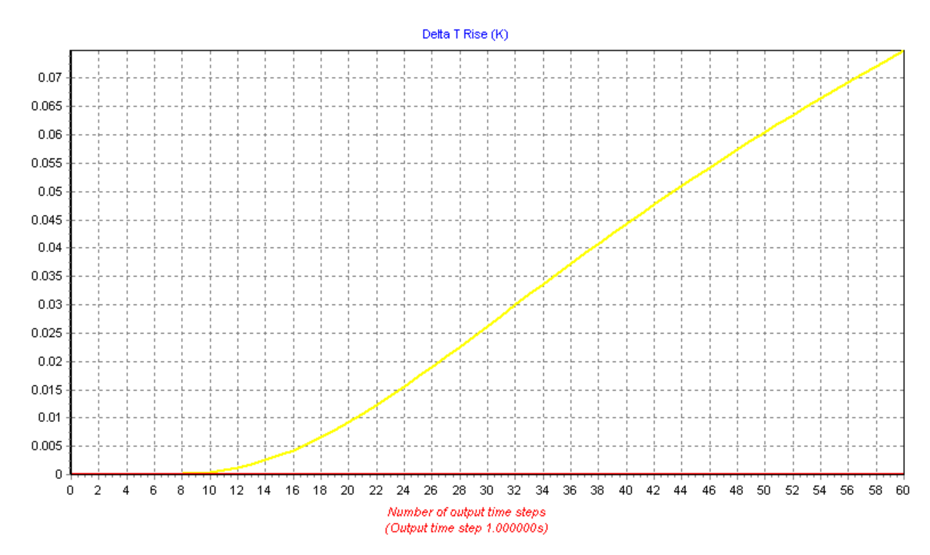

SL11

Figure 100 Thermal image for simulation SL11 using optical lockin: Heating density 11111 W/m^2, wave period 4s, Total time 90s

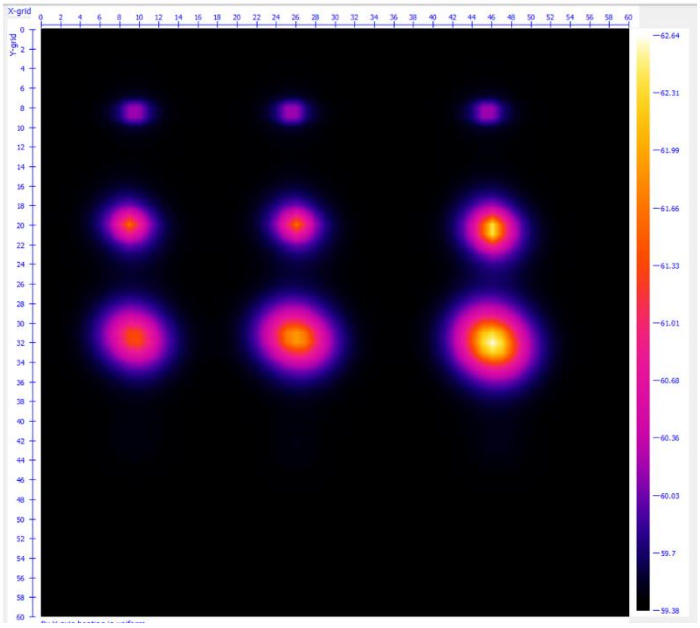

Graph 148 Space profiles of the different rows of defects using optical lockin simulation SL11 settings

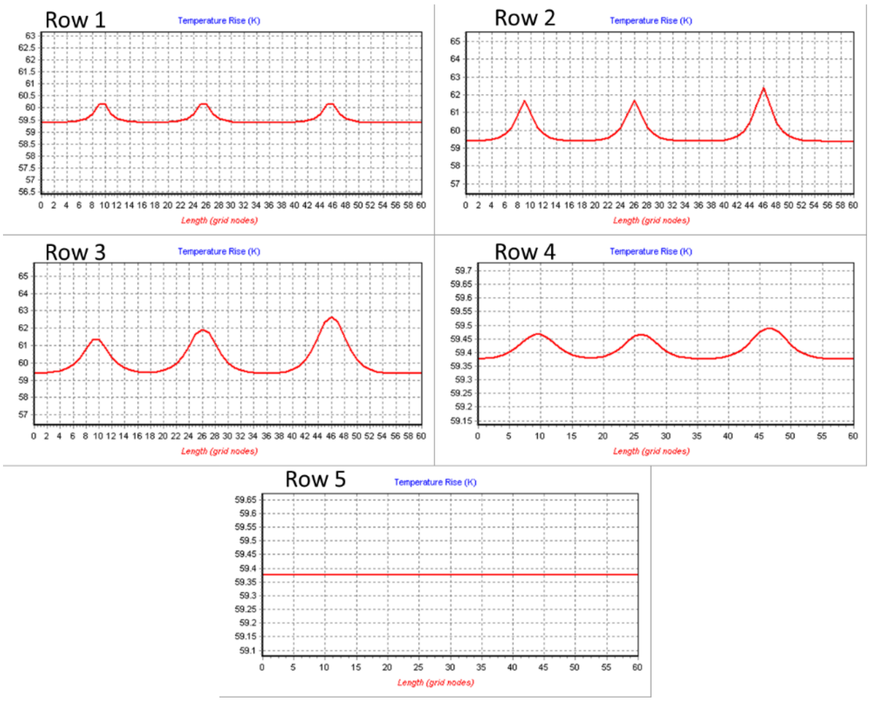

Graph 149 Delta T profiles for different rows of defects using optical pulsed thermography simulation SL10. Row#1 in blue, Row #2 in green, Row# 3 in Orange, Row# 4 yellow and Row #5 in red

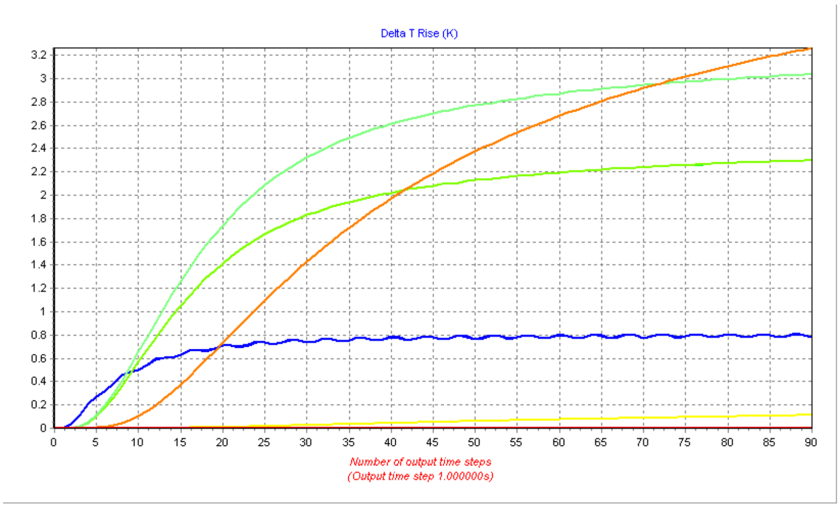

Graph 150 Delta T profiles for Row #4 and #5 of defects using optical lockin simulation SL10. Row# 4 in yellow and Row#4 in red

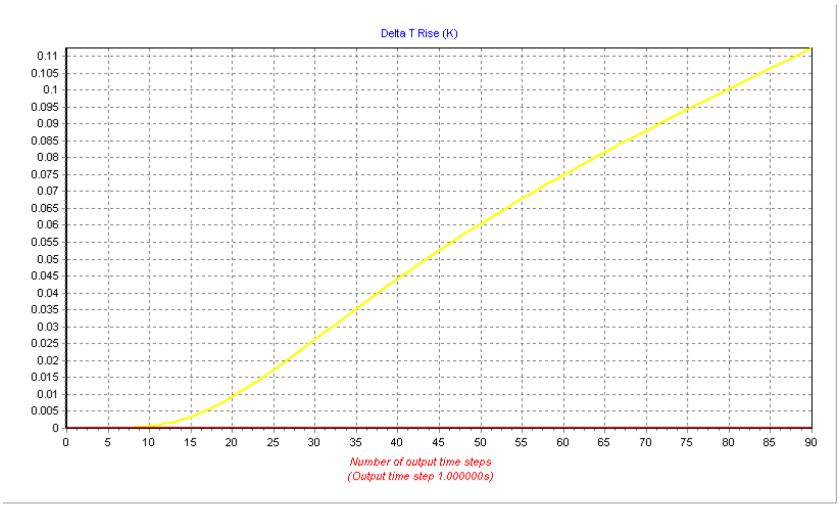

SL12

Figure 101 Thermal image for simulation SL12 using optical lockin: Heating density 11111 W/m^2, wave period 4s, Total time 120s

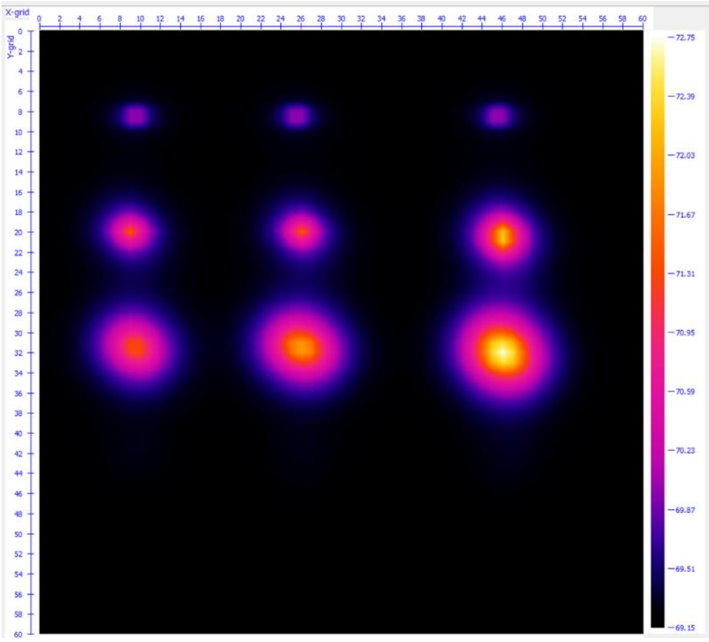

Graph 151 Space profiles of the different rows of defects using optical lockin simulation SL12 settings

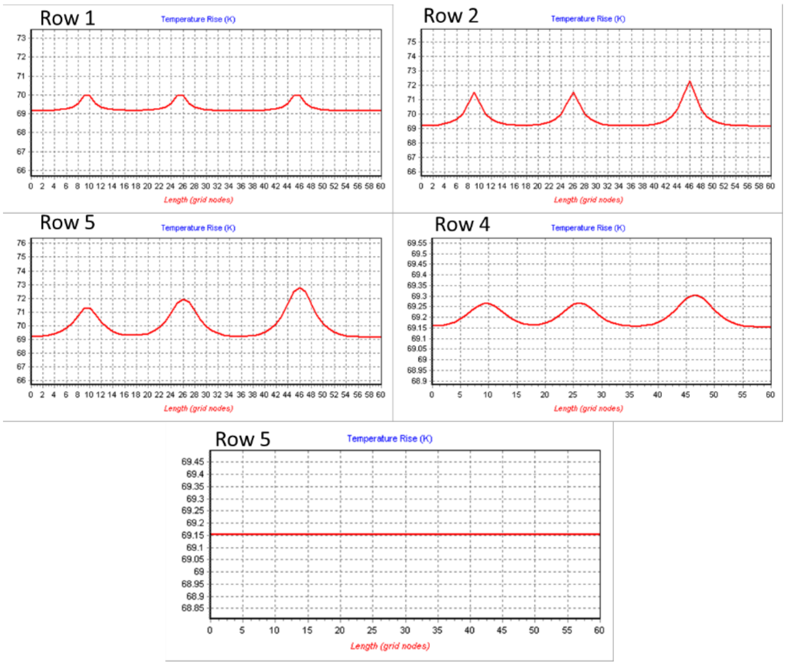

Graph 152 Delta T profiles for different rows of defects using optical pulsed thermography simulation SL10. Row#1 in blue, Row #2 in green, Row# 3 in Orange, Row# 4 yellow and Row #5 in red

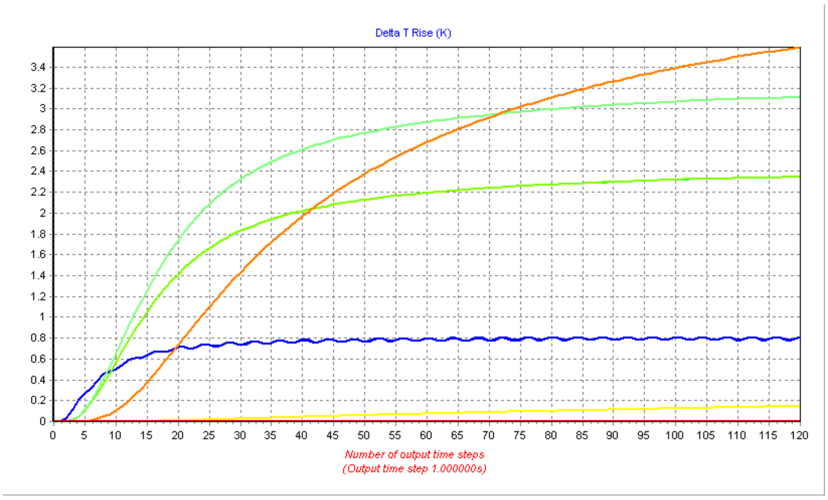

Graph 153 Delta T profiles for Row #4 and #5 of defects using optical lockin simulation SL10. Row# 4 in yellow and Row#4 in red

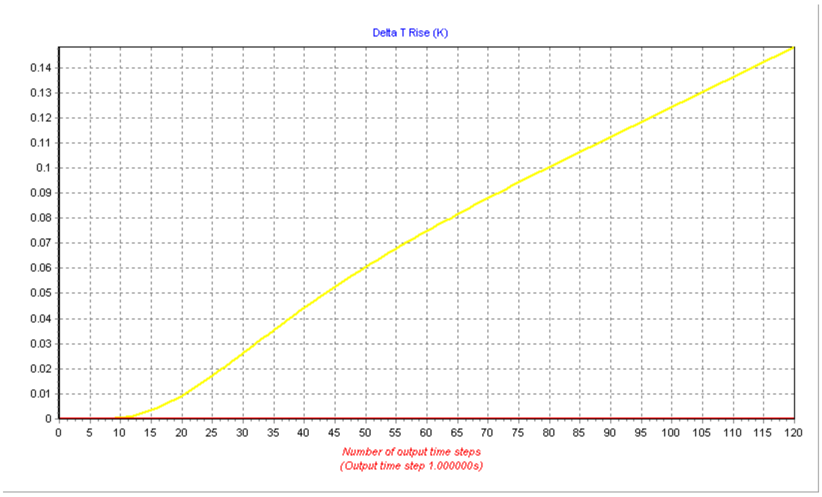

SL13

Figure 102 Thermal image for simulation SL13 using optical lockin: Heating density 22222 W/m^2, wave period 4s, Total time 30s

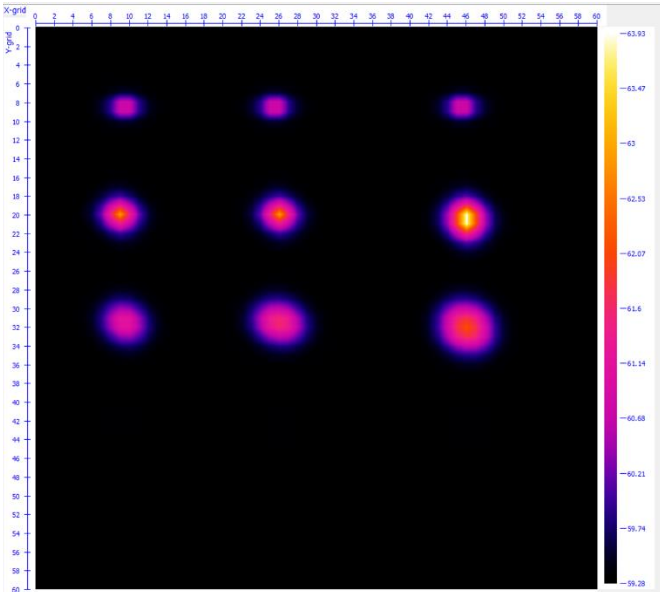

Graph 154Space profiles of the different rows of defects using optical lockin simulation SL13 settings

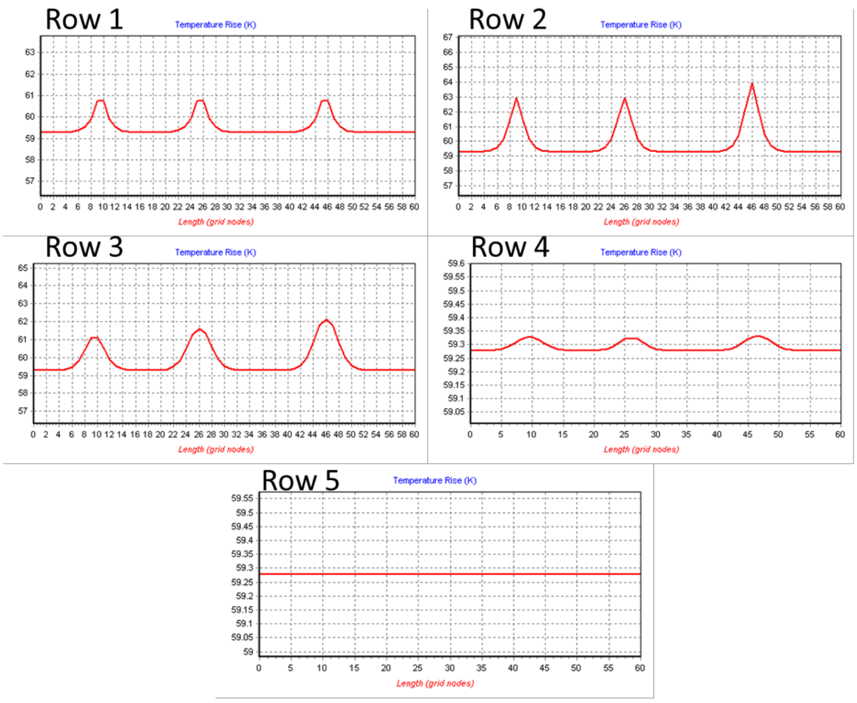

Graph 155 Delta T profiles for different rows of defects using optical pulsed thermography simulation SL13. Row#1 in blue, Row #2 in green, Row# 3 in Orange, Row# 4 yellow and Row #5 in red

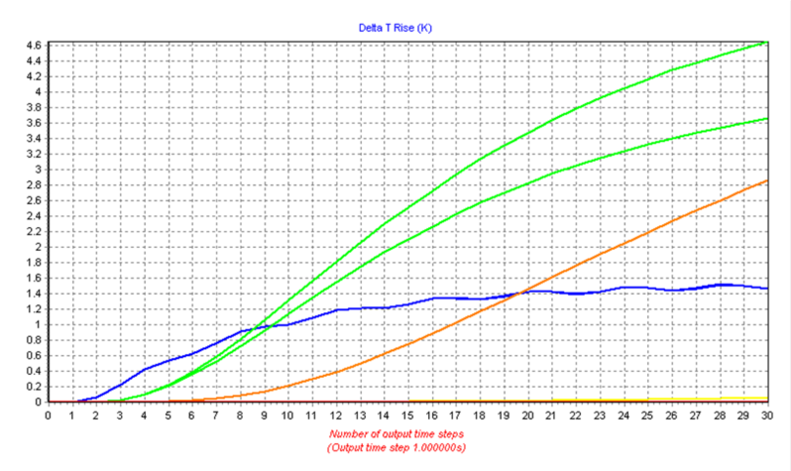

Graph 156 Delta T profiles for Row #4 and #5 of defects using optical lockin simulation SL13. Row# 4 in yellow and Row#4 in red

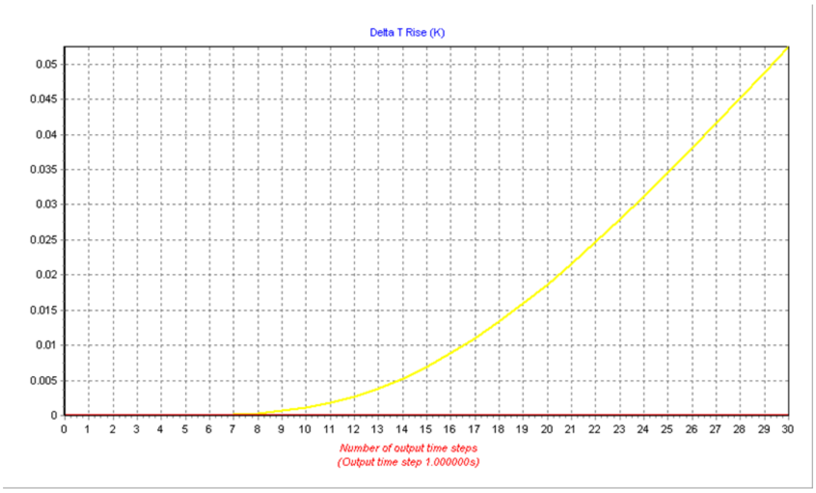

SL14

Figure 103 Thermal image for simulation SL14 using optical lockin: Heating density 22222 W/m^2, wave period 4s, Total time 600s

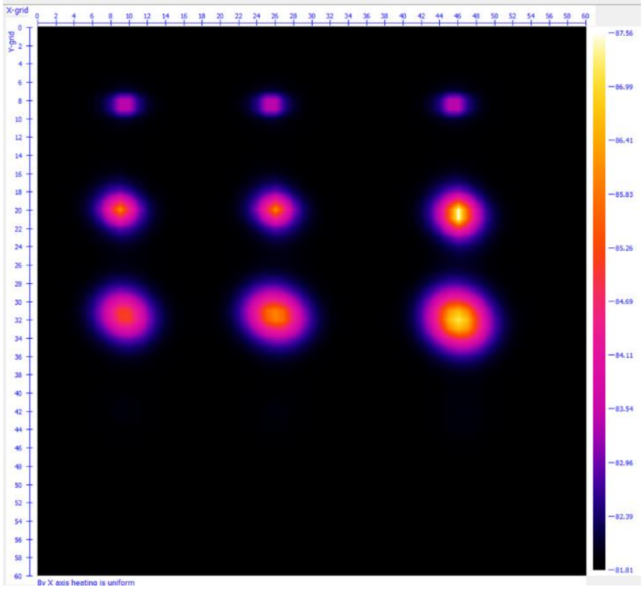

Graph 157 Space profiles of the different rows of defects using optical lockin simulation SL14 settings

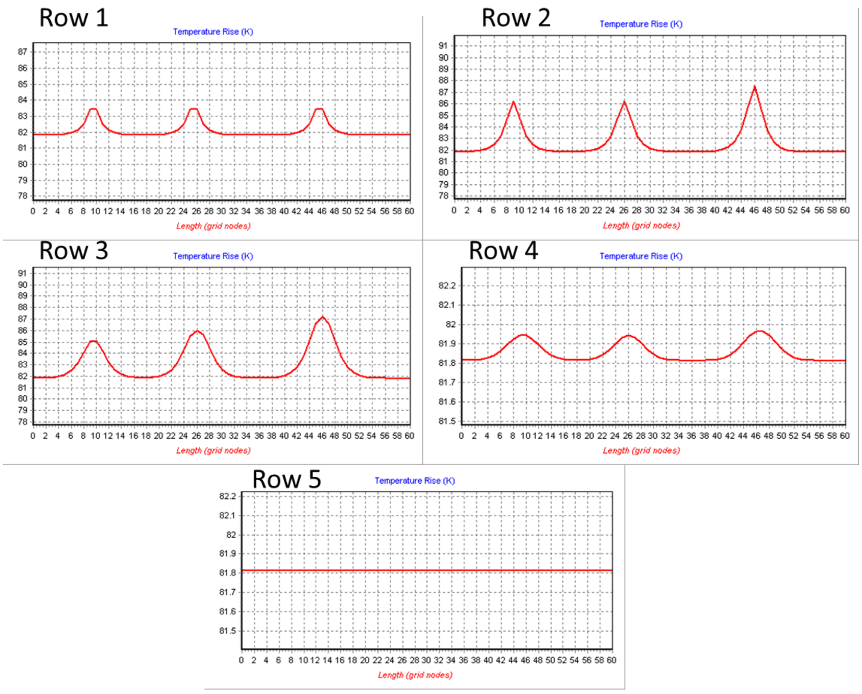

Graph 158 Delta T profiles for different rows of defects using optical pulsed thermography simulation SL14. Row#1 in blue, Row #2 in green, Row# 3 in Orange, Row# 4 yellow and Row #5 in red

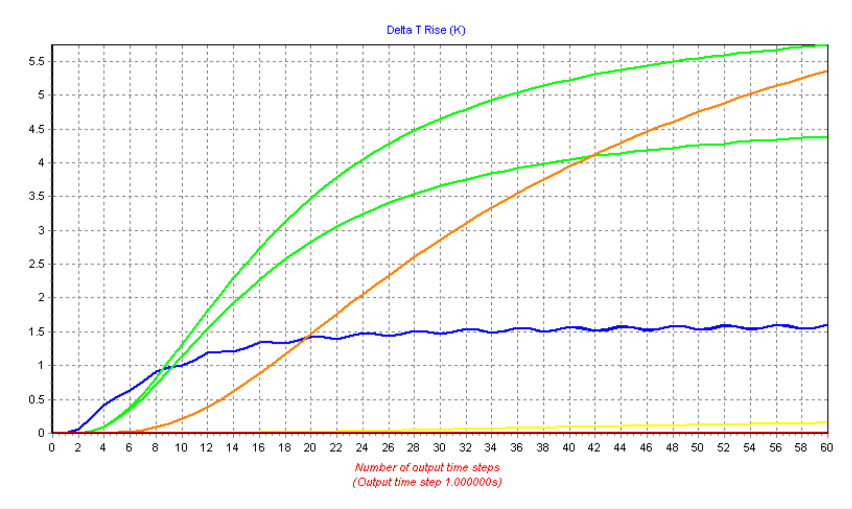

Graph 159 Delta T profiles for Row #4 and #5 of defects using optical lockin simulation SL14. Row# 4 in yellow and Row#4 in red

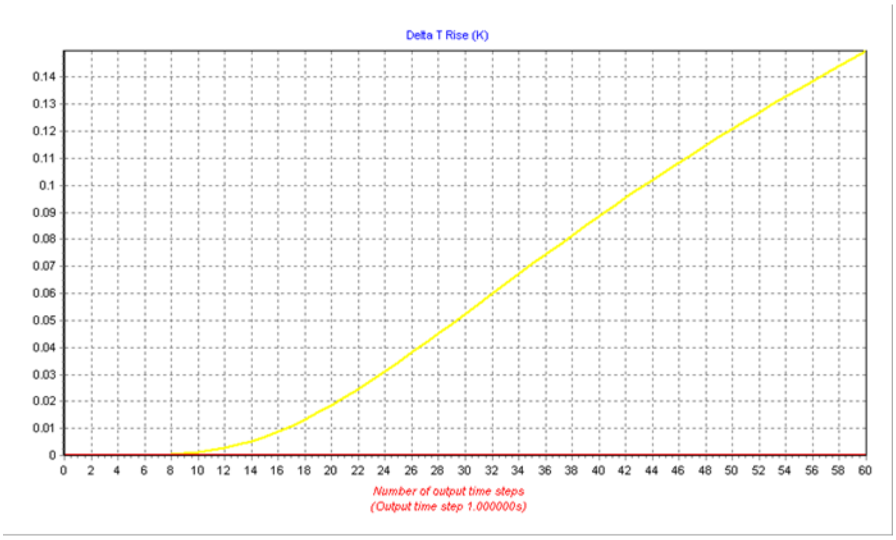

SL15

Figure 104Thermal image for simulation SL15 using optical lockin: Heating density 22222 W/m^2, wave period 4s, Total time 90s

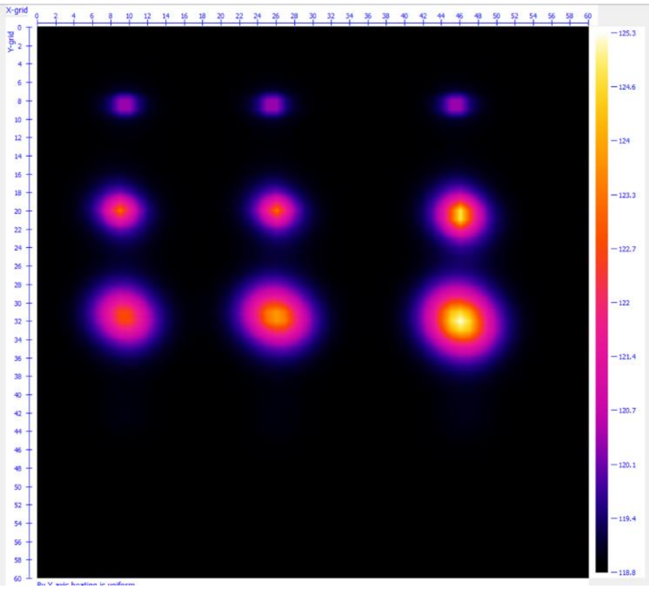

Graph 160 Space profiles of the different rows of defects using optical lockin simulation SL16 settings

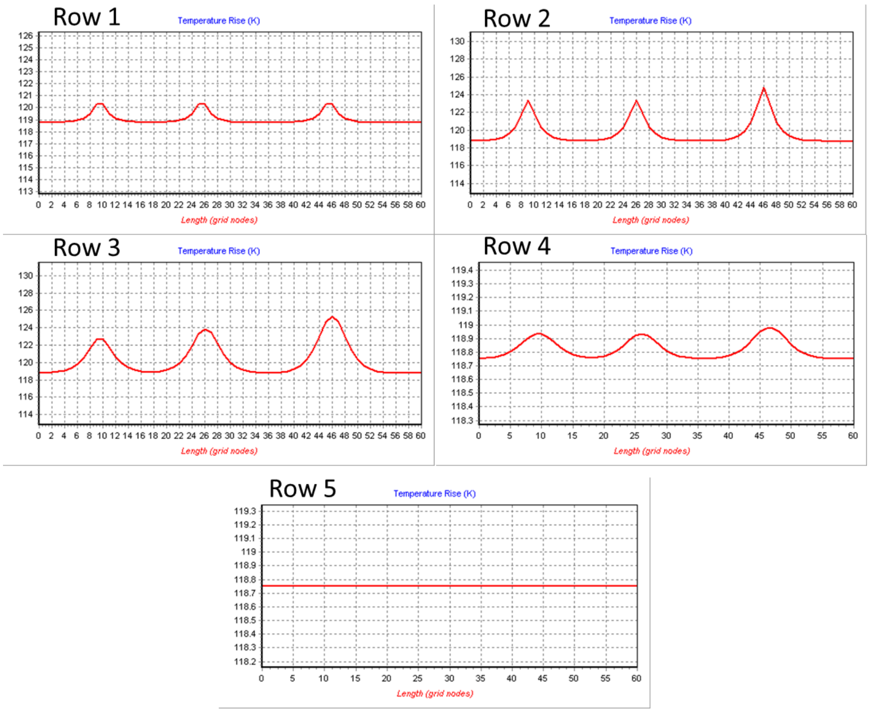

Graph 161 Delta T profiles for different rows of defects using optical pulsed thermography simulation SL15. Row#1 in blue, Row #2 in green, Row# 3 in Orange, Row# 4 yellow and Row #5 in red

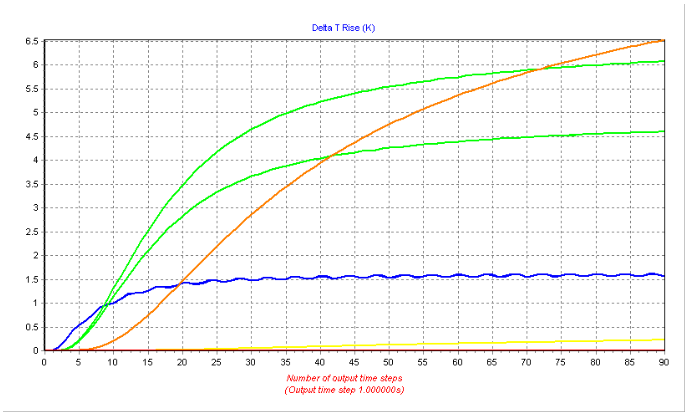

Graph 162 Delta T profiles for Row #4 and #5 of defects using optical lockin simulation SL15. Row# 4 in yellow and Row#4 in red

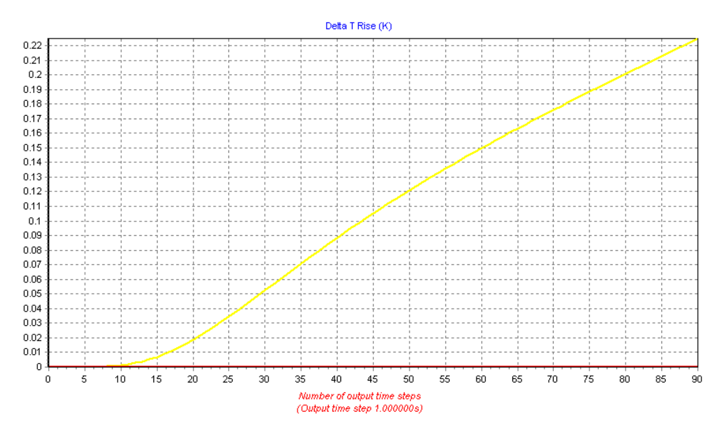

SL16

Figure 105 Thermal image for simulation SL16 using optical lockin: Heating density 22222 W/m^2, wave period 4s, Total time 120s

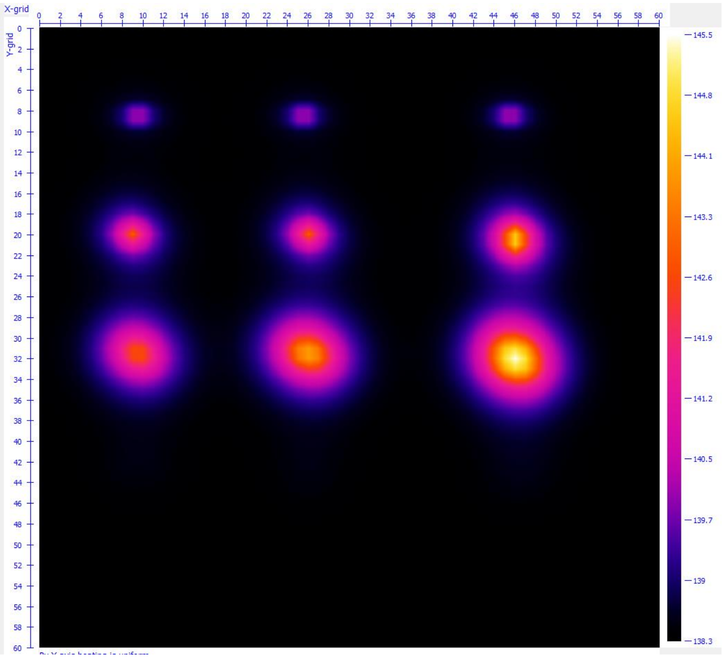

Graph 163 Space profiles of the different rows of defects using optical lockin simulation SL16 settings

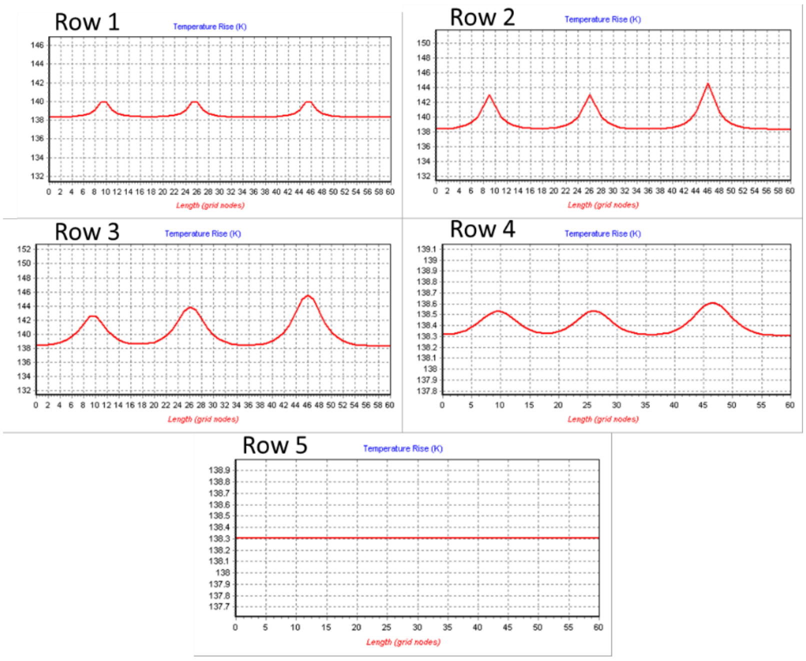

Graph 164 Delta T profiles for different rows of defects using optical pulsed thermography simulation SL16. Row#1 in blue, Row #2 in green, Row# 3 in Orange, Row# 4 yellow and Row #5 in red

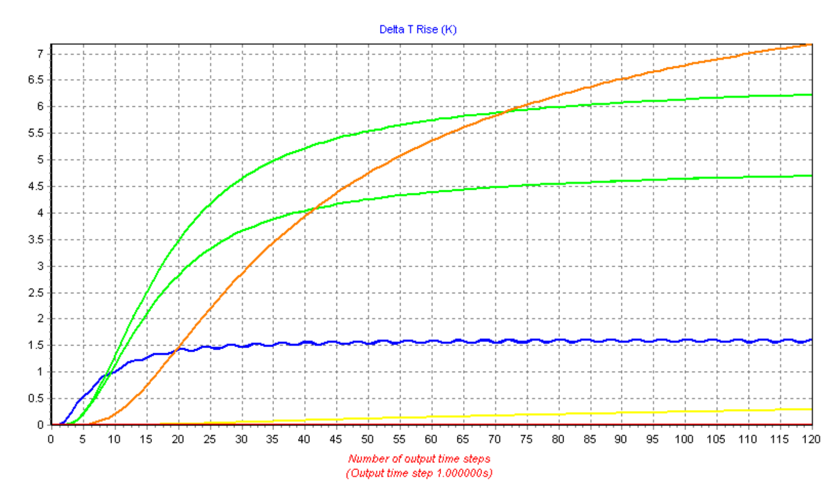

Graph 165 Delta T profiles for Row #4 and #5 of defects using optical lockin simulation SL16. Row# 4 in yellow and Row#4 in red

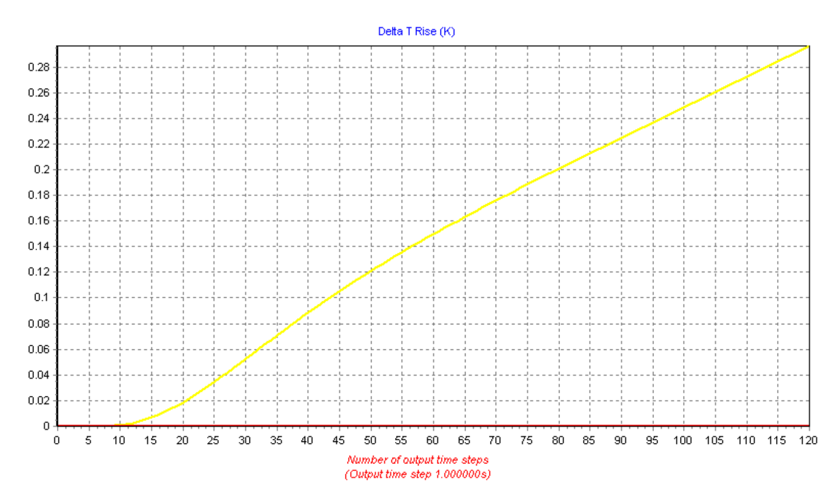

8.1 Optical pulsed thermography- sandwich component

SP1

Figure 106 Thermal image for simulation SP 1 using single square pulse: Heating density 11,111,111 W/m^2, Heating time 0.003s, Total time 5s

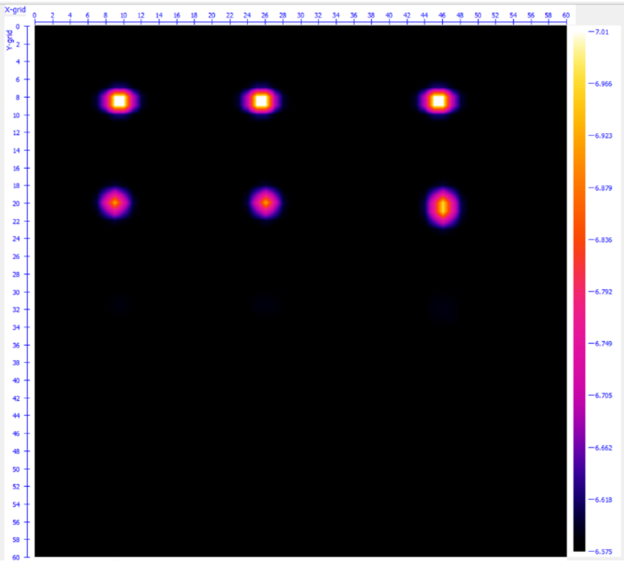

Graph 166 Space profiles of the different rows of defects using optical pulse simulation SP1 settings

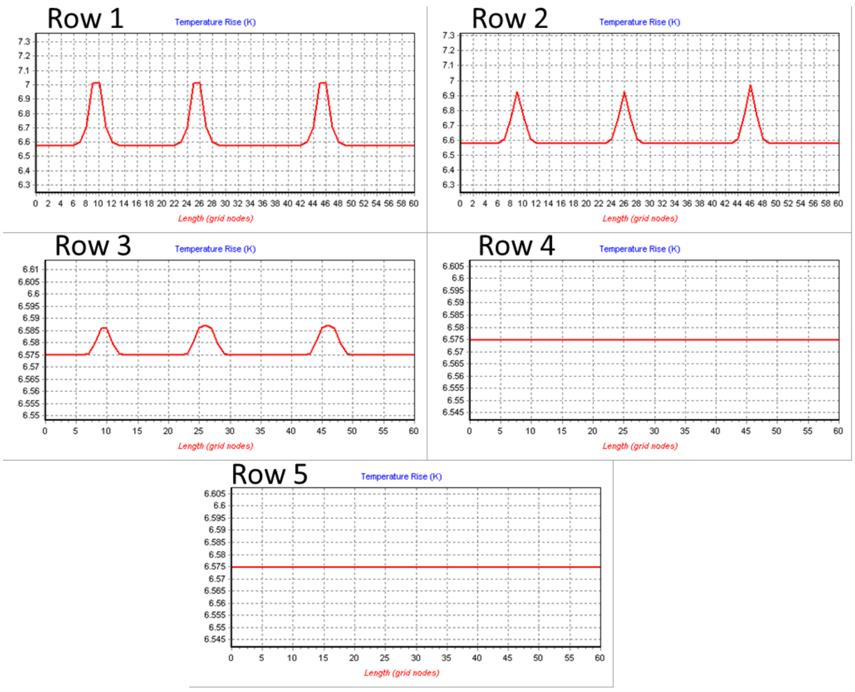

Graph 167 Delta T profiles for different rows of defects using optical pulsed thermography simulation SP1. Row#1 in blue, Row #2 in green, Row# 3 in Orange, Row# 4 yellow and Row #5 in red

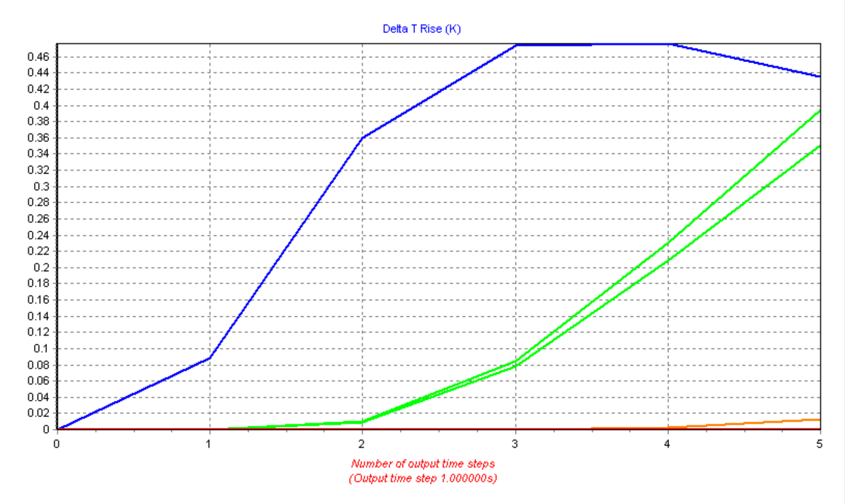

Graph 168 Delta T profiles for Row #3, Row #4 and #5 of defects using optical lockin simulation SP1. Row# 3 in orange, Row #4 yellow, Row #5 in red

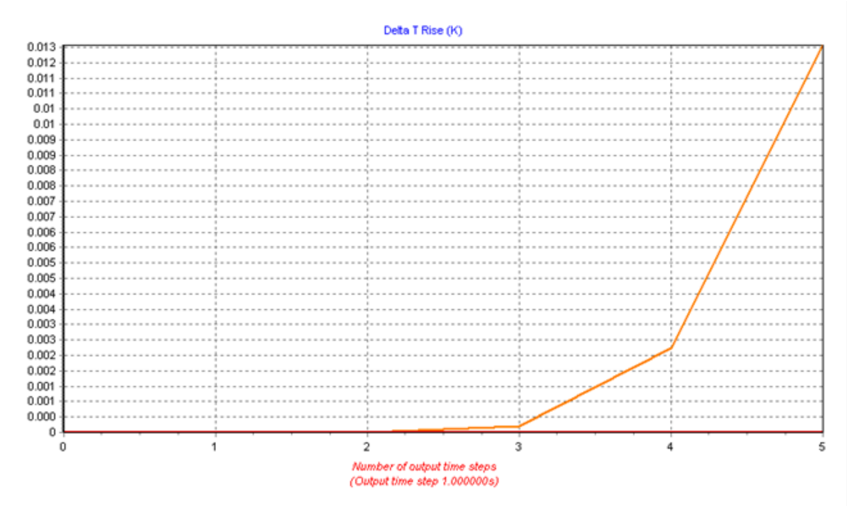

SP2

Figure 107 Thermal image for simulation SP 2 using single square pulse: Heating density 11,111,111 W/m^2, Heating time 0.003s, Total time 10s

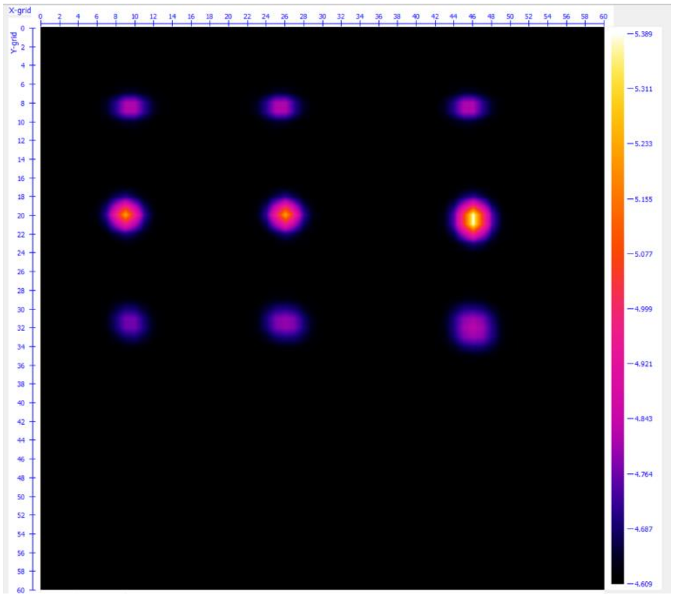

Graph 169 Space profiles of the different rows of defects using optical pulse simulation SP2 settings

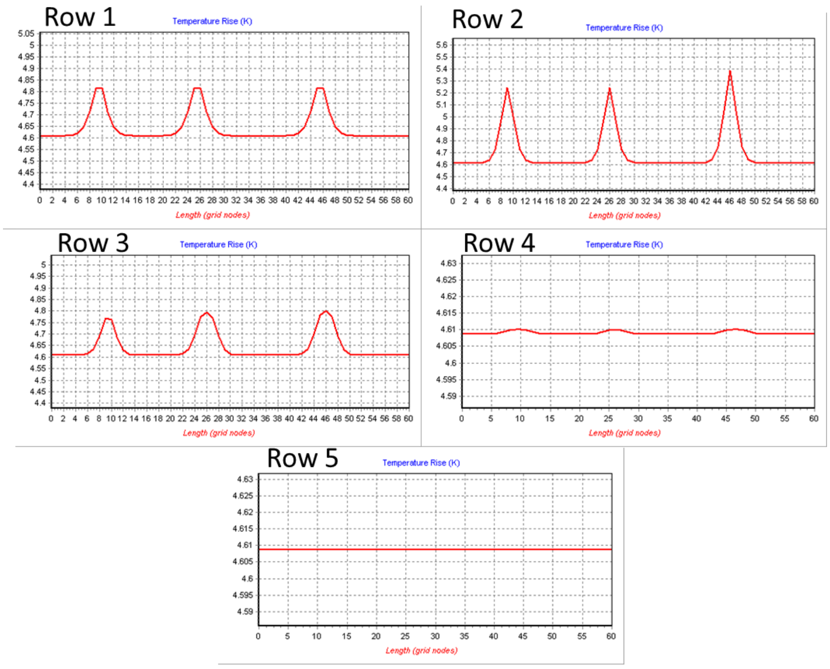

Graph 170 Delta T profiles for different rows of defects using optical pulsed thermography simulation SP2. Row#1 in blue, Row #2 in green, Row# 3 in Orange, Row# 4 yellow and Row #5 in red

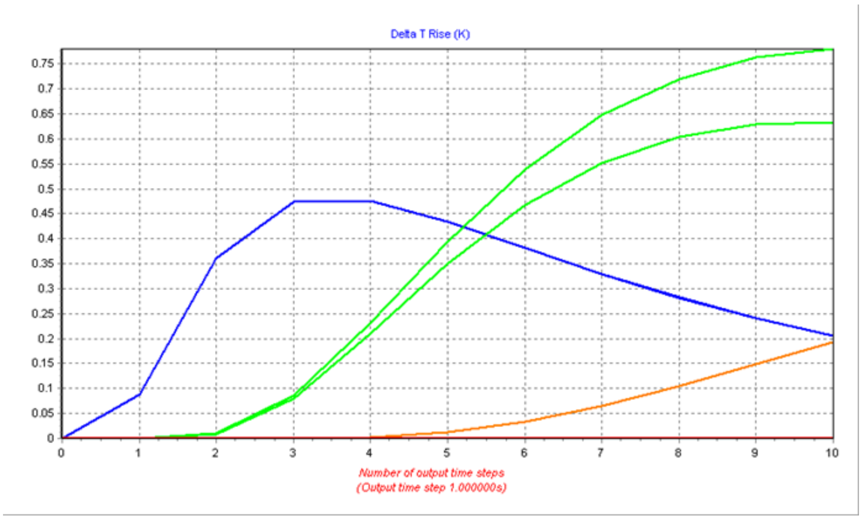

Graph 171 Delta T profiles for Row #3, Row #4 and #5 of defects using optical lockin simulation SP2. Row# 3 in orange, Row #4 yellow, Row #5 in red

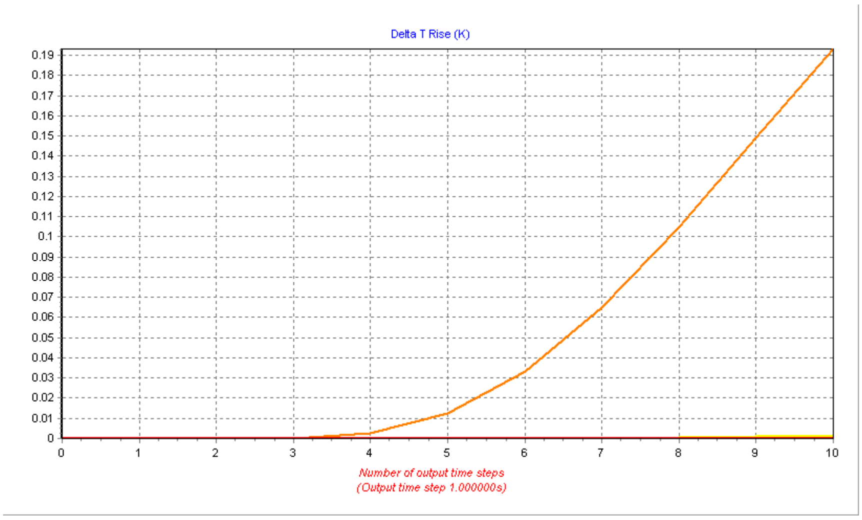

SP3

Figure 108 Thermal image for simulation SP 3 using single square pulse: Heating density 11,111,111 W/m^2, Heating time 0.006s, Total time 10s

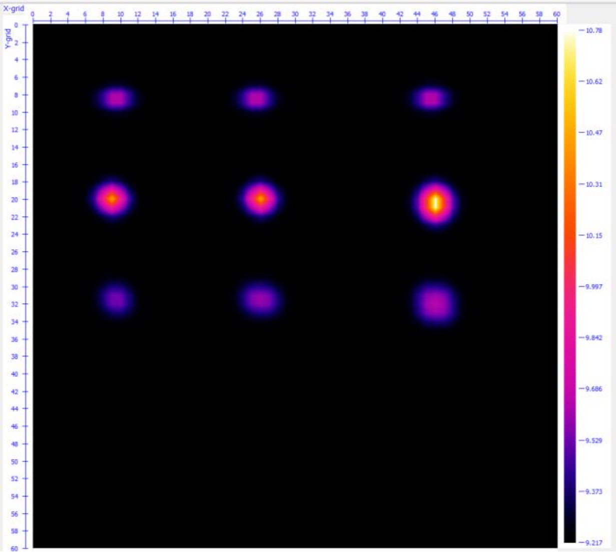

Graph 172 Space profiles of the different rows of defects using optical pulse simulation SP3 settings

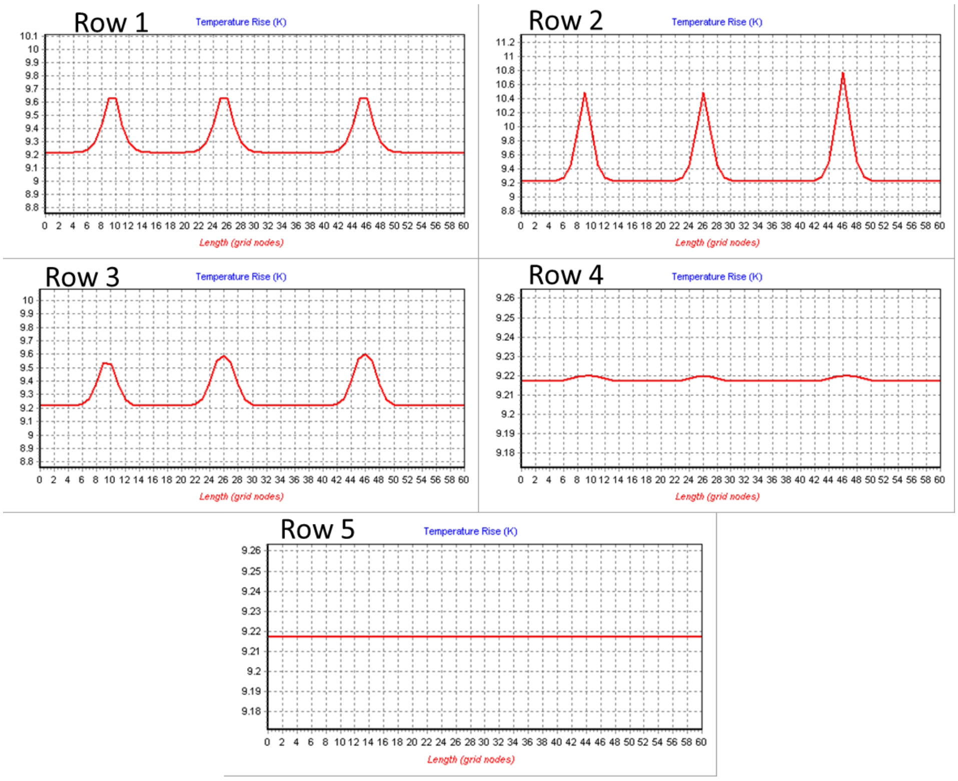

Graph 173 Delta T profiles for different rows of defects using optical pulsed thermography simulation SP3. Row#1 in blue, Row #2 in green, Row# 3 in Orange, Row# 4 in yellow and Row #5 in red

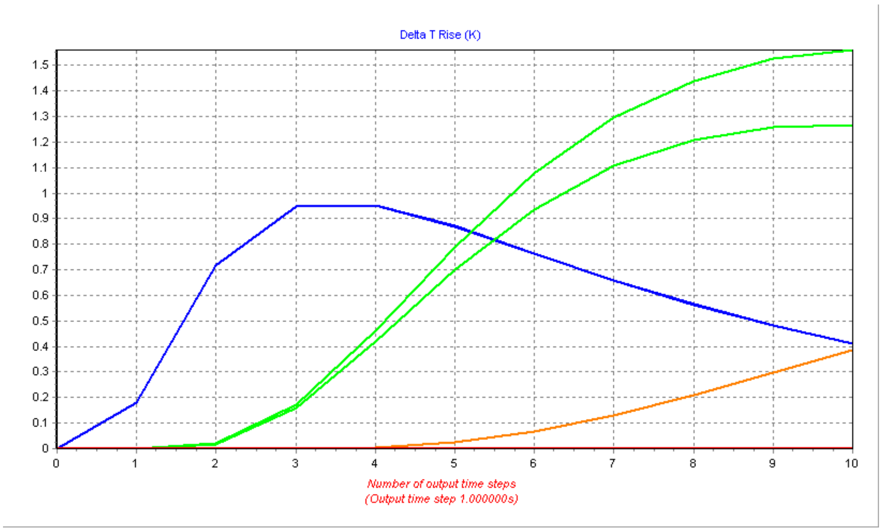

Graph 174 Delta T profiles for Row #3, Row #4 and #5 of defects using optical lockin simulation SP3. Row# 3 in orange, Row #4 yellow, Row #5 in red

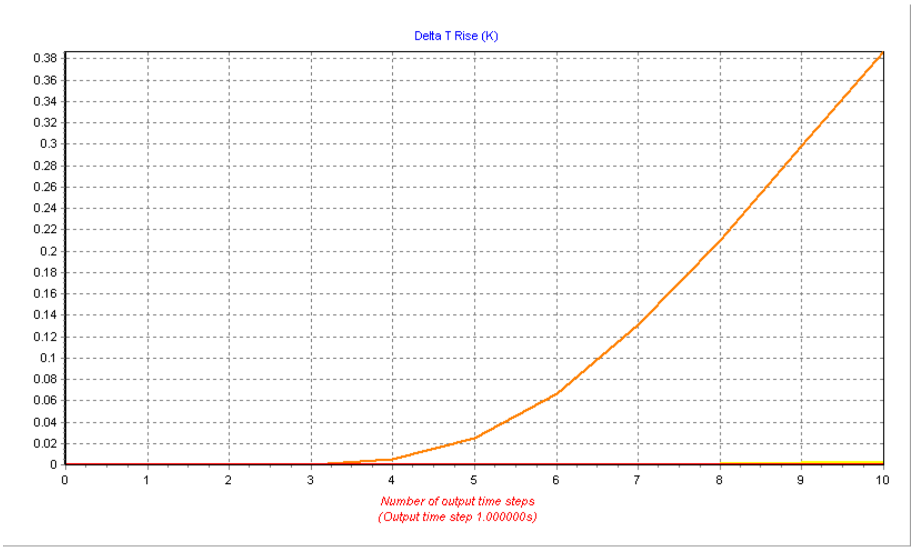

SP4

Figure 109 Thermal image for simulation SP 4 using single square pulse: Heating density 1,000,000 W/m^2, Heating time 0.05s, Total time 10s

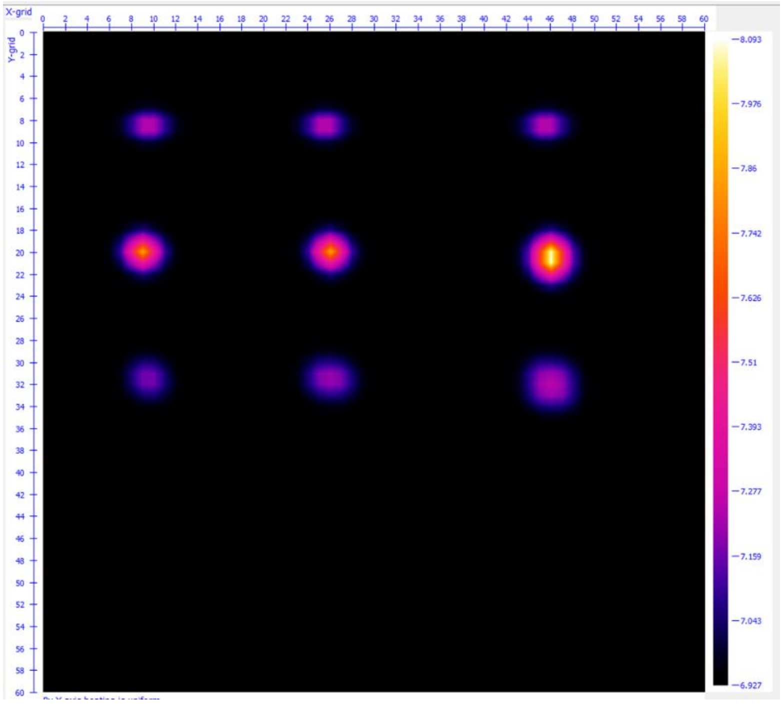

Graph 175 Space profiles of the different rows of defects using optical pulse simulation SP4 settings

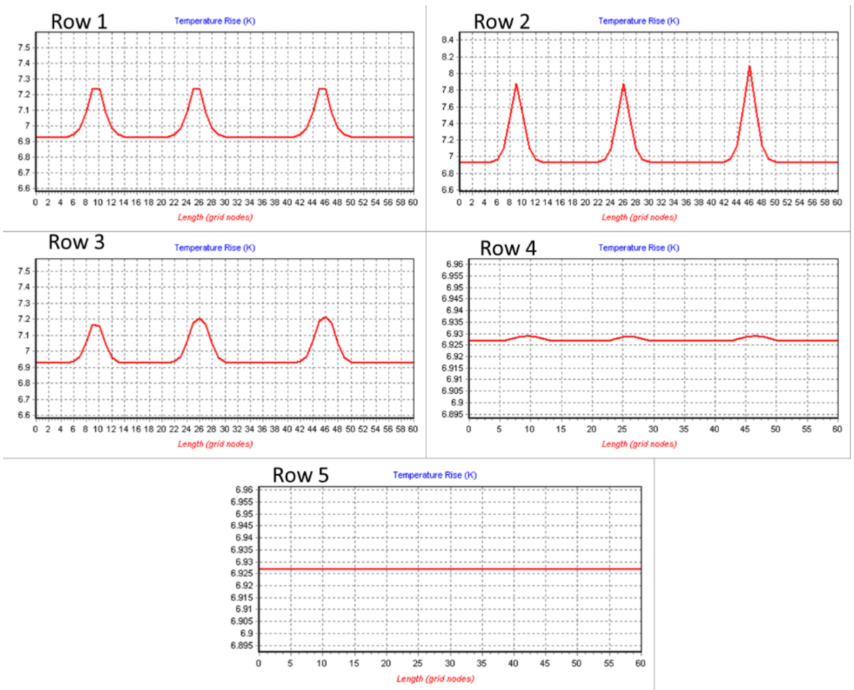

Graph 176 Delta T profiles for different rows of defects using optical pulsed thermography simulation SP4. Row#1 in blue, Row #2 in green, Row# 3 in Orange, Row# 4 in yellow and Row #5 in red

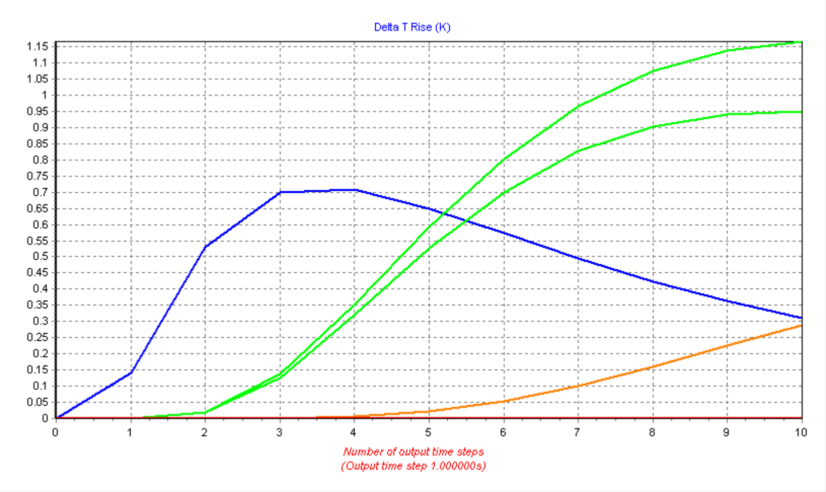

Graph 177 Delta T profiles for Row3, Row #4 and #5 of defects using optical lockin simulation SP4. Row# 3 in orange, Row #4 yellow, Row #5 in red

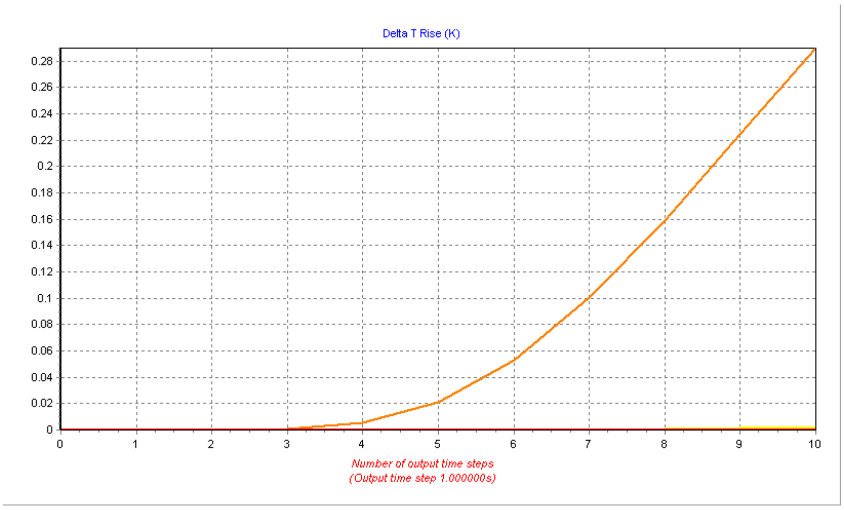

SP5

Figure 110 Thermal image for simulation SP 5 using single square pulse: Heating density 1,000,000 W/m^2, Heating time 0.05s, Total time 10s

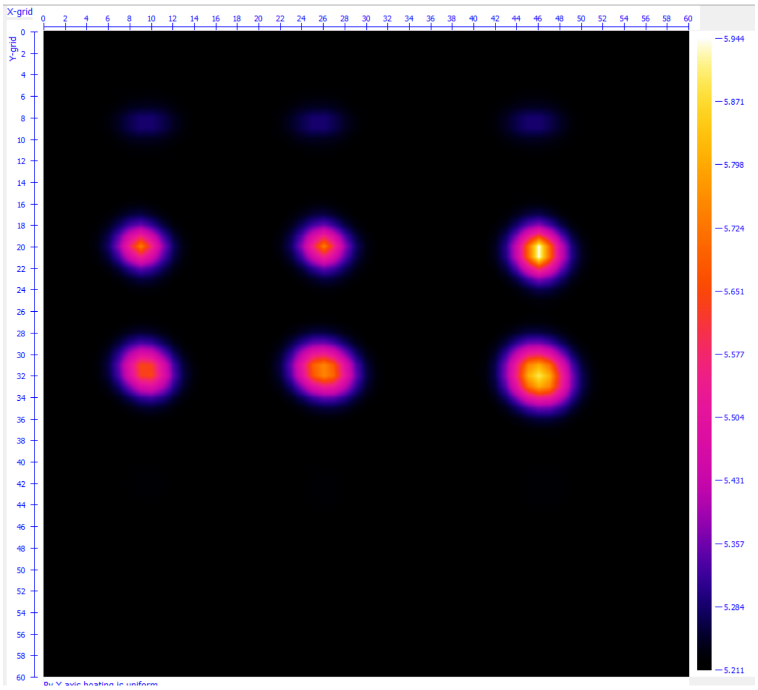

Graph 178 Space profiles of the different rows of defects using optical pulse simulation SP5 settings

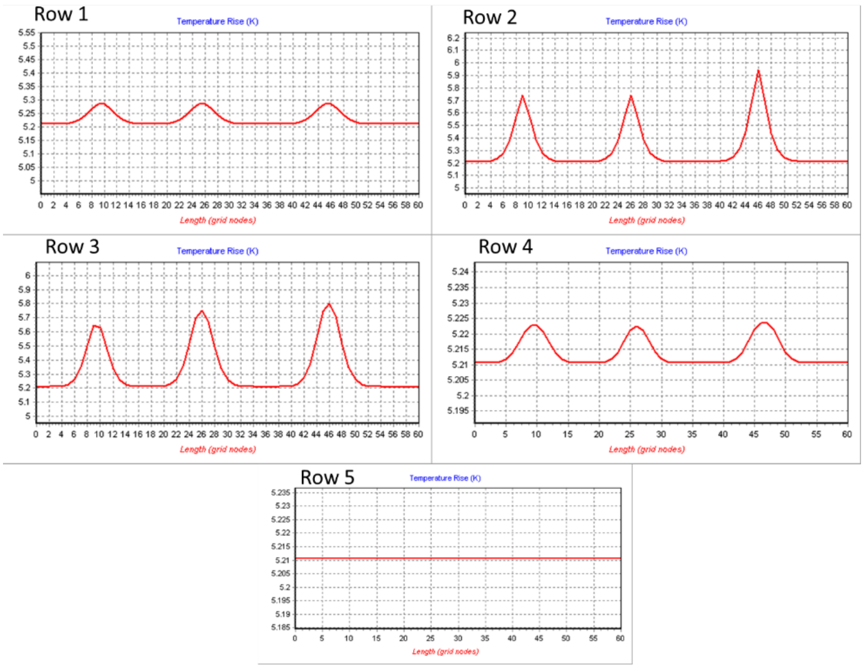

Graph 179 Delta T profiles for different rows of defects using optical pulsed thermography simulation SP5. Row#1 in blue, Row #2 in green, Row# 3 in Orange, Row# 4 in yellow and Row #5 in red

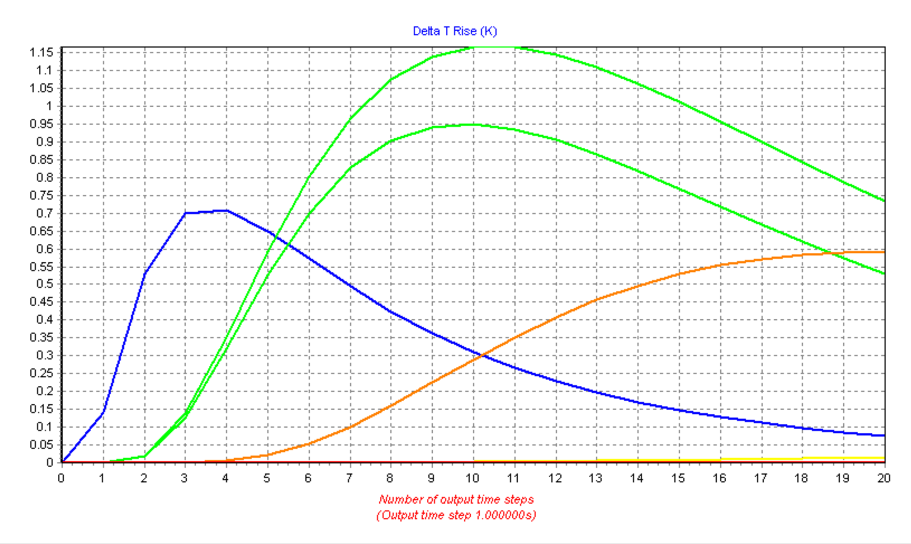

Graph 180 Delta T profiles for Row #4 and #5 of defects using optical lockin simulation SP4. Row #4 yellow, Row #5 in red

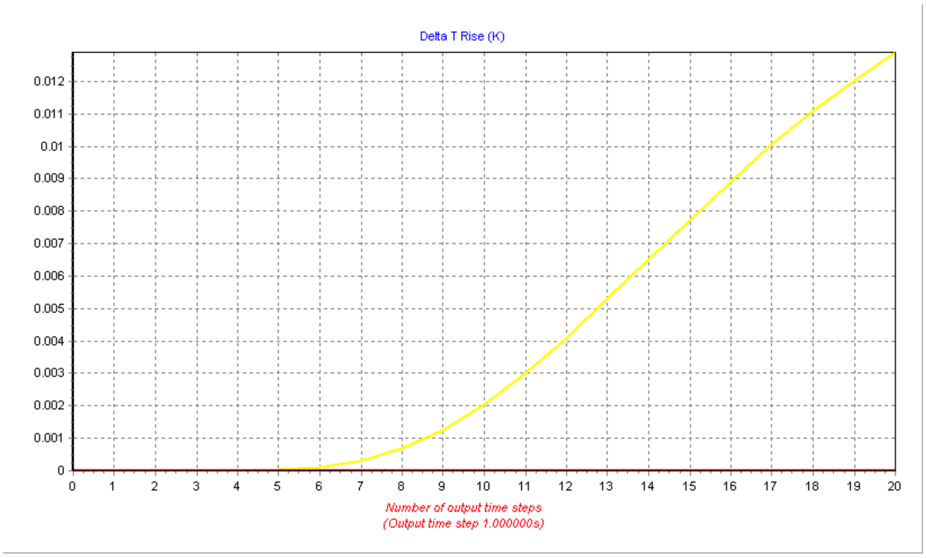

SP5

Figure 111 Thermal image for simulation SP 5 using single square pulse: Heating density 1,000,000 W/m^2, Heating time 0.05s, Total time 20s

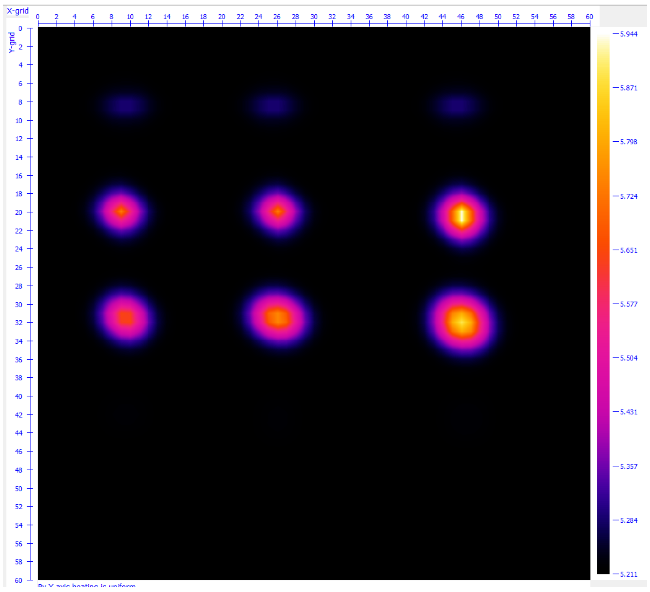

Graph 181 Space profiles of the different rows of defects using optical pulse simulation SP5 settings

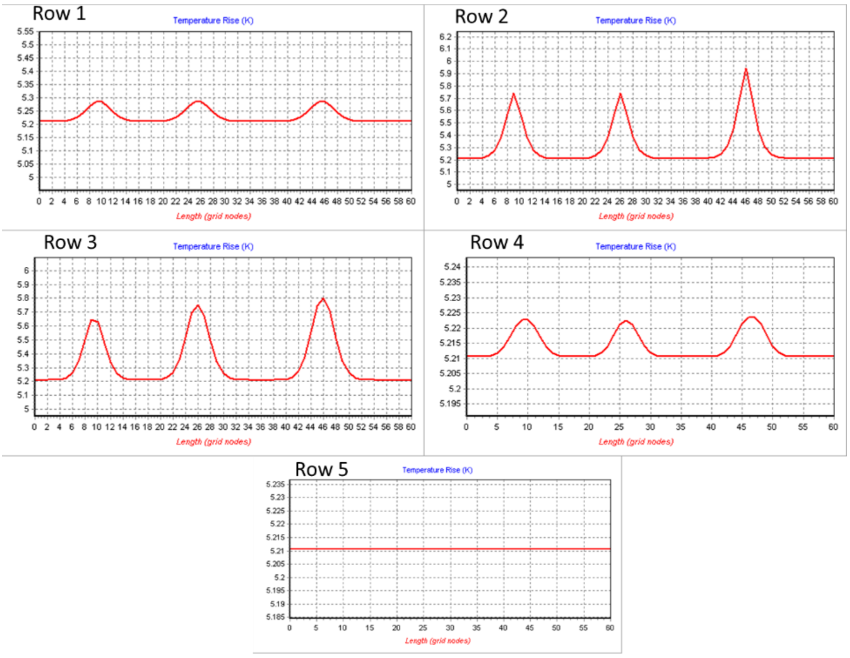

Graph 182 Delta T profiles for different rows of defects using optical pulsed thermography simulation SP5. Row#1 in blue, Row #2 in green, Row# 3 in Orange, Row# 4 yellow and Row #5 in red

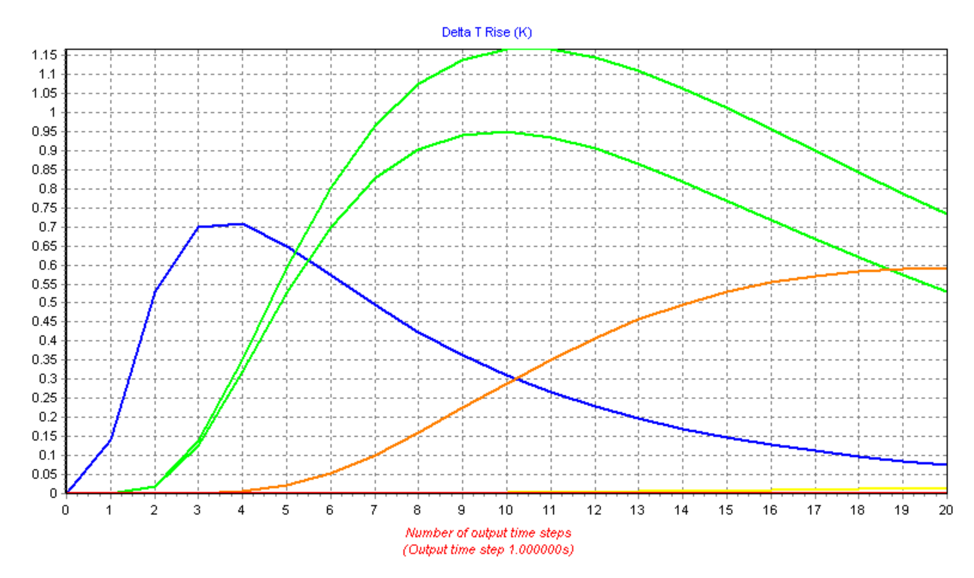

Graph 183 Delta T profiles for Row #4 and #5 of defects using optical lockin simulation SP5. Row #4 yellow, Row #5 in red

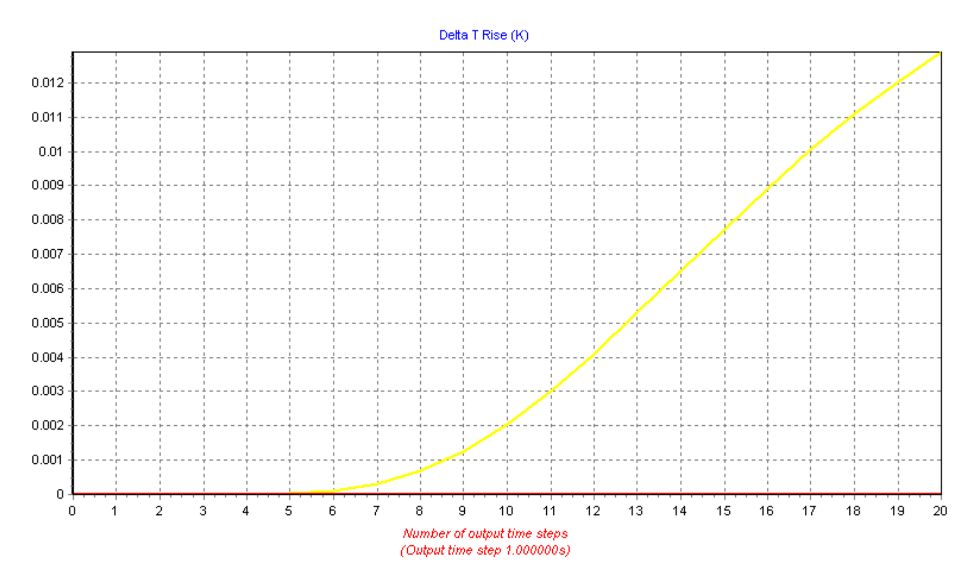

SP6

Figure 112 Thermal image for simulation SP 6 using single square pulse: Heating density 1,000,000 W/m^2, Heating time 0.05s, Total time 20s

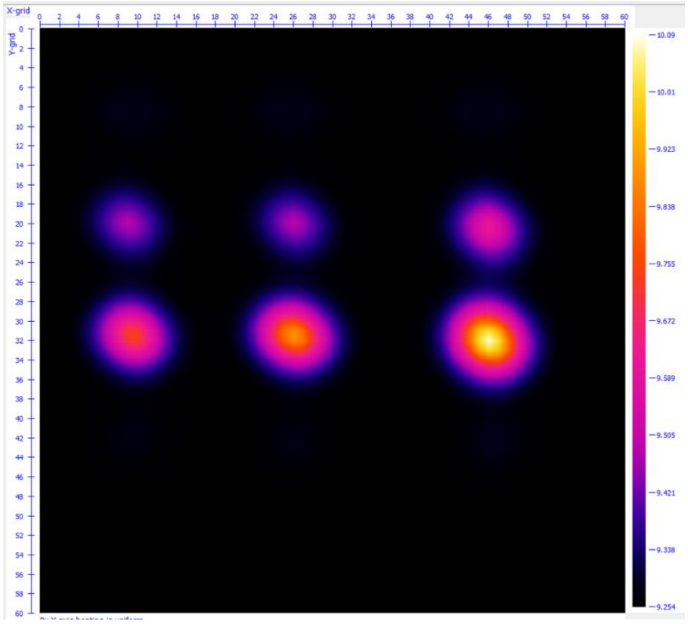

Graph 184 Space profiles of the different rows of defects using optical pulse simulation SP6 settings

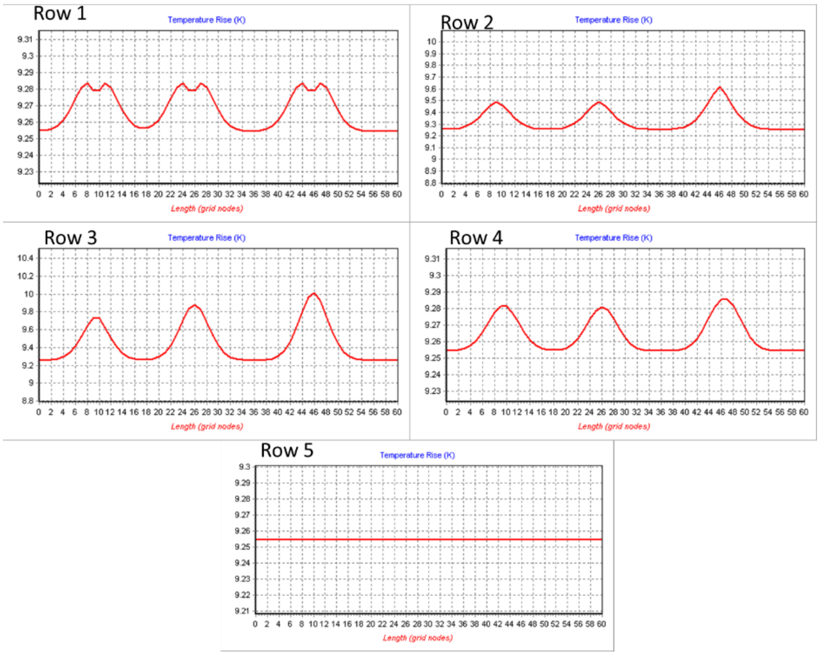

Graph 185 Delta T profiles for different rows of defects using optical pulsed thermography simulation SP6. Row#1 in blue, Row #2 in green, Row# 3 in Orange, Row# 4 in yellow and Row #5 in red

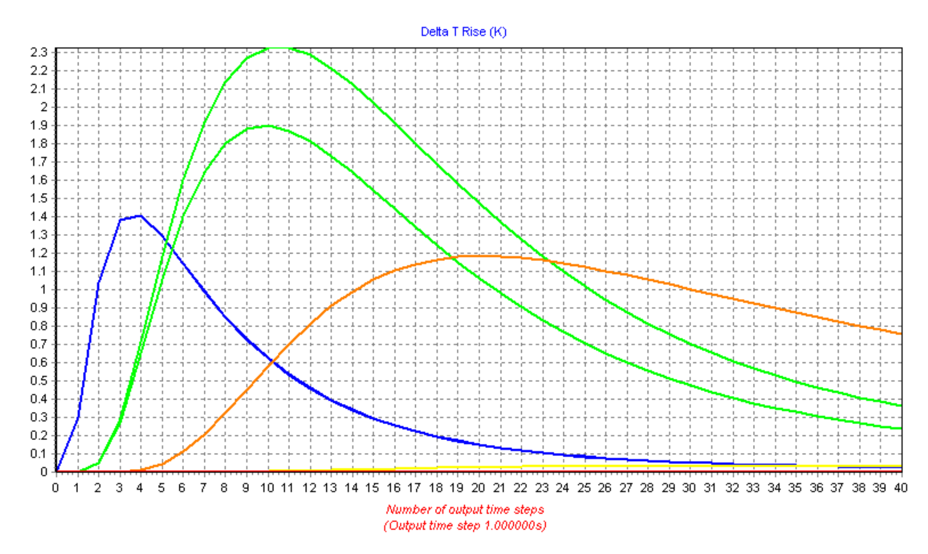

Graph 186 Delta T profiles for Row #4 and #5 of defects using optical lockin simulation SP4. Row #4 yellow, Row #5 in red

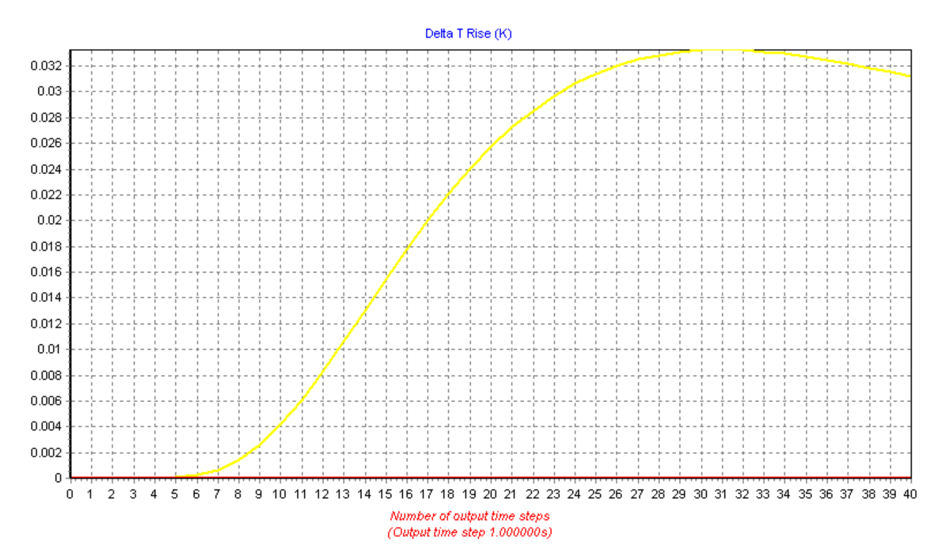

SP7

Figure 113 Thermal image for simulation SP 7 using single square pulse: Heating density 1,000,000 W/m^2, Heating time 0.05s, Total time 60s

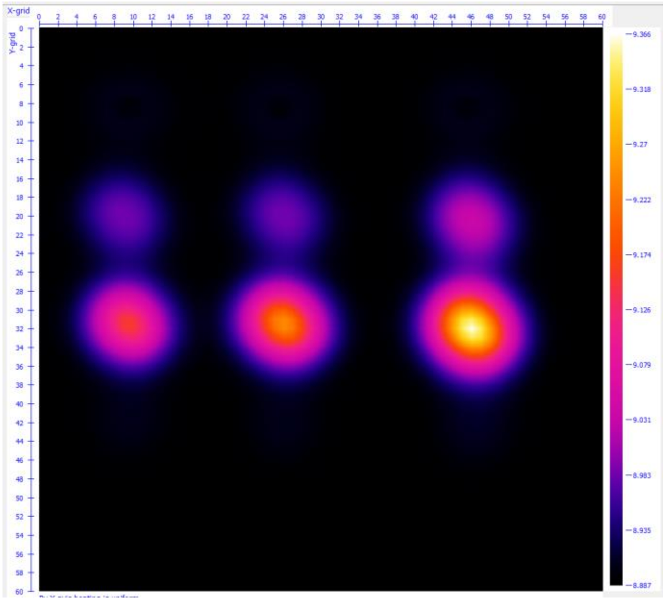

Graph 187 Space profiles of the different rows of defects using optical pulse simulation SP7 settings

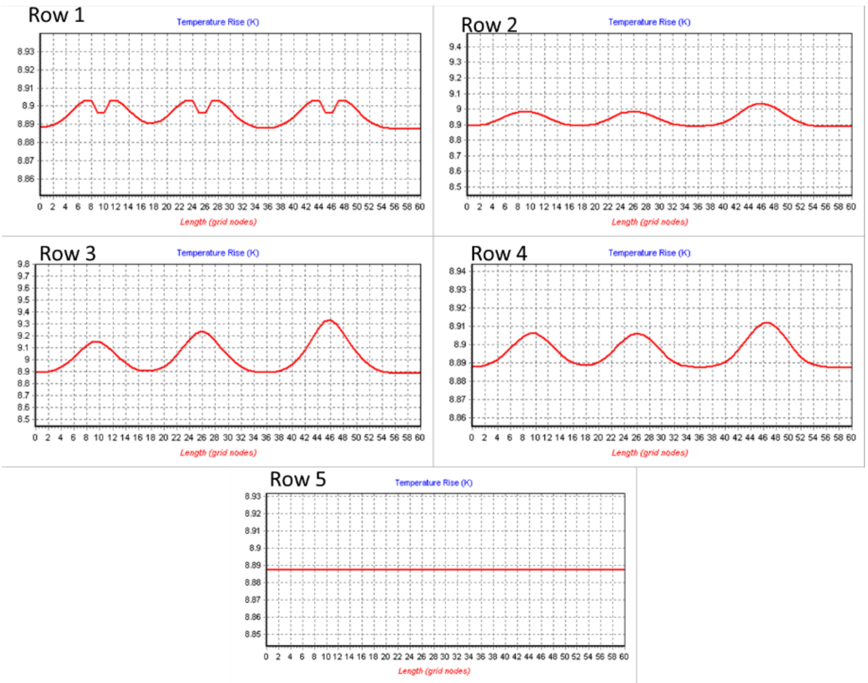

Graph 188 Delta T profiles for different rows of defects using optical pulsed thermography simulation SP7. Row#1 in blue, Row #2 in green, Row# 3 in Orange, Row# 4 in yellow and Row #5 in red

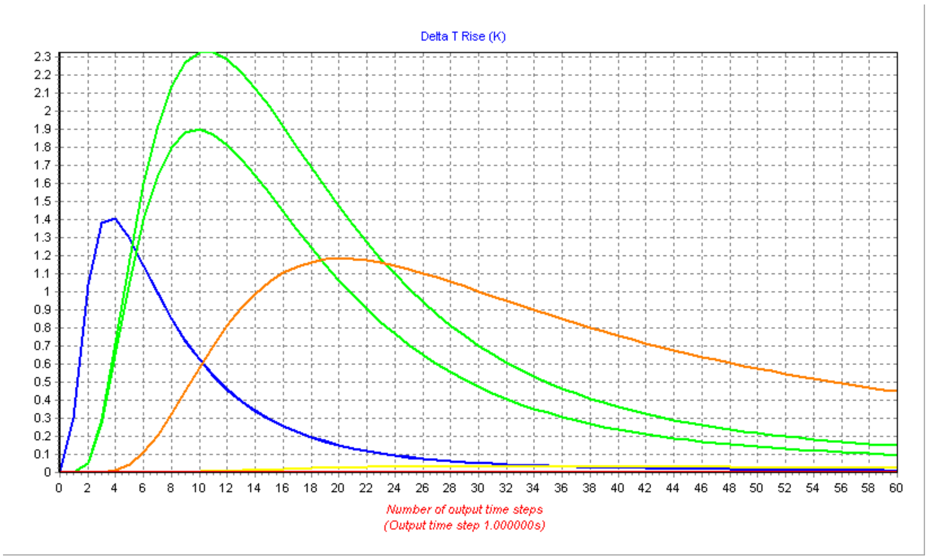

Graph 189 Delta T profiles for Row #4 and #5 of defects using optical lockin simulation SP7. Row #4 yellow, Row #5 in red

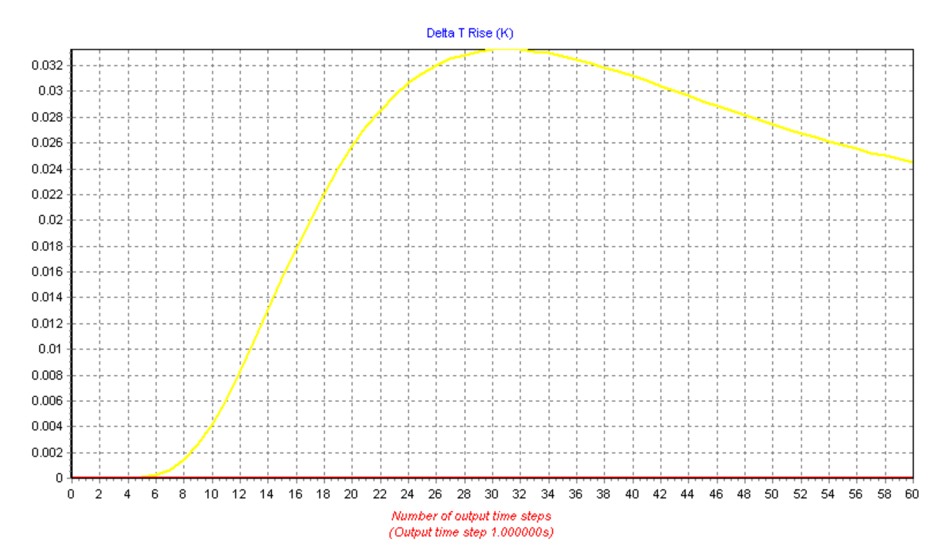

SP8

Figure 114 Thermal image for simulation SP 8 using single square pulse: Heating density 333,000 W/m^2, Heating time 0.1s, Total time 20s

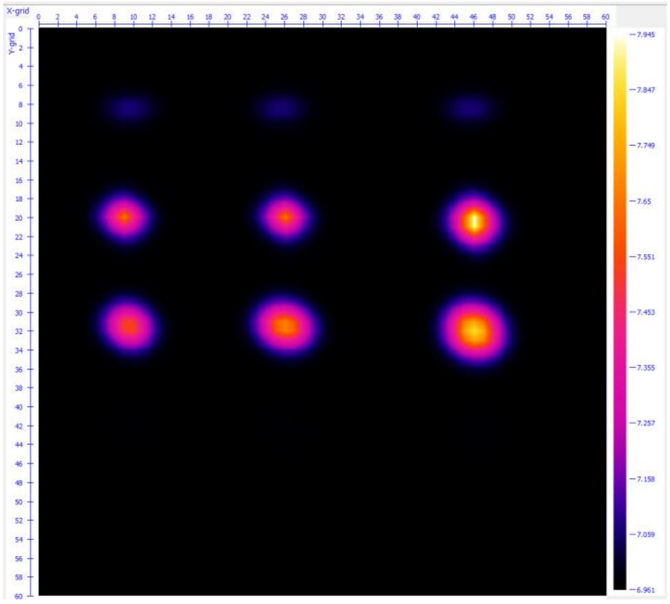

Graph 190 Space profiles of the different rows of defects using optical pulse simulation SP8 settings

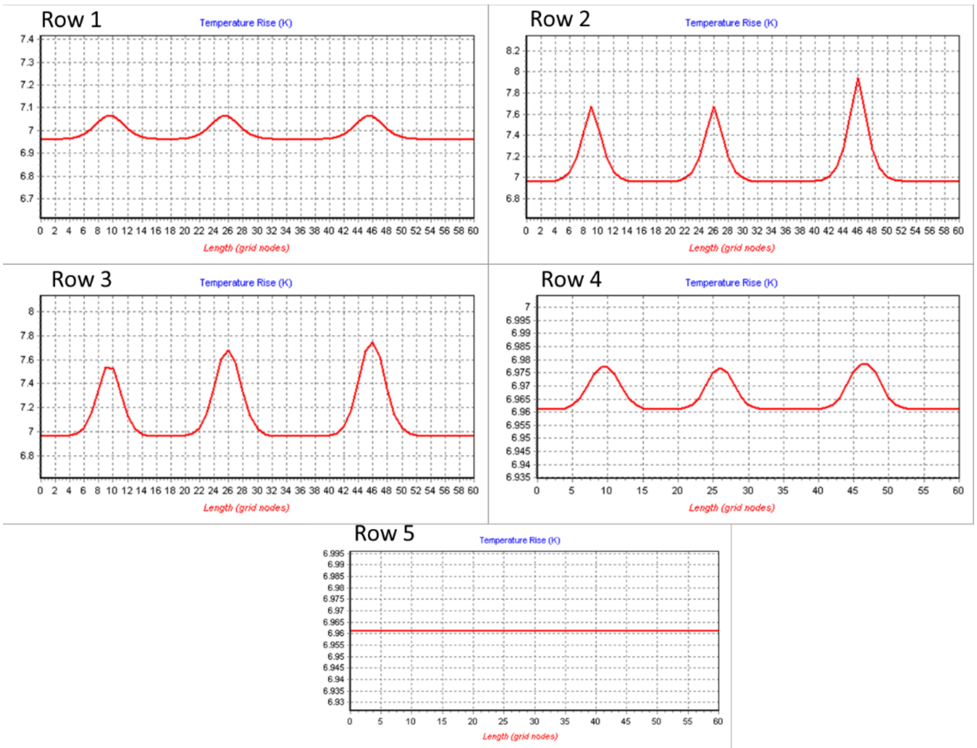

Graph 191 Delta T profiles for different rows of defects using optical pulsed thermography simulation SP8. Row#1 in blue, Row #2 in green, Row# 3 in Orange, Row# 4 in yellow and Row #5 in red

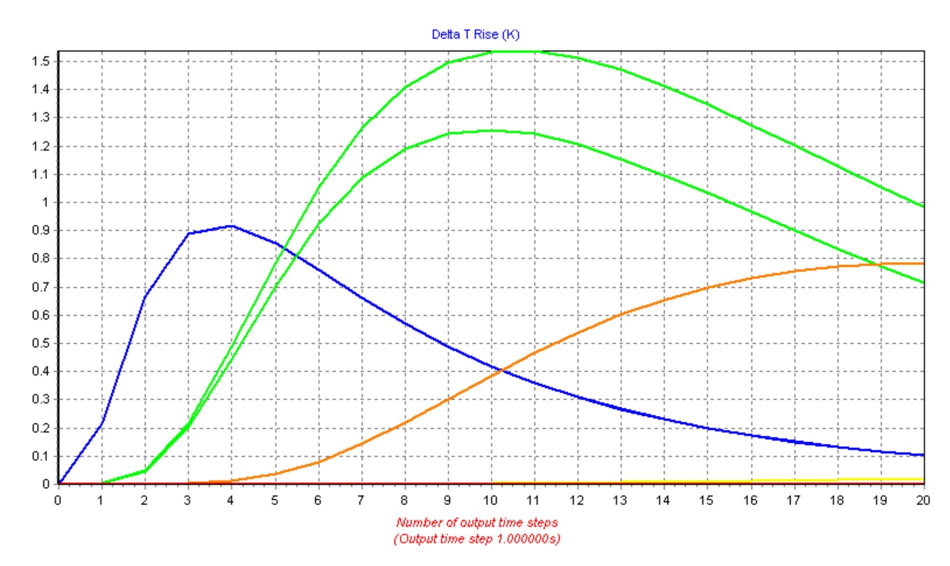

Graph 192 Delta T profiles for Row #4 (yellow) and Row#5 (red) of defects using optical lockin simulation SP8.

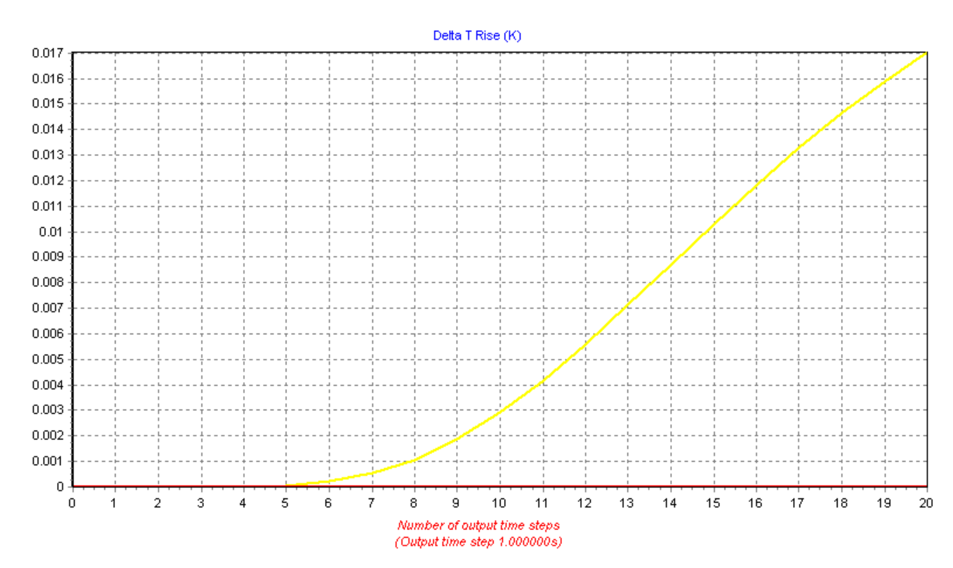

SP9

Figure 115 Thermal image for simulation SP 9 using single square pulse: Heating density 333,000 W/m^2, Heating time 0.1s, Total time 40s

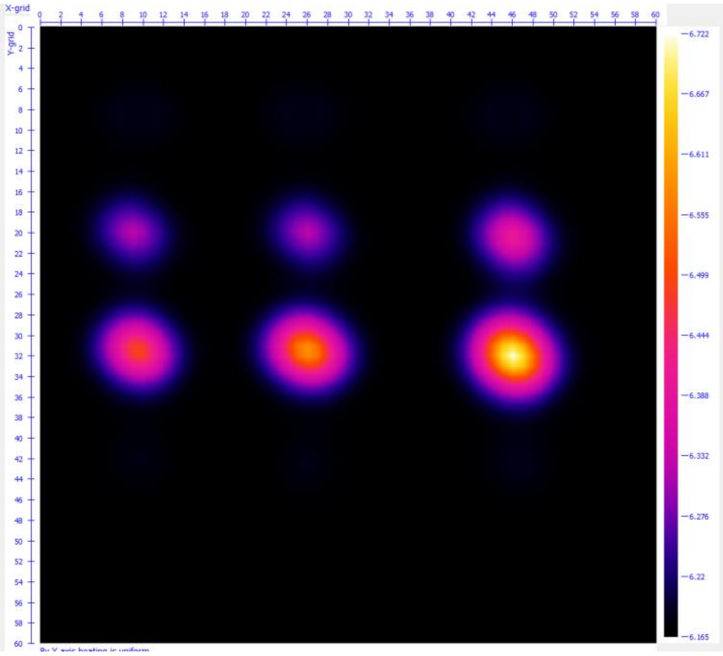

Graph 193 Space profiles of the different rows of defects using optical pulse simulation SP9 settings

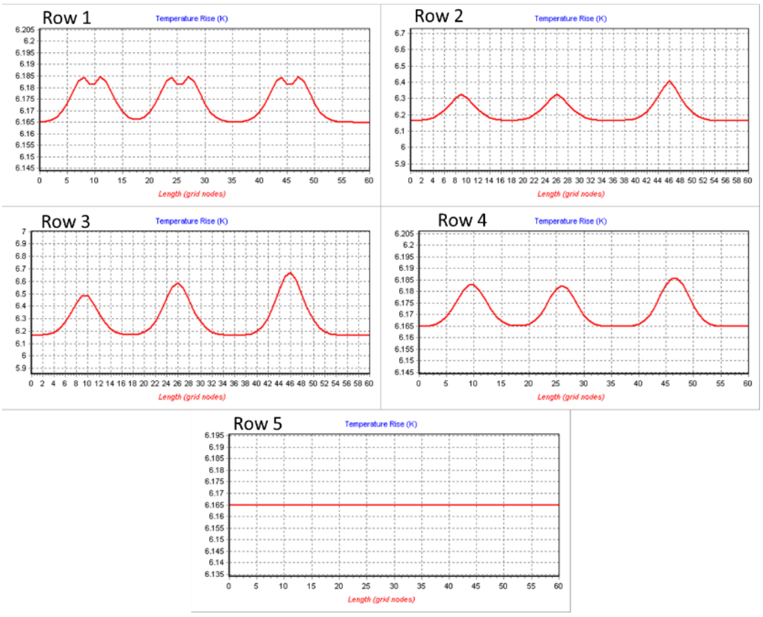

Graph 194 Delta T profiles for different rows of defects using optical pulsed thermography simulation SP9. Row#1 in blue, Row #2 in green, Row# 3 in Orange, Row# 4 in yellow and Row #5 in red

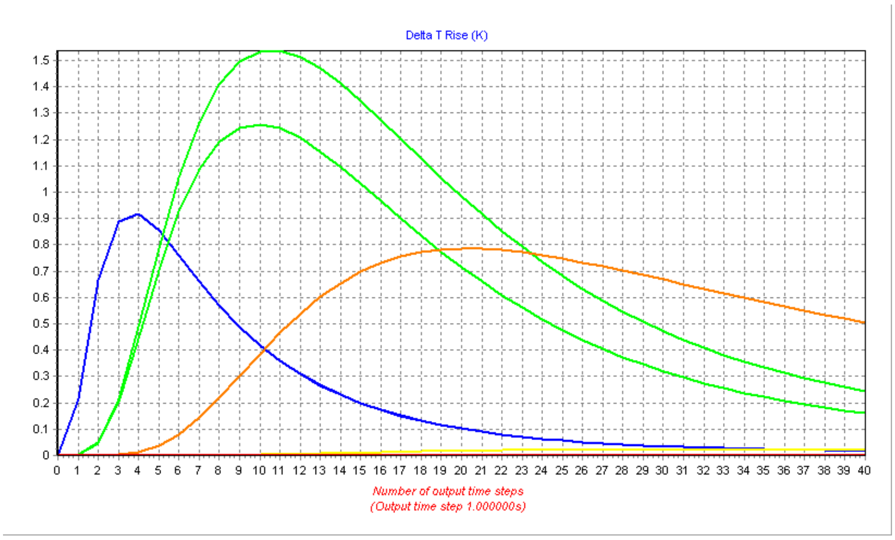

Graph 195 Delta T profiles for Row #4 and #5 of defects using optical lockin simulation SP9. Row #4 yellow, Row #5 in red

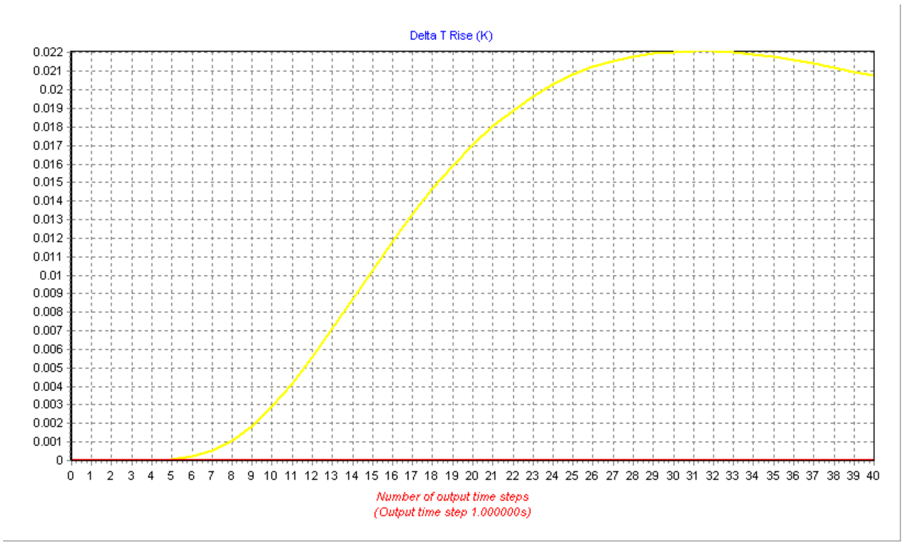

SP10

Figure 116 Thermal image for simulation SP 10 using single square pulse: Heating density 333,000 W/m^2, Heating time 0.1s, Total time 60s

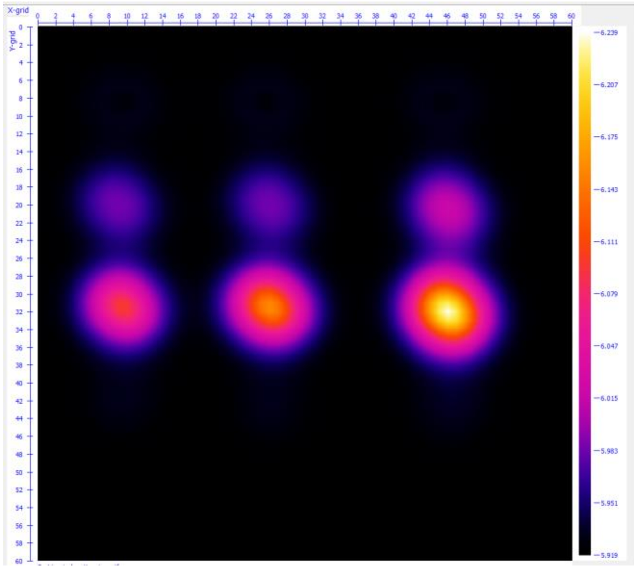

Graph 196 Space profiles of the different rows of defects using optical pulse simulation SP10 settings

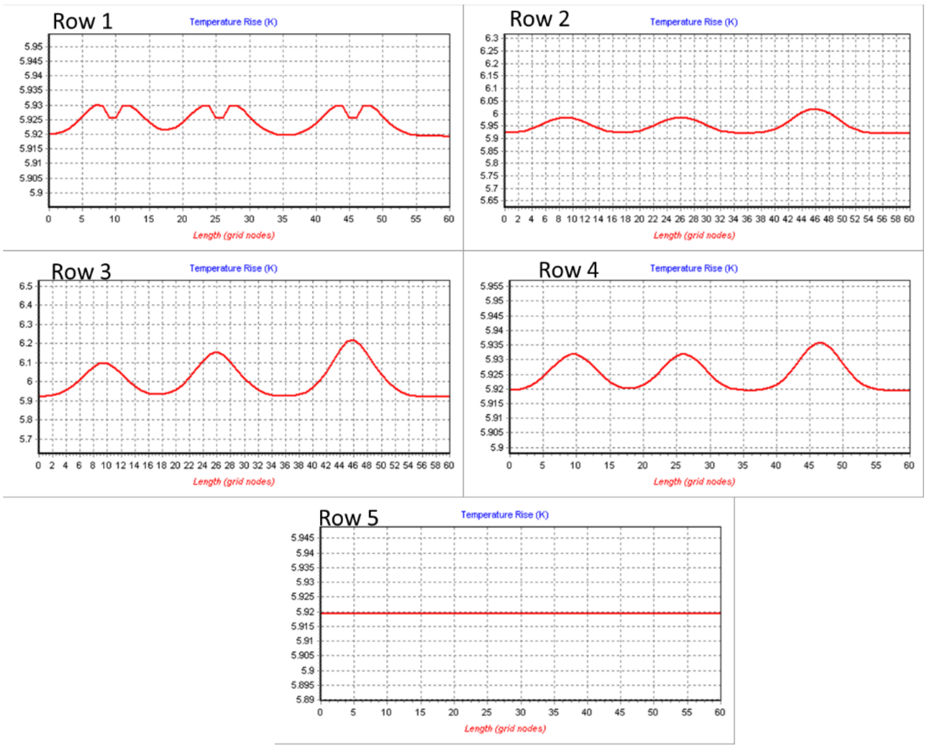

Graph 197 Delta T profiles for different rows of defects using optical pulsed thermography simulation SP10. Row#1 in blue, Row #2 in green, Row# 3 in Orange, Row# 4 in yellow and Row #5 in red

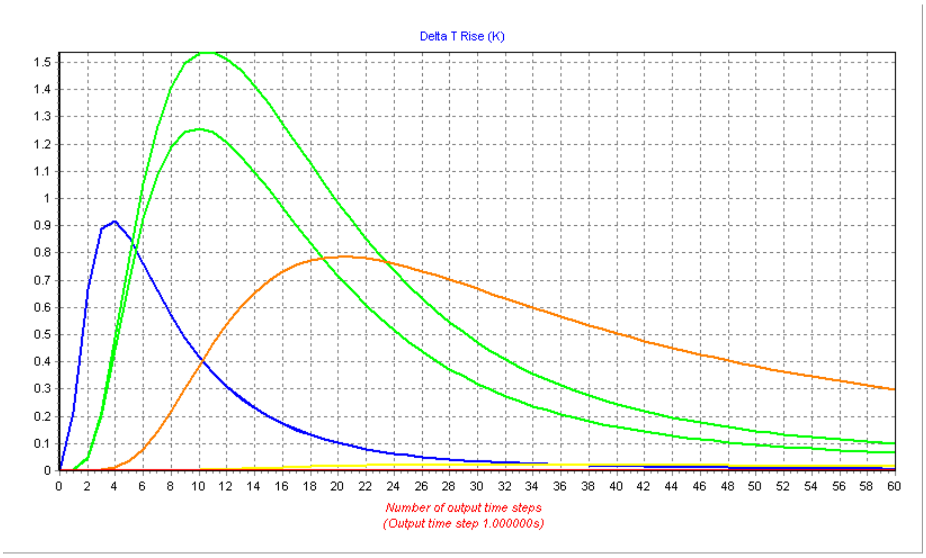

Graph 198 Delta T profiles for Row #4 and #5 of defects using optical lockin simulation SP10. Row #4 yellow, Row #5 in red

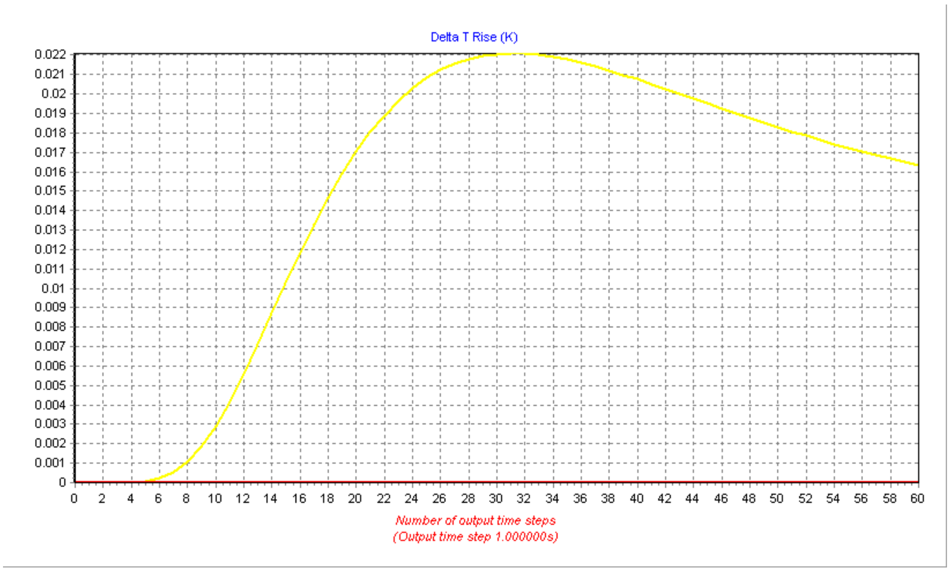

SP11

Figure 117 Thermal image for simulation SP 11 using single square pulse: Heating density 666,000 W/m^2, Heating time 0.1s, Total time 20s

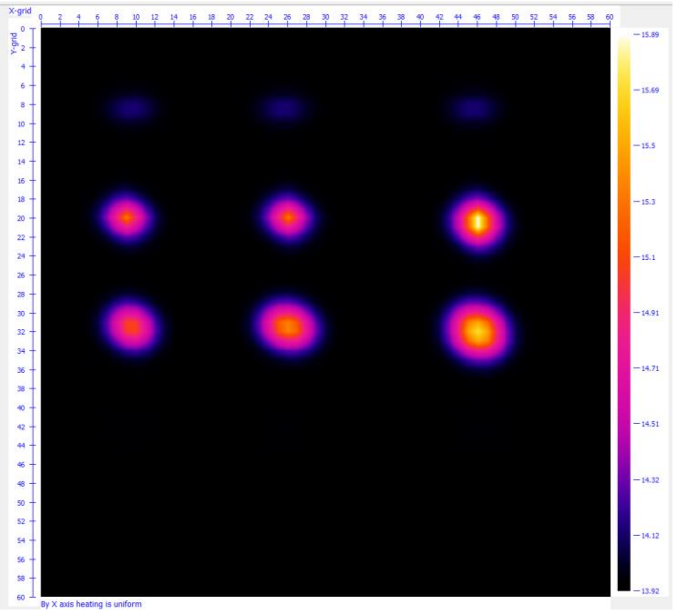

Graph 199 Space profiles of the different rows of defects using optical pulse simulation SP11 settings

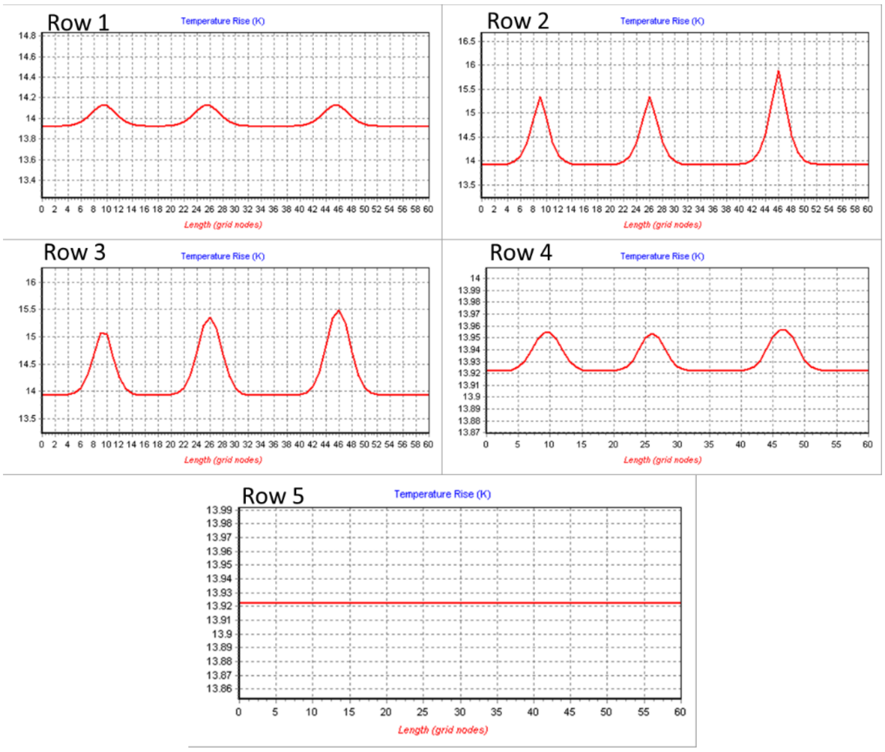

Graph 200 Delta T profiles for different rows of defects using optical pulsed thermography simulation SP11. Row#1 in blue, Row #2 in green, Row# 3 in Orange, Row# 4 in yellow and Row #5 in red

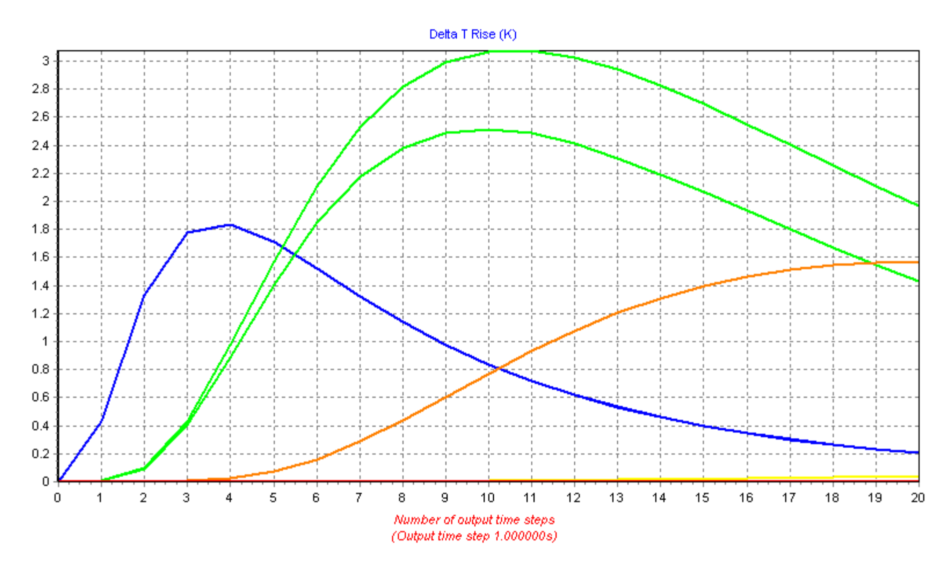

Graph 201 Delta T profiles for Row #4 and #5 of defects using optical lockin simulation SP11. Row #4 yellow, Row #5 in red

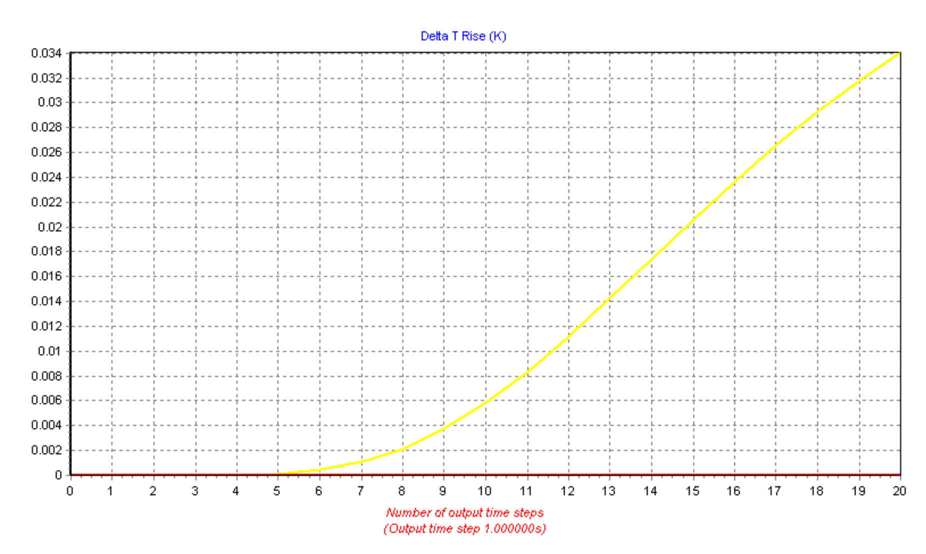

SP 12

Figure 118 Thermal image for simulation SP 12 using single square pulse: Heating density 666,000 W/m^2, Heating time 0.1s, Total time 40s

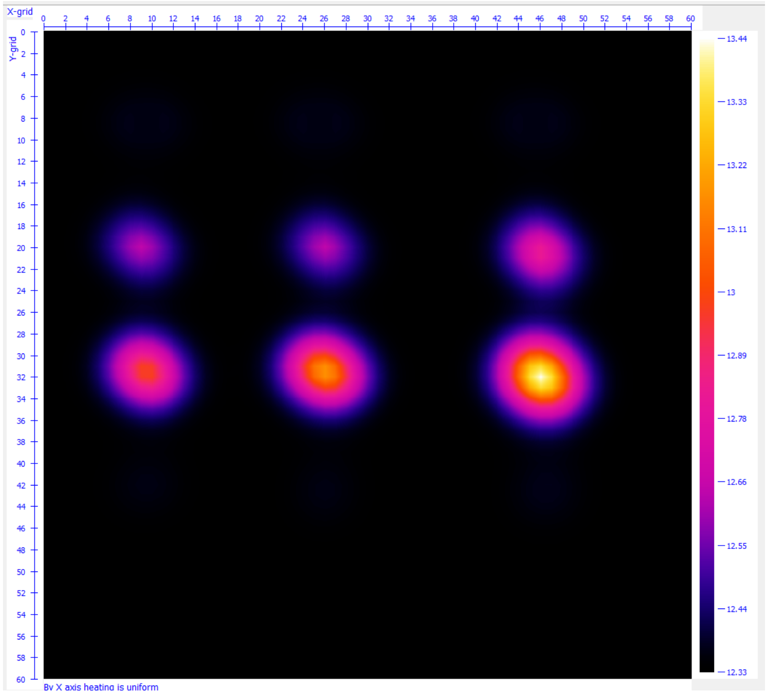

Graph 202 Space profiles of the different rows of defects using optical pulse simulation SP12 settings

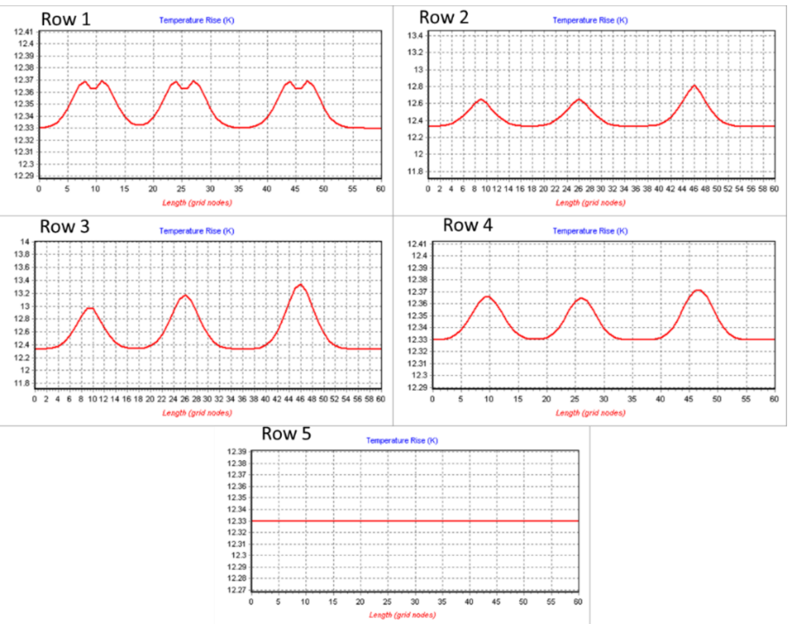

Graph 203 Delta T profiles for different rows of defects using optical pulsed thermography simulation SP12. Row#1 in blue, Row #2 in green, Row# 3 in Orange, Row# 4 in yellow and Row #5 in red

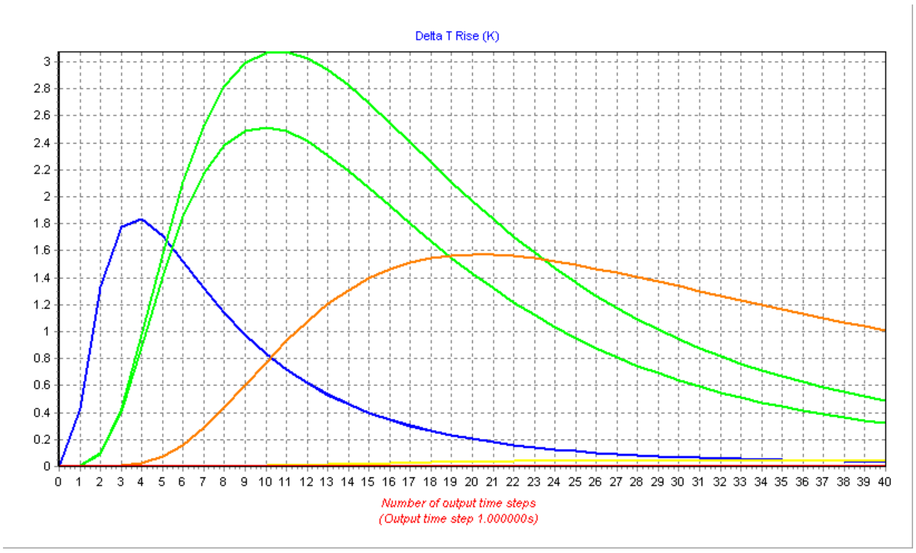

Graph 204 Delta T profiles for Row #4 and #5 of defects using optical lockin simulation SP12. Row #4 yellow, Row #5 in red